The Dissertation Committee for Matthew David Guild
certifies that this is the approved version of the following dissertation:

Acoustic Cloaking of Spherical Objects Using Thin Elastic Coatings

Committee:

Andrea Alù, Supervisor

Michael R. Haberman, Supervisor

Mark F. Hamilton

Preston S. Wilson

Loukas F. Kallivokas

Acoustic Cloaking of Spherical Objects Using Thin Elastic Coatings

by

Matthew David Guild, B.S.; M.S.E.

DISSERTATION

Presented to the Faculty of the Graduate School of

The University of Texas at Austin

in Partial Fulfillment

of the Requirements

for the Degree of

DOCTOR OF PHILOSOPHY

THE UNIVERSITY OF TEXAS AT AUSTIN

May 2012

Dedicated to Melissa

Acoustic Cloaking of Spherical Objects Using Thin Elastic Coatings

Publication No. _____

Matthew David Guild, Ph.D.
The University of Texas at Austin, 2012

Supervisors: Andrea Alù
Michael R. Haberman

In this thesis, a detailed description of acoustic cloaking is put forth using a coating consisting of discrete layers, enabling the cancellation of the scattered field around the object. This particular approach has previously only been applied to electromagnetic waves, for which it was observed that cloaking could be achieved using isotropic materials over a finite bandwidth. The analysis begins with a presentation of the theoretical formulation, which is developed using classical scattering theory for the scattered acoustic field of an isotropic sphere coated with multiple layers. Unlike previous works on acoustic scattering from spherical bodies, the criteria for acoustic cloaking is that the scattered field in the surrounding medium be equal to zero, and seeking a solution for the layer properties which achieve this condition.

To effectively investigate this situation, approximate solutions are obtained by assuming either quasi-static limits or thin shells, which provide valuable insight into the fundamental nature of the scattering cancellation. In addition, using these approximate solutions as a guide, exact numerical solutions can be obtained, enabling the full dynamics of the parameter space to be evaluated. Based on this

analysis, two distinct types of acoustic cloaking were found: a plasmonic cloak and an anti-resonance cloak.

The plasmonic cloak is a non-resonant type of cloak, named plasmonic because of its analogous behavior to the non-resonant cloak observed in electromagnetic waves which utilizes plasmonic materials to achieve the necessary properties. Due to the non-resonant behavior, this type of cloak offers the possibility of a much broader range of cloaking. To expand this design beyond wavelengths on the order of the uncloaked scatterer, multilayered cloak designs are investigated.

The anti-resonance cloak, as the name suggests, uses the anti-resonances of the modes within the cloaking layer to supplement the non-resonant plasmonic cloaking of the scattered field. Although somewhat more limited in bandwidth due to the presence of anti-resonances (and the accompanying resonances), this type of cloak enables a larger reduction in the scattering strength, compared with using a single elastic layer utilizing only non-resonant cloaking. A thorough investigation of the design space for a single isotropic elastic cloaking layer is performed, and the necessary elastic properties are discussed.

The work in this thesis describes the investigation of the theoretical formulation for acoustic cloaking, expanding upon the use of scattering cancellation previously developed for the cloaking of electromagnetic waves. This work includes a detailed look at the different physical phenomena, including both resonant and non-resonant mechanisms, that can be used to achieve the necessary scattering cancellation and which can be applied to a wide range of scattering configurations for which cloaking would be desirable. In addition to laying out a broad theoretical foundation, the use of limiting cases and practical examples demonstrates the effectiveness and feasibility of such an approach to the acoustic cloaking of a spherical object.

Table of Contents

List of Tables

List of Figures

Chapter 1

Introduction

For many years, the concept of cloaking has been a prevalent theme in science fiction and popular culture, from *Start Trek* to *Harry Potter*. The traditional approach taken by scientists and engineers to hide an object has been to apply an absorptive coating, thereby reducing the amount of energy reflected back to the source. Absorption alone, however, is limited by the physical properties of available lossy materials, and to compensate for this can require significantly increasing the thickness of the coating. Due to practical limitations in terms of size and weight, these absorptive layers are often not sufficient to eliminate the electromagnetic or acoustic 'visibility' due to the scattering from the object. Furthermore, even a perfect absorber casts a shadow, which can provide a means of detection. It has not been until more recently that the topic of cloaking has received serious attention from the scientific community. This research has been driven by theoretical works describing how waves could be effectively bent around an object, or alternatively, by applying a coating to the object which effectively cancels the scattered field.

1.1 Thesis objectives

The objective of this thesis is to investigate the physical parameters necessary for, and the feasibility of, designing an acoustic cloak using a scattering cancellation approach for an elastic sphere using fluid and elastic layers. To achieve this objective, two fundamental questions will be addressed throughout this work:

1. How can the acoustic field scattered from a spherical object be significantly reduced or cancelled?

2. How can a realizable cloak be achieved?

To address the first question, a thorough analysis of the existing body of scientific literature is required. For the case of acoustic cloaking, this includes previous approaches to cloaking, including both electromagnetic (EM) waves and those involving acoustic waves in fluids and elastic solids. To gain a deeper understanding also requires a detailed look at the fundamental physics of scattering from spherical elastic bodies. With this foundation, the investigation of how the scattered acoustic field can be eliminated and the relevant physical parameters needed to accomplish this can be determined.

To address the second question, the relevant cloaking parameters will need to be considered. In particular, it is important to account for elastic effects, which are inherent to any practical acoustic structure. Although the elastodynamics of a submerged spherical body will lead to significantly increased complexity, thereby limiting the ability to obtain explicit analytic solutions, except for some limiting cases or specific examples. It is important to be mindful of how these particular cases fit into the broader context of acoustic cloaking, and therefore the solutions will be developed in the most generalized manner possible. Even when it is impractical or impossible to express the configurations explicitly, exact systems of equations can be solved numerically to determine the results in these instances. In fact, under some circumstances for which approximate solutions can be obtained, it will still be necessary to solve for the exact solution to precisely determine the effectiveness of a particular cloak design.

1.2 Thesis overview

The chapters which follow have been laid out to address the objectives and research questions put forth in the previous section, and to convey the information in as clear a manner as possible. This process begins with a background on the basic theory and current approaches to cloaking, presented in Chapter 2. This includes approaches which have showed promise for EM or acoustic waves, examining how they work and identifying the potential limitations and challenges associated with each method.

To supplement this understanding of acoustic cloaking, a detailed formulation for the acoustic scattering from a submerged coated elastic sphere is developed in Chapter 3. Although classical scattering concepts have been studied extensively for over half a century, the vast majority of these works have focused on determining the scattered field for a given geometry and material properties, and the determination of distinctive features based on these results which can enable identification of the object [1]. Rather than using the scattered acoustic field for identification, the more recent concept of scattering cancellation developed for EM cloaking is applied, in which the scattered field in the surrounding medium is prescribed to be zero. Thus, instead of asking *what coated objected caused this acoustic scattering?*, the novel question considered here is *what sort of coatings can produce zero or minimal acoustic scattering?*.

The general formulations developed in Chapter 3 are analyzed in detail for particular configurations in Chapters 4, 5 and 6, presented in order of increasing complexity. In Chapter 4, the case of a submerged sphere coated with a single layer is investigated. Even in this simplest of cases, determining exact explicit expressions for the required cloaking layer properties is not feasible. Therefore, approximate solutions are developed for two different scenarios: (i) quasi-static limit, and (ii)

thin shells relative to the wavelength of the incident sound. Based on these results, the effects of using a fluid or an isotropic elastic solid as a cloak is examined, for the cloaking of both fluid and elastic spheres. Chapter 5 presents a means to increase the effectiveness of the single layer cloak presented in Chapter 4. To do this, shear-wave *anti-resonances* within an isotropic elastic cloaking layer are used to increase the reduction in the scattering strength.

The presence of resonances in the single elastic cloaking layer presented in Chapter 5, however, can lead to a reduction in the bandwidth. Building upon the non-resonant single configuration presented in Chapter 4, Chapter 6 presents an investigation of the use of multiple layers. To facilitate this, the case of two layers is examined in detail. Although conceptually it is a relatively minor step to move from a single homogeneous layer to two homogeneous layers, the scattering analysis becomes significantly more cumbersome. Due to this, development of analytic expressions is limited to cloak consisting of two fluid layers. Although a relatively simple configuration, the results developed are used to investigate more complicated multilayer cloaks, by using two alternating materials.

The analysis in Chapter 6 allows for an arbitrary number of fluid or isotropic elastic solids to be used to construct a cloak. Although the operation of these cloaks is focused on a single design frequency, a reduction in the scattering strength is seen for a broader range of frequencies. To extend this bandwidth, consideration of anisotropic layers is considered, which is presented in Chapter 7. In spherical coordinates, the formulation developed in Chapter 3 and used in Chapters 4-6 cannot be used. An alternative approach to describe the scattering from an elastic sphere with anisotropic spherical shells is developed in Chapter 7, to which the conditions for scattering cancellation can be applied.

Finally, Chapter 8 gives a summary of the results and some concluding

remarks. Potential future applications of this work and expansions of the analysis developed are considered.

Chapter 2

Background and fundamentals of acoustic cloaking

The topic of acoustic cloaking has gained significant attention in recent years, as the result of successful implementations in the electromagnetic (EM) domain. This chapter introduces several EM cloaking approaches which offer a means to achieving cloaking of acoustic waves. In Section 2.1, the transformation method is discussed, which prescribes anisotropic functionally-graded materials to re-route the incident energy around an object. This method has been the topic of much interest in the literature and has direct analogues in acoustics. In Section 2.2, another means of cloaking originally proposed for EM waves is described. This proposed method uses the anomalous resonances resulting from the interaction with negative-valued material properties to achieve cloaking. Finally, in Section 2.3, a promising method is discussed which utilizes a cloaking layer designed to eliminate the scattered field within the surrounding medium over a given bandwidth. This scattering cancellation approach has previously only been applied to the cloaking of EM waves. A qualitative comparison of the analogous behavior between EM and acoustic waves is presented, revealing that the main limitations and challenges encountered with implementation of this type of cloak for EM waves are mitigated in the case of acoustic waves.

2.1 Transformation cloaks for acoustic waves

One proposed approach to cloaking is to utilize materials whose properties lead to the re-routing of sound around the object of interest. This approach prevents acoustic energy from interacting with the object, and was originally described for EM waves [2], [3]-[11] and subsequently extended to acoustic [12], [13]-[20] and elastic waves [21], [22]-[25]. To understand how this is possible, consider an undisturbed acoustic wave traveling through a homogeneous medium. To achieve cloaking, the objective is to create an annulus-shaped region that is deformed in such a way as to preserve the undisturbed acoustic wave outside of this enclosed region. Thus, while outside of this deformed region the acoustic wave is undisturbed, there is no acoustic field present within the interior of the annulus, and therefore allows any object in this region to be cloaked.

Mathematically, this is accomplished by using a one-to-one mapping between the deformed and undeformed regions everywhere except at a single point, which is mapped onto the cloak's inner boundary [26]. This process is illustrated in Figure 2.1. Note that this process, which is formally called a coordinate transformation, alters the cloak's properties so that the modified wave equation in the cloak mimics the wave equation in the previously unaltered region. Due to the mathematics defining cloaks employing this approach, it is referred to here as the *transformation method*.

Mathematically, the general representation for relating the wave equation in the initial and transformed spaces is given by Norris [21]

$$\nabla^2 p - \ddot{p} = 0 \quad \Longleftrightarrow \quad K\mathbf{S} : \nabla\left(\boldsymbol{\rho}^{-1}\mathbf{S}\nabla p\right) - \ddot{p} = 0. \tag{2.1}$$

In the undeformed space, this relationship is simply the wave equation for a homogeneous fluid. The expression for the deformed space is more complicated, and

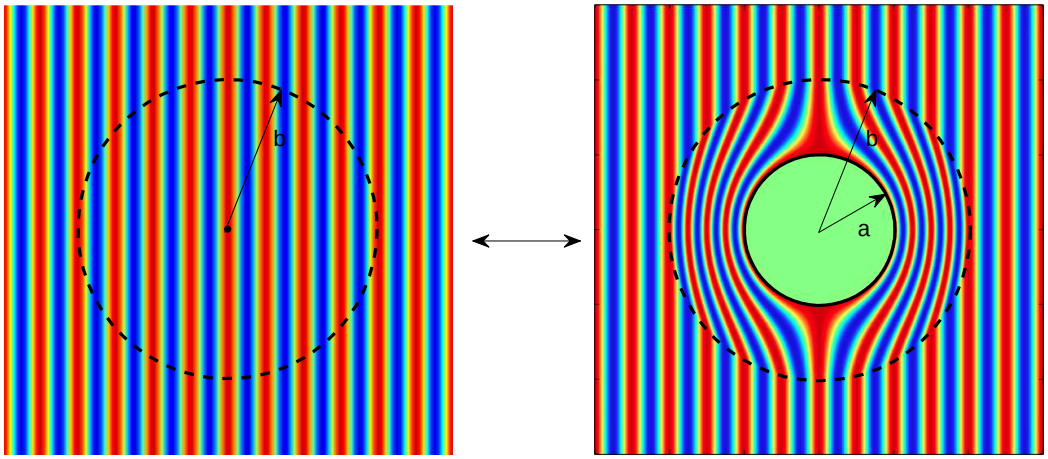

Figure 2.1: Illustration of the coordinate transformation between an undeformed space (left) and a symmetric deformed space (right). Any object placed within the interior region of radius a will be cloaked.

involves spatial variability of both the pressure p and a generalized material property called the density tensor $\boldsymbol{\rho}$. The parameters K and $\mathbf{S}$ describe the stress-strain relationship in the transformed region, which is $\boldsymbol{\sigma} = \mathbf{C}\boldsymbol{\varepsilon}$, where

$$\mathbf{C} = K\mathbf{S} \otimes \mathbf{S}. \tag{2.2}$$

In this relationship, the second order tensor $\mathbf{S}$ is the result of the transformation and satisfies the condition $\operatorname{div} \mathbf{S} = 0$. Note that the : and $\otimes$ in the above expressions denote the inner and outer tensor products, respectively. Two different types of cloaks arise from this transformation: *inertial cloaks* and *pentamode material cloaks*, which are explored in the next two sections.

2.1.1 Inertial cloak

The analysis of determining the necessary coordinate transformation with general elastic media and arbitrary geometries can be formidable. One case of interest, which was the first form of acoustic cloaking to be explored by Cummer

et al. [12], is when the compressibility is isotropic, like that of a fluid. This is equivalent to the case where **S** is equal to the identity matrix in Equations (2.1) and (2.2). The basic formulation for this case is presented in Section 2.1.1.1. Based on these theoretical values for the cloaking layer properties, Section 2.1.1.2 discusses current approaches to the realization of these cloaks.

2.1.1.1 Basic formulation

Simplification of the solution to the transformation in Equation (2.1) occurs when an isotropic compressibility is considered for canonical shapes in a rotationally symmetric coordinate system, like that shown in Figure 2.2(a). With these simplifications, expressions for the transformed cloaking layer properties become [21]

$$\frac{\rho_r}{\rho_0} = R' \left(\frac{r}{R}\right)^{N-1}, \tag{2.3}$$

$$\frac{\rho_\theta}{\rho_0} = \frac{1}{R'} \left(\frac{r}{R}\right)^{N-3}, \tag{2.4}$$

$$\frac{\kappa}{\kappa_0} = \frac{1}{R'} \left(\frac{r}{R}\right)^{N-1}, \tag{2.5}$$

where ρ_r and ρ_θ are the radial and azimuthal densities of the cloak, κ is the bulk modulus of the cloak, ρ_0 and κ_0 are the density and bulk modulus of the surrounding fluid, and N is the number of spatial dimensions. For solutions of practical significance, $N = 2$ or $N = 3$, corresponding to either cylindrical or spherical coordinates, respectively. The function R appearing in Equations (2.3)–(2.5) is the radius in the undeformed space shown on the left-hand side of Figure 2.1, which is related to the radius r in the deformed space by

$$R = \frac{b}{b-a}\left(r - a\right). \tag{2.6}$$

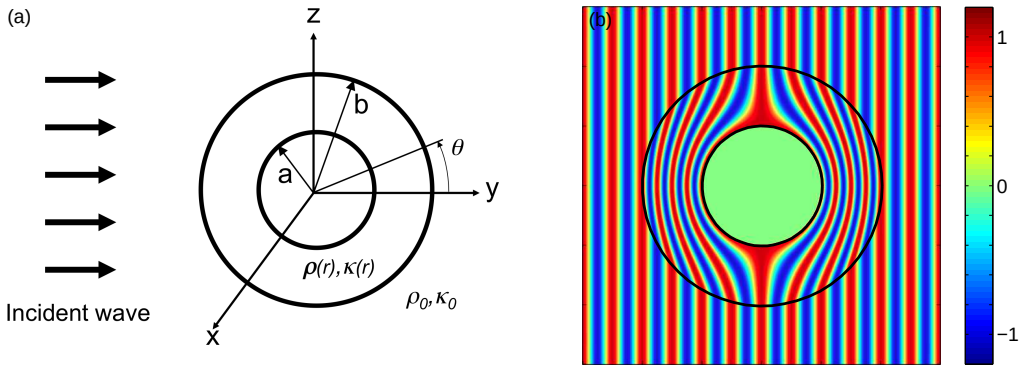

Figure 2.2: (a) An incident plane wave impinging upon a cylindrical body covered with an inertial cloak with density tensor $\boldsymbol{\rho}$ and bulk modulus κ. (b) Numerical simulation from Cummer *et al.* of the total pressure field for a perfect inertial cloak [14]. The amplitude is normalized by the magnitude of the incident wave, which is a time-harmonic plane wave traveling from left to right.

The function R' denotes the first derivative of R with respect to r, which is simply

$$R' = \frac{b}{b-a}. \tag{2.7}$$

Notice that the values of $r = a$ and $r = b$ in the right-hand side of Figure 2.1, representing the inner and outer edge of the cloak, correspond to the values $R = 0$ and $R = b$ in the undeformed space shown on the left-hand side of Figure 2.1.

Substituting Equations (2.6) and (2.7) into Equations (2.3)–(2.5), one can obtain the required physical properties necessary to achieve acoustic cloaking for a spherical (or cylindrical) object of radius a with an acoustic cloak of outer radius b

[14]

$$\frac{\rho_r}{\rho_0} = \left(\frac{b-a}{b}\right)^{N-2}\left(\frac{r}{r-a}\right)^{N-1}, \tag{2.8}$$

$$\frac{\rho_\theta}{\rho_0} = \left(\frac{b-a}{b}\right)^{N-2}\left(\frac{r}{r-a}\right)^{N-3}, \tag{2.9}$$

$$\frac{\kappa}{\kappa_0} = \left(\frac{b-a}{b}\right)^{N}\left(\frac{r}{r-a}\right)^{N-1}. \tag{2.10}$$

Since the wave speed in a fluid is given by $c = \sqrt{\frac{\kappa}{\rho}}$, the radial and azimuthal wave speeds can be written as

$$\frac{c_r}{c_0} = \left(\frac{b-a}{b}\right), \tag{2.11}$$

$$\frac{c_\theta}{c_0} = \left(\frac{b-a}{b}\right)\left(\frac{r}{r-a}\right), \tag{2.12}$$

where c_0 is the wave speed in the surrounding fluid. One of the defining characteristics of this type of cloak is the requirement that the density is *anisotropic*. Due to this unusual inertial effect, cloaks of this type are referred to as *inertial cloaks* [21].

Examining Equations (2.8)–(2.10), one finds these cloak properties possess a similar form, consisting of a scaling term proportional to $(b-a)/a$ and a radial dependence proportional to $r/(r-a)$. Although the exact functional dependence of $\rho_r(r)$, $\rho_\theta(r)$ and $\kappa(r)$ is different for these two coordinate systems, it is noted from Equations (2.11) and (2.12) that the radial and tangential wave speeds within the cloak are independent of the number of spatial dimensions. In particular, the radial wave speed is independent of r, and simply scales in magnitude depending on the values of the inner and outer radii, a and b. Since the wavelength is proportional to the wave speed for a given frequency, this means that the wavelength scales such that there are the same number of wavelengths over a distance a in the surrounding fluid as there are in the distance $(b-a)$ in the cloak. Furthermore, Equations (2.8)

and (2.11) reveal that the radial specific acoustic impedance, $\rho_r c_r$, is equal to that of the surrounding medium at the outer edge of the cloak.

A numerical example of the resulting pressure field obtained for an inertial cloak is given in Figure 2.2(b). In this figure, the compression of the radial wavefronts prescribed by Equation (2.11) is clearly observed. At the inner edge of the cloak near $r = a$, it is apparent that the phase front is the same on all sides of the object simultaneously. For this to occur, the tangential phase speed must become infinitely large. This is clear from inspection of Equation (2.11) which requires that $c_\theta \to \infty$ as $r \to a$. In the limit of $r = a$, this would present a clear violation of causality. Another significant problem that arises in both cylindrical and spherical coordinates is that the density and the bulk modulus of the cloak must become infinite at the inner edge of the cloak.

Despite the apparent non-physical requirements of anisotropic inertia, non-causal wave speeds and infinite mass, extensive research has been performed with the aim of developing a practical inertial cloak. To address these limitations, the primary focus has been on cloaks which allow a small but finite amount of scattering, which are sometimes referred to as *near perfect* cloaks [21] (though often times this distinction is not addressed in the literature).

For a perfect cloak, recall that the coordinate transformation creates a region which does not interact with the incident wave, so that any object can be placed inside without affecting the cloaking condition. Using a near perfect cloak, however, will inevitably allow some energy to penetrate into the interior. In this case, the effectiveness has been observed to depend on the properties of the object being cloaked, particularly near resonance frequencies of the object [13, 27]. Another challenge with inertial cloaking is dealing with the radially inhomogeneous (functionally-graded) properties of the cloak, which vary as a continuous function

of r. Overcoming this difficulty is accomplished by dividing the cloak into discrete, homogeneous layers [27].

For an inertial cloak, there is the unique problem of producing a material with anisotropic inertia, a property which can be achieved by utilizing the effective properties of a periodically layered fluid system. The characterization of this behavior, and the development of explicit expressions relating the different components of the effective density to the constituent fluid layers, is credited to Schoenberg and Sen [28]. Interestingly, this work was published well before there was serious scientific discussion of cloaking, and was presented with regards to the acoustical interactions of the ocean bottom. Originally derived for periodic fluid layers in a half-space, these results have been applied directly by assuming that the curved discrete layers within the cloak are sufficiently thin. Assuming two alternating fluids denoted by the subscripts 1 and 2, the resulting homogenized properties are

$$\rho_r = \frac{1}{d_1 + d_2}\big(d_1\rho_1 + d_2\rho_2\big), \tag{2.13}$$

$$\frac{1}{\rho_\theta} = \frac{1}{d_1 + d_2}\left(\frac{d_1}{\rho_1} + \frac{d_2}{\rho_2}\right), \tag{2.14}$$

$$\frac{1}{\kappa} = \frac{1}{d_1 + d_2}\left(\frac{d_1}{\kappa_1} + \frac{d_2}{\kappa_2}\right), \tag{2.15}$$

where d_m is the thickness of the m^{th} layer.

To address the issue of creating anisotropic inertia, Equations (2.13)–(2.15) provide a useful way for obtaining discrete layer properties using fluid layers. Unfortunately, the constitutive fluids needed to match the properties given in Equations (2.8)–(2.10) must also exhibit similarly extreme properties, and most proposed layering schemes require a mixture of extremely dense and extremely light fluids relative to the surrounding medium. As a result, inertial cloaks made from alternating fluid layers are impractical to construct and, for the most common ambient fluids

encountered (namely air and water), fluids possessing these vast material property contrasts do not exist in nature. Configurations using three fluid sublayers have been proposed by Norris and Nagy [29], which results in sublayers with low densities, near-neutral densities, and high densities. These three layer cases, however, also require the use of fluids which currently do not exist in order to achieve cloaking.

2.1.1.2 Use of acoustic metamaterials

Although homogeneous fluids are impractical to use in the construction of inertial cloaks, recent research has focused on creating fluids which exhibit the properties required. In particular, attention has been focused on *acoustic metamaterials*, which are materials containing organized microstructures that create extreme effective macroscopic properties that are difficult or impossible to achieve using ordinary materials. Acoustic metamaterials can be thought of as a type of composite structure, although they have the distinct feature of exhibiting effective properties beyond the normal bounds of an ordinary homogenized mixture.

Despite their exotic nature, acoustic metamaterials have been realized using basic physical mechanisms, including the lumped-element behavior of a series of ports and cavities by Zhang *et al.* [30] and the multiple scattering effects of a lattice of cylindrical scatterers by Torrent and Sánchez-Dehesa [16]. More recent efforts by Popa *et al.* [31] have used more complex engineered structures, but these fundamentally rely on the same basic principles of lumped-element and scattering effects within each structural unit, in addition to the periodic arrangement of these units, to achieve the desired extreme macroscopic properties.

Figure 2.3(a) shows one type of acoustic metamaterial for 2D acoustic cloaking applications proposed by Torrent and Sánchez-Dehesa [15]. In this configuration, each layer is made up of two fluid sublayers (shown in red and blue in the figure),

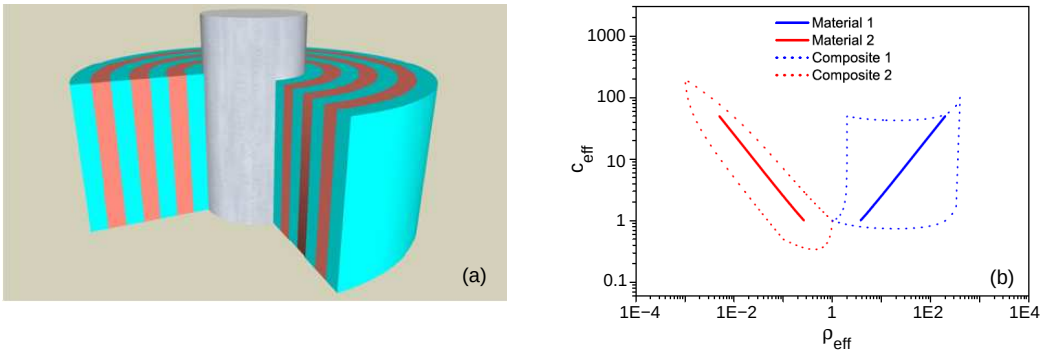

Figure 2.3: (a) Schematic view of a cloaked cylinder proposed by Torrent and Sánchez-Dehesa [15]. The cloak consists of alternating fluid sublayers of equal thickness. (b) Parametric plot showing the range of material properties needed to achieve cloaking using a configuration like that shown in part (a). The solid lines show the two fluid sublayer properties, and the dashed lines show the design space using a sonic crystal arrangement.

as described by Equations (2.13)–(2.15). To obtain the necessary fluid properties, each sublayer consists of a lattice of elastic scatterers. Utilizing the homogenized properties from this lattice (including multiple scattering effects) creates an acoustic metamaterial commonly referred to as a *sonic crystal* [16]. Through the use of sonic crystals, a more realistic design space can considered, as illustrated by the parametric plot presented in Figure 2.3(b). In this figure, the solid lines represent the necessary values for the fluid sublayers based on Equations (2.13)–(2.15), while the dotted lines represent the parameter space which can be used to achieve these values with a sonic crystal.

This noticeable increase in the range of material properties which can be used arises from the variation in the composition and volume fraction of elastic scatterers within each fluid sublayer. Although the choice of using elastic cylinders with a fluid layer is partially responsible for such a broad expansion of the parameter space shown in Figure 2.3(b), the range of achievable densities are extended beyond the

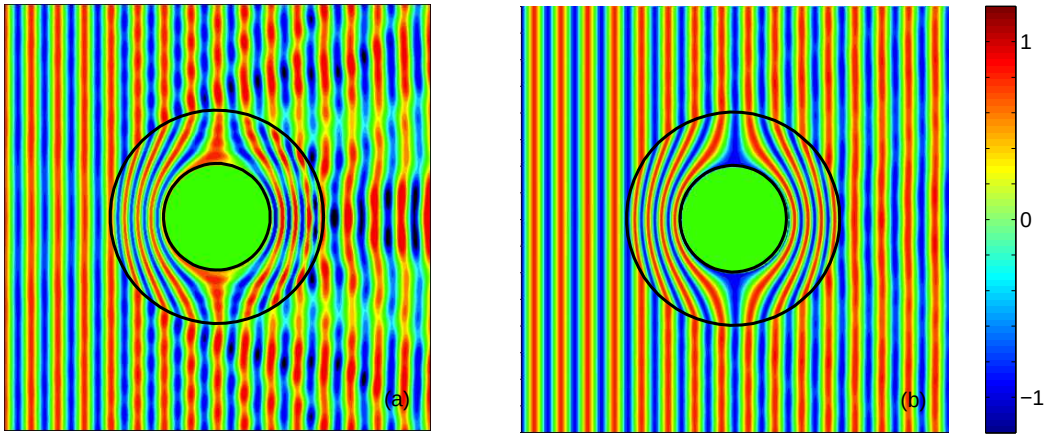

Figure 2.4: Numerical simulations of the total pressure field for a cloaked rigid cylinder, using an inertial cloak consisting of alternating fluid sublayers containing sonic crystals by Torrent and Sánchez-Dehesa [15], with (a) 50 layers, and (b) 200 layers.

traditional bounds of composite mixtures through the judicious design of the lattice arrangement of the elastic scatterers. Such an effect was verified experimentally by Torrent *et al.* [32], achieving the effective properties of argon gas using a closely packed lattice of wooden cylinders in air.

Despite the promising characteristics that sonic crystals offer, there are still significant obstacles with regards to implementation in a practical inertial cloak. Figure 2.4(a) and (b) show numerical simulations of the total acoustic pressure field using sonic crystals for 50 layers and 200 layers, respectively. Even with discretization of the cloak into 50 layers, there is still significant visible disruption of the field, even in the idealized case illustrated which does not include any losses.

Aside from the complexity of the structure, there are several other factors that significantly affect the realization of inertial cloaks. From Figure 2.3(b) it is observed that there are two distinct properties exhibited by the two sublayers, one

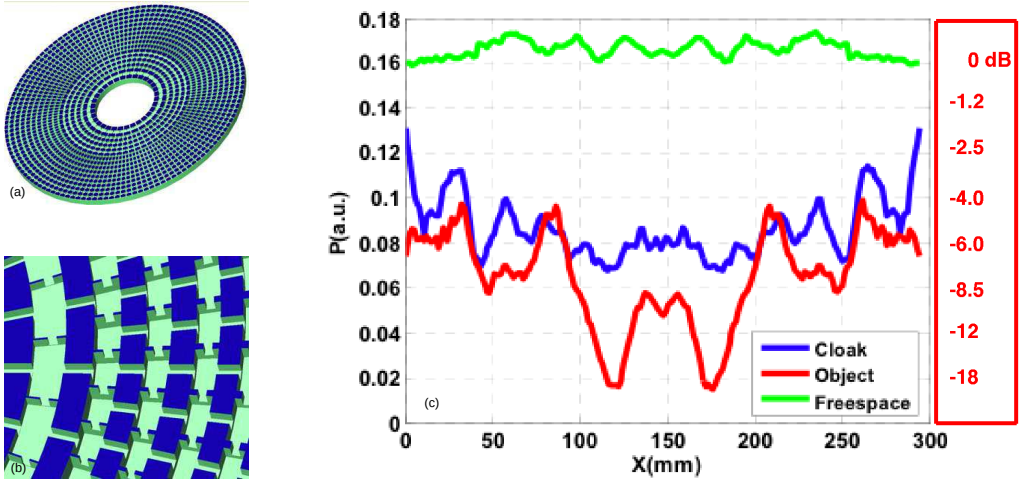

Figure 2.5: Experimental design by Zhang, Xia and Fang [30] for a cloaked steel cylinder in water, using an inertial cloak with 16 discrete layers of a radially symmetric lattice of ports and cavities, for (a) the entire cloak, and (b) a close up to show the arrangement of ports and cavities. The measured pressure field passing through the shadow zone of the rigid cylinder are shown in (c) for the cloaked (blue) and uncloaked (red) configurations, relative to a freefield measurement (green).

which is consistently lower in density than the surrounding fluid, and the other which is consistently heavier. Since the required cloak properties are normalized based on the surrounding fluid properties, the relative difficulty in realizing the necessary cloak depends on the particular properties of the surrounding fluid, and can be addressed by varying the filling fraction of each sublayer [33]. However, the most commonly encountered surrounding media in acoustic applications are air and water, which lie on opposite extremes of the range of material densities, potentially limiting the effectiveness of what cloaking layer properties can be achieved, even with an arbitrarily large number of layers.

Another type of acoustic metamaterial which has been developed utilizes transmission-line arrangements of acoustic lumped elements made up of ports and

cavities. Arrangements of acoustic lumped elements have been used for a cylindrical configuration, made up of discs that were stacked together, an example of which is shown in Figure 2.5(a) based on the work of Zhang, Xia and Fang [30]. A close up is shown in Figure 2.5(b), in which the individual ports and cavities can be clearly observed.

To design this cloak, the features illustrated in Figure 2.5(a) and (b) were machined out of aluminum discs, using the surrounding fluid (in this case water) to fill the resulting ports and cavities. To achieve anisotropic inertial effects, different sized ports were used in the radial and tangential directions while using a shared cavity. The cavity sizes were the same for each layer, but were allowed to change size with the radial distance from the inner cylinder.

Using the prescribed properties for ρ_r, ρ_θ and κ for an inertial cloak, expressions for the acoustical inductance in the radial and tangential directions, L_r and L_θ, and the acoustical compliance C become [30]

$$L_r = \rho_w \frac{l_r}{S_r}, \tag{2.16}$$

$$L_\theta = \rho_w \frac{l_\theta}{S_\theta} \left(\frac{r-a}{r} \right)^2, \tag{2.17}$$

$$C = \frac{V}{K_w} \left(\frac{a}{b-a} \right)^2, \tag{2.18}$$

where l is the port length, S is the cross-sectional area of the port, V is the volume of the cavity, and ρ_w and κ_w are the density and bulk modulus of water, respectively. Note that the sound speed for a transmission-line configuration of acoustic lumped elements is [34]

$$c = \sqrt{\frac{1}{LC}}. \tag{2.19}$$

Using Equations (2.16)–(2.18), the sound speed given by Equation (2.19) can be determined for the radial and tangential directions and equated with the prescribed

values given by Equations (2.11)–(2.12).

Figure 2.5(c) highlights typical data obtained from experimental results using this design. In this plot, the total pressure field was measure in the shadow zone directly behind the target. Note that the axis of symmetry along which the center of the target lies is located at $x = 150$ mm based on the data illustrated. To interpret the results presented in Figure 2.5(c), a scale in decibels has been added to right-hand side which gives a measure of the sound pressure level (SPL) relative to the freefield levels. Comparing the SPL, it can be seen that the change due to the addition of the cloaking layer is about 3 dB or less over most of the range, with a maximum change of about 12 dB. Even when the cloaking layer is present, there is still a difference about 6 dB in the shadow zone compared with the freefield measurements. Considering that the thickness of the cloak is three times the radius of the target and contains approximately 3000 helmholtz resonators, it is uncertain how much of these observed changes in the data with the cloak present are due to thermoviscous losses.

There are still more significant limitations of designs using this type of acoustic metamaterial. First, since water (or any ambient fluid) is used as the medium through which sound propagates, this limits how fast the information can propagate within the cloak. Although the high phase speeds needed can be achieved once the acoustic field reaches steady state, this means that the performance with transients will be significantly diminished. Furthermore, one design aspect which appears to have not been considered by Zhang *et al.* is the end correction of the ports to account for the mass of the entrained fluid [34]. Based on the design presented, thin wide ports are used to achieve the low inertia needed for the high phase speeds near the inner edge of the cloak. However, when the end corrections are properly accounted for, this significantly reduces the achievable phase speeds.

2.1.2 Pentamode materials and acoustic metafluids

To address the requirement for infinite mass necessary at the inner edge to achieve perfect cloaking with an inertial cloak, alternative solutions have been sought based on the general coordinate-transformation given by Equation (2.1). By assuming that the density tensor can vary with radial position, but is isotropic at any point in space, the transformed cloak properties are [21]

$$\frac{\rho}{\rho_0} = R' \left(\frac{R}{r}\right)^{N-1}, \tag{2.20}$$

$$\frac{\kappa_r}{\kappa_0} = \frac{1}{R'} \left(\frac{R}{r}\right)^{N-1}, \tag{2.21}$$

$$\frac{\kappa_\theta}{\kappa_0} = R' \left(\frac{R}{r}\right)^{N-3}, \tag{2.22}$$

where R and R' represent the radius in the undeformed space and its derivative, given by Equations (2.6) and (2.7), respectively. By prescribing isotropic density in this case, the anisotropy required to re-route incoming waves around the cloaked space is achieved through the bulk modulus, with radial and tangential components κ_r and κ_θ, respectively.

Under these conditions, the stress-strain relations simplify to a single expression. Note that the tensor $\mathbf{C}$ containing the elastic coefficients is 4^{th} order, though due to symmetry contains at most 21 independent coefficients for a general anisotropic elastic body [35]. As a result, the stress-strain relation is often written in a more compact form in which $\mathbf{C}$ is expressed as a 6×6 symmetric matrix where each column of a row relates a component of stress to one of six possible deformations, given by the *eigenmodes*. Therefore, of the six different possible ways of deforming an elastic body, the type of material needed for this type of cloak does not resist deformation in five of these modes. Another way of saying this is that no

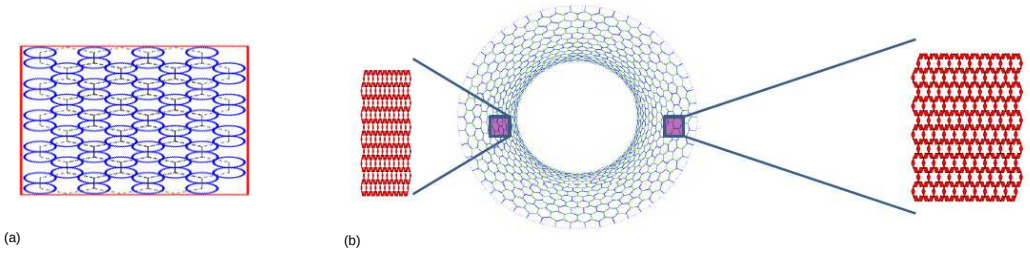

Figure 2.6: (a) Example of an acoustic metafluid by Norris [21], consisting of lubricated elliptical beads arranged in a hexagonal lattice. (b) A pentamode cloak using a proposed acoustic metafluid called *metal water* [37].

energy is required to deform the material in these modes. As a result, this type of material is known as a *pentamode material* [36].

The simplest example of a *pentamode material* is a fluid which does not resist deformation in five shear modes and only resists pure compression [21]. However, conventional fluids have isotropic compressibility and therefore cannot satisfy Equations (2.20)–(2.22). Pentamode materials which do satisfy the conditions for the transformed cloak are called *acoustic metafluids* [38].

Figure 2.6 shows two acoustic metafluids proposed by Norris. In Figure 2.6(a), the acoustic metafluid is created using a microstructure of lubricated elliptical beads in a hexagonal lattice [38]. Use of non-spherical beads ensures that the macroscopic properties will exhibit anisotropy, as prescribed by Equations (2.20)–(2.22). Another proposed acoustic metafluid is illustrated in Figure 2.6(b), for use as a cloak in water. The material for this cloak is made up of an air-filled, hinged metal lattice, so that an undeformed block will have the same density and bulk modulus as water, which has appropriately been called *metal water* [37]. A cloak can be created by physically deforming a cylinder (or sphere) of metal water to achieve a hole at the center with the desired radius. The deformation of the metal water represents the physical embodiment of the mathematical steps involved with the coordinate

transformation. This will lead to denser portions exhibiting strong anisotropy at the inner part of the cloak as prescribed by Equations (2.20)–(2.22), and observed in Figure 2.6(b).

Although the use of acoustic metafluids addresses many of the issues with inertial cloaks, challenges remain with the construction and implementation of such materials. Effects of small amounts of resistance in some of these modes, such as that which could occur in real hinges, has yet to be determined. Furthermore, due to the condition of having five modes which do not resist deformation, designing such a structure while ensuring sufficient stability is a significant issue.

2.2 Anomalous resonance cloaking

In addition to the transformation-based approach discussed in the previous section, cloaking effects can occur through other physical means. One such type is cloaking by *anomalous resonances*, which has been theorized based on the analysis of a device known as a *superlens*, which was devised to permit sub-wavelength electromagnetic imaging [39]. Superlens work by using materials with negative properties (either permittivity or permeability for electromagnetic waves), causing scattered evanescent waves to emanate from an illuminated surface and can therefore enable resolution beyond the tradition diffraction limits. This apparent evanescent wave 'amplification' is referred to as an *anomalous resonance*.

Based on the theoretical formulations for a cylindrical electromagnetic superlens, it was observed by Nicorovici *et al.* that transparency could also occur, analogous to planar mirroring effects from a material with negative properties [40]. Due to this mirroring effect, cloaking with anomalous resonances occurs in the region *external* to the cloak itself, unlike the transformation-based approach that occurs within the *interior* of the cloak [39]. Figure 2.7(a) shows a numerical simulation

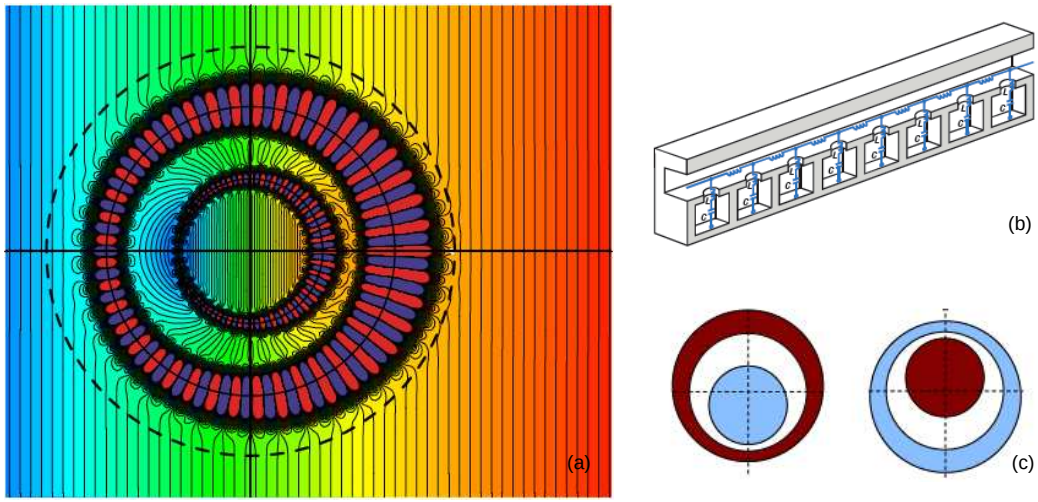

Figure 2.7: (a) Numerical simulation by Nicorovici *et al.* [39] of the electric potential field demonstrating anomalous resonance cloaking. The inner and outer edge of the cloak are denoted by solid lines, and the region of cloaking is denoted with a dashed line. (b) Layout of a 1D mass-spring system by Fang *et al.* [41] experimentally shown to exhibit negative effective mass. (c) Proposed resonant inclusion for an acoustic anomalous resonance cloak by Zhou *et al.* [42]. In this illustration, red denotes upward displacement and blue denotes downward displacement.

from Nicorovici *et al.* [39] of the electric potential field for an electromagnetic cloak using anomalous resonances. In this figure, resonances can clearly be seen near the inner and outer edge of the cloak, though the cloaking effect occurs beyond the edge of the cloak and the associated anomalous resonances.

One of the difficulties associated with this approach is that it requires negative material properties. For the acoustic analog to anomalous resonance cloaking, research has currently been focused on overcoming this particular challenge. Although negative mass or compressibility are not readily found in nature, the use of resonant elements within an acoustic material has been demonstrated to produce an effective negative mass.

One method which has been proposed by Fang *et al.* uses a transmission-

line arrangement of Helmholtz resonators operating near resonance [41]. This was experimentally demonstrated using a linear arrangement of the resonators along the length of a waveguide, shown in Figure 2.7(b), creating a 1D mass-spring system which exhibited effective negative mass for a small range of excitation frequencies. This is a similar approach taken to the one proposed for the inertial cloak using a lattice of ports and cavities shown in Figure 2.5(a) and (b). It is important to note that for the inertial cloak, the required effective mass is *positive*, whereas for the anomalous resonance it is *negative*, which can only be achieved over a very narrow frequency band near resonance. Another proposed method by Zhou *et al.* utilizes an acoustic metamaterial consisting of coated spherical inclusions [42]. The coated sphere is tuned to resonate so that the outer layer is moving out-of-phase with the sphere, as illustrated in Figure 2.7(c), thereby creating a net negative effective mass.

To achieve the necessary negative material properties for anomalous resonance cloaking of acoustic waves, acoustic metamaterials with resonant structures are required. However, the use of such resonances are highly sensitive to real world factors, such as the internal losses and perturbations from the design specifications encountered during the fabrication process [43]. Furthermore, to achieve these negative effective properties requires highly resonant systems which are inherently narrowband, therefore presenting a significant challenge in achieving a realizable broadband cloak.

2.3 EM plasmonic cloaking

An alternative approach which has been investigated extensively for electromagnetic waves is the use of a coating which cancels the scattered field from the object, thereby achieving cloaking. This corresponds to mathematically solving the classical scattering problem, often referred to as Mie scattering for electromagnetic

waves, for the coated object, and then solving to determine what coating properties will produce a null in the scattered field under a given set of conditions. As a result, this is typically referred to as a *scattering cancellation* approach.

Since it is only the scattered field at the outer edge of the cloak which is eliminated, there is no restriction on the interaction of the incident wave with the object being cloaked, as observed in Figure 2.8(a). This is conceptually different from the transformation method presented in Section 2.1, for which the incident wave is re-routed around the object to prevent any interaction with it. Previous work by Alù and Engheta [43] has shown that scattering cancellation can occur using non-resonant or resonant wave interactions within the cloaking layer, with either positive or negative cloak properties to achieve this effect. This differs from the anomalous resonance method described in Section 2.2, which used the anomalous resonances resulting from the negative cloak properties combined with the positive properties of the surrounding medium to achieve cloaking at a distance away from the edge of the cloak. With scattering cancellation, the cloaking effect occurs everywhere in the surrounding medium, even in the case where negative properties are used.

To enable the reader to examine the scattering cancellation approach in more detail, the basic theory which has been developed for electromagnetic waves is summarized in Section 2.3.1. In addition, the type of material properties which are necessary will be discussed in Section 2.3.2. Based on this analysis of the EM scattering cancellation, an overview of how this relates to the possibility of being applied for acoustics waves is presented in Section 2.3.3.

2.3.1 Basic formulation

For electromagnetic waves, the general scattering problem may be solved using the Mie expansion technique. The fields scattered by an arbitrary object

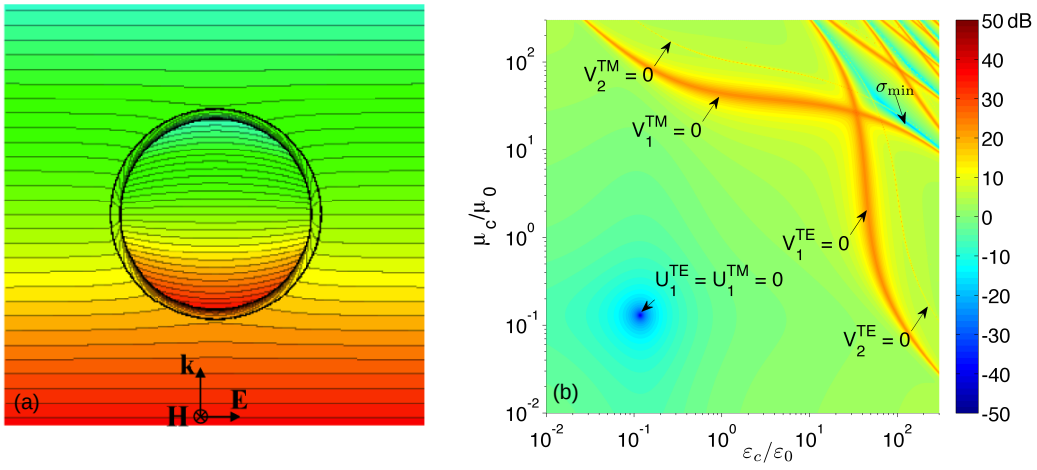

Figure 2.8: (a) Demonstration of EM scattering cancellation using a plasmonic cloak [44], originally developed by Alù and Engheta [45]. (b) Parametric plot for the cloaking layer properties of a single layer cloak utilizing EM scattering cancellation for a magnetodielectric sphere [44]. The color scale represents the scattering strength relative to the uncloaked scatterer.

subject to a time-harmonic excitation, which in this work are described using a $e^{-i\omega t}$ convention, may be represented by a sum of electric ($\mathbf{E}_\mathrm{S}$) and magnetic ($\mathbf{H}_\mathrm{S}$) outgoing waves, often referred to as *transverse electric* (TE) and *transverse magnetic* (TM), expanded in terms of spherical harmonics as [46]

$$\begin{aligned}\mathbf{E}_\mathrm{S} &= \sum_{n=1}^{\infty}\sum_{m=-n}^{n} c_{nm}^{\mathrm{TM}} b_{nm} \nabla\times\nabla\times(\boldsymbol{r}\psi_n^m) + i\omega\mu_0 \sum_{n=1}^{\infty}\sum_{m=-n}^{n} c_{nm}^{\mathrm{TE}} d_{nm} \nabla\times(\boldsymbol{r}\psi_n^m)\,,\\ \mathbf{H}_\mathrm{S} &= \sum_{n=1}^{\infty}\sum_{m=-n}^{n} c_{nm}^{\mathrm{TE}} d_{nm} \nabla\times\nabla\times(\boldsymbol{r}\psi_n^m) - i\omega\varepsilon_0 \sum_{n=1}^{\infty}\sum_{m=-n}^{n} c_{nm}^{\mathrm{TM}} b_{nm} \nabla\times(\boldsymbol{r}\psi_n^m)\,, \end{aligned} \quad (2.23)$$

where ψ_n^m is a spherical potential function, ε_0 and μ_0 are permittivity and permeability of the background, $k_0 = \omega\sqrt{\varepsilon_0\mu_0}$ is the background wavenumber, b and d represent the known amplitudes of the spherical expansion of the impinging wave, and the scattering coefficients c depend on the geometry of the scatterer and on the frequency of operation. For the case of a spherical scatterer enclosed in a spherical

shell, the expression for ψ_n^m reduces to

$$\psi_n^m = i^n \frac{2n+1}{n(n+1)} \, k_0 r h_n^{(1)}(k_0 r) P_n^m(\cos\theta), \tag{2.24}$$

where P_n^m are the associated Legendre polynomials, θ is the polar angle, and $h_n^{(1)}(\cdot)$ is the spherical Hankel function of the first kind. Note that for the axisymmetric case of an incident plane wave impinging on a spherical target, $m=1$ for the transverse electromagnetic (TE and TM) waves. For this case, the resulting TE and TM scattering coefficients can be written in the form [47]

$$c_n^{\mathrm{TE}} = -\frac{U_n^{\mathrm{TE}}}{U_n^{\mathrm{TE}} + iV_n^{\mathrm{TE}}}, \tag{2.25}$$

$$c_n^{\mathrm{TM}} = -\frac{U_n^{\mathrm{TM}}}{U_n^{\mathrm{TM}} + iV_n^{\mathrm{TM}}}, \tag{2.26}$$

where U_n and V_n are determinants for each mode n of the spherical harmonic expansion, the size and composition of which are based on the applied boundary conditions at each interface and the number of unknown scattering coefficients.

The total scattering cross-section of an object, σ_{total}, represents a measure of its overall visibility to an impinging wave at the frequency of interest, which under time-harmonic excitation and axial symmetry is given by [48]

$$\sigma_{\mathrm{total}} = \frac{2\pi}{|k_0|^2} \sum_{n=1}^{\infty} (2n+1) \left(|c_n^{\mathrm{TE}}|^2 + |c_n^{\mathrm{TM}}|^2 \right). \tag{2.27}$$

Cloaking requires the suppression of scattering for *any* position of an external observer, positioned in the near or far field of the object. It is evident, however, that if one could cancel all the relevant c coefficients with a proper cover, $\sigma_{\mathrm{total}} \to 0$ and cloaking may be achieved.

Based on the form of the scattering coefficients c given in Equations (2.25)–(2.26), the condition to eliminate the total scattering cross-section can be met by

prescribing $U_n^{\mathrm{TE}} = U_n^{\mathrm{TM}} = 0$. Notice that in the case when $V_n = 0$, the scattering coefficient is equal to unity, corresponding to a modal resonance. Figure 2.8(b) shows a parametric plot of the scattering cross-section of a cloaked magnetodielectric sphere (exhibiting contrast of both the TE and TM waves), normalized by that of the uncloaked sphere [44].

In the example illustrated in Figure 2.8(b), the cloak consists of a single homogeneous magnetodielectric coating, with positive, isotropic material properties. Even using such a simple cloak, a region of significant scattering reduction can be observed, where $U_1^{\mathrm{TE}} = U_1^{\mathrm{TM}} = 0$. Note that here only the leading order mode for the TE and TM scattered waves have been cancelled, but a scattering reduction of over 40 dB is achieved. This scattering reduction is obtained in the non-resonant region of the parameter space, away from the modal resonances where $V_n^{\mathrm{TE}} = 0$ and $V_n^{\mathrm{TM}} = 0$.

2.3.2 Use of plasmonic materials

Based on the results illustrated in Figure 2.8(b), it is of particular interest to examine what type of materials would be needed to achieve the significant scattering reduction in the non-resonant region of the parameter space. In the figure, it is observed that both the permittivity and permeability required to achieve this cloaking are much less than the background medium. For most cases of interest for electromagnetic waves, the background medium is free space, and most ordinary materials have $\varepsilon, \mu > 1$. Depending on the frequency range of interest, several options are available. The most broadly applicable choice is the use of metamaterials, which can be used to create materials with low values of ε and/or μ, using similar means as described in Section 2.1.1.2.

Alternatively, *plasmonic materials* have been shown to have electromagnetic

permittivity less than free space [45]. An electromagnetic *plasma* is any medium that possesses freely mobile charges, including not only ionized gases traditionally referred to as 'plasmas' but also solids with free moving electrons, like metals in certain frequency bands [49]. Oscillations of these free charges may be excited by the interaction with electromagnetic radiation, and the resonant modes of these free charges are called *plasmons*, with the study and utilization of this phenomenon known as *plasmonics*. The frequency dependence of a plasmonic material in the absence of losses can be expressed as [49]

$$\varepsilon_{\mathrm{p}}(\omega) = \varepsilon \left(1 - \frac{\omega_{\mathrm{p}}^2}{\omega^2}\right), \tag{2.28}$$

where ω is the angular frequency, ω_{p} is the plasma frequency and ε is permittivity of the material. From Equation (2.28), it can be seen that the permittivity of a plasmonic material at frequencies slightly below the plasma frequency can be used to achieve the necessary properties to achieve scattering cancellation, referred to as *plasmonic cloaking*.

Plasmonic cloaking has been investigated quite extensively for EM waves, including exploration of single and multiple frequencies, and for collections of multiple particles [45, 43, 47, 50, 51]. Furthermore, plasmonic cloaking has been found to be quite robust to design and frequency variations [52, 53]. Recently, a 3D EM plasmonic cloak for a finite length cylinder was designed and tested at ARL:UT and UT Austin demonstrating its effectiveness [54].

A novel feature of the plasmonic cloak, as illustrated in Figure 2.8(a), is that it allows the incident wave to penetrate the object while still canceling the scattered field in the surrounding medium. This provides for the possibility of a cloaked sensor, which can simultaneously measure the incident field without disrupting it, with applications in near-field scanning and imaging demonstrated by Alù and Engheta

[55]-[57].

Although EM plasmonic cloaking shows strong promise for providing a feasible means of cloaking, it faces several obstacles. Use of plasmonic materials, both as ordinary materials or as part of a metamaterial, ultimately is based on plasmonic resonances modes to achieve their properties. This inherently limits the bandwidth and increases the losses, potentially limiting the size of the objects to be cloaked. Furthermore, the realizable parameter space is limited by causality, since the wave speed within the cloak cannot exceed the wave speed in free space.

2.3.3 Physical analogy between EM and acoustic waves

To provide a comparison between scattering cancellation of EM waves and acoustic waves, the relationship between the relevant cloaking parameters is now considered. Cummer and Schurig showed a direct mapping between EM and acoustic waves for 2D cylindrical geometries [12]:

$$[p, v_r, v_\phi, \rho_r, \rho_\phi, \kappa^{-1}] \Leftrightarrow [-E_z, H_\phi, -H_r, \mu_\phi, \mu_r, \varepsilon_z], \tag{2.29}$$

which gives an exact duality whether the material has an isotropic or anisotropic density/permeability. However, as noted by Cummer and Schurig, this result does not hold for 3D geometries, which includes the spherically symmetric cases of interest here [12]. This result is not surprising, based on the fundamental physical differences: the 2D cylindrical EM scattering problem is inherently separable into TE and TM orthogonal polarizations (relative to the cylinder axis), which allows the reduction of the electromagnetic problem to a scalar boundary-value problem mappable into the acoustic equivalent for the specific polarization of interest. In 3D scattering problems, however, the TE- and TM-polarized spherical waves (relative to the radial coordinate in this case) inherently coexist for plane wave incidence,

making a mapping between electromagnetic and acoustic problems generally impossible.

Although a formal mapping between EM and acoustic waves may not be possible, it would be expected that some similarities common to wave phenomena in the two scattering problems do exist. Consider that the relative size of the scatterers compared to the wavelength in each domain is given by $k_0 a$, where the wavenumber is $k_0 = \omega\sqrt{\varepsilon_0 \mu_0}$ for EM waves and $k_0 = \omega\sqrt{\rho_0/\kappa_0}$ for acoustic waves. In both scenarios, larger scattering is expected for larger $k_0 a$. Qualitatively, there will be an analogy between the two EM constitutive parameters permittivity and permeability (ε and μ) and the acoustic material properties, i.e., density and compressibility (ρ and $1/\kappa$).

Considering the case of acoustic waves scattering in an ambient fluid like water, there are a wide range of homogeneous materials which exist that have densities and bulk moduli either much less than or much greater than that of water. In addition, there is no practical limit on the wave speed which could limit the design of an acoustic 'plasmonic' cloak. Although acoustic plasmonic cloaking has previously never been explored explicitly, in the quasi-static limit a plasmonic cloak essentially behaves as a *neutral inclusion* [58]. In this case, the full-wave expressions simplify considerably, and for fluids the scattering is dominated by only two modes (three modes for elastic solids). Using quasi-static expressions, simplified relations for single layer acoustic cloaks have been developed, and shown to yield realizable material properties [59].

In the next chapter, the full-wave solutions for the scattering from spherical acoustic objects is formulated, following a similar approach taken in Section 2.3.1. Unlike previous work examining acoustic cloaking in the quasi-static limit, the full dynamics of the scattered field are retained through the entirety of this work, taking

limiting cases to provide illustrative examples and highlight fundamental aspects. Although the resulting expressions are quite complex, retaining the full dynamics becomes critically important when considering wavelengths on the order of the scatterer diameter, multilayered configurations and internal resonances within the cloaking layer, all of which are addressed in the following chapters.

Chapter 3

Theoretical formulation of acoustic scattering cancellation

The dynamic behavior of a linear elastic material can be described by the equations of motion, which in the absence of body forces can be written as

$$\nabla \cdot \mathbf{T} = \rho\, \ddot{\mathbf{u}}, \tag{3.1}$$

where $\mathbf{T}$ is the stress tensor, $\mathbf{u}$ is the displacement vector, and ρ is the density. The stress and displacement of a linear elastic material are related by the small strain tensor $\boldsymbol{\varepsilon}$, which is given by

$$\boldsymbol{\varepsilon} = \frac{1}{2}\left[\nabla \mathbf{u} + (\nabla \mathbf{u})^{\mathrm{T}}\right]. \tag{3.2}$$

Using a generalized form of Hooke's law, the constitutive linear relationship between stress and strain can be expressed as

$$\mathbf{T} = \mathbf{C}\,\boldsymbol{\varepsilon}, \tag{3.3}$$

where $\mathbf{C}$ is a fourth-order stiffness tensor. Due to the symmetry of $\mathbf{T}$ and $\boldsymbol{\varepsilon}$, $\mathbf{C}$ contains a maximum of 21 independent elastic constants. In the case of an isotropic elastic material, only 2 independent elastic properties are needed, in which case Equation (3.3) reduces to [60]

$$\mathbf{T} = \lambda\, \mathrm{tr}(\boldsymbol{\varepsilon}) + 2\mu\, \boldsymbol{\varepsilon}. \tag{3.4}$$

where λ and μ are Lamé constants. Combining Equations (3.1), (3.2) and (3.4), one obtains

$$(\lambda + \mu)\,\nabla\,(\nabla \cdot \mathbf{u}) + \mu \boldsymbol{\nabla}^2 \mathbf{u} = \rho \ddot{\mathbf{u}}, \tag{3.5}$$

commonly referred to as Navier's equations of motion, which describe the elastodynamic behavior of an *isotropic* linear elastic solid.

3.1 Method of potentials

Although Navier's equations provide a full description of the elastodynamics for an isotropic solid, the solution for the resulting displacements can be simplified by looking at the displacement potential fields. Using the vector identity for the vector Laplacian operator

$$\boldsymbol{\nabla}^2 \mathbf{u} = \nabla\,(\nabla \cdot \mathbf{u}) - \nabla \times (\nabla \times \mathbf{u}), \tag{3.6}$$

one finds that Equation (3.5) reduces to [61]

$$(\lambda + 2\mu)\,\nabla\,(\nabla \cdot \mathbf{u}) - \mu \nabla \times (\nabla \times \mathbf{u}) = \rho \ddot{\mathbf{u}}. \tag{3.7}$$

From this expression, it is clear that the solution can be simplified by separating $\mathbf{u}$ into irrotational ($\nabla \times \mathbf{u} = \mathbf{0}$) and solenoidal ($\nabla \cdot \mathbf{u} = \mathbf{0}$) components. Using the Helmholtz decomposition of the displacement vector yields an expression in terms of an irrotational scalar potential ϕ, and a solenoidal vector potential $\boldsymbol{\Psi}$

$$\mathbf{u} = \nabla \phi + \nabla \times \boldsymbol{\Psi}. \tag{3.8}$$

Substitution of Equation (3.8) into Equation (3.7) yields decoupled expressions for the displacement potentials

$$\nabla^2 \phi - \frac{1}{c_{\mathrm{d}}^2} \frac{\partial^2 \phi}{\partial t^2} = 0, \tag{3.9}$$

$$\nabla^2 \boldsymbol{\Psi} - \frac{1}{c_{\mathrm{s}}^2} \frac{\partial^2 \boldsymbol{\Psi}}{\partial t^2} = \mathbf{0}, \tag{3.10}$$

where

$$c_{\mathrm{d}} = \sqrt{\frac{\lambda + 2\mu}{\rho}}, \quad c_{\mathrm{s}} = \sqrt{\frac{\mu}{\rho}}, \tag{3.11}$$

are the dilatational (i.e. longitudinal) and shear wave speeds, respectively. For the spherical geometry under consideration in this work, illustrated in Figure 3.1, the vector potential $\mathbf{\Psi}$ can be written as [62]

$$\mathbf{\Psi} = r\psi\,\hat{\mathbf{e}}_{\mathrm{r}} + \nabla\times(r\chi\,\hat{\mathbf{e}}_{\mathrm{r}})\,, \tag{3.12}$$

where ψ and χ are two scalar Debye potentials, and $\hat{\mathbf{e}}_{\mathrm{r}}$ denotes the unit vector in the radial direction. As illustrated in Figure 3.1, an incident compressional plane wave propagating along the z-direction impinges on a spherically symmetric object, so the scalar potential ψ is zero due to the azimuthal symmetry. Therefore, the stress and displacement fields can be completely described using only the two scalar potentials ϕ and χ. With the assumption of time-harmonic waves, Equations (3.9) and (3.10) can be written in the form of Helmholtz equation

$$\nabla^2\phi + \frac{\omega^2}{c_{\mathrm{d}}^2}\phi = 0, \tag{3.13}$$

$$\nabla^2\chi + \frac{\omega^2}{c_{\mathrm{s}}^2}\chi = 0. \tag{3.14}$$

Assuming spherical geometry, the reader finds the solution to these equations can be written as a summation of spherical harmonics

$$\phi_{\mathrm{inc}}(r,\theta,t) = \phi_0 e^{-i\omega t}\sum_{n=0}^{\infty} i^n(2n{+}1)\,j_n(k_{d0}r)P_n(\cos\theta), \tag{3.15}$$

$$\phi_{\mathrm{sc}}(r,\theta,t) = \phi_0 e^{-i\omega t}\sum_{n=0}^{\infty} i^n(2n{+}1)\,A_n^{(0)}h_n^{(1)}(k_{d0}r)P_n(\cos\theta), \tag{3.16}$$

$$\begin{aligned}\phi_{\mathrm{m}}(r,\theta,t) = \phi_0 e^{-i\omega t}&\sum_{n=0}^{\infty} i^n(2n{+}1)\\ &\times\left[A_n^{(m)}j_n(k_{d,m}r) + B_n^{(m)}n_n(k_{d,m}r)\right]P_n(\cos\theta),\end{aligned} \tag{3.17}$$

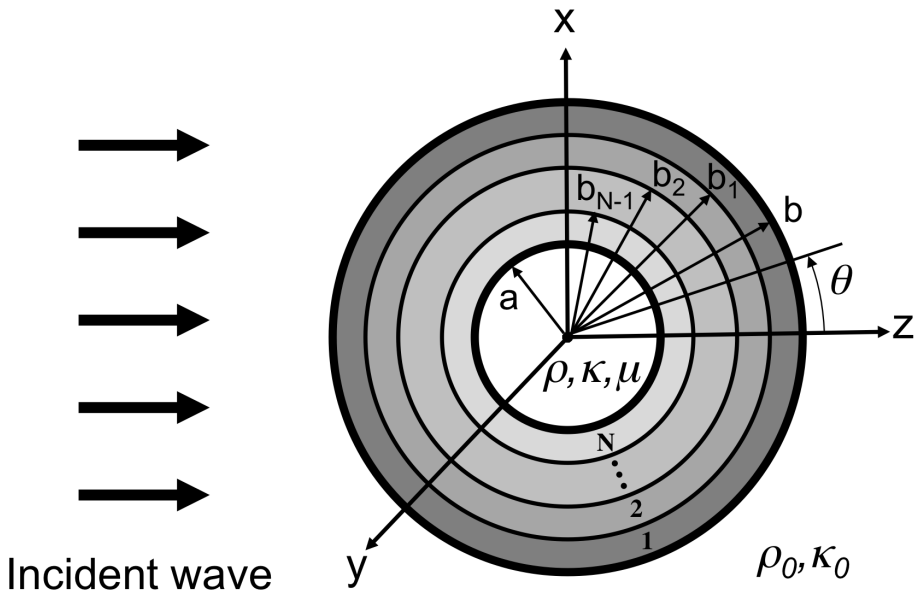

Figure 3.1: A time-harmonic incident plane wave in a fluid medium impinging on an isotropic elastic core of radius a coated with multiple shells with outer radius b. The surrounding medium has density ρ_0 and bulk modulus κ_0, and the elastic core has density ρ, bulk modulus κ and shear modulus μ.

$$\chi_{\mathrm{m}}(r,\theta,t) = \phi_0 e^{-i\omega t} \sum_{n=0}^{\infty} i^n (2n+1) \times \left[C_n^{(m)} j_n(k_{s,m} r) + D_n^{(m)} n_n(k_{s,m} r) \right] P_n(\cos\theta), \tag{3.18}$$

where ϕ_{inc} is the incident plane wave displacement potential of amplitude ϕ_0, ϕ_{sc} is the scattered displacement potential in the surrounding fluid, ϕ_{m} and χ_{m} are the displacement potentials accounting for the compressional and shear waves in the m^{th} material, j_n and $h_n^{(1)}$ are the spherical Bessel and Hankel functions of the first kind, respectively, n_n is the spherical Bessel function of the second kind, P_n is the

Legrendre polynomial, and θ is the polar angle. Further, the dilatational and shear wave numbers in the m^{th} layer material are known to be

$$k_{\text{d},m} = \frac{\omega}{c_{\text{d}}^{(m)}}, \quad k_{\text{s},m} = \frac{\omega}{c_{\text{s}}^{(m)}}, \tag{3.19}$$

and $A_n^{(m)}$, $B_n^{(m)}$, $C_n^{(m)}$, and $D_n^{(m)}$ are the scattering coefficients for the m^{th} layer material.

Although the modes n fundamentally arise as a result of expressing the potentials in terms of infinite series, these modes hold an important physical significance. The modes for the scattered field in the surrounding medium, which throughout this work will be referred to as *scattering modes*, determine not only the complex magnitude of the scattered field (corresponding to $A_n^{(0)}$), but also the directivity based on θ-dependence arising from the Legendre polynomial $P_n(\cos\theta)$. As a result, the scattering modes correspond to basic physical scattering patterns, such as a *monopole* ($n=0$), *dipole* ($n=1$) and *quadrupole* ($n=2$).

3.2 Solution for scattering coefficients and scatter cancellation

The boundary conditions at the radial interfaces for elastic solids consist of the continuity of the normal and tangential components of the stress $\mathbf{T}$ and displacement $\mathbf{u}$. At the interface between an inviscid fluid and an elastic solid, the boundary conditions are zero shear stress in the solid and the continuity of the normal components of stress and displacement, and for the interface of two inviscid fluids only continuity of the radial stress (pressure) and displacement are required. Although the analysis above was derived for isotropic elastic solids, to obtain the behavior for an inviscid fluid it suffices to set the shear modulus, μ, to zero. Evaluating the above expressions in this case implies that the potential χ is equal to a constant, and therefore gives a solution which is described using only the

potential ϕ, in agreement with linear acoustic theory derived using fluid dynamic principles [34].

Applying the boundary conditions to Equations (3.15)–(3.18) yields a linear system of equations for the unknown scattering coefficients at the n^{th} mode of the form

$$\boldsymbol{\mathcal{D}}^{(n)} \cdot \vec{\mathcal{A}}^{(n)} = \vec{\mathsf{r}}^{(n)}, \tag{3.20}$$

where $\boldsymbol{\mathcal{D}}^{(n)}$ is the system matrix with coefficients containing the material properties and shell geometry, $\vec{\mathsf{r}}^{(n)}$ is the input vector describing the incident wave, and $\vec{\mathcal{A}}^{(n)}$ is a vector containing the unknown scattering coefficients. For an isotropic spherical core coated by N isotropic layers (either elastic or fluid), Equation (3.20) can be written as

$$\begin{bmatrix} \mathbf{D}_{1,0}^{(n)} & \mathbf{D}_{1,1}^{(n)} & \mathbf{0} & \mathbf{0} & \dots & \mathbf{0} \\ \mathbf{0} & \mathbf{D}_{2,1}^{(n)} & \mathbf{D}_{2,2}^{(n)} & \mathbf{0} & \dots & \mathbf{0} \\ \vdots & \ddots & \ddots & \ddots & \ddots & \vdots \\ \mathbf{0} & \dots & \mathbf{0} & \mathbf{D}_{N,N-1}^{(n)} & \mathbf{D}_{N,N}^{(n)} & \mathbf{0} \\ \mathbf{0} & \dots & \mathbf{0} & \mathbf{0} & \mathbf{D}_{N+1,N}^{(n)} & \mathbf{D}_{N+1,\text{core}}^{(n)} \end{bmatrix} \begin{bmatrix} \vec{A}_0^{(n)} \\ \vec{A}_1^{(n)} \\ \vec{A}_2^{(n)} \\ \vdots \\ \vec{A}_{N-1}^{(n)} \\ \vec{A}_N^{(n)} \\ \vec{A}_{\text{core}}^{(n)} \end{bmatrix} = \begin{bmatrix} \vec{r}_0^{(n)} \\ \vec{0} \\ \vec{0} \\ \vdots \\ \vec{0} \\ \vec{0} \\ \vec{0} \end{bmatrix}, \tag{3.21}$$

where $\mathbf{D}_{q,m}^{(n)}$ is a coefficient matrix for the m^{th} material at the q^{th} interface, $\vec{A}_m^{(n)}$ is a vector of the unknown scattering coefficients in the m^{th} material, and $\vec{r}_0^{(n)}$ is a vector of coefficients due to the incident wave. The number of rows in $\mathbf{D}$ depends on the boundary condition at the interface, while the number of columns in is determined by the number of unknown scattering coefficients in that particular layer. Explicit expressions for $\mathbf{D}$ are given in Appendix A.

To determine the scattered field, Cramer's rule can be used to solve Equation (3.21) for the scattering coefficient in the surrounding fluid

$$A_0^{(n)} = \frac{\det \boldsymbol{\mathcal{R}}^{(n)}}{\det \boldsymbol{\mathcal{D}}^{(n)}}, \tag{3.22}$$

where $\boldsymbol{\mathcal{D}}^{(n)}$ is the system matrix and $\boldsymbol{\mathcal{R}}^{(n)}$ is $\boldsymbol{\mathcal{D}}^{(n)}$ with the first column replaced by $\vec{\mathsf{r}}^{(n)}$. Therefore, given that

$$\boldsymbol{\mathcal{D}}^{(n)} = \begin{bmatrix} d_{1,1}^{(n)} & d_{1,2}^{(n)} & \dots & d_{1,Q}^{(n)} \\ d_{2,1}^{(n)} & d_{2,2}^{(n)} & \dots & d_{2,Q}^{(n)} \\ \vdots & \vdots & \ddots & \vdots \\ d_{Q,1}^{(n)} & d_{Q,2}^{(n)} & \dots & d_{Q,Q}^{(n)} \end{bmatrix}, \quad \vec{\mathsf{r}}^{(n)} = \begin{bmatrix} r_{1,1}^{(n)} \\ r_{2,1}^{(n)} \\ \vdots \\ r_{Q,1}^{(n)} \end{bmatrix}, \tag{3.23}$$

for a $Q \times Q$ system, then

$$\boldsymbol{\mathcal{R}}^{(n)} = \begin{bmatrix} r_{1,1}^{(n)} & d_{1,2}^{(n)} & \dots & d_{1,Q}^{(n)} \\ r_{2,1}^{(n)} & d_{2,2}^{(n)} & \dots & d_{2,Q}^{(n)} \\ \vdots & \vdots & \ddots & \vdots \\ r_{Q,1}^{(n)} & d_{Q,2}^{(n)} & \dots & d_{Q,Q}^{(n)} \end{bmatrix}. \tag{3.24}$$

This implementation is a well-established approach which has been used to calculate acoustic scattering from an elastically coated elastic sphere, which can be found in scientific literature on the subject dating back to the 1950's [1], [63]-[66], including detailed work accounting for viscous and thermal effects [67]. In all these previous works, the scattering coefficients and the resulting scattered field have been determined for specific shell and core properties. For such cases, the coefficients of $\boldsymbol{\mathcal{R}}^{(n)}$ and $\boldsymbol{\mathcal{D}}^{(n)}$ are specified and the unknown scattering coefficient in the surrounding fluid can be solved explicitly using Equation (3.22).

For the case of acoustic cloaking, a solution is sought where the incident compressional wave passes unimpeded around the target. Mathematically, this means

that the total acoustic field is equal to the incident wave throughout the surrounding fluid, which requires that the scattered field throughout the surrounding fluid is zero. Written in terms of the scattering coefficient, this corresponds to the condition where $A_0^{(n)} = 0$ for each mode n of the expansion, and thus is referred to as *scattering cancellation* to distinguish it from the transformation-based acoustic cloaking discussed in Chapter 2.

By setting Equation (3.22) equal to zero, the expression for the cloaking condition can be simplified. Making use of the definition of the spherical Hankel function of the first kind,

$$h_n^{(1)}(k_{d0}r) = j_n(k_{d0}r) + i\, n_n(k_{d0}r), \tag{3.25}$$

Equation (3.22) can be expressed as

$$A_0^{(n)} = -\frac{U_n}{U_n + i\, V_n}, \tag{3.26}$$

where

$$U_n = \begin{vmatrix} \mathfrak{Re}\Big[d_{1,1}^{(n)}\Big] & d_{1,2}^{(n)} & \dots & d_{1,Q}^{(n)} \\ \mathfrak{Re}\Big[d_{2,1}^{(n)}\Big] & d_{2,2}^{(n)} & \dots & d_{2,Q}^{(n)} \\ \vdots & \vdots & \ddots & \vdots \\ \mathfrak{Re}\Big[d_{Q,1}^{(n)}\Big] & d_{Q,2}^{(n)} & \dots & d_{Q,Q}^{(n)} \end{vmatrix} = - \begin{vmatrix} r_{1,1}^{(n)} & d_{1,2}^{(n)} & \dots & d_{1,Q}^{(n)} \\ r_{2,1}^{(n)} & d_{2,2}^{(n)} & \dots & d_{2,Q}^{(n)} \\ \vdots & \vdots & \ddots & \vdots \\ r_{Q,1}^{(n)} & d_{Q,2}^{(n)} & \dots & d_{Q,Q}^{(n)} \end{vmatrix}, \tag{3.27}$$

and

$$V_n = \begin{vmatrix} \mathfrak{Im}\Big[d_{1,1}^{(n)}\Big] & d_{1,2}^{(n)} & \dots & d_{1,Q}^{(n)} \\ \mathfrak{Im}\Big[d_{2,1}^{(n)}\Big] & d_{2,2}^{(n)} & \dots & d_{2,Q}^{(n)} \\ \vdots & \vdots & \ddots & \vdots \\ \mathfrak{Im}\Big[d_{Q,1}^{(n)}\Big] & d_{Q,2}^{(n)} & \dots & d_{Q,Q}^{(n)} \end{vmatrix}. \tag{3.28}$$

This expression indicates that scattering cancellation of a given mode is achieved by finding cloak properties that lead to $U_n = 0$, provided that $V_n \neq 0$. When $V_n = 0$, $A_0^{(n)}$ has a magnitude of unity for any non-zero value of U_n and corresponds to a modal resonance, while the simultaneous conditions of $U_n = 0$ and $V_n = 0$ leads to an indeterminate form for $A_0^{(n)}$.

From this analysis, the design of an acoustic cloak using a scattering cancellation approach is in essence finding the cloak properties which achieve $U_n = 0$ for the dominant scattering modes. The properties of the cloak will depend on the frequency and the material properties and geometry of the object being cloaked. Furthermore, the number of modes which can be cancelled will be limited by the complexity of the cloak design, particularly the number of discrete layers used to construct it. This is an important factor to consider, since the number of modes which significantly affect the scattered field increase with frequency.

3.3 Relation to scattering cross-section

With an expression for $A_0^{(n)}$ in terms of the material properties of the isotropic cloaking layers, it is necessary to relate the displacement potential, which was expanded in terms of spherical harmonics with scattering coefficients for each mode, in terms of the scattered field in the surrounding fluid. From Equation (3.16), it follows that the scattered pressure can be written as

$$p_{\mathrm{sc}}(r,\theta,t) = p_0 e^{-i\omega t} \sum_{n=0}^{\infty} i^n (2n{+}1)\, A_n^{(0)} h_n^{(1)}(k_{d0} r) P_n(\cos\theta), \tag{3.29}$$

where $p_0 = \rho_0\, \omega^2 \phi_0$ due to conservation of momentum.

To describe the flow of energy through a unit area, the acoustic intensity for the scattered wave is defined as [34]

$$I_{\mathrm{sc}}\,(r,\theta) = \left\langle\, p_{\mathrm{sc}}\,(r,\theta)\, \dot{\mathbf{u}}_{\mathrm{sc}}\,(r,\theta) \cdot \hat{\mathbf{e}}_{\mathrm{r}} \right\rangle, \tag{3.30}$$

where $\dot{\mathbf{u}}_{\mathrm{sc}}$ is the time derivative of the particle displacement in the surrounding fluid, $\hat{\mathbf{e}}_{\mathrm{r}}$ is the unit vector pointing the radial direction, and $\langle\cdot\rangle$ represents the time average of the quantity in brackets. For time-harmonic waves, Equation (3.30) reduces to

$$I_{\mathrm{sc}} = \frac{1}{2}\frac{|p_{\mathrm{sc}}|^2}{|Z_{\mathrm{sc}}|}\cos\varphi, \tag{3.31}$$

where the specific acoustic impedance of the scattered field Z_{sc} is

$$Z_{\mathrm{sc}} = \frac{p_{\mathrm{sc}}}{\dot{\mathbf{u}}_{\mathrm{sc}}\cdot\hat{\mathbf{e}}_{\mathrm{r}}} = |Z_{\mathrm{sc}}|\, e^{-i\varphi}, \tag{3.32}$$

with φ denoting the phase difference between the scattered pressure and velocity in the radial direction.

The standard metric for determining the scattering strength of an object is the *scattering cross-section*, which represents a measure of the acoustic power scattered relative to the incident wave. This can be written per unit angle using the *bistatic cross-section* [68]

$$\sigma_{\mathrm{bi}}(r,\theta) = 4\pi r^2 \frac{I_{\mathrm{sc}}(r,\theta)}{I_{\mathrm{inc}}(r,\theta)}, \tag{3.33}$$

where I_{inc} is the intensity of the incident time-harmonic plane wave given by

$$I_{\mathrm{inc}} = \frac{1}{2}\frac{|p_{\mathrm{inc}}|^2}{\rho_0 c_0}. \tag{3.34}$$

A monostatic metric corresponding to the case where $\theta = -\pi$, the scattering cross-section is referred to as the *backscattering cross-section*,

$$\sigma_{\mathrm{back}}(r) = \sigma_{\mathrm{bi}}(r,-\pi) = 4\pi r^2 \frac{I_{\mathrm{sc}}(r,-\pi)}{I_{\mathrm{inc}}(r,-\pi)}. \tag{3.35}$$

To quantify the acoustic power scattered over all angles, the *total scattering cross-section* is used, which is determined by

$$\sigma_{\mathrm{total}}(r) = \int_S \frac{I_{\mathrm{sc}}}{I_{\mathrm{inc}}} dS, \tag{3.36}$$

where S represents a surface that fully encloses the object.

For the case when the distance r to the observation point is much larger than the radius a of the scatterer, the scattered acoustic intensity at any given angle is approximately equal to that of a progressive plane wave, such that

$$I_{\text{sc}} \approx \frac{1}{2} \frac{|p_{\text{sc}}|^2}{\rho_0 c_0}. \tag{3.37}$$

To simplify the expression for p_{sc}, the spherical Hankel function of the first kind in Equation (3.29) can be approximated for large arguments as [69]

$$h_n^{(1)}(z) \approx \frac{1}{z} e^{-i\left[z - \frac{1}{2}(n+1)\pi\right]}. \tag{3.38}$$

Thus, far from the scatterer, Equation (3.35) reduces to

$$\sigma_{\text{back}} = \frac{4\pi}{|k_{d0}|^2} \left| \sum_{n=0}^{\infty} (-1)^n (2n+1) A_n^{(0)} \right|^2. \tag{3.39}$$

A similar form can be obtained for σ_{total} by evaluating the integral in Equation (3.36) over the spherical surface enclosing the scatterer at a distance r, with $r \gg a$. Using the orthogonality of the Legendre polynomials [34]

$$\int_{-1}^{1} P_m(z) P_n(z)\, dz = \begin{cases} \frac{2}{2n+1}, & \text{if } m = n; \\ 0, & \text{otherwise,} \end{cases} \tag{3.40}$$

integration over the surface yields

$$\sigma_{\text{total}} = \frac{4\pi}{|k_{d0}|^2} \sum_{n=0}^{\infty} (2n+1) \left| A_n^{(0)} \right|^2. \tag{3.41}$$

To eliminate the backscatter from an object, prescribing σ_{back} to be zero in Equation (3.39) yields the condition

$$\sum_{n=0}^{\infty} (-1)^n (2n+1) A_n^{(0)} = 0. \tag{3.42}$$

From this expression, it is clear that $A_n^{(0)}$ in general can be nonzero as long as the summation of all the terms converges to zero. This can be achieved by a variety of solutions, including approaches which seek to absorb the incident sound or minimize the backscattered reflection. Although effective suppression of the backscatter may be obtained without absorption, these methods are not optimal for stealth applications since they achieve suppression by redirecting scattered energy. This inherently leads to an increase in the magnitude of the scattered field in other directions, particularly in the forward direction resulting in large shadow zones.

In the case of the total scattering cross-section, examination of Equation (3.41) reveals the presence of the squared magnitude of the scattering coefficients. With all other terms being nonzero, elimination of the total scattering cross-section can only be achieved when all $A_n^{(0)}$ are zero. As a result, the condition $A_n^{(0)} = 0$ represents the criteria for cloaking achieved using scattering cancellation.

Although the cloaking criterion $A_n^{(0)} = 0$ was determined using an expression obtained by integrating over all angles, it is important to note that this condition satisfies the cancellation of the scattering cross-section at *all angles individually* and not just the ensemble average of the scattered field over some range of angles. This is due to the fact that the formulation of the total scattering cross-section contains the integration of acoustic intensity, which is an expression for the flow of acoustic energy consisting of a quadratic term of the acoustic variables, such as the product of the acoustic pressure and particle velocity or the square of the acoustic pressure, as given by Equations (3.30) and (3.31), respectively. By comparison, integrating the scattered acoustic pressure over all angles and setting it equal to zero would simply give the condition where the *average* scattered pressure equals zero, but the scattered pressure at individual angles could be non-zero.

It is important to consider that although Equation (3.41) was obtained us-

ing a farfield assumption by using approximate forms for radially varying terms, the resulting cloaking condition of $A_n^{(0)} = 0$ is equally valid using the exact expressions. Thus, for this criteria, the total scattering cross-section becomes zero and the scattered acoustic energy is eliminated in the entire surrounding medium.

3.4 Numerical implementation

Based on the analysis presented in Section 3.2, it was shown that the criteria for determining the cloaking layer properties could be obtained by setting the scattering coefficient in the surrounding medium for each mode equal to zero. Examining the elements of $A_n^{(0)}$, even for the relatively simple configurations listed in Appendix A, show that many of the cloaking layer parameters are either products with, or arguments of, different spherical Bessel functions. Explicitly solving for the cloaking layers is made even more challenging by the fact that the determinant of $A_n^{(0)}$ can quickly become large for even a few layers, as can be seen from Equations (3.26), the elements of which are defined by Equation (3.21), or from the examples given in Appendix A.

3.4.1 Minimization of scattered field

Although analytic solutions for these equations can be determined for certain limiting cases, such as either low ka or thin shells, these are practical only for simple configurations (only approximate analytic expressions for configurations of up to two fluid layers are considered using solutions derived using the method of potentials in this work). Thus, a more general solution technique is sought for an arbitrary number of layers and thicknesses. This can be achieved by numerically evaluating the expression for $A_n^{(0)}$ to determine its roots within a given range of the cloaking layer properties, based on realistic material bounds or design considerations. However, for

a finite number of discrete layers, only a finite number of modes will be cancelled, meaning that some of the higher order modes will be non-zero. As a result, the scattered field will be significantly reduced, but not completely cancelled. To obtain the optimal solution, therefore, one can search for the combination of cloaking layer parameters that minimize the total scattering cross-section.

By defining the problem in terms of minimizing the total scattering cross-section, this ensures that the scattering coefficients are minimized, and not simply a minimal *average* scattered strength. As described in Section 3.3, use of the total scattering cross-section, as opposed to simply the backscattering cross-section, ensures that $A_n^{(0)} \to 0$ as $\sigma_{\text{total}} \to 0$, since σ_{total} is proportional to the sum of the *magnitude squared* of $A_n^{(0)}$, as seen in the farfield expression given by Equation (3.41). From this equation, it can be observed that the total scattering cross-section is simply a weighted root-mean-square of $A_n^{(0)}$, where each mode is weighted by $\frac{4\pi}{|k_{d0}|^2}(2n+1)$.

A minimization scheme was achieved using an algorithm to search the multi-dimensional cloaking layer parameter space to find those which yield the minimum total scattering cross-section at the frequency of interest. A schematic for this process is illustrated in Figure 3.2. To determine the minimum total scattering cross-section, the user provides the design frequency and an initial guess of the material properties and shell thicknesses of the cloak. A quasi-Newton minimization algorithm employing sequential quadratic programming (SQP) is then used to vary the cloaking layer properties within the allowable range, until a minimum value of the total scattering cross-section is achieved. To perform this operation, the code was implemented in MATLAB using the *fminsearch* function [70].

For the numerical simulations presented in Chapters 4-6, the farfield expression for the total scattering cross-section given by Equation (3.41) is used. The analysis presented in the remainder of this work is limited to optimization at sin-

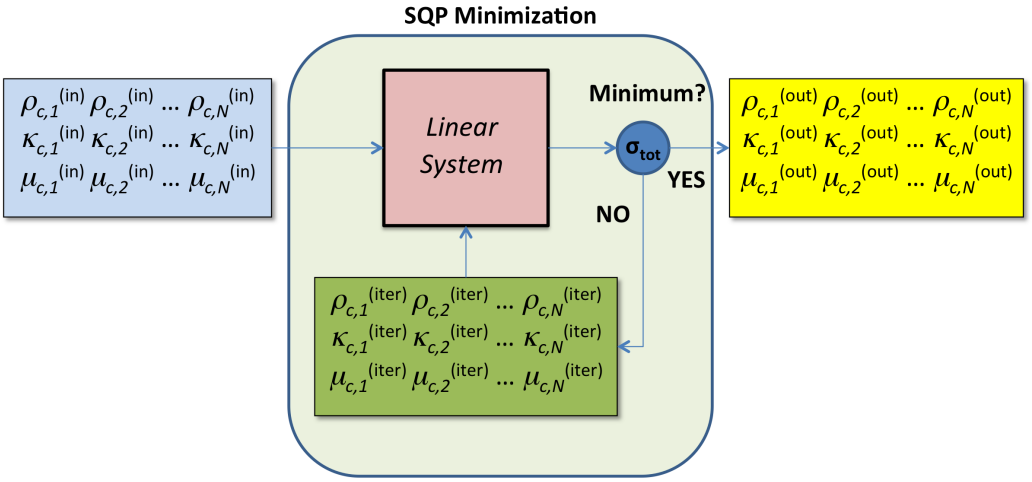

Figure 3.2: Schematic of the minimization algorithm used to find the properties and geometry of the cloak using the scattering cancellation approach.

gle design frequency, and the investigation of the subsequent bandwidth which is achieved, illustrating the physical nature of cloaks designed using a scattering cancellation approach. However, the method put forth here is quite robust, and could also be expanded to determining the cloaking layer properties which minimize the total scattering cross-section over a given frequency band. This could be achieved, for example, by changing the design criteria such that the total scattering cross-section over a finite range of frequencies is reduced below a minimum threshold.

Although the implementation of the numerical minimization scheme highlighted in Figure 3.2 is relatively straightforward, it is important to note that the output of such an algorithm is only as good as the input it is given. An important question, therefore, is whether or not the minimized solution represents a local minimum or a global minimum. To ensure that it is the global minima which are found,

it is crucial to understand the nature of the design space, and what type of cloaking layers are necessary to achieve scattering cancellation.

3.4.2 Parameter space

Before proceeding with a detailed look at solution techniques for determining the cloaking layer properties which achieve a sufficient level of scattering cancellation, it is worthwhile to examine the design space to understand the nature of the solutions being sought. Consider the variation in the scattering gain as a function of the the cloaking material parameters, $\frac{\rho_c}{\rho_0}$ and $\frac{\kappa_c}{\kappa_0}$, which have been normalized by the properties of the surrounding fluid, as illustrated in Figure 3.3 for a design frequency of $ka = 0.5$ with $b = 1.10a$.

In this figure, the scattering gain is represented with a color scale, ranging from shades of blue, representing a significant reduction in the scattering gain due to the presence of the cloak, to yellows and reds representing an increase in the scattering gain. From this figure, it can be seen for small values of $\frac{\kappa_c}{\kappa_0}$ there is a region in which the scattering gain is large, which corresponds to the resonances of the cloaking layer for which $V_n = 0$. Away from this resonance region, there is a localized region of significant reduction resulting from non-resonant scattering cancellation where the first two scattering modes are zero, corresponding to $U_0 = U_1 = 0$. This occurs at the point in the design space where $\rho_c = 0.175\rho_0$ and $\kappa_c = 0.244\kappa_0$, which results in a scattering reduction of 40 dB relative to an uncloaked rigid sphere.

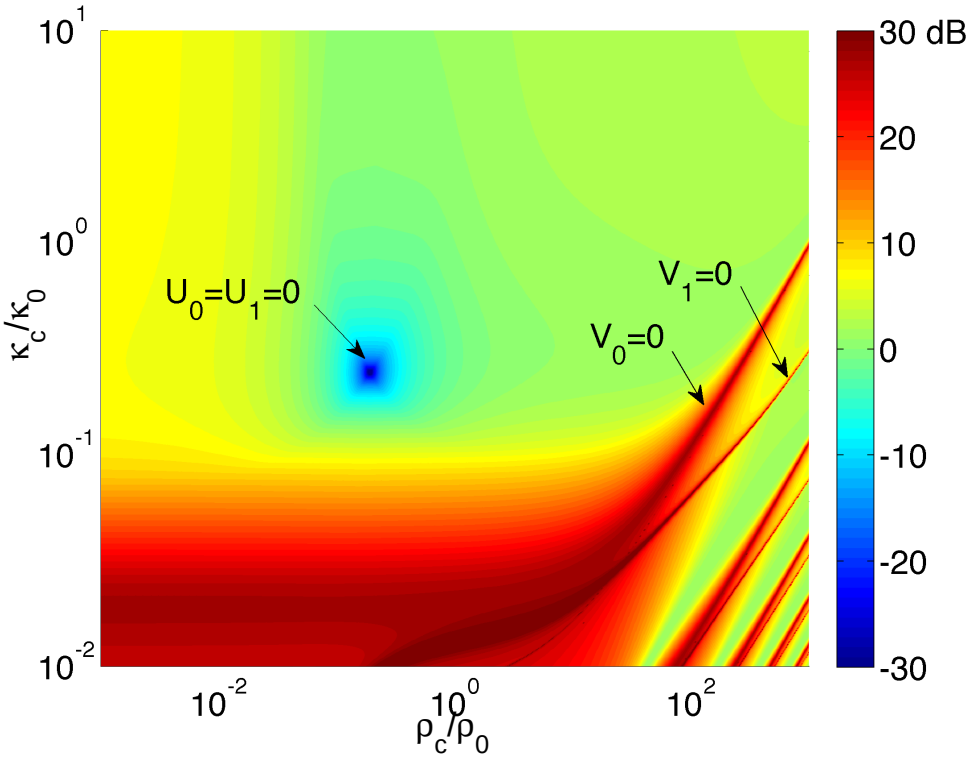

Figure 3.3: Parametric plot of the optimized cloaking layer density (top panel), cloaking layer bulk modulus (middle panel) and scattering gain (bottom panel) as a function of the density and bulk modulus of a penetrable fluid scatterer relative to the external fluid. The results are given for a cloaking layer with a thickness ratio of $b/a = 1.10$ at $ka = 0.5$.

Chapter 4

Investigation of acoustic plasmonic cloaking using a single layer

In Chapter 3, the existence of a non-resonant type of acoustic scattering cancellation called *plasmonic cloaking* was formulated. The simplest possible design of an acoustic *plasmonic* cloak is that of a single isotropic fluid layer with uniform thickness, as illustrated in Figure 4.1. In this configuration, there are only three cloaking layer design parameters: the bulk modulus, κ_c, the density, ρ_c, and the shell thickness ratio b/a. Investigating this configuration for a given spherical scatterer and design frequency allows for the fundamental behavior of an acoustic plasmonic cloak to be examined in detail, while limiting the analysis to the minimum number of parameters.

The analysis of a single layer acoustic plasmonic cloak is presented in five sections. In Section 4.1, the generalized analytic results developed in Chapter 3 are applied to the specific case of a single fluid cloaking layer. To gain further insight, explicit expressions for the cloaking layer parameters are obtained by considering two different approximations: (i) low frequency, and (ii) a thin shell. Using these analytic expressions as a guide, parametric investigations of increasing complexity are presented in the remaining four sections. In Section 4.2, the cloaking of an impenetrable rigid sphere is considered. The application of an acoustic plasmonic cloak to a penetrable spherical scatterer is discussed next in Section 4.3 for fluid targets and Section 4.4 for isotropic elastic targets. Finally, a comparison is presented between the use of a single layer fluid and an isotropic elastic shell to achieve

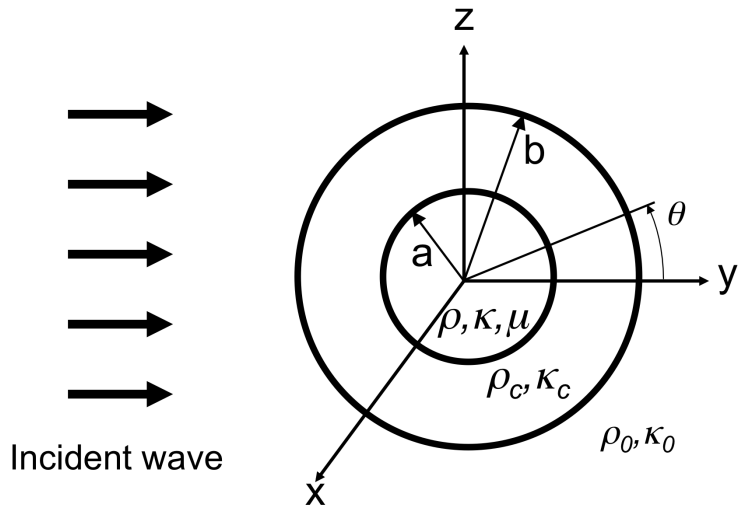

Figure 4.1: A time-harmonic incident plane wave in a fluid medium impinging on an isotropic elastic core of radius a coated with a single fluid shell with outer radius b. The surrounding medium has density ρ_0 and bulk modulus κ_0, the fluid shell has density ρ_c and bulk modulus κ_c, and the elastic core has density ρ, bulk modulus κ and shear modulus μ.

acoustic plasmonic cloaking.

4.1 Analytic expressions for a single fluid cloaking layer

The general form for the solution of the cloaking layer properties necessary to achieve the cloaking condition $A_n^{(0)}=0$ for an arbitrary number of isotropic fluid or elastic layers was derived in Section 3.2, resulting in the expression given by Equation (3.26). In this expression, the modal scattering coefficient A_n is equal to zero when the determinants $U_n = 0$ and $V_n \neq 0$. In this section, approximate analytic solutions for the specific case of a single fluid cloaking layer coating an isotropic sphere (either fluid or elastic) will be developed, based on determining

where $U_n = 0$, and confirming that $V_n \neq 0$. Although these solutions will represent approximate solutions limited to either low ka or thin shell conditions, they will enable explicit expressions for the density and bulk modulus of the cloaking layer to be obtained, which can provide insight into the behavior of an acoustic plasmonic cloak.

For the case of an isotropic elastic core and a fluid cloaking layer, Equations (3.26) and (3.27) become

$$\begin{vmatrix} u_{11}^{(n)} & u_{12}^{(n)} & u_{13}^{(n)} & 0 & 0 \\ u_{21}^{(n)} & u_{22}^{(n)} & u_{23}^{(n)} & 0 & 0 \\ 0 & u_{32}^{(n)} & u_{33}^{(n)} & u_{34}^{(n)} & u_{35}^{(n)} \\ 0 & u_{42}^{(n)} & u_{43}^{(n)} & u_{44}^{(n)} & u_{45}^{(n)} \\ 0 & 0 & 0 & u_{54}^{(n)} & u_{55}^{(n)} \end{vmatrix} = 0, \tag{4.1}$$

where the non-zero terms are developed in Appendix A and are given by

$$u_{11}^{(n)} = k_{d,0} b \, j_n'(k_{d,0} b), \tag{4.2}$$

$$u_{12}^{(n)} = k_{d,c} b \, j_n'(k_{d,c} b), \tag{4.3}$$

$$u_{13}^{(n)} = k_{d,c} b \, n_n'(k_{d,c} b), \tag{4.4}$$

$$u_{21}^{(n)} = j_n(k_{d,0} b), \tag{4.5}$$

$$u_{22}^{(n)} = \overline{\rho}_c \, j_n(k_{d,c} b), \tag{4.6}$$

$$u_{23}^{(n)} = \overline{\rho}_c \, n_n(k_{d,c} b), \tag{4.7}$$

$$u_{32}^{(n)} = k_{d,c} a \, j_n'(k_{d,c} a), \tag{4.8}$$

$$u_{33}^{(n)} = k_{d,c} a \, n_n'(k_{d,c} a), \tag{4.9}$$

$$u_{34}^{(n)} = -k_{\mathrm{d}} a \, j_n'(k_{\mathrm{d}} a), \tag{4.10}$$

$$u_{35}^{(n)} = -n(n+1) \, j_n(k_{\mathrm{s}} a), \tag{4.11}$$

$$u_{42}^{(n)} = \overline{\rho}_c \, j_n(k_{d,c} a), \tag{4.12}$$

$$u_{43}^{(n)} = \overline{\rho}_c \, n_n(k_{d,c}a), \tag{4.13}$$

$$u_{44}^{(n)} = 2\overline{\rho}\left\{\left[\frac{n(n+1)}{(k_s a)^2} - \frac{1}{2}\right] j_n(k_d a) - 2\frac{k_d a}{(k_s a)^2} j_n'(k_d a)\right\}, \tag{4.14}$$

$$u_{45}^{(n)} = 2\overline{\rho}\frac{n(n+1)}{(k_s a)^2}\left[k_s a j_n'(k_s a) - j_n(k_s a)\right], \tag{4.15}$$

$$u_{54}^{(n)} = k_d a \, j_n'(k_d a) - j_n(k_d a), \tag{4.16}$$

$$u_{55}^{(n)} = \left[n(n+1) - 1 - \frac{1}{2}(k_s a)^2\right] j_n(k_s a) - k_s a \, j_n'(k_s a), \tag{4.17}$$

with $\overline{\rho}_c = \rho_c/\rho_0$ and $\overline{\rho} = \rho/\rho_0$. Similarly, for this to represent cancellation of the scattered field, the condition $V_n \neq 0$ must also be met. For a single fluid cloaking layer with an elastic core, Equation (3.28) reduces to

$$\begin{vmatrix} v_{11}^{(n)} & u_{12}^{(n)} & u_{13}^{(n)} & 0 & 0 \\ v_{21}^{(n)} & u_{22}^{(n)} & u_{23}^{(n)} & 0 & 0 \\ 0 & u_{32}^{(n)} & u_{33}^{(n)} & u_{34}^{(n)} & u_{35}^{(n)} \\ 0 & u_{42}^{(n)} & u_{43}^{(n)} & u_{44}^{(n)} & u_{45}^{(n)} \\ 0 & 0 & 0 & u_{54}^{(n)} & u_{55}^{(n)} \end{vmatrix} = 0, \tag{4.18}$$

where the only differing terms from those in U_n are $v_{11}^{(n)}$ and $v_{21}^{(n)}$, which are given by

$$v_{11}^{(n)} = -k_{d,0} b \, n_n'(k_{d,0} b), \tag{4.19}$$

$$v_{21}^{(n)} = -n_n(k_{d,0} b). \tag{4.20}$$

Based on Equations (4.1)–(4.20), a fluid core can be treated as a specific case of an isotropic elastic core by considering the limit as the shear modulus of the core material, μ, approaches zero. Under these conditions, Equation (4.1) (and likewise Equation (4.18)) can be modified by eliminating the 5^{th} column, corresponding to shear wave scattering coefficient in the core material, and the 5^{th} row, corresponding to the continuity of shear displacement at $r = a$ boundary condition.

For the case of an isotropic elastic core, the determinant of Equation (4.1) can be written as

$$u_{11}^{(n)}\left|\begin{array}{cc:cc} u_{22}^{(n)} & u_{23}^{(n)} & 0 & 0 \\ u_{32}^{(n)} & u_{33}^{(n)} & u_{34}^{(n)} & u_{35}^{(n)} \\ \hdashline u_{42}^{(n)} & u_{43}^{(n)} & u_{44}^{(n)} & u_{45}^{(n)} \\ 0 & 0 & u_{54}^{(n)} & u_{55}^{(n)} \end{array}\right| - u_{21}^{(n)}\left|\begin{array}{cc:cc} u_{12}^{(n)} & u_{13}^{(n)} & 0 & 0 \\ u_{32}^{(n)} & u_{33}^{(n)} & u_{34}^{(n)} & u_{35}^{(n)} \\ \hdashline u_{42}^{(n)} & u_{43}^{(n)} & u_{44}^{(n)} & u_{45}^{(n)} \\ 0 & 0 & u_{54}^{(n)} & u_{55}^{(n)} \end{array}\right| = 0. \tag{4.21}$$

To evaluate the determinants in Equation (4.21), each determinant can be divided into 4 block matrices, which are denoted by the dashed lines. The determinant of a 2×2 matrix consisting of block matrix elements is given by [71]

$$\left|\begin{array}{cc} \mathbf{A} & \mathbf{B} \\ \mathbf{C} & \mathbf{D} \end{array}\right| = \big|\mathbf{D}\big|\big|\mathbf{A}-\mathbf{B}\mathbf{D}^{-1}\mathbf{C}\big|, \tag{4.22}$$

where $\mathbf{A}$, $\mathbf{B}$, $\mathbf{C}$ and $\mathbf{D}$ are matrices with dimensions $p\times p$, $p\times q$, $q\times p$ and $q\times q$, respectively, with $\mathbf{D}$ assumed to be non-singular. Application of Equation (4.22) to the two determinants in Equation (4.21) yields

$$u_{11}^{(n)}\left|\begin{array}{cc} u_{22}^{(n)} & u_{23}^{(n)} \\ u_{32}^{(n)}-\Upsilon_n u_{42}^{(n)} & u_{33}^{(n)}-\Upsilon_n u_{43}^{(n)} \end{array}\right| - u_{21}^{(n)}\left|\begin{array}{cc} u_{12}^{(n)} & u_{13}^{(n)} \\ u_{32}^{(n)}-\Upsilon_n u_{42}^{(n)} & u_{33}^{(n)}-\Upsilon_n u_{43}^{(n)} \end{array}\right| = 0, \tag{4.23}$$

which reduces to

$$\Big(u_{11}^{(n)}u_{22}^{(n)}-u_{21}^{(n)}u_{12}^{(n)}\Big)\Big(u_{33}^{(n)}-\Upsilon_n u_{43}^{(n)}\Big)-\Big(u_{11}^{(n)}u_{23}^{(n)}-u_{21}^{(n)}u_{13}^{(n)}\Big)\Big(u_{32}^{(n)}-\Upsilon_n u_{42}^{(n)}\Big)=0, \tag{4.24}$$

where the function Υ_n depends only on the core material properties, and can be expressed as

$$\Upsilon_n = \begin{cases} \frac{u_{34}^{(n)}u_{55}^{(n)}-u_{35}^{(n)}u_{54}^{(n)}}{u_{44}^{(n)}u_{55}^{(n)}-u_{45}^{(n)}u_{54}^{(n)}}, & \text{for an elastic core,} \\ \frac{u_{34}^{(n)}}{u_{44}^{(n)}}, & \text{for a fluid core.} \end{cases} \tag{4.25}$$

Substitution of Equations (4.2)–(4.17) into Equation (4.24) produces an expression in terms of the cloaking layer properties for the cancellation of the n^{th} mode,

$$\begin{aligned}
&\overline{\rho}_c\, k_{d,c}a\, k_{d,0}a\, j_n'(k_{d,0}b)\left[j_n(k_{d,c}b)\, n_n'(k_{d,c}a) - j_n'(k_{d,c}a)\, n_n(k_{d,c}b)\right] \\
&\quad - (k_{d,c}a)^2\, j_n(k_{d,0}b)\left[j_n'(k_{d,c}b)\, n_n'(k_{d,c}a) - j_n'(k_{d,c}a)\, n_n'(k_{d,c}b)\right] \\
&\quad - \overline{\rho}_c^2\, k_{d,0}a\, \Upsilon_n\, j_n'(k_{d,0}b)\left[j_n(k_{d,c}b)\, n_n(k_{d,c}a) - j_n(k_{d,c}a)\, n_n(k_{d,c}b)\right] \\
&\quad + \overline{\rho}_c\, k_{d,c}a\, \Upsilon_n\, j_n(k_{d,0}b)\left[j_n'(k_{d,c}b)\, n_n(k_{d,c}a) - j_n(k_{d,c}a)\, n_n'(k_{d,c}b)\right] \quad = 0. \qquad (4.26)
\end{aligned}$$

This expression describes the properties necessary for cancellation of the n^{th} mode with a single fluid cloaking layer, in terms of the design frequency $k_{d,0}a$ with a thickness of $b-a$ and the uncloaked core properties given by Υ_n. Although this expression is exact, it is observed from the equation that the cloaking layer properties are imbedded in the arguments of the spherical Bessel function and their derivatives, since

$$k_{d,c}a = k_{d,0}a\sqrt{\frac{\overline{\rho}_{\text{c}}}{\overline{\kappa}_{\text{c}}}}, \qquad (4.27)$$

where $\overline{\rho}_c = \rho_c/\rho_0$ and $\overline{\kappa}_c = \kappa_c/\kappa_0$.

To obtain an analytic expression for the cloaking properties through the use of Equation (4.26), investigation of the terms containing the spherical Bessel functions must be addressed. Since the argument of the Bessel functions include the parameters of interest and due to the harmonic nature of Bessel functions, trying to determine all the possible solutions which satisfy this expression leads to many possible solutions for a given configuration. Only the lowest order solutions, however, correspond to the non-resonant plasmonic cloaking. The other solutions correspond to the conditions for achieving anti-resonance cloaks, which are explored in more detail in Chapter 5.

For the case of acoustic plasmonic cloaking, two different approximations can be made to simplify Equation (4.26) and yield only the non-resonant cloaking solution: assuming either *low frequency*, or a *thin shell*. For both approximations, the assumption of a small argument of the Bessel functions allows for the use of only the leading order terms of a series expansion, enabling the spherical Bessel functions to be reduced to algebraic functions. These solutions are developed in the next two subsections, and provide a guide for analysis of a single fluid layer acoustic plasmonic cloak.

4.1.1 Low frequency approximation

In the case when the wavelength of sound traveling in the surrounding fluid, Λ, is much larger than the outer radius b of the scatterer, then

$$k_{d,0}b = 2\pi\frac{b}{\Lambda} \ll 1. \tag{4.28}$$

Applying this approximation will yield a *quasi-static* solution. By comparison, a solution can be developed using only static forces and displacements, in which case the resulting solution is referred to as the *static* solution.

In addition to the long wavelength assumption given by Equation (4.28) for the solution of Equation (4.26) being sought, it will also be assumed that the wavelength in the cloaking layer is much larger than the outer radius of the scatterer, which from Equation (4.27) yields

$$k_{d,c}b = k_{d,0}b\sqrt{\frac{\overline{\rho}_{\mathrm{c}}}{\overline{\kappa}_{\mathrm{c}}}} \ll 1. \tag{4.29}$$

It is important to note that this assumption is not valid for all possible combinations of $\overline{\rho}_{\mathrm{c}}$ and $\overline{\kappa}_{\mathrm{c}}$, in particular, for the situation where $\sqrt{\frac{\overline{\rho}_{\mathrm{c}}}{\overline{\kappa}_{\mathrm{c}}}} \gg 1$. Although this range of cloaking layer material properties is valid in general, it leads to a very low sound

speed with a correspondingly short wavelength, giving rise to modal resonances within the cloaking layer. Although the use of anti-resonances can be used to achieve scattering cancellation, as described in Chapter 5, the analysis here is focused on isolating the solutions which yield a *non-resonant* scattering cancellation, namely, acoustic plasmonic cloaking.

Given the conditions prescribed by Equations (4.28) and (4.29), the spherical Bessel functions of the first and second kind can be written using the leading order term of the Maclaurin series, such that[69]

$$j_n(z) \approx \frac{\sqrt{\pi}}{2^{n+1}} \frac{z^n}{\Gamma(n+\frac{3}{2})} \equiv C_n^{(1)} z^n, \qquad z \ll 1, \tag{4.30}$$

$$n_n(z) \approx -\frac{2^n}{\sqrt{\pi}} \frac{\Gamma(n+\frac{1}{2})}{z^{(n+1)}} \equiv -\frac{C_n^{(2)}}{z^{n+1}}, \qquad z \ll 1, \tag{4.31}$$

where Γ is the Gamma function. Using the recursion relations for spherical Bessel functions, the first derivatives can be written as

$$j_n'(z) = \frac{n}{z} j_n(z) - j_{n+1}(z) \quad \approx n C_n^{(1)} z^n - C_{n+1}^{(1)} z^{n+1}, \qquad z \ll 1, \tag{4.32}$$

$$n_n'(z) = \frac{n}{z} n_n(z) - n_{n+1}(z) \quad \approx \left(-n C_n^{(2)} + C_{n+1}^{(2)}\right) z^{-(n+2)}, \qquad z \ll 1. \tag{4.33}$$

The relationship between the coefficients $C_n^{(1)}$ and $C_n^{(2)}$ can be simplified through use of the recurrence formula of the Gamma function [69]

$$\Gamma(z) = (z-1)\Gamma(z-1), \tag{4.34}$$

which gives

$$C_n^{(1)} C_n^{(2)} = \frac{1}{2n+1}, \tag{4.35}$$

$$C_{n+1}^{(1)} = \frac{1}{2n+3} C_n^{(1)}, \tag{4.36}$$

$$C_{n+1}^{(2)} = (2n+1) C_n^{(2)}. \tag{4.37}$$

Substituting Equations (4.29)–(4.37) into Equation (4.26), one finds that the expression for cancellation of the n^{th} mode becomes

$$\begin{aligned}&\left\{\left[\Upsilon_n\left(\frac{b}{a}\right)^{2n+1}-\frac{(k_{d,0}a)^2}{2n+3}\right]\left[n(2n+3)-(k_{d,0}b)^2\right]-\Upsilon_n\left[n(2n+3)-2(k_{d,0}b)^2\right]\right\}\overline{\rho}_c^2\\&-n(+1)(k_{d,0}a)^2\left[1-\left(\frac{b}{a}\right)^{2n+3}\right]\overline{\rho}_c+\left\{\left[n(2n+3)-(k_{d,0}b)^2\right]\left[n+(n+1)\left(\frac{b}{a}\right)^{2n+1}\right]\right.\\&\left.-(2n+3)\Upsilon_n\left[(n+1)+\left(\frac{b}{a}\right)^{2n+1}\right]\right\}\overline{\rho}_c\overline{\kappa}_c+n(n+1)(2n+3)\left[1-\left(\frac{b}{a}\right)^{2n+1}\right]\overline{\kappa}_c=0,\end{aligned}\tag{4.38}$$

where the function Υ_n given by Equation (4.25) reduces to

$$\Upsilon_n=\begin{cases}-\frac{1}{2\overline{\rho}}\frac{\left[n-\frac{(k_{\mathrm{d}}a)^2}{2n+3}\right]\overline{f}_n-n(n+1)\overline{g}_n}{\left[\frac{n(n-1)}{(k_{\mathrm{s}}a)^2}-\frac{1}{2}+\frac{2}{2n+3}\frac{(k_{\mathrm{d}}a)^2}{(k_{\mathrm{s}}a)^2}\right]\overline{f}_n-\frac{n(n+1)}{(k_{\mathrm{s}}a)^2}\left[n-1-\frac{(k_{\mathrm{s}}a)^2}{2n+3}\right]\overline{g}_n}, & \text{for an elastic core,}\\ \frac{1}{\overline{\rho}}\left[n-\frac{1}{2n+3}(k_{\mathrm{d}}a)^2\right], & \text{for a fluid core,}\end{cases}\tag{4.39}$$

with $\overline{f}_n$ and $\overline{g}_n$ defined by

$$\overline{f}_n=n^2-1-\frac{1}{2}\frac{2n+1}{2n+3}(k_{\mathrm{s}}a)^2,\tag{4.40}$$

$$\overline{g}_n=n-1-\frac{(k_{\mathrm{d}}a)^2}{2n+3}.\tag{4.41}$$

At first glance, Equations (4.38)–(4.41) hardly seem to have simplified the analytic expressions. Upon a closer examination of Equation (4.38), however, it is apparent that the properties of the cloaking layer have been isolated, and appear explicitly as the normalized density $\overline{\rho}_c$ and bulk modulus $\overline{\kappa}_c$. Specifically, Equation (4.38) represents an expression for the necessary cloaking layer properties of the form

$$A\,\overline{\rho}_c^2+B\,\overline{\rho}_c+C\,\overline{\rho}_c\overline{\kappa}_c+D\,\overline{\kappa}_c=0,\tag{4.42}$$

where A, B, C and D depend only on the design frequency, given by the wave number in the surrounding fluid $k_{d,0}$, the geometric dimensions, given by the inner radius a and outer radius b, and the core material properties contained in the function Υ_n.

It is important to consider that the expressions given by Equations (4.38)–(4.41) are generalized to represent the n^{th} mode, and not all the terms in these expressions appear in each mode. In particular, even though the approximation of $k_{d,0}b \ll 1$ is made, some of these higher order terms are retained, since for the $n = 0$ mode $(k_{d,0}b)^2$ is the leading order term, while all other modes ($n \geq 1$) are of order unity. Evaluating Equations (4.38)–(4.41) at $n=0$, retaining only the terms of order $(k_{d,0}b)^2$ eliminates $\overline{\rho_c}$ and leads to an explicit solution for the bulk modulus,

$$\overline{\kappa}_c = \overline{\kappa}\frac{1-\phi}{\overline{\kappa}-\phi}, \tag{4.43}$$

where $\phi = \left(\frac{a}{b}\right)^3$ is the volume fraction of the inner sphere to that of the total sphere with the cloaking layer present, and

$$\Upsilon_0 = -\frac{1}{3\,\overline{\kappa}}(k_{d,0}a)^2. \tag{4.44}$$

Note that Equation (4.44) is obtained for *both* expressions given in Equation (4.39) (for a fluid core *and* an elastic core), demonstrating that the bulk modulus of the core material dominates the monopole ($n = 0$) modal response and that the shear effects are negligible in the low frequency limit.

Similarly, evaluating Equations (4.38)–(4.41) at $n = 1$ leads to the simple relation

$$\Upsilon_1 = \frac{1}{\overline{\rho}} - \frac{1}{5}\frac{(k_{d,0}a)^2}{\overline{\kappa}}, \tag{4.45}$$

which is valid when the core is a fluid or an isotropic elastic solid. In the low frequency limit, the $(k_{d,0}a)^2$ term can be neglected, leaving only the dependence on the density of the core material, which dominates the dipole modal response. Combining this result with Equation (4.38) and retaining only the terms of order unity eliminates $\overline{\kappa_c}$, this yields a quadratic expression for the cloaking layer density,

$$(1-\phi)\overline{\rho}_c^2 - \beta_{\text{QS}}(\phi)\overline{\rho}_c - 2(1-\phi)\overline{\rho} = 0, \tag{4.46}$$

where the function $\beta_{\text{QS}}(\phi)$ is defined as

$$\beta_{\text{QS}}(\phi) = (1 + 2\phi) - (2 + \phi)\overline{\rho}. \tag{4.47}$$

Using the quadratic formula, solving for the positive root of Equation (4.46) gives

$$\overline{\rho}_c = \frac{\beta_{\text{QS}}(\phi) + \sqrt{\left(\beta_{\text{QS}}(\phi)\right)^2 + 8\overline{\rho}(1-\phi)^2}}{2(1-\phi)}. \tag{4.48}$$

Since the volume fraction ranges from $0 < \phi < 1$ and the core material density is positive, Equation (4.48) will give a cloaking layer density which is both positive and real.

The results developed in Equations (4.43) and (4.48) for the quasi-static solution of a single fluid cloaking layer are in agreement with those found in the literature [59, 72, 73]. For the case of the bulk modulus, these results match those developed by static analysis, and corresponds to a *neutral inclusion* under volumetric changes [72]. For the density, though, the static analysis does not yield the same solution as obtained in the quasi-static analysis [73]. Using the static analysis, the density of the coating material is obtained from conservation of mass, but it fails to account for the reactive motion of the surrounding fluid. The existence of this fluid motion adds an effective inertia known as the *accession to inertia*, so that the resulting effective density is higher than that of the static average density of the interior sphere and cloaking layer [34].

These results are in agreement with other comparable acoustic cloaking work, such as that of Zhou *et al.* [59]. In the work of Zhou *et al.*, the cloaking of an isotropic elastic sphere was developed in the quasi-static limit using a similar approach as described in this section. The stresses and displacements were expanding using spherical harmonics, and the analysis was performed using similar expressions to Equations (4.30) and (4.31) to obtain the quasi-static behavior. However, unlike

the analysis developed here, in which a linear system for the scattering coefficients in the form of Equation (3.21) is obtained by applying the boundary conditions at each interface, Zhou *et al.* used a Hashin-Shtrikman effective medium model to determine the effective properties of a composite sphere, consisting of the core and the cloaking layer [74]. This allowed the problem to be formulated simply as scattering from a single isotropic elastic sphere, with the cloaking layer properties being determined based on the expressions for those of the effective sphere. To obtain the condition for cloaking, these effective properties are set equal to those of the surrounding medium, which in the quasi-static limit also leads to cancellation of the leading order scattering coefficients.

In the work presented by Zhou *et al.*, the resulting expressions for cloaking were left in terms of the effective moduli as a function of the core material and cloaking layer properties. It is interesting to note that although the results given by Zhou *et al.* can be solved to obtain the explicit expressions for the cloaking layer properties given by Equations (4.43) and (4.48), they were instead left in an implicit form in terms of the effective density and effective elastic moduli. Although such a form can make more intuitive sense to emphasize how such a cloak behaves as a neutral inclusion, it is arguably more important to have an explicit solution for the necessary cloaking layer properties in terms of understanding and designing such a cloak.

4.1.2 Thin shell approximation

Although the quasi-static solutions yield simple explicit expressions for the cloaking layer density and bulk modulus, they are inherently limited to situations in which the wavelength is much larger than the object and therefore cannot be applied to higher frequencies. Alternatively, a useful approximation can be made by

assuming that the cloaking layer is *thin* relative to the wavelength in the cloaking layer, such that

$$k_{d,c} a\, \delta \ll 1, \tag{4.49}$$

where $\delta = \frac{b-a}{a}$ is the thickness of the cloaking layer, and a and b are the inner and outer radius of the shell, respectively. Although limited to thin shells, such an assumption is in fact not as restrictive from a design perspective as the condition prescribed by Equation (4.49) may seem. This is due to the fact that, for most situations of practical interest, one would prefer a cloaking layer that does not significantly increase the size of the scatterer. In addition, a thinner layer reduces the risk of inducing higher order scattering harmonics.

The spherical Bessel functions containing the argument $k_{d,c}b$ can be rewritten by assuming a thin shell and using a Taylor series expanded about the value $k_{d,c}a$, which to leading order gives

$$j_n(k_{d,c}b) = j_n(k_{d,c}a(1+\delta)) \;\approx\; j_n(k_{d,c}a) \;+\; k_{d,c}a\, \delta j_n'(k_{d,c}a), \tag{4.50}$$

$$n_n(k_{d,c}b) = n_n(k_{d,c}a(1+\delta)) \approx n_n(k_{d,c}a) + k_{d,c}a\, \delta n_n'(k_{d,c}a). \tag{4.51}$$

Similarly, the first derivative of the spherical Bessel functions can be expressed as

$$j_n'(k_{d,c}b) = j_n'(k_{d,c}a(1+\delta)) \;\approx\; j_n'(k_{d,c}a) \;+\; k_{d,c}a\, \delta j_n''(k_{d,c}a), \tag{4.52}$$

$$n_n'(k_{d,c}b) = n_n'(k_{d,c}a(1+\delta)) \approx n_n'(k_{d,c}a) + k_{d,c}a\, \delta n_n''(k_{d,c}a). \tag{4.53}$$

From Equations (4.50)–(4.53), it is important to note that, although the shell thickness is assumed to be small, there is no such restriction on $k_{d,c}a$, provided the condition of Equation (4.49) is met. With the spherical Bessel functions in terms of $k_{d,c}a$, this allows the dynamics of the scattering to be retained. Substituting

Equations (4.50)–(4.53) into Equation (4.26) and neglecting terms of order δ^2 yields

$$\begin{aligned}\left[\Upsilon_n \delta k_{d,0} a j_n'(k_{d,0}a)\overline{\rho}_c^2 + \left(\mathcal{F}_n' - \Upsilon_n \mathcal{F}_n\right)\overline{\rho}_c\right]\left[j_n(k_{d,c}a)\, n_n'(k_{d,c}a) - j_n'(k_{d,c}a)\, n_n(k_{d,c}a)\right] \\ -\Upsilon_n \delta j_n(k_{d,0}a)\overline{\rho}_c\, k_{d,c}a\left[j_n(k_{d,c}a)\, n_n''(k_{d,c}a) - j_n''(k_{d,c}a)\, n_n(k_{d,c}a)\right] \\ +\delta j_n(k_{d,0}a)\,(k_{d,c}a)^2\left[j_n'(k_{d,c}a)\, n_n''(k_{d,c}a) - j_n''(k_{d,c}a)\, n_n'(k_{d,c}a)\right] = 0,\end{aligned} \tag{4.54}$$

where the coefficients $\mathcal{F}_n$ and $\mathcal{F}_n'$ are

$$\mathcal{F}_n = j_n(k_{d,0}a) + k_{d,0}a\,\delta\, j_n'(k_{d,0}a), \tag{4.55}$$

$$\mathcal{F}_n' = k_{d,0}a\left[j_n'(k_{d,0}a) + k_{d,0}a\,\delta\, j_n''(k_{d,0}a)\right], \tag{4.56}$$

In Equations (4.54)–(4.55), the spherical Bessel functions and their derivatives are grouped such that those with $k_{d,c}a$ in the argument are contained within the square brackets. To write a solution for the cloaking layer density and bulk modulus explicitly, a form is sought such that these terms in brackets can be written in terms of algebraic functions of $k_{d,c}a$. To do this, the products of the spherical Bessel functions of the first and second kind can be reformulated as

$$j_n(z)n_n'(z) - j_n'(z)n_n(z) = \frac{1}{z^2}, \tag{4.57}$$

$$j_n(z)n_n''(z) - j_n''(z)n_n(z) = -\frac{2}{z^3}, \tag{4.58}$$

$$j_n'(z)n_n''(z) - j_n''(z)n_n'(z) = \frac{1}{z^2} - \frac{n(n+1)}{z^4}. \tag{4.59}$$

The derivation of these expressions is given in detail in Appendix B. For the case of a single fluid cloaking layer, consideration will be limited to $n=0$ and $n=1$ only, in which case Equation (4.59) reduces to

$$j_n'(z)n_n''(z) - j_n''(z)n_n'(z) = \begin{cases} \frac{1}{z^2}, & n=0, \\ \frac{1}{z^2} - \frac{2}{z^4}, & n=1. \end{cases} \tag{4.60}$$

Examining Equations (4.57)–(4.60), it is clear that the expressions on the left-hand side, which contain the products of spherical Bessel functions, can be described using only the simple algebraic quantities given on the right-hand side. Although similar in form to those developed in Equations (4.30)–(4.33) for the low frequency approximation, it is important to note that the relationships given by Equations (4.57)–(4.60) are *exact*.

The substitution of Equations (4.57)–(4.60) into Equation (4.54) yields

$$\Upsilon_n \delta k_{d,0} a j_n'(k_{d,0}a)\overline{\rho}_c^2 + \left[\mathcal{F}_n' - \Upsilon_n \mathcal{F}_n + 2\delta \Upsilon_n j_n(k_{d,0}a)\right]\overline{\rho}_c + \delta j_n(k_{d,0}a)\left[(k_{d,0}a)^2 \frac{\overline{\rho}_c}{\overline{\kappa}_c} - n(n+1)\right] = 0. \quad (4.61)$$

Evaluating Equation (4.61) for $n=0$ and $n=1$, one obtains two equations in terms of the two variables of interest, $\overline{\rho}_c$ and $\overline{\kappa}_c$, which reduces to

$$\Upsilon_0 \delta k_{d,0} a j_0'(k_{d,0}a)\overline{\rho}_c + \left[\mathcal{F}_0' - \Upsilon_0 \mathcal{F}_0 + 2\delta \Upsilon_0 j_0(k_{d,0}a)\right] + \delta j_0(k_{d,0}a)(k_{d,0}a)^2 \frac{1}{\overline{\kappa}_c} = 0, \quad (4.62)$$

$$\Upsilon_1 \delta k_{d,0} a j_1'(k_{d,0}a)\overline{\rho}_c^2 + \left[\mathcal{F}_1' - \Upsilon_1 \mathcal{F}_1 + 2\delta \Upsilon_1 j_1(k_{d,0}a)\right]\overline{\rho}_c + \delta j_1(k_{d,0}a)\left[(k_{d,0}a)^2 \frac{\overline{\rho}_c}{\overline{\kappa}_c} - 2\right] = 0, \quad (4.63)$$

where Υ_n, $\mathcal{F}_n$ and $\mathcal{F}_n'$ are given by Equations (4.25), (4.55) and (4.56), respectively. Solving Equation (4.62) for $\overline{\kappa}_c$ as a function of $\overline{\rho}_c$ yields

$$\overline{\kappa}_c = \frac{-\delta (k_{d,0}a)^2 j_0(k_{d,0}a)}{\Upsilon_0 \delta k_{d,0} a j_0'(k_{d,0}a)\overline{\rho}_c + \left[\mathcal{F}_0' - \Upsilon_0 \mathcal{F}_0 + 2\delta \Upsilon_0 j_0(k_{d,0}a)\right]}. \quad (4.64)$$

Substituting this expression into Equation (4.63), a quadratic equation in $\overline{\rho}_c$ is obtained,

$$\alpha_{\text{thin}} \delta \overline{\rho}_c^2 + \beta_{\text{thin}} \overline{\rho}_c - 2\delta j_0(k_{d,0}a) j_1(k_{d,0}a) = 0, \quad (4.65)$$

where

$$\alpha_{\text{thin}} = k_{d,0} a \left[\Upsilon_1 j_0(k_{d,0}a) j_1'(k_{d,0}a) - \Upsilon_0 j_0'(k_{d,0}a) j_1(k_{d,0}a)\right], \quad (4.66)$$

$$\beta_{\text{thin}} = \left[j_0(k_{d,0}a)\mathcal{F}_1' - j_1(k_{d,0}a)\mathcal{F}_0'\right] - \left[j_0(k_{d,0}a)\Upsilon_1\mathcal{F}_1 - j_1(k_{d,0}a)\Upsilon_0\mathcal{F}_0\right] + 2\delta j_0(k_{d,0}a)j_1(k_{d,0}a)\left(\Upsilon_1 - \Upsilon_0\right). \tag{4.67}$$

When α_{thin} and β_{thin} are nonzero, there will be two roots of Equation (4.65) given by

$$\overline{\rho}_c = \frac{-\beta_{\text{thin}} \pm \sqrt{\beta_{\text{thin}}^2 + 8\delta^2 j_0(k_{d,0}a)j_1(k_{d,0}a)\alpha_{\text{thin}}}}{2\delta\,\alpha_{\text{thin}}}. \tag{4.68}$$

Assuming $\delta \ll 1$, this expression reduces to

$$\overline{\rho}_c^{(1)} = \frac{2\delta j_0(k_{d,0}a)j_1(k_{d,0}a)}{\beta_{\text{thin}}}, \tag{4.69}$$

$$\overline{\rho}_c^{(2)} = -\frac{\beta_{\text{thin}}}{\delta\,\alpha_{\text{thin}}}, \tag{4.70}$$

where the superscripts $^{(1)}$ and $^{(2)}$ denote the different roots of Equation (4.65).

Although Equations (4.64)–(4.70) are more complex that those developed using a low frequency approximation, these expressions still enable one to explicitly determine $\overline{\kappa}_c$ and $\overline{\rho}_c$, for a fluid or isotropic elastic spherical scatterer at a specific design frequency $k_{d,0}a$ and shell thickness δ. For the case of the low frequency approximation results (Equations (4.43) and (4.48)), it was observed that $\overline{\kappa}_c$ is independent of the core density $\overline{\rho}$, and $\overline{\rho}_c$ is independent of core elastic moduli $\overline{\kappa}$ and $\overline{\mu}$. Using a thin shell approximation, the results of Equations (4.64)–(4.70) can be obtained for an arbitrary frequency $k_{d,0}a$, provided that $k_{d,c}a\delta \ll 1$, but at these finite frequencies $\overline{\kappa}_c$ and $\overline{\rho}_c$ are both dependent on $\overline{\rho}$, $\overline{\kappa}$ and $\overline{\mu}$ (for the case of an isotropic elastic core material).

4.2 Cloaking of a rigid sphere

To better understand the analytic expressions for the cloaking layer properties developed in Section 4.1, the specific limiting case of a rigid, immovable core will be considered. This limit is obtained in a two step process, first by applying

the condition $\kappa \to \infty$ for a *rigid* scatterer, followed by taking the limit $\rho \to \infty$ for an *immovable* scatterer [64]. Note that for an isotropic elastic core material, the shear modulus can be written in terms of the bulk modulus κ and Poisson's ratio ν,

$$\mu = \frac{3\kappa(1-2\nu)}{2(1+\nu)}. \tag{4.71}$$

With the physical bounds on Poisson's ratio for an isotropic elastic solid limited to $-1 \leq \nu < \frac{1}{2}$ [75], taking $\kappa \to \infty$ corresponds to $\mu \to \infty$. This process ensures the limit $k_d a \to 0$ (and $k_s a \to 0$ for an elastic core) is obtained, leading to the solution for a rigid, immovable scatterer.

Taking these limits using the analysis developed in Section 3.2, the scattered pressure for an uncloaked rigid, immovable sphere of radius a can be obtained [76]

$$p_{\text{sc}}(r,\theta,t) = p_0 e^{-i\omega t} \sum_{n=0}^{\infty} i^n (2n+1)\, A_n^{(\text{rigid})} h_n^{(1)}(k_{d0} r) P_n(\cos\theta), \tag{4.72}$$

where

$$A_n^{(\text{rigid})} = \frac{j_n'(k_{d0}a)}{h_n'^{(1)}(k_{d0}a)}, \tag{4.73}$$

and p_0 is the amplitude of the incident pressure.

The amplitude of the scattered field for each mode is determined by the scattering coefficient, $A_n^{(\text{rigid})}$. From Equation (4.73), it is seen that this coefficient depends on the relative amplitudes of $j_n'(k_{d0}a)$ and $h_n'(k_{d0}a)$, which will vary as a function frequency. These functions are plotted in the top panel of Figure 4.2 for the first three modes. From this plot, it can be seen that the magnitude of the scattering coefficient, given by the ratio $|j_n'(k_{d0}a)|/|h_n'(k_{d0}a)|$, varies between 0 and 1. The zeroes of the resulting scattering coefficients, which are shown in the bottom panel of Figure 4.2, correspond to where $j_n'(k_{d0}a) = 0$.

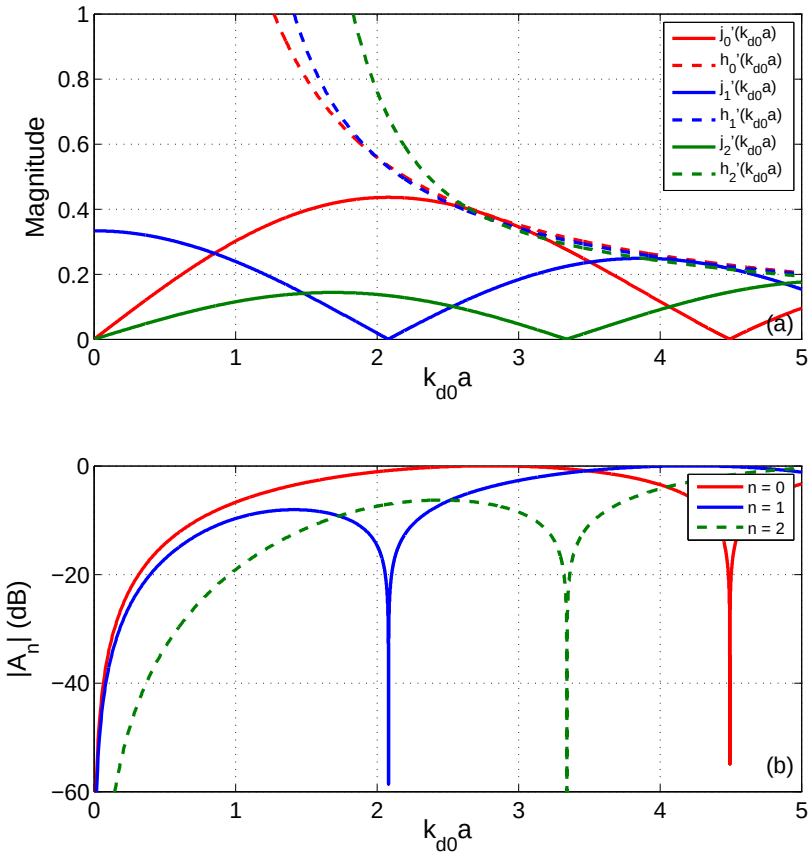

Figure 4.2: Magnitude of the spherical Bessel functions (top) which make up the numerator and denominator of the scatter coefficients for a rigid, immovable sphere (bottom). The magnitude of the scattering coefficients are given in dB.

Although all of the modal scattering coefficients pass through zero, these occur at different frequencies. The total scattering strength, which is the sum of the contribution from all the modes, can therefore still be significant without these modal nulls being apparent. Using the approach described in Section 3.2, these modal nulls can be aligned at a single frequency, thereby eliminating the scattered field from the leading modes.

For the case of a rigid, immovable sphere, the low frequency solutions given by Equations (4.43) and (4.48) become

$$\overline{\kappa}_c = 1-\phi, \tag{4.74}$$

$$\overline{\rho}_c = \frac{2(1-\phi)}{2+\phi}. \tag{4.75}$$

To apply this limiting condition to the thin shell solution, it is necessary to determine the limiting value of Υ_n. To do this, consider the expression for the low frequency limit given by Equation (4.39). Since this expression only depends on the the wavenumber within the core material, it is valid for any finite incident frequency, provided that $k_d a \ll 1$. Taking the limit as $k_d a \to 0$ (and $k_s a \to 0$ for an elastic core), it is seen that $\Upsilon_n \to 0$ for both a fluid and an isotropic elastic core material. Applying the condition $\Upsilon_0, \Upsilon_1 \to 0$ to Equation (4.64) yields

$$\overline{\kappa}_c = \frac{-\delta(k_{d,0}a)^2 j_0(k_{d,0}a)}{\mathcal{F}'_0}. \tag{4.76}$$

In this limiting case, $\alpha_{\text{thin}} \to 0$, leading to only a single solution for $\overline{\rho}_c$ in Equation (4.65), which is given by Equation (4.69) and reduces to

$$\overline{\rho}_c = \frac{2\delta j_0(k_{d,0}a) j_1(k_{d,0}a)}{j_0(k_{d,0}a)\mathcal{F}'_1 - j_1(k_{d,0}a)\mathcal{F}'_0}. \tag{4.77}$$

The coefficient $\mathcal{F}'_n$, which is given by Equation (4.56), is independent of the core material and therefore remains unchanged.

Equations (4.74) and (4.75) can be contrasted with the quasi-static solutions for the normalized effective bulk modulus $\overline{\kappa}_{\text{eff}}$ and density $\overline{\rho}_{\text{eff}}$ of a rigid sphere coated by a single fluid layer, which can be written as [59]

$$\overline{\kappa}_{\text{eff}} = \frac{\overline{\kappa}_c}{1-\phi}, \tag{4.78}$$

$$\overline{\rho}_{\text{eff}} = \overline{\rho}_c \frac{2+\phi}{2(1-\phi)}. \tag{4.79}$$

Comparing these expressions for the normalized effective properties with Equations (4.74) and (4.75) leads to $\overline{\kappa}_{\text{eff}} = 1$ and $\overline{\rho}_{\text{eff}} = 1$, illustrating that application of the cloaking layer allows the effective behavior of the total system (spherical core plus cloaking layer) to equal the properties of the surrounding fluid medium in the quasi-static limit.

In the quasi-static limit, $\overline{\rho}_c$ and $\overline{\kappa}_c$ are only functions of the total volume fraction $\phi = (\frac{a}{b})^3$, which is illustrated in Figure 4.3. For the case of a rigid, immovable scatterer, the normalized cloaking layer properties range from approaching zero, as the thickness of the shell approaches zero (corresponding to $b \to a$), to approaching unity, as the outer shell radius approaches infinity. Due to the normalization of the cloaking layer properties (referenced to the properties of the surrounding fluid medium), this latter condition implies that as the cloaking layer thickness becomes infinitely large (or conversely, the radius of the rigid scatterer becomes infinitely small), so that the cloaking layer properties approach the values of the surrounding medium.

As described in Section 4.1, the cloaking layer properties given by Equations (4.74)–(4.77) were developed by canceling the first two scattering modes. For any non-zero frequencies, there will be higher order modes which will allow some small amount of scattering to occur, even in the quasi-static limit. To determine the overall effectiveness of such a cloaking layer at a given frequency, the total scattering cross-section σ_{total}, given by Equation (3.36) and numerically calculated using the method outlined in Section 3.4, can be used to determine the overall strength of the scattered field with and without the cloak present. The calculation of the total scattering cross-section is performed by summing the effects of a large (but finite) number of scattering modes, which enables the total scattering to be accounted for, including the contributions from the higher order scattering modes which were not

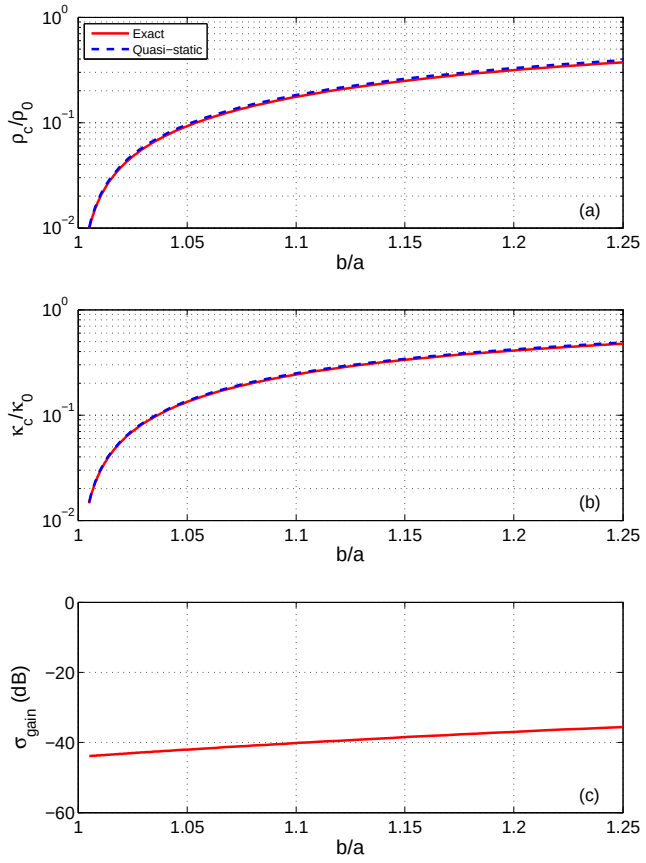

Figure 4.3: Variation of the cloaking layer parameters as a function of the ratio of the outer radius of the cloaking layer b to the outer radius of the scatterer a. The cloaking layer properties, given by ρ_c/ρ_0 (top panel) and κ_c/κ_0 (middle panel), represent the values which cancel the first two modes at $k_{d,0}a = 0.5$ using a single fluid plasmonic cloak coating a rigid, immovable sphere. The bottom panel gives the scattering gain in dB, relative to the uncloaked scatterer.

cancelled. To express the relative change in σ_{total} that occurs with the addition of the cloaking layer, the *scattering gain* can be defined as

$$\sigma_{\text{gain}} = 10 \log_{10} \left[\frac{\sigma_{\text{total}}}{\sigma_{\text{total}}^{(\text{ref})}} \right], \tag{4.80}$$

where σ_{total} is the total scattering cross-section of the cloaked target, and $\sigma_{\text{total}}^{(\text{ref})}$ is

the reference value of the total scattering cross-section, which for this case is that of the uncloaked target.

In Figure 4.3(c), the scattering gain relative to the uncloaked rigid immovable sphere at $k_{d,0}a = 0.5$. It can be seen that, using a single fluid cloaking layer, 40 dB or more of scattering reduction can be obtained at this frequency. The overall scattering reduction varies slightly with shell thickness, decreasing as $\frac{b}{a}$ increases. This is due to the corresponding increase in $k_{d,c}b$, which affects total scattering strength due to the non-zero higher order modes, since a thicker shell shifts the affects of the higher modes (including the fundamental shell resonances) to lower frequencies.

To more thoroughly analyze such frequency dependent affects, the magnitude of each scattering mode ($A_n^{(0)}$ in the notation used in Chapter 3) can be plotted for the uncloaked and cloaked configuration, as shown in the top and middle panels of Figure 4.4, respectively, for the case of $\frac{b}{a} = 1.10$. Comparing these two panels of the figure, the effect of adding the cloaking layer is clearly demonstrated at the design frequency of $k_{d,0}a = 0.5$, where the first and second scattering modes (monopole and dipole modes) are driven to zero. These two modes dominate the scattering in the uncloaked case, while the higher order modes have nearly the same magnitude in the cloaked condition as for the uncloaked scatterer. The resulting residual scattered field at the design frequency $k_{d,0}a = 0.5$ is left with the quadrupole ($n = 2$) as the dominant scattering mode, and from the bottom panel of Figure 4.4 achieves a scattering reduction of 40 dB.

An interesting characteristic of suppressing the two leading order modes, when the cloaking layer is present, is a significant reduction in these modes away from the design frequency. Recall that throughout the development of the cloaking layer formulation presented in Section 4.1 and Chapter 3 focused only on the cancellation

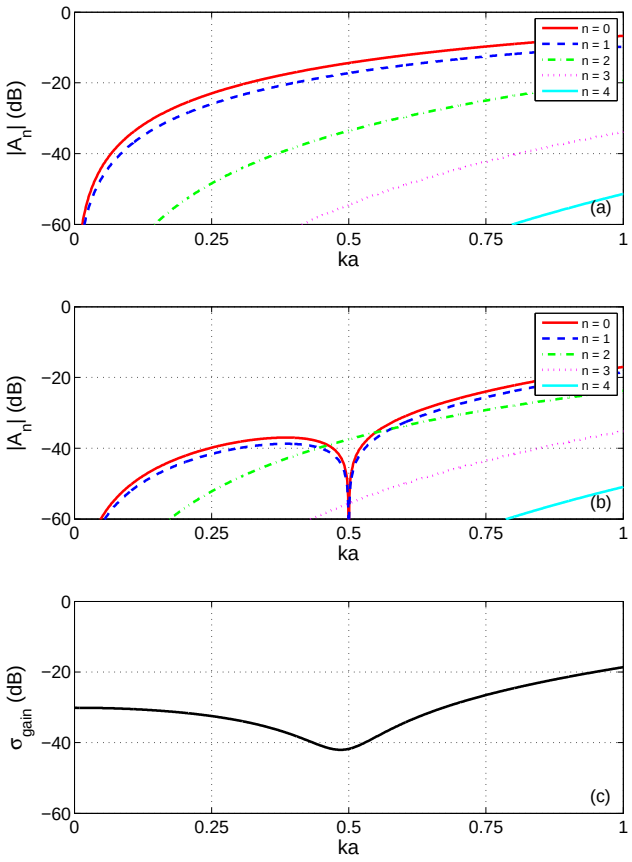

Figure 4.4: Scattering coefficients (in dB) for an uncloaked (top panel) and cloaked (middle panel) rigid, immovable sphere. The cloak consists of a single fluid layer with $\frac{b}{a} = 1.10$ which cancels the first two scattering modes at $k_{d,0}a = 0.5$. The scattering gain in dB, relative to the uncloaked scatterer, is given in the bottom panel

.

of scattering modes at a single frequency. Since each individual scattering mode is only one term in the summation of modes producing the total scattered field, the scattering gain is given in the lower panel of Figure 4.4 to characterize the total scattering reduction achieved by the cloaking layer relative to an uncloaked rigid, immovable sphere. A scattering reduction of at least 20 dB of scattering reduction

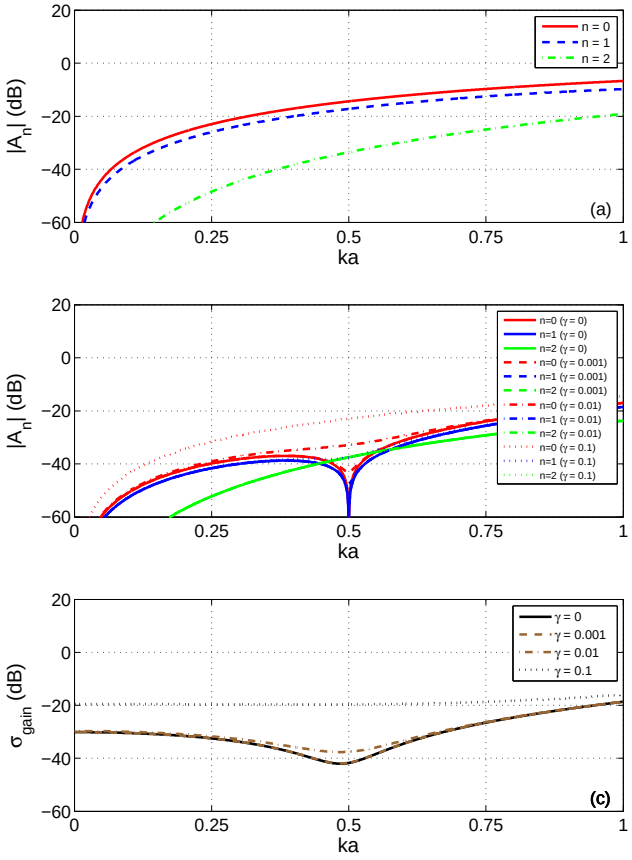

Figure 4.5: Scattering coefficients (in dB) for an uncloaked (top panel) and cloaked (middle panel) rigid, immovable sphere. The cloak consists of a single fluid layer with $\frac{b}{a} = 1.10$ which cancels the first two scattering modes at $k_{d,0}a = 0.5$. Results for loss factors of $\gamma = 0$ (lossless), $\gamma = 0.001$, $\gamma = 0.01$ and $\gamma = 0.1$ are shown. The scattering gain in dB, relative to the uncloaked scatterer, is given in the bottom panel.

over the range of $k_{d,0}a \lesssim 1$ is achieved using a single fluid cloaking layer, with 40 dB of reduction occurring at the design frequency.

Thus far, only ideal conditions have been examined, namely, a lossless cloak with the exact values needed to achieve cancellation. One of the challenges faced

with transformation-based cloaks discussed in Section 2.1.1.2 is the high sensitivity to perturbations in the cloak properties. These problems arise in large part because of the requirement for large gradients in the cloak prescribed by the coordinate-transformation, which are not required for the scattering cancellation approach. For plasmonic cloaks, this was examined for electromagnetic waves by Alù and Engheta [52], who demonstrated the robustness of such cloaks by varying the losses within the cloaking layer and surface variations of the target.

To examine the robustness of acoustic plasmonic cloaking, Figures 4.5(b) and (c) illustrate the effect of losses within the cloaking layer on the magnitude of the scattering coefficient and scattering gain, respectively, which is referenced to an uncloaked (lossless) sphere. For comparison, the magnitude of the scattering coefficient for the uncloaked is plotted in Figure 4.5(a). Losses are included in the cloak by using a complex bulk modulus, κ_c', which is given by

$$\kappa_c' = \kappa_c(1 - \gamma i), \tag{4.81}$$

where γ is a dimensionless parameter which quantifies the effects of the losses. In Figures 4.5(b) and (c), results are presented for values of γ ranging from 0 (lossless) to 0.1 (heavily damped). It is observed that with low to moderate losses (up to $\gamma = 0.01$), an increase of only a few dB in scattering gain is observed in the vicinity of the design frequency, which corresponds to a decrease in the cloak performance. Note that at $\gamma = 0.01$, the null in the $n = 0$ mode is essentially removed, and yet significant scattering reduction is still observed. In addition, the performance of the cloak away from the design frequency remains nearly unchanged from the results observed in the lossless case. Even in the extreme case of $\gamma = 0.1$, a scattering reduction of approximately 20 dB relative to the uncloaked sphere is still achieved.

The results presented in Figure 4.5 illustrate the robustness of a plasmonic cloak to the effects of losses in the cloaking layer. Although these results represent a

significant reduction in scattering strength over a relatively broad frequency range, the core properties considered here represents only a limiting case, leading to an idealized condition of an impenetrable target. More generally, a penetrable target with a finite acoustic impedance will affect the performance and the necessary cloaking layer properties, which is investigated in the next section.

4.3 Cloaking of a fluid sphere

Taking the limiting case of a rigid, immovable core performed in the last section enabled simplification of the analytic expressions and parametric design space, allowing for the plasmonic cloaking behavior to be explored for a simple yet relevant spherical scatterer. To fully explore the behavior of a single fluid cloaking layer, however, it is necessary to consider the properties of the core material, which strongly affect the required cloaking layer properties and effectiveness in the reducing the scattering gain.

To investigate such a configuration, the variation in the necessary cloaking layer properties will be considered due to the normalized density $\overline{\rho}$ and bulk modulus $\overline{\kappa}$ of the core material, for a fixed design frequency and layer thickness. To do this, a surface plot can be constructed depicting the required cloaking layer property as a function of the core material properties, which can be obtain through implicitly solving Equation (4.26), using the expression in Equation (4.25) for a fluid core.

A demonstration of such a plot, indicating the required value of the cloaking layer properties for a particular combination of $\overline{\rho}$ and $\overline{\kappa}$, is given by Figure 4.6 for the case of $k_{d,0}a = 0.5$ and $\frac{b}{a} = 1.10$, illustrating the values for $\overline{\rho}_c$ (top panel) and $\overline{\kappa}_c$ (middle panel), with the magnitude denoted by a change in color. In these two panels, values less than unity are are represented by blues and greens, and values greater than unity are represented by yellows and reds. Due to the large range of

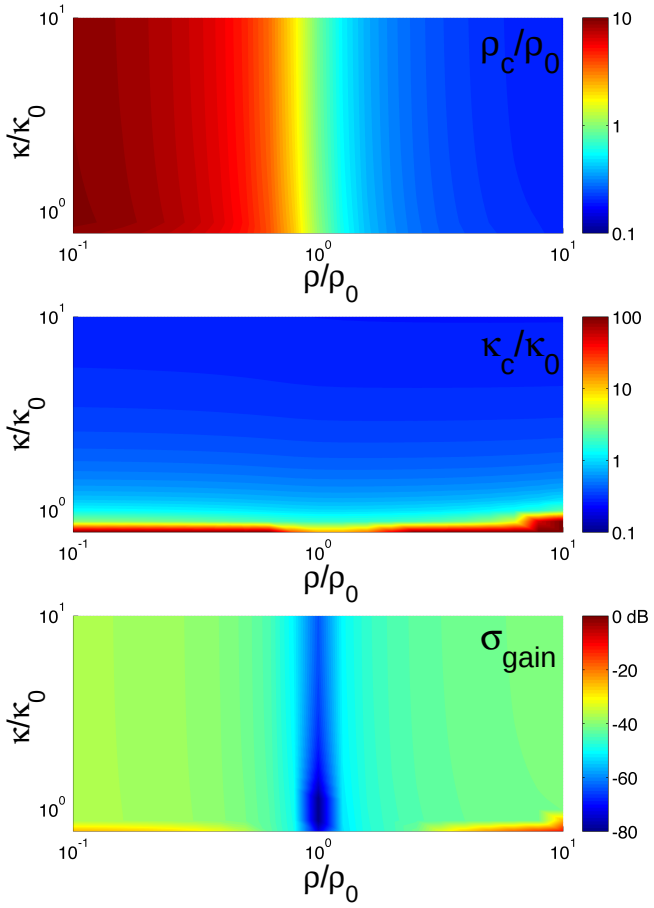

Figure 4.6: Parametric plot of the optimized cloaking layer density (top panel), cloaking layer bulk modulus (middle panel) and scattering gain (bottom panel) as a function of the density and bulk modulus of a penetrable fluid scatterer relative to the external fluid. The results are given for a cloaking layer with $b/a = 1.10$, which cancels the first two modes at $k_{d,0}a = 0.5$.

the material properties illustrated in the figure, a logarithmic scale has been used for both the core material properties (on the axes) and the cloaking layer properties

(on the color scale). For the case illustrated in Figure 4.6, the variations in $\overline{\rho}_c$ and $\overline{\kappa}_c$ change monotonically and largely dependent on only $\overline{\rho}$ and $\overline{\kappa}$, respectively. Given the moderately low frequency, this behavior is to be expected, as seen in the quasi-static solutions presented in Equations (4.43) and (4.48).

As with the case of a rigid, immovable sphere, the density and bulk modulus of a single fluid cloaking layer will only serve to cancel the first two scattering modes, and the total scattering cross-section can be used to quantify the scattering strength of the remaining higher order modes. The change in this quantity was given by the scattering gain in Equation (4.80), which is plotted in the lower panel of Figure 4.6. Although typically referenced to the uncloaked scatterer, the values given in the lower panel of Figure 4.6 are normalized by the scattering strength of an uncloaked rigid, immovable sphere. In the previous section, the uncloaked sphere considered was rigid and immovable, which does not exhibit any internal acoustic field. For the penetrable fluid scatterers considered here, there is an internal acoustic field within the uncloaked sphere, which can lead to the presence of internal resonances, particularly for cases when $\overline{\kappa} \ll \overline{\rho}$. Depending on the particular core material properties, these resonances could occur either above or below the design frequency. Due to the large scattered field generated near resonance for the uncloaked sphere, and the fact that this resonance frequency will shift due to the presence of the cloaking layer, artificially low or high scattering gain values can be obtained, which are not due to the effectiveness of the cloaking layer. To avoid such problems, the use of an impenetrable reference will be used, which in this case is that of a rigid, immovable sphere of radius a.

From the lower panel of Figure 4.6, it is apparent that nearly all of the regions throughout the parameter space show a scattering reduction of 30 dB or more. The magnitude of the scattering reduction is relatively consistent, except in

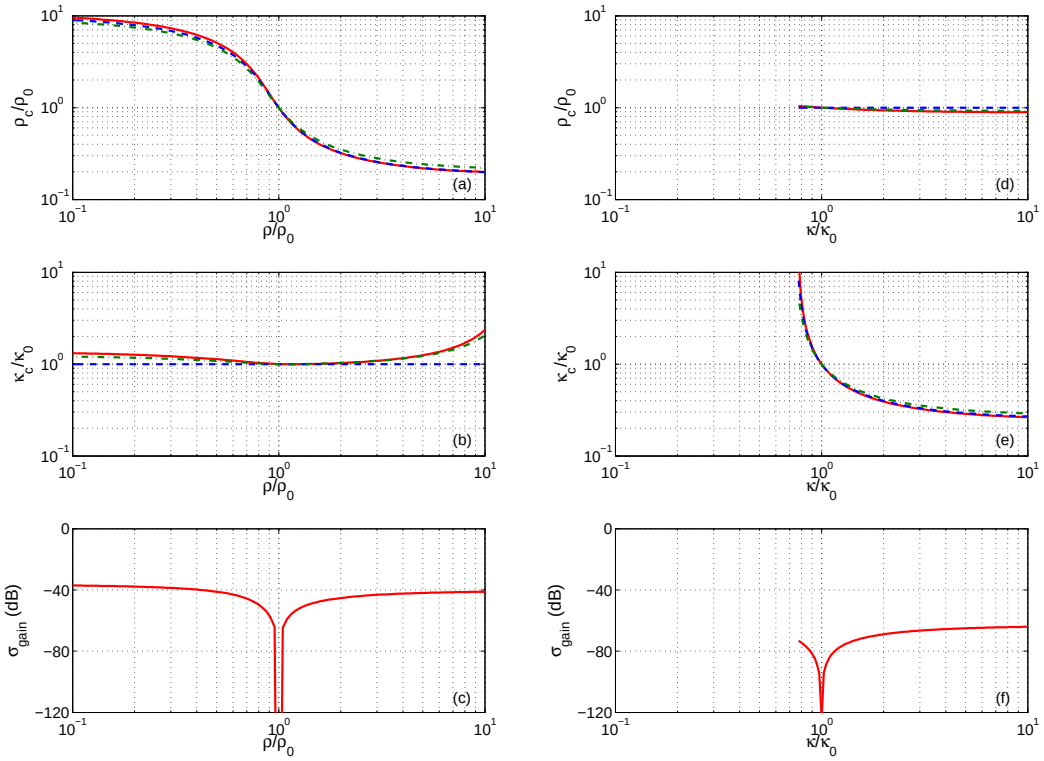

Figure 4.7: Slices of the parametric plots of Figure 4.6 for constant scatterer bulk modulus of $\kappa/\kappa_0 = 1$ (left column) and scatterer density of $\rho/\rho_0 = 1$ (right column). The rows depict resulting changes in the cloaking layer density (top row), cloaking layer bulk modulus (middle row) and scattering gain (bottom row).

the vicinity of $\overline{\rho}$ near unity (in particular, when $\overline{\kappa}$ is also near unity), and in the region $\overline{\kappa} < 1$. In the vicinity of $\overline{\rho} = 1$ and $\overline{\kappa} = 1$, this corresponds to the point where the fluid sphere is the same as the surrounding fluid, leading to no scattered energy. It is clear that for the case of $\overline{\rho} = 1$ with $\overline{\kappa} \neq 1$, the effects of the scattering reduction occurs over a much broader region of the parameter space than when $\overline{\kappa} = 1$ with $\overline{\rho} \neq 1$.

To examine this phenomenon further and to understand the rapid increase in

scattering gain occurring in the region $\overline{\kappa}<1$, Figure 4.7 illustrates the required cloaking layer properties and resulting scattering gain for two particular cases presented in Figure 4.6. Specifically, these results represent slices of the multi-parameter plots shown in Figure 4.6, taken along a constant value of $\overline{\kappa}=1$ to obtain the results in the left column, and $\overline{\rho}=1$ for the right column. In this figure, the exact numerical solution is represented by the solid line, the quasi-static solution calculated using Equations (4.43) and (4.48) is represented by the dashed line, and the thin shell solution calculated using Equations (4.64) and (4.69) is represented by the dotted line.

Examining Figure 4.7, one can see that there is very good agreement of the quasi-static solution with the exact solution for describing the variation of $\overline{\rho}_c$ with $\overline{\rho}$ (top left panel) and the variation of $\overline{\kappa}_c$ with $\overline{\kappa}$ (middle right panel). As expected, these solutions pass through the points $\overline{\rho}_c=1$ and $\overline{\kappa}_c=1$ when $\overline{\rho}=1$ and $\overline{\kappa}=1$, which is the trivial case of the core fluid having the same properties as the surrounding fluid, and therefore yields cloaking layer properties also equal to the surrounding fluid. Even at the moderately low frequency of $k_{d,0}a=0.5$ considered here, there is coupling between the density of the core material and the bulk modulus of the cloaking layer illustrated in the middle left panel, particularly in the regions $\overline{\rho}\ll 1$ and $\overline{\rho}\gg 1$, which is not captured by the quasi-static approximation. These effects on $\overline{\kappa}_c$, however, are captured by the thin shell approximation, which includes an explicit dependence on density which appears in the denominator of Equation (4.64).

Looking at the values of $\overline{\rho}_c$ at upper and lower extremes of $\overline{\rho}$ shown in Figure 4.6(a), it is apparent that the cloaking layer density asymptotically approaches finite limits. Thus, in a similar manner to the limit of $\overline{\rho}\to\infty$ taken in Section 4.2, an equivalent finite value could be achieved for the limit $\overline{\rho}\to 0$. For $\overline{\kappa}_c$, the upper limit of $\overline{\kappa}$ illustrated in the Figure 4.6(e) demonstrates a similar behavior. Taking

Parameter	Steel	Aluminum	Glass
Density, ρ(kg/m^3)	7700	2700	2300
Bulk Modulus, κ(GPa)	170	75	39
Poisson's Ratio, ν	0.28	0.33	0.24

Table 4.1: Properties of elastic spheres to be cloaked for the three examples considered in this section.

the lower limit of $\overline{\kappa}$ presents a much different result, with $\overline{\kappa}_c$ approaching infinity as $\overline{\kappa}$ decreases below unity. This behavior is in excellent agreement with both the quasi-static and thin shell approximations, and its source can clearly be identified as a pole in Equation (4.43). From this equation, the denominator becomes zero when $\overline{\kappa}=\phi$, which for $\frac{b}{a}=1.10$ corresponds to $\overline{\kappa}=0.7513$. For $\overline{\kappa}$ below this critical value, the required cloaking layer bulk modulus is *negative*, making the plasmonic cloaking of compliant scatterers a significant challenge. To overcome this challenge, it is possible to use a thicker shell, since the critical value scales as $(\frac{a}{b})^3$, or to use an anti-resonance cloaking layer, which is described in Chapter 5. Although seemingly a strange physical phenomenon, it is actually not limited to plasmonic cloaking, and has previously been observed in the static analysis of elastic coated spheres [72].

4.4 Cloaking of an isotropic elastic sphere

In the previous section, the analysis was limited to a fluid core material. Many scatterers of practical interest, including metals, ceramics and plastics, are isotropic elastic solids, and it would therefore be useful to determine the effect that elasticity in the core material has on the cloaking layer properties. Analytic expressions to include an isotropic elastic core material were developed as a general case for an isotropic scatterer, and characterized using a coefficient, Υ_n. For the exact full-

	Steel			**Aluminum**			**Glass**		
ka	**0.50**	**0.75**	**1.00**	**0.50**	**0.75**	**1.00**	**0.50**	**0.75**	**1.00**
$\rho_c\,(\mathrm{kg/m^3})$	103.53	98.30	91.28	138.55	129.28	117.25	152.13	141.10	126.86
κ_c(MPa)	295.85	287.80	276.25	300.83	293.34	282.38	307.41	299.87	288.67

Table 4.2: Properties of single fluid layer plasmonic cloak of an *elastic* core for $ka = 0.5$, 0.75, and 1.00.

wave solution (as well as the thin shell approximation), Υ_n can be determined from Equation (4.25), making it straightforward to include in the analysis of an isotropic elastic core. It was observed in Section 4.1.1, however, that the expressions for Υ_0 and Υ_1 for an isotropic elastic core in the quasi-static limit are equal to those of a fluid core with the same bulk modulus $\overline{\kappa}$ and density $\overline{\rho}$. For a single cloaking layer, when the wavelength in the surrounding fluid is on the order of the diameter or larger, these elastic effects will be minimal on the two leading order modes ($n=0$ and $n=1$), and will predominantly affect the scattering from the scattering modes for $n=2$ and above.

To highlight the behavior of a single fluid cloaking layer for an isotropic elastic core, three different materials will be examined: stainless steel, aluminum and glass. The material properties of each are obtained from Kinsler *et al.* [77] and listed in Table 4.1, and in each case the surrounding medium is assumed to be water ($\rho_0 = 1000\,\mathrm{kg/m^3}$, and $\kappa_0 = 2.193\,\mathrm{GPa}$). These materials provide a broad range of density and elastic moduli, representing materials which are commonly used in scientific and engineering applications, and provide significant scattering in an aqueous environment.

To illustrate the scattering reduction obtained for each of these materials, as well as the relative effects due to the non-zero shear modulus of the core material,

	Steel fluid			**Alum. fluid**			**Glass fluid**		
ka	**0.50**	**0.75**	**1.00**	**0.50**	**0.75**	**1.00**	**0.50**	**0.75**	**1.00**
$\rho_c\,(\mathrm{kg/m^3})$	103.47	98.06	90.66	138.49	129.10	116.70	151.98	140.84	126.32
$\kappa_c(\mathrm{MPa})$	294.97	287.89	277.72	298.05	290.85	280.49	300.44	293.13	282.63

Table 4.3: Properties of single fluid layer plasmonic cloak of a *fluid* core for $ka = 0.5$, 0.75, and 1.00.

three different design frequencies will be considered: $k_{d,0}a = 0.5$, $k_{d,0}a = 0.75$, and $k_{d,0}a = 1.0$. The properties for of the single fluid layer plasmonic cloak, determined through numerically solving Equations (4.26) for each design frequency, are given in Table 4.2 for the case of $\frac{b}{a} = 1.05$.

As a guide for comparison, the analogous results are also obtained for scatterers with the same density and bulk modulus, but zero shear modulus (corresponding to a Poisson's ratio of $\frac{1}{2}$). This represents the equivalent of a stainless steel 'fluid', aluminum 'fluid', and glass 'fluid', which in the quasi-static limit produce the same scattered field. The single fluid plasmonic cloaking properties for these fluids is obtained in the same manner as for the cloaking of the elastic scatterers, and the results are presented in Table 4.3 for the case of $\frac{b}{a} = 1.05$.

To demonstrate the effectiveness of these various cloaking configurations, the scattering gain is plotted as a function of $k_{d,0}a$ in Figure 4.8 for stainless steel (top panel), aluminum (middle panel) and glass (bottom panel). In the figure, the solid lines denote the case of the elastic core material, and the dashed lines represent the case of the 'fluid' equivalent. The results for the different plasmonic cloaking layers for each scatterer given in Tables 4.2 and 4.3 are presented in different colors to denote the different design frequencies: $k_{d,0}a = 0.5$ (black), $k_{d,0}a = 0.75$ (blue) and $k_{d,0}a = 1.0$ (green).

Examining the curves presented in Figure 4.8, it is clear that all the plasmonic cloaks show similar trends in the overall performance, achieving 30 dB or more of scattering reduction at the design frequency, while producing significant reductions over a wide range of frequencies before returning to zero scattering gain around $k_{d,0}a = 2.5 - 3.0$. This figure illustrates that, by using the non-resonant cancellation of the leading order modes, application of a simple plasmonic cloak can achieve significant scattering reduction for common materials, which extend well above and below the design frequency.

As observed in Figure 4.8, broadband, non-resonant scattering reduction is not dependent on the elastic effects of the core material. However, looking in the vicinity of the design frequencies, it can be seen that, for fluid core materials, there is a less significant reduction as the design frequency is increased. This is to be expected, since as the design frequency increases, the contribution from the higher order modes increases, limiting the effectiveness of canceling only the two leading order modes. For the cloaked elastic core materials, this is generally true as well, but there is some distinct variations to changes in magnitude with respect to the equivalent fluid core for aluminum and glass. For these cases, there is significantly more scattering reduction than for the comparable fluid cores, particularly for the cloaked aluminum with a design frequency of $k_{d,0}a = 0.5$, and for the cloaked glass with a design frequency of $k_{d,0}a = 1.0$.

To determine the specific modal responses of the elastic and fluid cores, Figure 4.9 shows the magnitude of the modal scattering coefficients for a 'fluid' glass core (left column) and an elastic glass core (right column) using a single plasmonic cloaking layer with a design frequency of $k_{d,0}a = 1$. For each case, the scattering coefficients are shown for the uncloaked configuration (top) and cloaked configuration (bottom). Comparing the top row (uncloaked) with the bottom row (cloaked), the

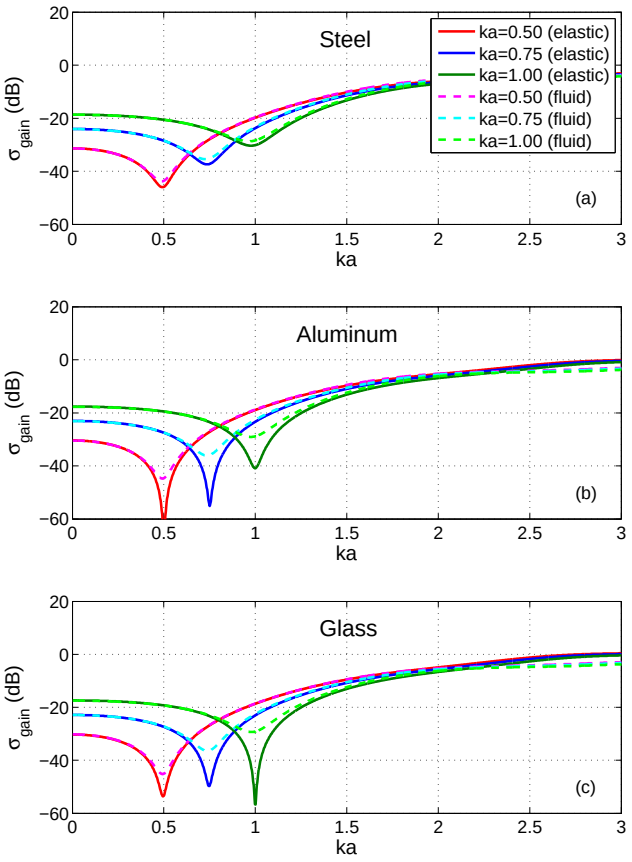

Figure 4.8: Scattering gain as a function of ka for a cloaked sphere of stainless steel (top), aluminum (middle) and glass (bottom). The scattering gain is given in dB relative to the scattering strength of the uncloaked sphere. Three plasmonic cloaking layers are presented for each case, optimized for $ka = 0.5$ (red), $ka = 0.75$ (blue) and $ka = 1.0$ (green). The cloaking layer material properties for each case are listed in Tables 4.2 and 4.3. The cloaking layer thickness ratio in all cases was $b/a = 1.05$.

effect of the plasmonic cloaking layer on the first two scattering modes are clearly illustrated, with the nulls of these two modes being aligned at the design frequency $k_{d,0}a = 1$. It is interesting to note that these nulls exist naturally in the scattering modes of the uncloaked scatterer, with each occurring at a different frequency.

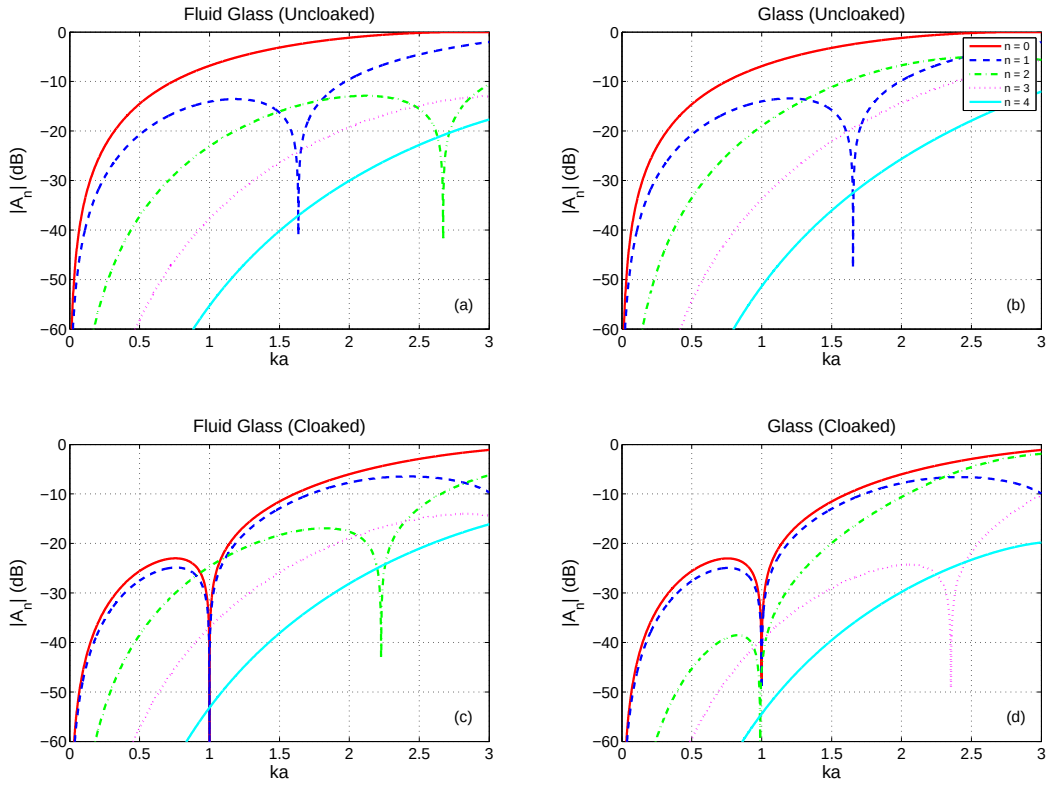

Figure 4.9: Comparison of the scattering coefficients for an elastic glass sphere (right column), and a fluid glass sphere (left column). For each case, the first 5 scattering coefficients are given for the uncloaked sphere (top row) and cloaked sphere (bottom row). The cloaking layer properties are given by Table 4.2 for the elastic glass sphere, and Table 4.3 for the fluid glass sphere.

However, it is the presence of the cloaking layer which aligns multiple nulls at a single frequency, allowing for the significant reduction in the scattering strength to be obtained.

Comparing the left column (fluid glass) with the right column (glass), the effects of a non-zero shear modulus can be observed. In both the uncloaked and cloaked cases, the $n=0$ and $n=1$ modes are nearly identical, which is in agreement

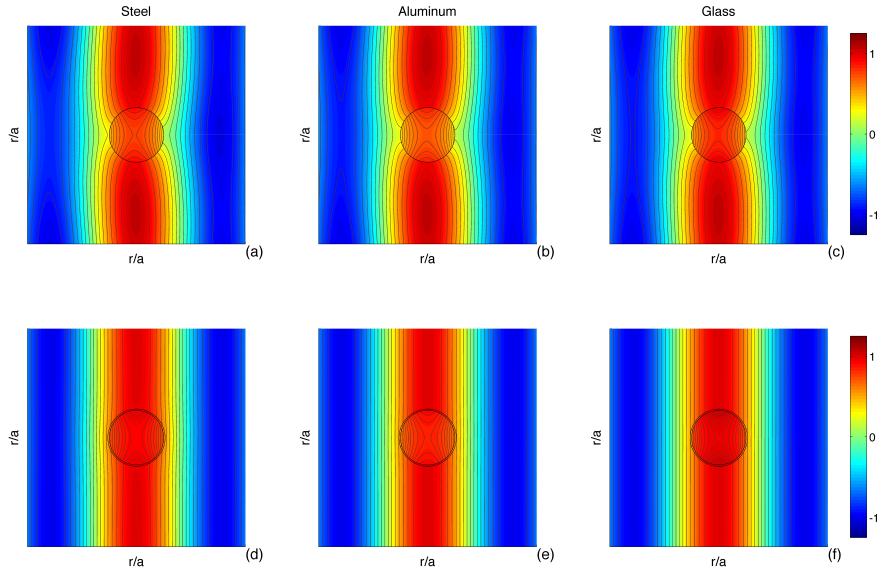

Figure 4.10: Real part of total pressure field for an isotropic sphere of stainless steel (left column), aluminum (middle column) and glass (right column). For each case, the uncloaked sphere is presented in the top row, and with a plasmonic cloak consisting of a single fluid layer with a thickness ratio of $b/a = 1.05$ presented in the bottom row. The cloaking layer properties for each case are listed in Table 4.2. The color scale for the pressure is normalized to the amplitude of the incident wave, which is a time-harmonic plane wave traveling from left to right with a frequency of $k_{d,0}a = 1$. The length scale r is normalized by the uncloaked sphere radius a.

with the quasi-static analytic results. For the $n = 2$ mode, however, there is a distinctly different location of the modal null. Although this difference is negligible for the uncloaked cases due to the relatively high frequency at which the null occurs, the null of the $n=2$ mode for the cloaked elastic glass core lies in the vicinity of the design frequency, leading to a much larger reduction in the total scattering strength than for the case of the fluid glass core.

Throughout the analysis thus far, the scattering gain and the magnitude of

the scattering coefficients have been used to demonstrate the capability of a single fluid layer plasmonic cloak to reduce the overall level of the scattered field, for both the design frequency and the broadband behavior. Although using the total scattering cross-section to determine the scattering gain ensures that the scattering coefficient of the cancelled scattering modes is zero for each angle, further insight can be gained by looking at the changes in phase which occur as a result of the cloaking layer. To illustrate this, consider the real part of the *total* acoustic pressure field (consisting of the scattered field plus the incident wave), which is illustrated in Figure 4.10 for stainless steel, aluminum and glass in water. In this figure, an uncloaked configuration shown in the top row, while the case of a single fluid plasmonic cloaking layer is shown in the bottom row. In each case, a time-harmonic incident plane wave passing from left to right is impinging upon the target at a frequency of $k_{d,0}a=1$, which also corresponds to the design frequency of the cloaking layer. To highlight the finer phase structure, lines of constant phase are shown and are denoted by the brown lines.

Within the region of the spherical isotropic elastic core, the pressure p is given by

$$p = -\frac{1}{3}(T_{rr} + T_{\theta\theta} + T_{\varphi\varphi}), \tag{4.82}$$

where T_{rr}, $T_{\theta\theta}$ and $T_{\varphi\varphi}$ are the normal stresses in the r-, θ- and φ-direction, respectively. The negative sign in Equation (4.82) is due to the fact that a *positive* pressure acting on the sphere corresponds to an applied force acting on the sphere in the *negative* r-direction.

From the top row of Figure 4.10, the disturbance of the incident field is clear, which, in the absence of the uncloaked scatterers, would appear as vertical lines of constant phase. This is in contrast with the corresponding cloaked spheres given in the bottom row, in which application of the thin plasmonic cloaking layer

effectively restores the total pressure field in the surrounding medium to that of the incident wave. In addition, this effect is clearly visible even within the nearfield, demonstrating that the scattered field within the surrounding medium has been sufficiently reduced. Although such effectiveness within the nearfield may seem surprising, recall that the objective of the cloaking layer design was the cancellation of the dominant terms of the scattering coefficient in the surrounding medium. This critieria is *range independent*, and therefore effective throughout the entire surrounding fluid.

Although the design of the cloaking layer has focused exclusively on the cancellation of the exterior scattered field, it is clear that there is still a substantial pressure field which exists within the core material. This is distinctly different than cloaks obtained using a transformation-based method, which seek a design that prevents the incident wave from interacting with the interior of the cloaked object. Furthermore, it can be seen from Figure 4.10 that although the interior pressure field is curved due to the curved contour of the object, it is in phase with incident wave. This is due to the cancellation of the scattered field, for which the resulting magnitude of the total pressure acting on the outside of the cloaking layer is nearly equal to the incident wave. Since the cloaking layer is thin and non-resonant, the pressure is relatively uniform across the thickness of the layer, so that the pressure acting on the interior very closely matches that of the incident wave front moving past the cloaked object. This fidelity between the incident and interior pressure without significantly disrupting the exterior field allows for possible applications as an ideal acoustic sensor. This concept has successfully been developed for electromagnetic detectors [55], and the potential for an acoustic sensor is discussed in Section 8.2.

4.5 Comparison with a single elastic cloaking layer

Thus far, a detailed analysis of acoustic plasmonic cloaking has been presented which has focused on the use of a single fluid layer to achieve scattering cancellation. In the present section, a basic description of a single *elastic* cloaking layer will be described and compared with the results previously obtained using a fluid layer. Although only allowing for a non-zero shear modulus, representing an addition of a single parameter, the determinant U_n (which is set equal to zero to determine the cloaking condition for each mode) becomes significantly more complicated. This is due to the fact that accounting for shear in the cloaking layer allows for the propagation of shear waves in the layer, which adds two more scattering coefficients and two more boundary conditions at the layer interfaces. As a result, U_n becomes the determinant of a 7×7 matrix for an isotropic elastic core (6×6 for a fluid core), the full expressions for which can be found in Appendix A. Furthermore, coupling between the shear and compressional modes leads to added complexity in many of the elements of U_n, making it difficult to evaluate in closed form. Although not impossible, exact solutions do not offer simple, closed form expressions, and fail to offer insight into the effects of elasticity within the cloaking layer.

Given the complexity of accounting for the cloaking layer elasticity using exact relations, the analytic results developed in this section will be limited to quasi-static results. In addition, since the cancellation of the two leading order terms is independent of the shear properties of the core material, results can be determined using only the core density and bulk modulus, while still being equally valid for either a fluid or isotropic elastic core. To obtain explicit expressions for the quasi-static cloaking layer properties, the same process will be followed as outlined in Section 4.1.1. Applying the quasi-static approximation for the spherical Bessel functions given by Equations (4.30)–(4.33) to each element of U_n, the determinant

can be evaluated using block matrices according to Equation (4.22) and set equal to zero. For the limiting case under consideration here, an equivalent expression can be obtained using static analysis for the effective bulk modulus of a coated sphere, with the cloaking achieved when the effective bulk modulus of the core plus coating layer is equal to the bulk modulus of the surrounding fluid [59].

Although the terms in U_n given in Appendix A are defined using the cloaking layer shear modulus μ_c, in the current analysis the Poisson's ratio of the cloaking layer ν_c will be used instead to characterize the shear effects. Based on the normalized bulk and shear modulus of the cloaking layer, these parameters are related by

$$\overline{\mu}_c = \frac{3\overline{\kappa}_c(1-2\nu_c)}{2(1+\nu_c)}. \tag{4.83}$$

In this expression, it is noted that although μ_c and κ_c have been normalized by κ_0 to yield non-dimensional quantities, ν_c is already dimensionless. Furthermore, the range of $\overline{\mu}_c$ is $0 \leq \overline{\mu}_c < \infty$, and depends on the value of $\overline{\kappa}_c$, which is determined (in the quasi-static limit) by $\overline{\kappa}$ and the thickness of the cloaking layer. The physical bounds on Poisson's ratio for an isotropic elastic material, however, are $-1 \leq \nu_c \leq \frac{1}{2}$, with $0 < \nu_c \leq \frac{1}{2}$ for most naturally-occurring homogeneous materials [75]. The upper limit $\nu_c = \frac{1}{2}$ corresponds to an incompressible material and zero shear modulus (as seen from Equation (4.83)), which is equivalent to the solution for an incompressible fluid.

Evaluating the resulting expression for $U_n = 0$ at $n = 0$ yields a quadratic expression for the normalized bulk modulus of the elastic cloaking layer,

$$\alpha_{\mathrm{QS}}^{(E)}\overline{\kappa}_c^2 - \beta_{\mathrm{QS}}^{(E)}\overline{\kappa}_c - \gamma_{\mathrm{QS}}^{(E)} = 0, \tag{4.84}$$

where $\phi = \left(\frac{a}{b}\right)^3$ and

$$\alpha_{\mathrm{QS}}^{(\mathrm{E})} = 2(1-\phi)(1-2\nu_c), \tag{4.85}$$

$$\beta_{\mathrm{QS}}^{(\mathrm{E})} = \big[2(1-2\nu_c) + (1+\nu_c)\phi\big] - \big[(1+\nu_c) + 2(1-2\nu_c)\phi\big]\overline{\kappa}, \tag{4.86}$$

$$\gamma_{\mathrm{QS}}^{(\mathrm{E})} = (1-\phi)(1+\nu_c)\overline{\kappa}. \tag{4.87}$$

Use of the quadratic formula yields the roots of Equation (4.84)

$$\overline{\kappa}_c = \frac{\beta_{\mathrm{QS}}^{(\mathrm{E})} + \sqrt{\big(\beta_{\mathrm{QS}}^{(\mathrm{E})}\big)^2 + 4\,\alpha_{\mathrm{QS}}^{(\mathrm{E})}\gamma_{\mathrm{QS}}^{(\mathrm{E})}}}{2\,\alpha_{\mathrm{QS}}^{(\mathrm{E})}}. \tag{4.88}$$

From this expression, the bulk modulus of the cloaking layer is given as a function of the core bulk modulus, the layer thickness, and the Poisson's ratio of the cloaking layer. In Equations (4.84)–(4.87), it is observed that $\alpha_{\mathrm{QS}}^{(\mathrm{E})} > 0$ and $\gamma_{\mathrm{QS}}^{(\mathrm{E})} > 0$ within the bounds of $0 < \phi < 1$ and $-1 \leq \nu_c < \frac{1}{2}$, regardless of $\overline{\kappa}$. Conversely, the sign of $\beta_{\mathrm{QS}}^{(\mathrm{E})}$ depends on the relative difference of the two bracketed terms in Equation (4.86), which depends on the value of $\overline{\kappa}$.

Examining Equation (4.88), the coefficient $\beta_{\mathrm{QS}}^{(\mathrm{E})}$ only appears under the square root as $(\beta_{\mathrm{QS}}^{(\mathrm{E})})^2 \geq 0$, which is added to the product of $\alpha_{\mathrm{QS}}^{(\mathrm{E})}$ and $\gamma_{\mathrm{QS}}^{(\mathrm{E})}$, ensuring that the solution given by Equation (4.88) is real. Furthermore, since

$$\sqrt{\big(\beta_{\mathrm{QS}}^{(\mathrm{E})}\big)^2 + 4\,\alpha_{\mathrm{QS}}^{(\mathrm{E})}\gamma_{\mathrm{QS}}^{(\mathrm{E})}} \geq \big\|\beta_{\mathrm{QS}}^{(\mathrm{E})}\big\|, \tag{4.89}$$

where $\|\beta_{\mathrm{QS}}^{(\mathrm{E})}\|$ denotes the magnitude of $\beta_{\mathrm{QS}}^{(\mathrm{E})}$. Thus, the choice of the "+" sign in Equation (4.88) will ensure a non-negative value for $\overline{\kappa}_c$. Although these results are derived from the elastodynamic relationship by taking the quasi-static limit, Equations (4.84)–(4.88) are identical to those obtained using static analysis and the concept of a neutral inclusion [59].

The non-zero shear effects characterized by ν_c on $\overline{\kappa}_c$, in addition to the normalized core bulk modulus $\overline{\kappa}$ which dominated the quasi-static behavior for the fluid layer case, are illustrated in Figure 4.11 for $\frac{b}{a} = 1.10$. In this figure, the value of $\overline{\kappa}_c$ is represented by the color scale for a given ν_c and $\overline{\kappa}$. It is clear that over the range $0 \leq \nu_c < \frac{1}{2}$, $\overline{\kappa}_c$ is real and positive for the entire range of $\overline{\kappa}_c$ considered.

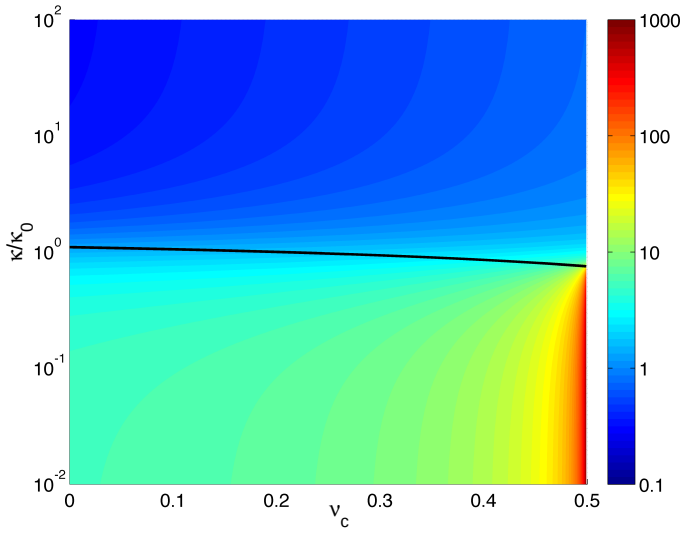

Figure 4.11: Parametric plot of elastic effects on the cloaking layer parameter $\overline{\kappa}_c$ in the quasi-static limit, as a function of the cloaking layer Poisson's ratio ν_c and the core material bulk modulus $\overline{\kappa}$, obtained from Equation (4.88). The different colors represent the (dimensionless) values of $\overline{\kappa}_c$ on a logarithmic scale.

Given the expression for $\overline{\kappa}_c$ in Equation (4.88), it is clear that the resulting behavior of the solution depends on the value and sign of $\beta_{\text{QS}}^{(\text{E})}$. An important transitional point in the behavior of $\overline{\kappa}_c$ occurs where $\beta_{\text{QS}}^{(\text{E})}=0$. Using Equation (4.86), this yields a value of $\overline{\kappa}$ under these conditions denoted by $\overline{\kappa}_{\text{crit}}$, which is given by

$$\overline{\kappa}_{\text{crit}} = \frac{2(1-2\nu_c)+(1+\nu_c)\phi}{(1+\nu_c)+2(1-2\nu_c)\phi}. \tag{4.90}$$

This expression is denoted in Figure 4.11 by the black line. In the figure, it is observed that this line denotes two distinct regions in the vicinity of ν_c near $\frac{1}{2}$. Evaluating Equation (4.90) at $\nu_c = \frac{1}{2}$ yields $\overline{\kappa}_{\text{crit}} = \phi$, which corresponds to the critical value of $\overline{\kappa}$ for the case of a fluid cloaking layer, for which $\overline{\kappa}_c \to \infty$.

For the case when $\beta_{\rm QS}^{\rm (E)} \neq 0$, Equation (4.88) can be expressed as

$$\overline{\kappa}_c = \frac{1}{2\alpha_{\rm QS}^{\rm (E)}}\left[\beta_{\rm QS}^{\rm (E)} + \|\beta_{\rm QS}^{\rm (E)}\|\sqrt{1+4\,\varepsilon_{\rm QS}}\right], \tag{4.91}$$

$$\varepsilon_{\rm QS} = \frac{\alpha_{\rm QS}^{\rm (E)}\gamma_{\rm QS}^{\rm (E)}}{\left(\beta_{\rm QS}^{\rm (E)}\right)^2} = \frac{2(1-2\nu_c)(1+\nu_c)(1-\phi)^2\overline{\kappa}}{\left\{\left[2(1-2\nu_c)+(1+\nu_c)\phi\right] - \left[(1+\nu_c)+2(1-2\nu_c)\phi\right]\overline{\kappa}\right\}^2}\,. \tag{4.92}$$

From these expressions, it is observed that away from $\beta_{\rm QS}^{\rm (E)} = 0$ the value of $\varepsilon_{\rm QS}$ is much less than unity. To highlight this, recall that $\overline{\kappa} = \overline{\kappa}_{\rm crit}$ when $\beta_{\rm QS}^{\rm (E)} = 0$, which based on Equation (4.90) varies over the range $0 \leq \nu_c \leq \frac{1}{2}$ between

$$\phi \leq \overline{\kappa}_{\rm crit} \leq \frac{2+\phi}{1+2\phi}. \tag{4.93}$$

Since $0 < \phi < 1$, this leads to a relatively narrow range for $\overline{\kappa}_{\rm crit}$, as illustrated in Figure 4.11. Away from $\overline{\kappa} = \overline{\kappa}_{\rm crit}$, the value of $\varepsilon_{\rm QS}$ becomes

$$\varepsilon_{\rm QS} = \begin{cases} \dfrac{2(1-2\nu_c)(1+\nu_c)(1-\phi)^2\overline{\kappa}}{\left[2(1-2\nu_c)+(1+\nu_c)\phi\right]^2}, & \overline{\kappa} \ll 1, \\ \dfrac{2(1-2\nu_c)(1+\nu_c)(1-\phi)^2}{\left[(1+\nu_c)+2(1-2\nu_c)\phi\right]^2\overline{\kappa}}, & \overline{\kappa} \gg 1, \end{cases} \tag{4.94}$$

which leads to $\varepsilon_{\rm QS} \ll 1$ in both cases.

Assuming that $\varepsilon_{\rm QS} \ll 1$, the expression for $\overline{\kappa}_c$ given by Equation (4.91) simplifies to

$$\overline{\kappa}_c \approx \begin{cases} \dfrac{\beta_{\rm QS}^{\rm (E)}}{\alpha_{\rm QS}^{\rm (E)}}, & \overline{\kappa} \ll 1, \\ \dfrac{-\gamma_{\rm QS}^{\rm (E)}}{\beta_{\rm QS}^{\rm (E)}}, & \overline{\kappa} \gg 1. \end{cases} \tag{4.95}$$

From Equation (4.86), it is noted that the case of $\overline{\kappa} \ll 1$ corresponds to $\beta_{\rm QS}^{\rm (E)} > 0$, whereas $\overline{\kappa} \gg 1$ corresponds to $\beta_{\rm QS}^{\rm (E)} < 0$. Thus, the resulting value for $\overline{\kappa}_c$ is positive for both cases, as observed in Figure 4.11. However, a striking feature of Figure 4.11 is seen as $\nu_c \to \frac{1}{2}$, where values of $\overline{\kappa}_c$ become increasing large for $\overline{\kappa} < \overline{\kappa}_{\rm crit}$, but remain relatively constant for the region where $\overline{\kappa} < \overline{\kappa}_{\rm crit}$.

To examine this difference between these two regions, consider the behavior of the solution given by Equation (4.95). Taking the limit $\nu_c \to \frac{1}{2}$ leads to $\alpha_{\mathrm{QS}}^{(\mathrm{E})} \to 0$, which from Equation (4.95) gives $\overline{\kappa}_c \to \infty$ when $\overline{\kappa} \ll 1$. When $\overline{\kappa} \gg 1$, however, $\overline{\kappa}_c$ is independent of $\alpha_{\mathrm{QS}}^{(\mathrm{E})}$. It is therefore unaffected by this limit and the solutions remains finite, as observed in Figure 4.11.

In a similar manner to $\overline{\kappa}_c$, an expression for the cloaking layer density can be obtained from the $n=1$ case, which yields

$$\overline{\rho}_c = \frac{1-\phi\overline{\rho}}{1-\phi}. \tag{4.96}$$

This relationship is the same as the one obtained using conservation of mass for the effective density of a coated sphere used in the static analysis of this configuration. Unlike the case of a fluid layer, there is no flow of the cloaking layer, and no inertial effects determining the required density. In addition, to achieve acoustic plasmonic cloaking with a single elastic layer with a positive density, from Equation (4.96) it is clear that this is only possible when $\overline{\rho} < (\frac{b}{a})^3$. For the fluid cloaking layer, there was no limitation on the density of the core material.

To examine the effectiveness of a single elastic layer as an acoustic plasmonic cloak, consider the limiting case of a pressure-release spherical core. This limit can be obtained by taking $\overline{\rho} \to 0$, and $\overline{\kappa} \to 0$, for which Equations (4.88) and (4.96) reduce to

$$\overline{\kappa}_c = \frac{2(1-2\nu_c) + (1+\nu_c)\phi}{2(1-\phi)(1-2\nu_c)}, \tag{4.97}$$

$$\overline{\rho}_c = \frac{1}{1-\phi}, \tag{4.98}$$

respectively. Using these expressions for $\overline{\kappa}_c$ and $\overline{\rho}_c$ as a guide, the first 5 scattering coefficients are plotted in Figure 4.12 for an uncloaked pressure-release sphere (top panel) and for a pressure-release sphere coated by an single elastic cloaking layer

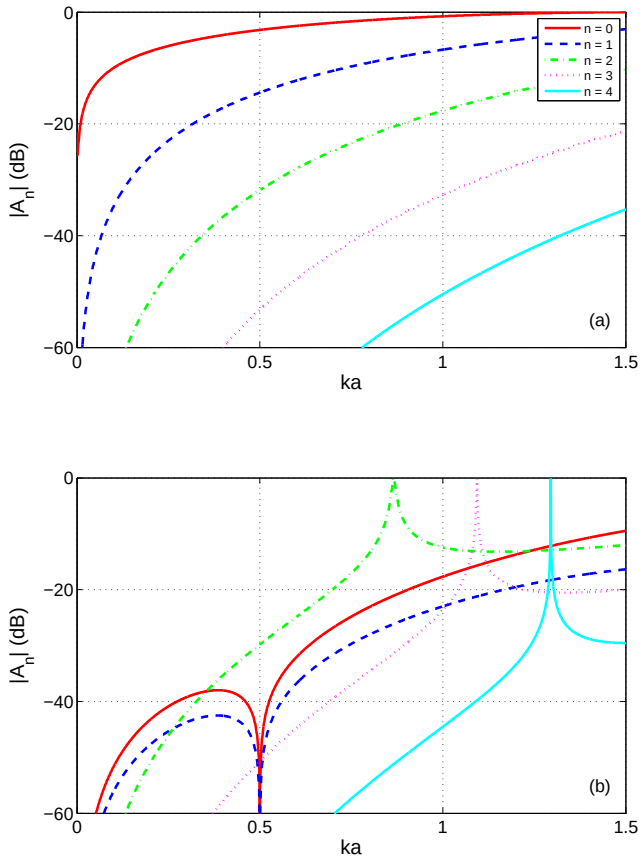

Figure 4.12: Scattering coefficients (in dB) for an uncloaked (top) and cloaked (bottom) pressure-release sphere. The cloak consists of a single elastic layer with $\nu_c = 0.3$ and $\frac{b}{a} = 1.10$, which cancels the first two scattering modes at $k_{d,0}a = 0.5$.

with $\frac{b}{a} = 1.10$ and a design frequency of $k_{d,0}a = 0.5$. Although cancellation of the first two modes is achieved at the desired frequency, there are significant contributions from higher order modes which mitigate the effectiveness of such a design, even at the relatively low frequency considered in this example. To improve the effectiveness, therefore, the cancellation of higher order modes must be addressed, which is addressed in the following chapters.

Chapter 5

Investigation of acoustic anti-resonance cloaking

In Chapter 4, analytic expressions for the simultaneous cancellation of acoustic scattering modes from a coated elastic sphere were developed, and approximate solutions were obtained for two cases: low-frequencies and thin shells, which are dependent on the relative size of the object and the wavelength of the incident wave. For frequencies beyond this range, resonances within the cloaking layer can occur which are not accounted for using either of these approximations. Consideration of the exact set of equations prescribing the cancellation of scattering modes allows for these effects to be analyzed. Furthermore, the anti-resonance features of the modal resonant structure within the cloaking layer can be utilized to cancel particular scattering modes, in addition to the plasmonic cloaking described in the Chapter 4. As for the case of plasmonic cloaks, this results in the alignment of multiple modal nulls at a single design frequency. A cloaking layer which utilizes this phenomenon is referred to in the following as an *anti-resonance cloak*, which will be investigated in this chapter.

To properly account for resonances within the cloaking layer, exact solutions for the cancellation of acoustic waves from an elastic sphere will be used. Since resonances can occur with both compressional and shear waves, a single cloaking layer consisting of an isotropic elastic solid will be considered. Due to the complexity of the resulting equations, it is not feasible to find explicit expressions for the cloaking layer properties. Instead, these properties will be determined numerically, with

insight obtained from how these properties change with respect to different parameters. The formulation of the necessary expressions to achieve cloaking are presented in Section 5.1. Since the focus of this chapter is on establishing physical insight into this particular type of cloak, only the simplest case of a single elastic layer will be discussed here, though all the concepts can be applied to more complicated configurations.

5.1 Formulation for a single elastic layer

As described in Section 3.3, the condition which must be prescribed to achieve cloaking is $A_n^{(0)}=0$. From Equation (3.26), it can be seen that the value of $A_n^{(0)}$ can be expressed in terms of two quantities: U_n and V_n. With U_n appearing in the numerator, the cloaking condition can be written as $|U_n|=0$, which was utilized in Chapter 4.

Consider an elastic sphere coated with a single elastic shell, the configuration and geometry of which are illustrated in Figure 5.1. For this case, Equations (3.26) and (3.27) become

$$\begin{vmatrix} u_{11}^{(n)} & u_{12}^{(n)} & u_{13}^{(n)} & u_{14}^{(n)} & u_{15}^{(n)} & 0 & 0 \\ u_{21}^{(n)} & u_{22}^{(n)} & u_{23}^{(n)} & u_{24}^{(n)} & u_{25}^{(n)} & 0 & 0 \\ 0 & u_{32}^{(n)} & u_{33}^{(n)} & u_{34}^{(n)} & u_{35}^{(n)} & 0 & 0 \\ 0 & u_{42}^{(n)} & u_{43}^{(n)} & u_{44}^{(n)} & u_{45}^{(n)} & u_{46}^{(n)} & u_{47}^{(n)} \\ 0 & u_{52}^{(n)} & u_{53}^{(n)} & u_{54}^{(n)} & u_{55}^{(n)} & u_{56}^{(n)} & u_{57}^{(n)} \\ 0 & u_{62}^{(n)} & u_{63}^{(n)} & u_{64}^{(n)} & u_{65}^{(n)} & u_{66}^{(n)} & u_{67}^{(n)} \\ 0 & u_{72}^{(n)} & u_{73}^{(n)} & u_{74}^{(n)} & u_{75}^{(n)} & u_{76}^{(n)} & u_{77}^{(n)} \end{vmatrix} = 0, \tag{5.1}$$

where the non-zero terms are developed in Appendix A and are given by

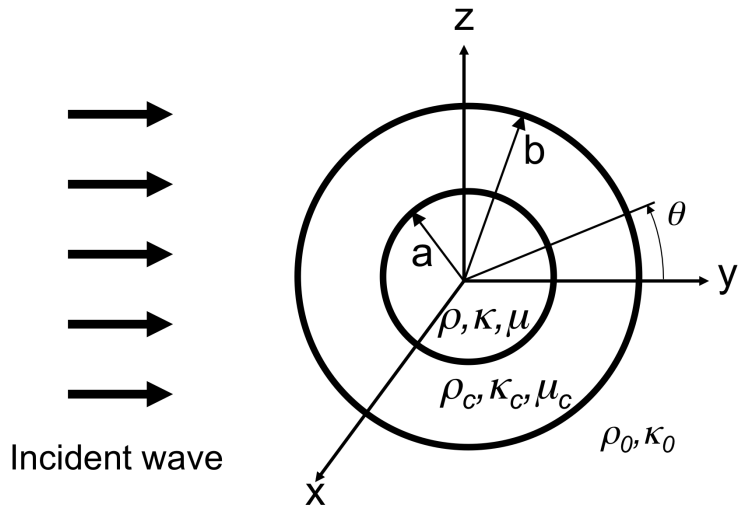

Figure 5.1: A time-harmonic incident plane wave in a fluid medium impinging on an isotropic elastic core of radius a coated with a single isotropic elastic shell with outer radius b. The surrounding medium has density ρ_0 and bulk modulus κ_0, and the elastic shell has density ρ_c, bulk modulus κ_c, and shear modulus μ_c. The elastic core has density ρ, bulk modulus κ and shear modulus μ.

$$u_{11}^{(n)} = k_{d,0}b\, j_n'(k_{d,0}b), \tag{5.2}$$

$$u_{12}^{(n)} = (k_{d,c}b)\, j_n^{'}(k_{d,c}b), \tag{5.3}$$

$$u_{13}^{(n)} = (k_{d,c}b)\, n_n^{'}(k_{d,c}b), \tag{5.4}$$

$$u_{14}^{(n)} = n(n+1)\, j_n(k_{s,c}b), \tag{5.5}$$

$$u_{15}^{(n)} = n(n+1)\, n_n(k_{s,c}b), \tag{5.6}$$

$$u_{21}^{(n)} = -\frac{1}{2}\, j_n(k_{d,0}b), \tag{5.7}$$

$$u_{22}^{(n)} = \overline{\rho}_c \frac{1}{(k_{s,c}b)^2}\left\{\left[n(n+1)-\frac{1}{2}(k_{s,c}b)^2\right] j_n(k_{d,c}b) - 2(k_{d,c}b) j_n^{'}(k_{d,c}b)\right\}, \tag{5.8}$$

$$u_{23}^{(n)} = \overline{\rho}_c \frac{1}{(k_{s,c}b)^2}\left\{\left[n(n+1) - \frac{1}{2}(k_{s,c}b)^2\right] n_n(k_{d,c}b) - 2(k_{d,c}b) n_n^{'}(k_{d,c}b)\right\}, \tag{5.9}$$

$$u_{24}^{(n)} = \overline{\rho}_c \frac{1}{(k_{s,c}b)^2} n(n+1)\left[(k_{s,c}b)\, j_n^{'}(k_{s,c}b) - j_n(k_{s,c}b)\right], \tag{5.10}$$

$$u_{25}^{(n)} = \overline{\rho}_c \frac{1}{(k_{s,c}b)^2} n(n+1)\left[(k_{s,c}b)\, n_n^{'}(k_{s,c}b) - n_n(k_{s,c}b)\right], \tag{5.11}$$

$$u_{32}^{(n)} = (k_{d,c}b) j_n^{'}(k_{d,c}b) - j_n(k_{d,c}b), \tag{5.12}$$

$$u_{33}^{(n)} = (k_{d,c}b) n_n^{'}(k_{d,c}b) - n_n(k_{d,c}b), \tag{5.13}$$

$$u_{34}^{(n)} = \left[n(n+1) - 1 - \frac{1}{2}(k_{s,c}b)^2\right] j_n(k_{s,c}b) - (k_{s,c}b) j_n^{'}(k_{s,c}b), \tag{5.14}$$

$$u_{35}^{(n)} = \left[n(n+1) - 1 - \frac{1}{2}(k_{s,c}b)^2\right] n_n(k_{s,c}b) - (k_{s,c}b) n_n^{'}(k_{s,c}b), \tag{5.15}$$

$$u_{42}^{(n)} = (k_{d,c}a) j_n^{'}(k_{d,c}a), \tag{5.16}$$

$$u_{43}^{(n)} = (k_{d,c}a) n_n^{'}(k_{d,c}a), \tag{5.17}$$

$$u_{44}^{(n)} = n(n+1) j_n(k_{s,c}a), \tag{5.18}$$

$$u_{45}^{(n)} = n(n+1) n_n(k_{s,c}a), \tag{5.19}$$

$$u_{46}^{(n)} = -\,(k_{\mathrm{d}}a) j_n^{'}(k_{\mathrm{d}}a), \tag{5.20}$$

$$u_{47}^{(n)} = -\,n(n+1) j_n(k_{\mathrm{s}}a), \tag{5.21}$$

$$u_{52}^{(n)} = j_n(k_{d,c}a), \tag{5.22}$$

$$u_{53}^{(n)} = n_n(k_{d,c}a), \tag{5.23}$$

$$u_{54}^{(n)} = (k_{s,c}a) j_n^{'}(k_{s,c}a) + j_n(k_{s,c}a), \tag{5.24}$$

$$u_{55}^{(n)} = (k_{s,c}a) n_n^{'}(k_{s,c}a) + n_n(k_{s,c}a), \tag{5.25}$$

$$u_{56}^{(n)} = -j_n(k_{\mathrm{d}}a), \tag{5.26}$$

$$u_{57}^{(n)} = -\,(k_{\mathrm{s}}a) j_n^{'}(k_{\mathrm{s}}a) - j_n(k_{\mathrm{s}}a), \tag{5.27}$$

$$u_{62}^{(n)} = \overline{\rho}_c \frac{1}{(k_{s,c}a)^2}\left\{\left[n(n+1) - \frac{1}{2}(k_{s,c}a)^2\right] j_n(k_{d,c}a) - 2(k_{d,c}a) j_n^{'}(k_{d,c}a)\right\}, \tag{5.28}$$

$$u_{63}^{(n)} = \overline{\rho}_c \frac{1}{(k_{s,c}a)^2}\left\{\left[n(n+1) - \frac{1}{2}(k_{s,c}a)^2\right] n_n(k_{d,c}a) - 2(k_{d,c}a) n_n^{'}(k_{d,c}a)\right\}, \tag{5.29}$$

$$u_{64}^{(n)} = \overline{\rho}_c \frac{1}{(k_{s,c}a)^2} n(n+1)\Big[(k_{s,c}a)j_n^{'}(k_{s,c}a) - j_n(k_{s,c}a)\Big], \tag{5.30}$$

$$u_{65}^{(n)} = \overline{\rho}_c \frac{1}{(k_{s,c}a)^2} n(n+1)\Big[(k_{s,c}a)n_n^{'}(k_{s,c}a) - n_n(k_{s,c}a)\Big], \tag{5.31}$$

$$u_{66}^{(n)} = -\overline{\rho} \frac{1}{(k_{\mathrm{s}}a)^2} \left\{ \left[n(n+1) - \frac{1}{2}(k_{\mathrm{s}}a)^2 \right] j_n(k_{\mathrm{d}}a) - 2(k_{\mathrm{d}}a) j_n^{'}(k_{\mathrm{d}}a) \right\}, \tag{5.32}$$

$$u_{67}^{(n)} = -\overline{\rho} \frac{1}{(k_{\mathrm{s}}a)^2} n(n+1)\Big[(k_{\mathrm{s}}a)j_n^{'}(k_{\mathrm{s}}a) - j_n(k_{\mathrm{s}}a)\Big], \tag{5.33}$$

$$u_{72}^{(n)} = \overline{\rho}_c \frac{1}{(k_{s,c}a)^2} \Big[(k_{d,c}a)j_n^{'}(k_{d,c}a) - j_n(k_{d,c}a)\Big], \tag{5.34}$$

$$u_{73}^{(n)} = \overline{\rho}_c \frac{1}{(k_{s,c}a)^2} \Big[(k_{d,c}a)n_n^{'}(k_{d,c}a) - n_n(k_{d,c}a)\Big], \tag{5.35}$$

$$u_{74}^{(n)} = \overline{\rho}_c \frac{1}{(k_{s,c}a)^2} \left\{ \left[n(n+1) - 1 - \frac{1}{2}(k_{s,c}a)^2 \right] j_n(k_{s,c}a) - (k_{s,c}a) j_n^{'}(k_{s,c}a) \right\}, \tag{5.36}$$

$$u_{75}^{(n)} = \overline{\rho}_c \frac{1}{(k_{s,c}a)^2} \left\{ \left[n(n+1) - 1 - \frac{1}{2}(k_{s,c}a)^2 \right] n_n(k_{s,c}a) - (k_{s,c}a) n_n^{'}(k_{s,c}a) \right\}, \tag{5.37}$$

$$u_{76}^{(n)} = -\overline{\rho} \frac{1}{(k_{\mathrm{s}}a)^2} \Big[(k_{\mathrm{d}}a)j_n^{'}(k_{\mathrm{d}}a) - j_n(k_{\mathrm{d}}a)\Big], \tag{5.38}$$

$$u_{77}^{(n)} = -\overline{\rho} \frac{1}{(k_{\mathrm{s}}a)^2} \left\{ \left[n(n+1) - 1 - \frac{1}{2}(k_{\mathrm{s}}a)^2 \right] j_n(k_{\mathrm{s}}a) - (k_{\mathrm{s}}a) j_n^{'}(k_{\mathrm{s}}a) \right\}, \tag{5.39}$$

with $\overline{\rho}_c = \rho_c/\rho_0$ and $\overline{\rho} = \rho/\rho_0$.

Unlike the condition $|U_n| = 0$, $|V_n| = 0$ identifies the modal resonances, which result in a value of $A_n^{(0)}$ equal to unity. It is worthwhile to note that the solutions for $|V_n| = 0$ do not directly relate to the condition for cloaking. However, the location of the modal resonances within the parameter space is valuable for identifying anti-resonances. Anti-resonances occur in between two resonances, and like the plasmonic solutions obtained in Section 4.1 correspond to $|U_n| = 0$. For a single elastic cloaking

layer with an elastic core, Equation (3.28) reduces to

$$\begin{vmatrix} v_{11}^{(n)} & u_{12}^{(n)} & u_{13}^{(n)} & u_{14}^{(n)} & u_{15}^{(n)} & 0 & 0 \\ v_{21}^{(n)} & u_{22}^{(n)} & u_{23}^{(n)} & u_{24}^{(n)} & u_{25}^{(n)} & 0 & 0 \\ 0 & u_{32}^{(n)} & u_{33}^{(n)} & u_{34}^{(n)} & u_{35}^{(n)} & 0 & 0 \\ 0 & u_{42}^{(n)} & u_{43}^{(n)} & u_{44}^{(n)} & u_{45}^{(n)} & u_{46}^{(n)} & u_{47}^{(n)} \\ 0 & u_{52}^{(n)} & u_{53}^{(n)} & u_{54}^{(n)} & u_{55}^{(n)} & u_{56}^{(n)} & u_{57}^{(n)} \\ 0 & u_{62}^{(n)} & u_{63}^{(n)} & u_{64}^{(n)} & u_{65}^{(n)} & u_{66}^{(n)} & u_{67}^{(n)} \\ 0 & u_{72}^{(n)} & u_{73}^{(n)} & u_{74}^{(n)} & u_{75}^{(n)} & u_{76}^{(n)} & u_{77}^{(n)} \end{vmatrix} = 0, \tag{5.40}$$

where the only differing terms from those in U_n are $v_{11}^{(n)}$ and $v_{21}^{(n)}$, which are given by

$$v_{11}^{(n)} = -k_{d,0} b \, n_n'(k_{d,0} b), \tag{5.41}$$

$$v_{21}^{(n)} = \frac{1}{2} n_n(k_{d,0} b), \tag{5.42}$$

Equations (5.1) and (5.40) could be expanded using the analytic techniques described in Section 4.1, yielding expressions analogous to Equation (4.26). However, without the further simplifications of either quasi-static conditions or a thin shell, an expression of this form does not allow for explicit solutions in terms of the cloaking layer properties. These simplifications preclude capturing resonant behavior, thus solutions for the anti-resonance cloaking layer properties must be solved implicitly. To do this, Equation (5.1) can be solved for N cloaking layer properties by prescribing $|U_n| = 0$ for the first N modes at the same design frequency, with the remaining cloaking layer material properties and geometric variables treated as

independent parameters. This gives a system of N equations with N unknowns,

$$\begin{aligned} |U_0(x_1, x_2, \ldots, x_N)| &= 0, \\ |U_1(x_1, x_2, \ldots, x_N)| &= 0, \\ &\vdots \\ |U_N(x_1, x_2, \ldots, x_N)| &= 0, \end{aligned} \tag{5.43}$$

where $x_1, x_2, \ldots, x_N$ are the cloaking layer properties to be determined. Note that the cloaking layer properties in Equation (5.1) appear within the arguments of spherical Bessel functions, which are multiplied together with spherical Bessel functions containing other cloaking layer properties. Thus, Equation (5.43) represents a nonlinear system of equations, for which various numerical solution techniques exist. In this work, this system is solved using the *fsolve* function in MATLAB, which utilizes a nonlinear least-squares algorithm [70].

5.2 Anti-resonance cloaking of a rigid sphere

To investigate the nature of anti-resonance cloaks further, consider the limiting case of a rigid, immovable sphere which was considered in Section 4.2. Although many different combinations of anti-resonance alignment are possible, the combinations of interest here are those which build upon the effectiveness of plasmonic cloaking, with the objective of using these anti-resonances to cancel more modes than otherwise possible.

5.2.1 Determining anti-resonance behavior

For a rigid, immovable sphere, plasmonic cloaking was demonstrated with a fluid layer in Section 4.2. However, the presence of an elastic layer presents a potential problem. As observed in Section 4.5, use of the quasi-static solution showed

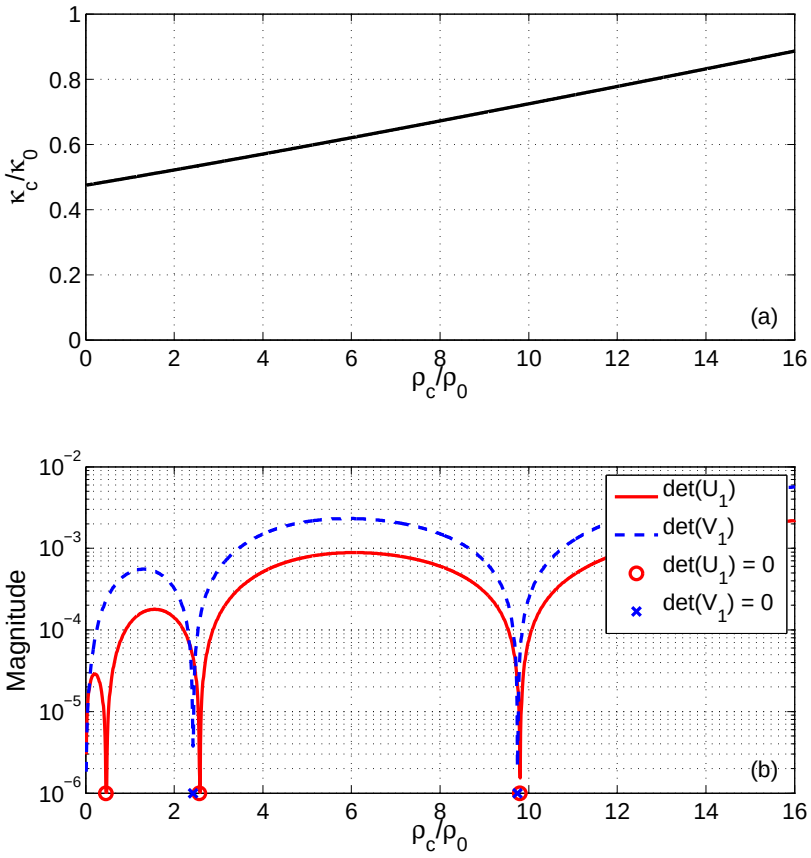

Figure 5.2: Parametric study of the solutions satisfying $|U_n|=0$ for a rigid, immovable sphere coated in a single elastic cloaking layer with $\nu_c=0.49$ and $\frac{b}{a}=1.30$ at $k_{d,0}a=1.0$. In (a), $|U_0|=0$ is solved for $\overline{\kappa}_c$ as a function of $\overline{\rho}_c$. In (b), the magnitude of $|U_1|$ and $|V_1|$ are plotted as a function of $\overline{\rho}_c$.

that achieving a plasmonic cloak which cancels the first two scattering modes is only possible when $\overline{\rho} < (\frac{b}{a})^3$. This means that, based on the analysis in Chapter 4, a plasmonic cloak cannot be achieved for a rigid, immovable sphere (for which $\overline{\rho}\to\infty$).

Despite this limitation on $\overline{\rho}$, it was noted in Section 4.5 that there was no restrictions on the compressibility of the core material. Since the monopole ($n=0$)

Parameter	1^{st} Anti-Res.	2^{nd} Anti-Res.	3^{rd} Anti-Res.
ρ_c/ρ_0	0.4656	2.5767	9.8060
κ_c/κ_0	0.4852	0.5352	0.7191
ν_c	0.49	0.49	0.49

Table 5.1: Material properties of a single elastic cloaking layer designed at $k_{d,0}a=1.0$ with $\dfrac{b}{a}=1.30$ for a rigid, immovable sphere.

mode is dominated by $\overline{\kappa}$, this suggests that the values of $\overline{\kappa}_c$ developed for a plasmonic cloak should still lead the same non-resonant cancellation for this particular mode. To achieve cancellation of the $n=0$ and $n=1$ simultaneously, an anti-resonance of the $n=1$ mode can be aligned with the non-resonant null in the $n=0$ mode.

Although an initial guess of $\overline{\kappa}_c$ can be based on a fluid plasmonic cloak, there is no basis for an initial guess of $\overline{\rho}_c$. In addition, since the nulls in this particular case arise from a resonance phenomenon, there can potentially be an infinite number of solutions giving rise to significantly different values of $\overline{\rho}_c$. To examine how these various solutions vary with $\overline{\rho}_c$, Figure 5.2 shows $\overline{\kappa}_c$, $|U_1|$ and $|V_1|$ plotted versus $\overline{\rho}_c$. Figure 5.2(a) shows the value of $\overline{\kappa}_c$ for a given $\overline{\rho}_c$, obtained by solving Equation (5.43) with $n=0$, using the plasmonic value of $\overline{\kappa}_c$ as an initial guess, at $k_{d,0}a = 1.0$ with $b/a = 1.30$ and $\nu_c = 0.49$. Using these layer properties, the magnitude of $|U_1|$ and $|V_1|$ can be calculated, as shown in Figure 5.2(b). From Figure 5.2(b), the layer properties which achieve cancellation of both $n = 0$ and $n=1$ correspond to the points where $|U_1|=0$, which are denoted by the red circles. Similarly, modal resonances for $n = 1$ can be determined from the points where $|V_1|=0$, which are denoted by the blue x's.

Over the range of $\overline{\rho}_c$ shown in Figure 5.2, there are three points for which $|U_0|=|U_1|=0$, corresponding to the first three anti-resonances and give three possi-

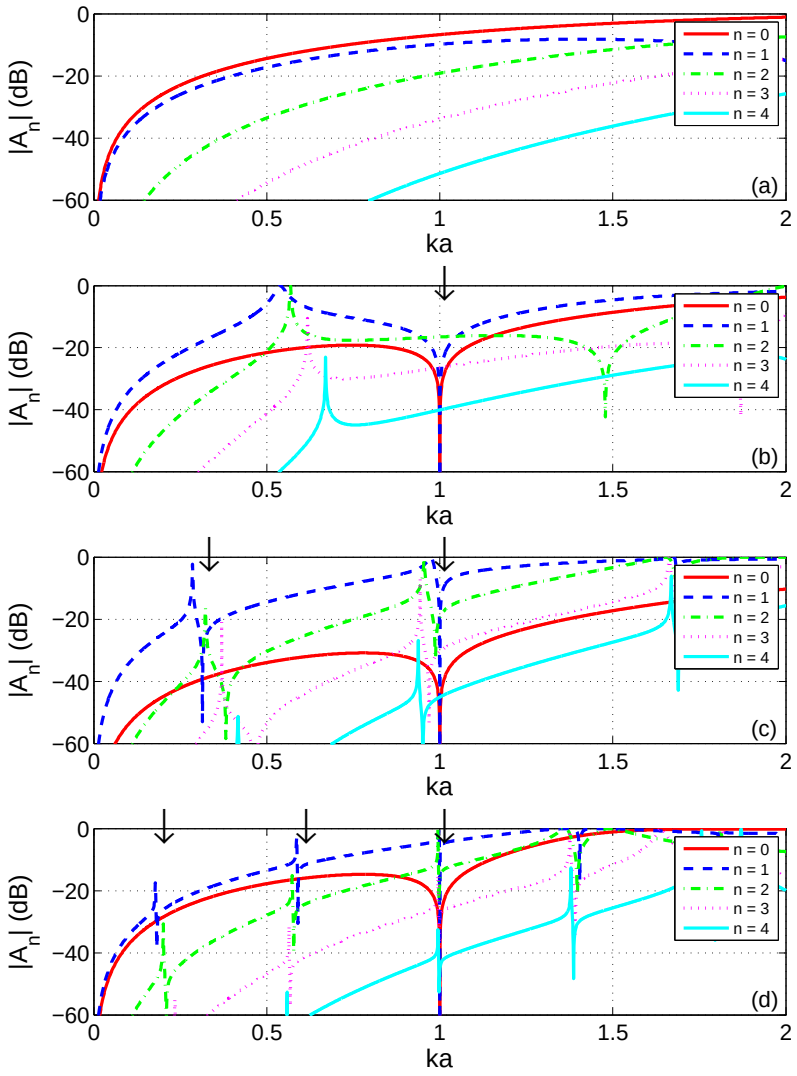

Figure 5.3: Magnitude of the scattering coefficients (in dB) for a rigid, immovable sphere: (a) uncloaked, (b) cloaked using the first anti-resonance, (c) cloaked using the second anti-resonance, and (d) cloaked using the third anti-resonance. All the cloaks consist of a single elastic layer with $\nu_c = 0.49$ and $\frac{b}{a} = 1.30$, designed to cancel the first two modes at $k_{d,0}a = 1.0$, with the material properties listed in Table 5.1.

ble anti-resonance cloaks. The cloaking layer properties for each case are listed in Table 5.1. To examine these three anti-resonance cloaks, the magnitude of the first 5 scattering coefficients are displayed in Figure 5.3. Figure 5.3(a) shows the scattering coefficients for an uncloaked rigid, immovable sphere. Without any coating, it is clear that there are no nulls present over the range of $k_{d,0}a$ shown.

In Figure 5.3(b), cancellation occurs in the scattering coefficients at $k_{d,0}a = 1.0$ for $n = 0$ and $n = 1$. For $n = 0$, this is a non-resonant null, similar to those seen in plasmonic cloaks. For $n = 1$, the null at $k_{d,0}a = 1.0$ which corresponds to the first anti-resonance and is denoted by a black arrow. Although resonances are present within the frequency band shown, it can be seen that the the first modal resonance for $n = 1$ occurring near $k_{d,0}a = 0.55$, away from the anti-resonance at $k_{d,0}a = 1.0$. In Figure 5.3(c), however, there is a resonance much closer to the anti-resonance at $k_{d,0}a = 1.0$. Furthermore, it can be observed that there are two anti-resonances, which are denoted by the black arrows. In this case, the second anti-resonance is aligned with the non-resonant null for the $n = 0$ mode to create the anti-resonance cloak.

In Figure 5.3(d), the first three anti-resonances in the $n = 1$ mode are denoted with a black arrow. In this case, the third anti-resonance is used to cancel the scattering coefficient at $k_{d,0}a = 1.0$. Comparing Figures 5.3(b)–(d), it can be seen that the available cloaking bandwidth decreases significantly as higher anti-resonances are used. In addition to the presence of more resonances which accompany these anti-resonances, a more significant effect is the shift in the location of the resonance upwards in frequency towards the associated anti-resonances, due to the observed reduction in bandwidth. This effect is quite extreme using the second anti-resonance or above, effectively limiting the cancellation to a very narrow notch, as illustrated in Figures 5.3(c) and (d). This indicates that cloaks designed using these higher

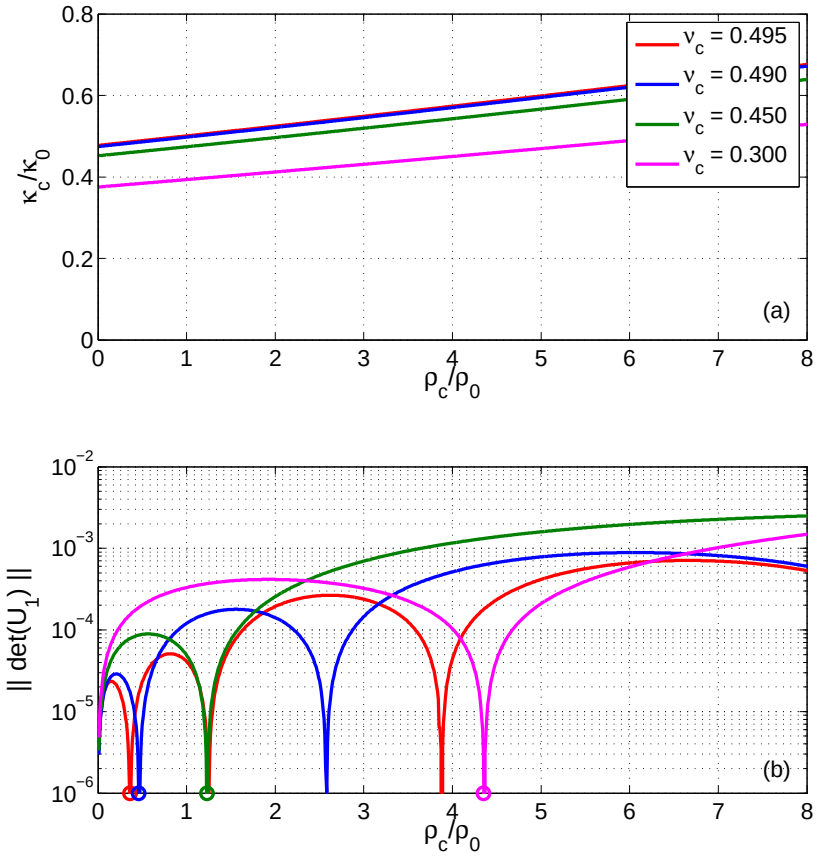

Figure 5.4: Parametric study of the solutions satisfying $|U_n|=0$ for a rigid, immovable sphere coated in a single elastic cloaking layer with $\frac{b}{a}=1.30$ at $k_{d,0}a=1.0$. In (a), $|U_0|=0$ is solved for $\overline{\kappa}_c$ as a function of $\overline{\rho}_c$. In (b), the magnitude of $|U_1|$ is plotted as a function of $\overline{\rho}_c$. Results are shown for $\nu_c=0.495$ (red), $\nu_c=0.490$ (blue), $\nu_c=0.450$ (green), and $\nu_c=0.300$ (magenta).

anti-resonances may be less robust in the presence of losses.

5.2.2 Effects of elastic shear within the cloaking layer

Based on the results presented in Figures 5.2 and 5.3, and tabulated in Table 5.1, it is clear that, despite the existence of a large number of possible anti-

Parameter	Case 1	Case 2	Case 3	Case 4
ρ_c/ρ_0	0.3640	0.4656	1.2311	4.3596
κ_c/κ_0	0.4858	0.4852	0.4791	0.4571
ν_c	0.495	0.490	0.450	0.300

Table 5.2: Material properties of a single elastic cloaking layer designed at $k_{d,0}a=1.0$ with $\dfrac{b}{a}=1.30$ for a rigid, immovable sphere, based on the first anti-resonance of the $n=1$ mode.

resonances, it is the lowest anti-resonances that are of most interest for practical applications. Thus, it is important to examine how these fundamental anti-resonances depend on the cloaking layer properties. As noted in Table 5.1, the anti-resonance cloaking results investigated up until this point were at $\nu_c=0.49$. This represents a nearly incompressible elastic solid, with a very low shear modulus compared to the bulk modulus and correspondingly low shear wave speed. With a low shear wave speed, this allows for resonance and anti-resonance modal patterns to be present in the layer for higher modes, while retaining the non-resonant compressibility effects of the monopole mode.

To examine the effects of the shear properties of the cloaking layer, Figure 5.4 presents the $\overline{\kappa}_c$ and $|U_1|$ as a function $\overline{\rho}_c$ for several values of ν_c. These results are obtained in the same manner as those presented in Figure 5.2, which are plotted in blue ($\nu_c=0.49$) in Figure 5.4. From Figure 5.4(a), there is slight decrease observed in the overall magnitude of $\overline{\kappa}_c$ with decreasing values of ν_c (corresponding to an increase in $\overline{\mu}_c$). Such a variation is to be expected, since an increase in the shear modulus produces an increase in the effective compressibility due to the Poisson effect, thereby leading to a lower value of $\overline{\kappa}_c$ required to yield the same effective stiffness. Besides this modest reduction in the overall magnitude, however, the

overall functional dependence of $\overline{\kappa}_c$ on $\overline{\rho}_c$ does not change with ν_c.

In Figure 5.4(b), the magnitude of $|U_1|$ is plotted versus $\overline{\rho}_c$ for each value of ν_c. In each case, the first zero crossing (i.e. first anti-resonance) is highlighted with a circle. From this figure, it is seen that there is strong dependence of the solutions for $|U_1| = 0$ on ν_c. In particular, it is observed that the number of zero crossings increases as $\nu_c \to 0.5$, while the corresponding $\overline{\rho}_c$ at which the first zero-crossing occurs decreases. The resulting cloaking layer properties based on the first anti-resonances for each Poisson's ratio are listed in Table 5.2.

Although the first anti-resonances show a distinct trend in Figure 5.4(b), this figure shows the importance of understanding which anti-resonances are being sought and determining an accurate initial guess. This is highlighted by the fact that in the figure, the first anti-resonance with $\nu_c = 0.45$ is nearly identical to the second anti-resonance with $\nu_c = 0.49$. The corresponding values of $\overline{\kappa}_c$ are very close, yet previous results clearly indicate that the achievable bandwidth would be significantly reduced by using the second anti-resonance.

Even using only the first anti-resonance, the bandwidth of an anti-resonance cloak can be significantly affected by the value of ν_c. The magnitude of the first five scattering coefficients are illustrated in Figure 5.5(a)–(c) for $\nu_c = 0.3$, 0.45 and 0.49, respectively. As ν_c increases from $\nu_c = 0.3$ in (a) to $\nu_c = 0.45$ in (b) and $\nu_c = 0.49$ in (c), there is significant movement of the resonance peak away from the anti-resonance null at $k_{d,0}a = 1.0$. By comparison, the changes in the monopole appear almost negligible when plotted on the decibel scale shown in the figures. With respect to the cancellation of the first two modes, it is clear that the bandwidth steadily improves as $\nu_c \to 0.5$.

Although the anti-resonance cloaking layers illustrated in Figure 5.5(a)–(c) were designed based on minimizing contributions from the $n = 0$ and $n = 1$ modes,

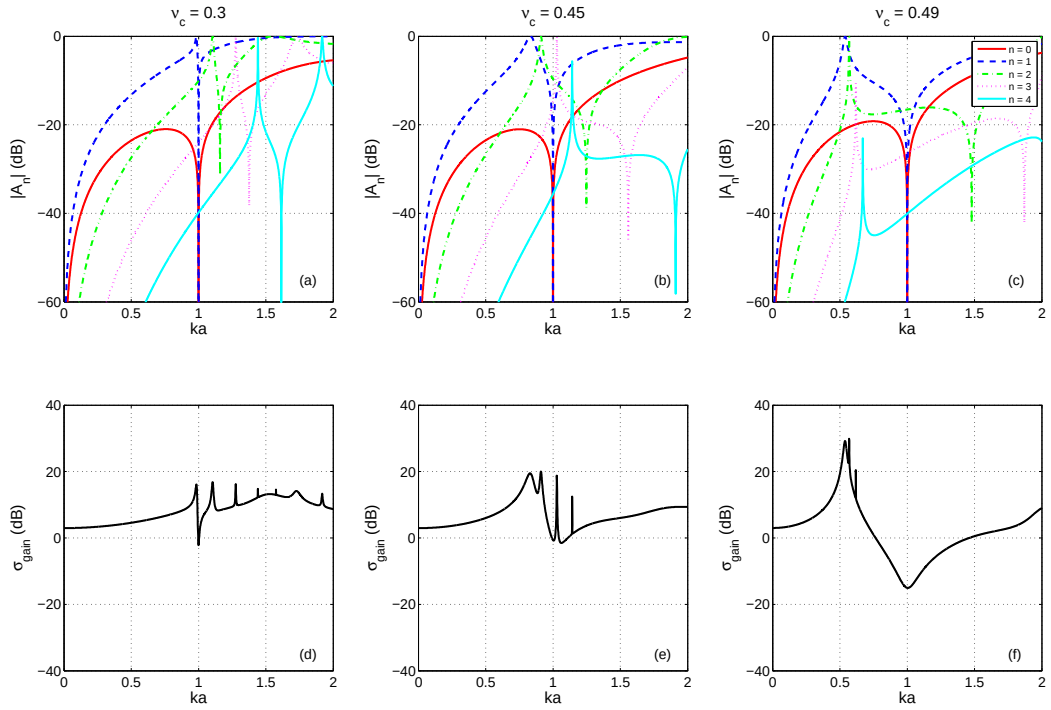

Figure 5.5: Magnitude of the scattering coefficients (in dB) for a rigid, immovable sphere cloaked using a single elastic layer with $\frac{b}{a} = 1.30$ and: (a) $\nu_c = 0.3$, (b) $\nu_c = 0.45$, (c) $\nu_c = 0.49$. The cloaks are designed to cancel the first 2 modes at $k_{d,0}a = 1.0$, with the material properties listed in Table 5.2. The scattering gain in dB, relative to the uncloaked scatterer, is given for (d) $\nu_c = 0.3$, (e) $\nu_c = 0.45$, (f) $\nu_c = 0.49$.

it is important to recall that the $n \geq 2$ modes also contribute to the total scattered field. With an anti-resonance cloak, these higher modes can provide a significant source of the scattering, especially in the vicinity of the modal resonances for these modes. These effects are observed in Figure 5.5(a)–(c), in which the first resonance of the higher modes start off above $k_{d,0}a = 1.0$ for $\nu_c = 0.3$, and are significantly reduced in frequency as the resonance of the $n = 1$ mode is decreased. As a result, there are certain configurations for which the resonances of the higher order modes

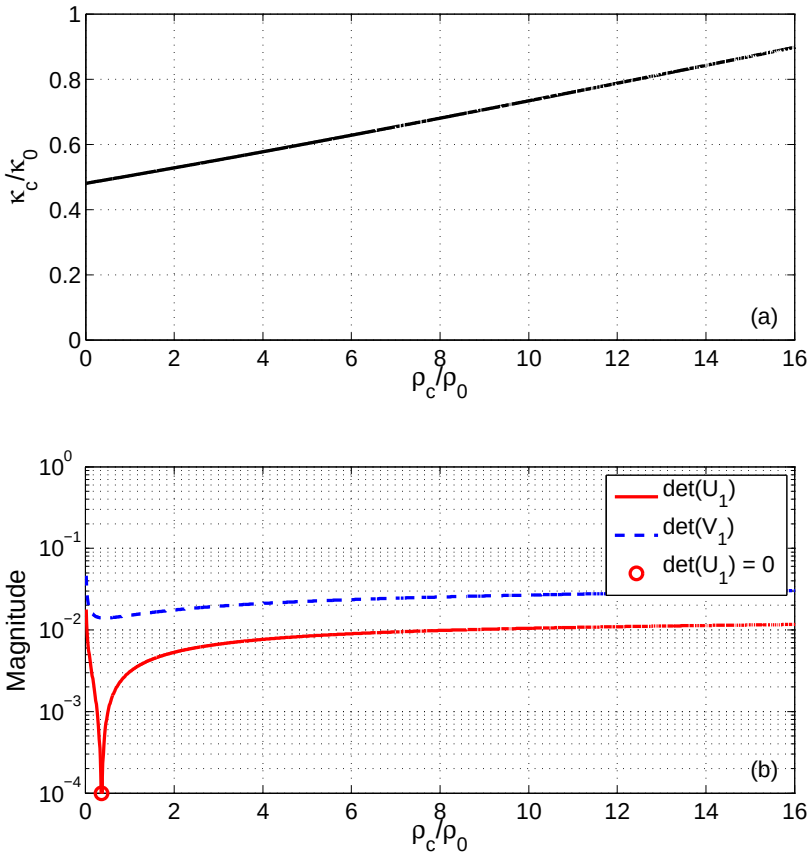

Figure 5.6: Parametric study of the solutions satisfying $|U_n| = 0$ for a rigid, immovable sphere coated in a single fluid cloaking layer with $\frac{b}{a} = 1.30$ at $k_{d,0}a = 1.0$. In (a), $|U_0| = 0$ is solved for $\overline{\kappa}_c$ as a function of $\overline{\rho}_c$. In (b), the magnitude of $|U_1|$ and $|V_1|$ are plotted as a function of $\overline{\rho}_c$.

occur at $k_{d,0}a = 1.0$, which occurs in this example when $\nu_c = 0.45$.

To quantify the total effect of each scattering mode and the overall change in scattering strength compared to an uncloaked scatterer, the scattering gain is given in Figure 5.5(d)–(f) for $\nu_c = 0.3$, 0.45 and 0.49, respectively. In Figure 5.5(d) and (e), it is apparent that the resulting anti-resonance cloak fails to provide any

reduction in scattering gain. This is due to the close proximity of the $n=2$ resonance to $k_{d,0}a = 1.0$. However, by moving the resonances of the $n \geq 1$ modes well below $k_{d,0}a = 1.0$, about 15 dB of scattering reduction can be achieved at the design frequency over a wide bandwidth using $\nu_c = 0.49$, as shown in Figure 5.5(f).

5.2.3 Limiting case of a fluid cloaking layer

It is clear from the analysis that ν_c close to 0.5 yields the best performance for an anti-resonance cloak in the case of a rigid, immovable sphere. It is therefore of interest to compare these results with those of a fluid cloaking layer, which is equivalent to having $\nu_c = 0.5$, with no shear waves present in the cloaking layer. In a similar manner to the elastic cloaking layer, $\overline{\kappa}_c$ and $|U_1|$ are presented as a function of $\overline{\rho}_c$ in Figure 5.6(a) and (b), respectively. As expected, $\overline{\kappa}_c$ is nearly identical to the one obtained with ν_c close to 0.5, which are shown in Figure 5.4(a).

Figure 5.6(b), in contrast, is significantly different compared with the results in Figure 5.4(b). For the case of a fluid cloaking layer, there is only one solution for which $|U_1| = 0$, occurring in a region for which $|V_n| \neq 0$. This indicates that the only available solution corresponds to a non-resonant plasmonic cloak, and that no anti-resonance solution exists. To confirm this, the magnitude of the first 5 scattering coefficients are plotted in Figure 5.7 using the solution for $|U_0| = |U_1| = 0$. This illustrates that the first two scattering modes are cancelled using non-resonant nulls, which is indicative of a plasmonic cloak as described in Chapter 4.

5.3 Anti-resonance cloaking of an elastic sphere

For some applications, non-rigid scatterers must be considered, which can significantly affect the scattering reduction achieved with an anti-resonance cloak as well as the necessary cloaking layer properties. As was discovered in the previous

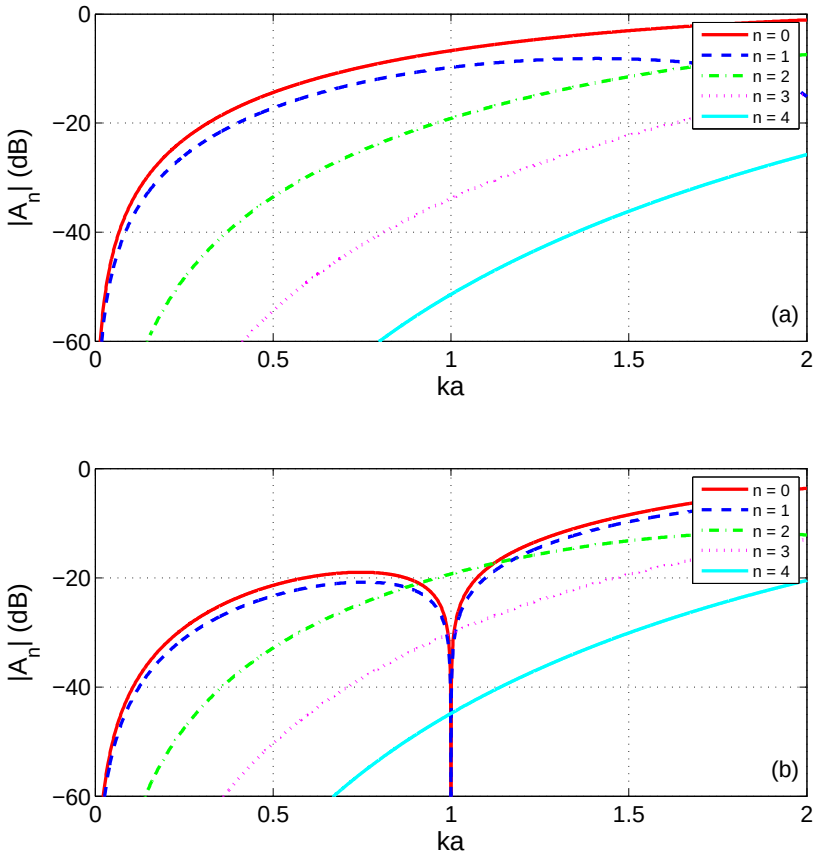

Figure 5.7: Magnitude of the scattering coefficients (in dB) for a rigid, immovable sphere: (a) uncloaked, and (b) cloaked using a single fluid layer with $\frac{b}{a} = 1.30$, designed to cancel the first two modes at $k_{d,0}a = 1.0$.

section, an anti-resonance cloak for a rigid, immovable sphere requires a wide range of cloaking layer densities, depending on the shear properties of the layer and anti-resonance utilized. It is therefore expected that such a cloak might also be sensitive to the density of the core material. In addition, it is important to consider the potential existence of plasmonic cloaking effects when $\overline{\rho} < (\frac{b}{a})^3$, which was not applicable for the case of the rigid, immovable sphere with an elastic cloaking layer

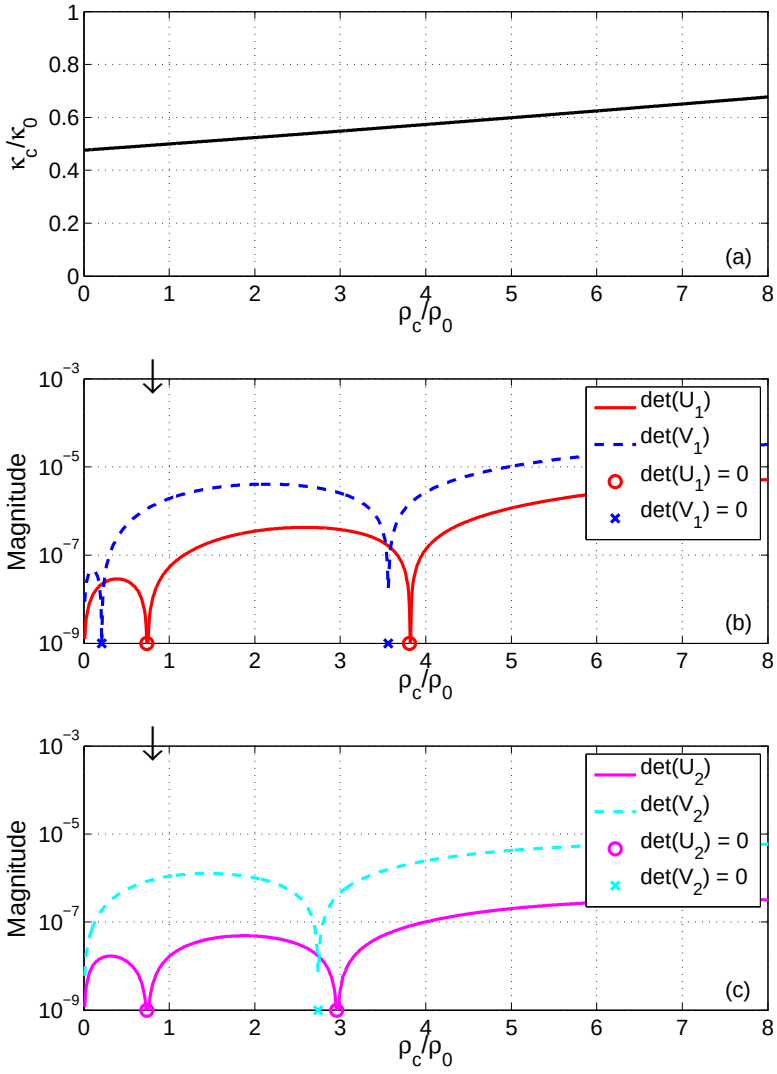

Figure 5.8: Parametric study of the solutions satisfying $|U_n|=0$ for a stiff, neutrally buoyant sphere coated in a single elastic cloaking layer with $\nu_c=0.4884$ and $\frac{b}{a}=1.30$ at $k_{d,0}a = 1.0$. In (a), $|U_0| = 0$ is solved for $\overline{\kappa}_c$ as a function of $\overline{\rho}_c$. In (b), the magnitude of $|U_1|$ and $|V_1|$ are plotted as a function of $\overline{\rho}_c$. In (c), the magnitude of $|U_2|$ and $|V_2|$ are plotted as a function of $\overline{\rho}_c$.

discussed in Section 5.2.

Parameter	Water	Stiff, Neutrally Buoyant	Air
Density, ρ(kg/m^3)	1000	1000	1.21
Bulk Modulus, κ(GPa)	2.19	419	1.42×10^{-4}
Shear Modulus, μ(GPa)	0	175	0

Table 5.3: Material properties of spheres to be cloaked in Sections 5.3 and 5.4.

To examine these factors, one can consider the case of a stiff, neutrally buoyant sphere in water, the properties of which are given in Table 5.3. For this example, the bulk modulus is much larger than that of the surrounding water, behaving almost like a rigid target with respect to the compressibility. Unlike the immovable sphere, the density in this case is not only finite but equal to that of the surrounding water. In addition to providing insight into the nature of anti-resonance cloaking, this example represents a situation of practical importance, since a primary design objective for many underwater vehicles and submerged structures is achieving the stiffness to withstand large hydrostatic pressures while maintaining a near-neutral buoyancy to enable movement through the water.

To determine the values of $\overline{\rho}_c$ which can be used to create an anti-resonance cloak, $\overline{\kappa}_c$, $|U_1|$ and $|U_2|$ are plotted versus $\overline{\rho}_c$ in Figure 5.8 (a)–(c), respectively. From Figure 5.8 (a), the $\overline{\kappa}_c$ based on $|U_0| = 0$ matches the results observed for the rigid, immovable sphere. Given that the neutrally buoyant sphere considered here has such a large compressibility, this is to be expected. Examining Figure 5.8 (b) and (c), there are two distinct points where $|U_n| = 0$ for each mode over the range of $\overline{\rho}_c$ shown. In particular, the first zeros in (b) and (c), which are highlighted by a black arrow, occur at the same value of $\overline{\rho}_c$. As a result, an anti-resonance cloak for this particular configuration provides cancellation of the first three modes ($n = 0$, 1, and 2) using a single elastic layer, with the properties listed in Table 5.4.

Parameter	Stiff, Neutrally Buoyant	Vaccuum	Air
ρ_c/ρ_0	0.7461	3.9148	3.9183
κ_c/κ_0	0.4934	6.3811	6.3879
ν_c	0.4884	0.3	0.3
Design $k_{d,0}a$	1.0	1.75	1.75

Table 5.4: Properties of a single elastic cloaking layer with $\frac{b}{a}=1.30$ for the different core materials examined in Sections 5.3 and 5.4.

To examine the frequency dependence in this case, the magnitude of the first 5 scattering coefficients are presented in Figure 5.9(a) and (b) for the uncloaked and cloaked configurations, respectively. As seen in Figure 5.8, the first three scattering modes are cancelled at $k_{d,0}a=1.0$. As with the rigid, immovable sphere, the choice of $\nu_c=0.4884$ in this case produces an anti-resonance cloak with a sufficient bandwidth over which the scattering strength is reduced, as illustrated in Figure 5.9(c). In Figure 5.9(c), the benefits of canceling the first three modes while moving the modal resonances away from the design frequency are readily apparent, with nearly 40 dB of scattering reduction achieved relative to the uncloaked scatterer. To independently verify these results, a numerical simulation using COMSOL was implemented, as described in Appendix C. The results of this analysis are given in Figure 5.9(c), showing excellent agreement with the theoretical solution developed in this section.

To illustrate this further, the real part of the total pressure field is shown in Figure 5.10(a) and (b) for the uncloaked and cloaked configurations, respectively. In these plots, the incident wave is a time harmonic plane wave moving from the bottom to the top of the figure. For the uncloaked stiff, neutrally buoyant sphere, disruption in the phase fronts of the incident wave due to the presence of the scatterer are apparent. With the addition of the anti-resonance cloaking layer, the incident

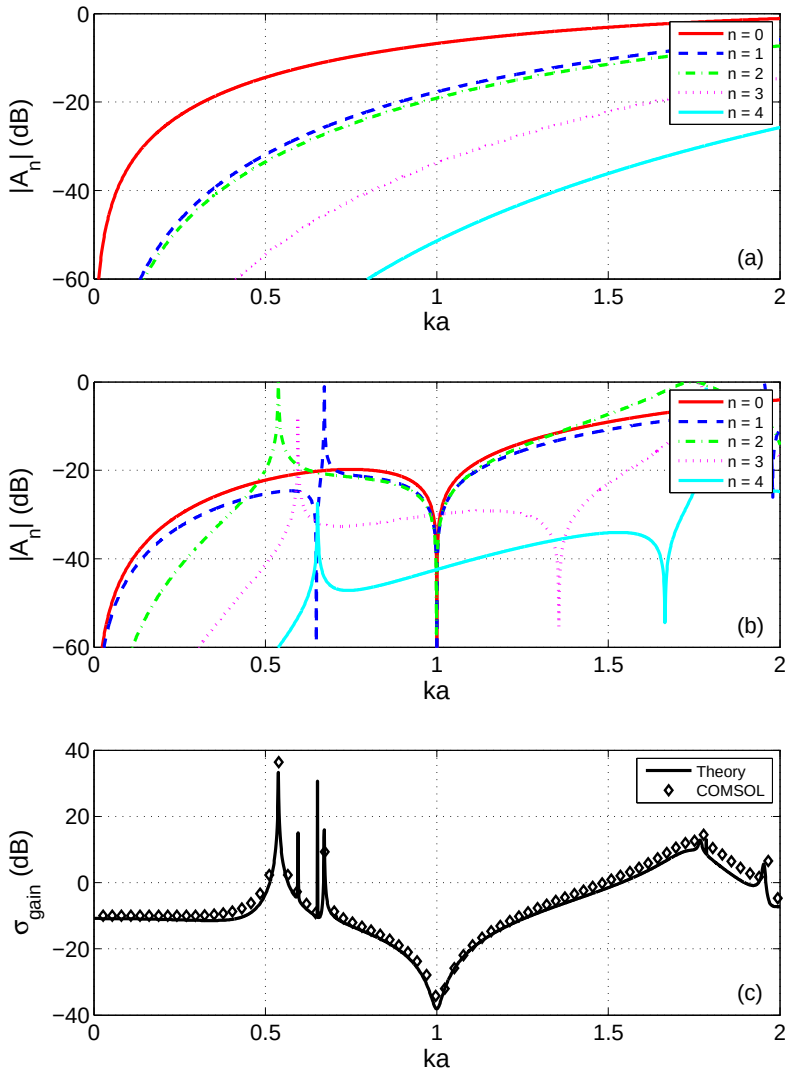

Figure 5.9: Magnitude of the scattering coefficients (in dB) for a stiff, neutrally buoyant sphere: (a) uncloaked, and (b) cloaked using a single elastic layer with $\nu_c = 0.4884$ and $\dfrac{b}{a} = 1.30$, designed to cancel the first two modes at $k_{d,0}a = 1.0$, with the material properties listed in Table 5.4. The scattering gain in dB, relative to the uncloaked scatterer, is given in (c) for the exact theoretical solution and using finite elements (COMSOL).

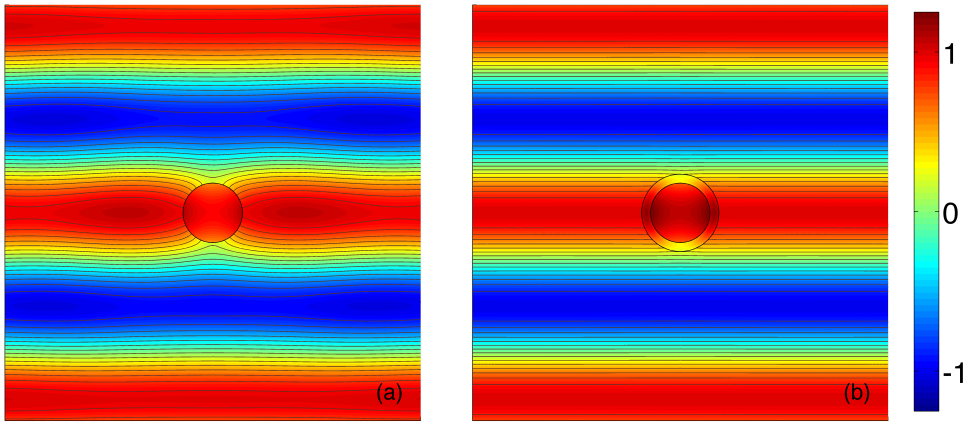

Figure 5.10: Real part of total pressure field for a stiff, neutrally buoyant sphere: (a) uncloaked, and (b) cloaked using a single elastic layer with $\nu_c = 0.4884$ and $\frac{b}{a} = 1.30$, designed to cancel the first two modes at $k_{d,0}a = 1.0$, with the material properties listed in Table 5.4. The color scale for the pressure is normalized to the amplitude of the incident wave, which is a time-harmonic plane wave traveling from bottom to top with a frequency of $k_{d,0}a = 1.0$.

wave passes around the target nearly unaffected. It is interesting to note that even though there are standing shear waves within the cloaking layer, there are no significant pressure gradients observed in Figure 5.10(b). Based on the similarity of the scattering coefficients (and scattering gain) for the anti-resonance cloak shown in Figure 5.9 and those of plasmonic cloaks examined in Chapter 4, this apparently non-resonant pressure field within the cloaking layer is not surprising.

5.4 Anti-resonance cloaking of a hollow sphere

Based on the results using an anti-resonance cloak for the stiff, neutrally buoyant sphere, it is clear that cancellation of the first three modes with a single

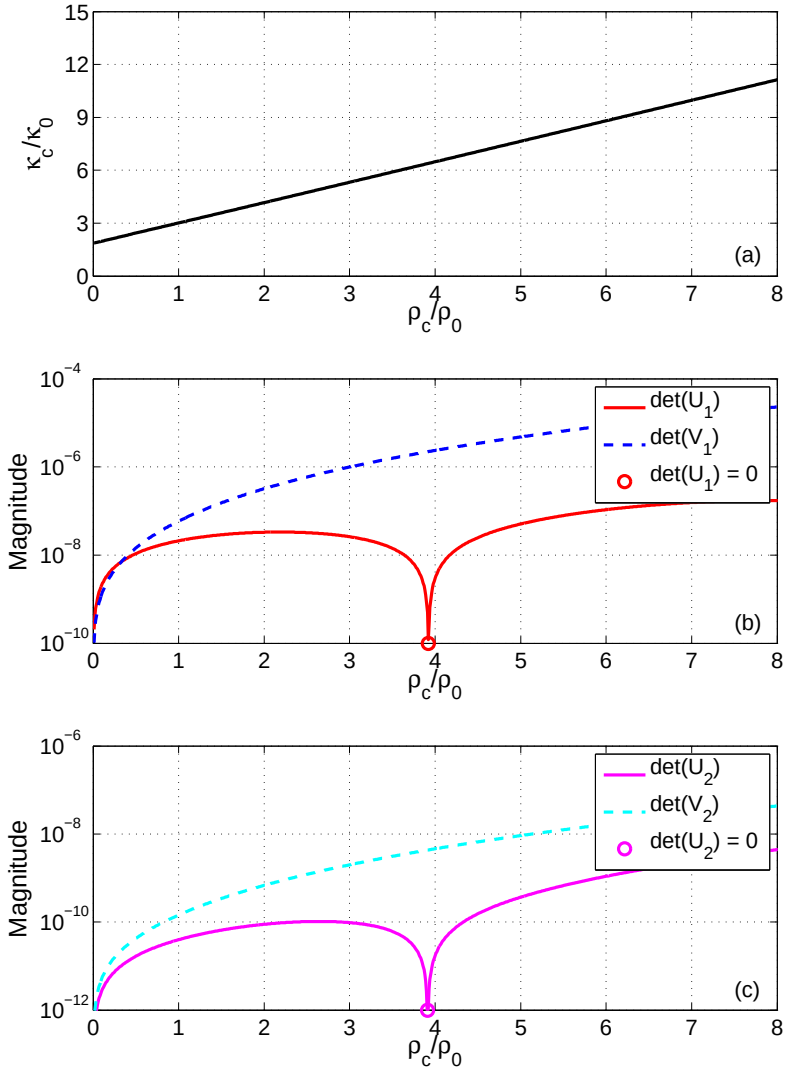

Figure 5.11: Parametric study of the solutions satisfying $|U_n| = 0$ for a hollow (pressure-release) sphere coated in a single elastic cloaking layer with $\nu_c = 0.3$ and $\frac{b}{a} = 1.30$ at $k_{d,0}a = 1.75$. In (a), $|U_0| = 0$ is solved for $\overline{\kappa}_c$ as a function of $\overline{\rho}_c$. In (b), the magnitude of $|U_1|$ and $|V_1|$ are plotted as a function of $\overline{\rho}_c$. In (c), the magnitude of $|U_2|$ and $|V_2|$ are plotted as a function of $\overline{\rho}_c$.

layer can yield a significant reduction in the scattering strength. As mentioned in Section 5.2.1, plasmonic cloaks are limited to the case when $\overline{\rho} < (\frac{b}{a})^3$ when using a single elastic layer. A practical example of such a target is that of a hollow (pressure-release) sphere, which was considered in Section 4.5.

For the case of a pressure-release sphere, the parametric study in terms of $\overline{\rho}_c$ is presented in Figure 5.11 at $k_{d,0}a = 1.75$. Although $\overline{\kappa}_c$ does vary linearly with $\overline{\rho}_c$ as observed in the scatterers analyzed in Sections 5.2 and 5.3, the magnitude of $\overline{\kappa}_c$ is significantly larger than in the previous cases, which is in agreement with the results observed for plasmonic cloaks. Examining $|U_1|$ and $|U_2|$ in Figure 5.11(b) and (c), respectively, the zero crossings for both occur at the same value of $\overline{\rho}_c$, verifying that this choice of an anti-resonance cloak (the properties of which are tabulated in Table 5.4) will cancel at least the first three scattering modes.

To determine the effectiveness of this cloak, the magnitude of the first 6 scattering coefficients are given in Figure 5.12(a) and (b) for the uncloaked and cloaked configurations, respectively. With the anti-resonance cloak, it can be seen that the first 4 scattering modes are successfully cancelled at $k_{d,0}a = 1.75$, leaving the $n = 4$ mode as the dominant contribution to the scattering strength.

To quantify the scattering reduction achieved using this anti-resonance cloak, it is important to consider what reference level is desired. The natural choice for the scattering reduction for a cloaked target is to compare it to the uncloaked scattering strength, which is shown in the dashed black line in Figure 5.12(c). However, very compliant targets, such as a pressure-release sphere, exhibit a large low frequency monopole response, which is evident upon inspection of in Figure 5.12(a). The simple act of adding a stiff coating eliminates this effect. Since the cloaking layer used is stiff and dense when compared to the surrounding fluid, comparison of the cloaked object's response to that of a stiff target might be worthwhile. The scattering

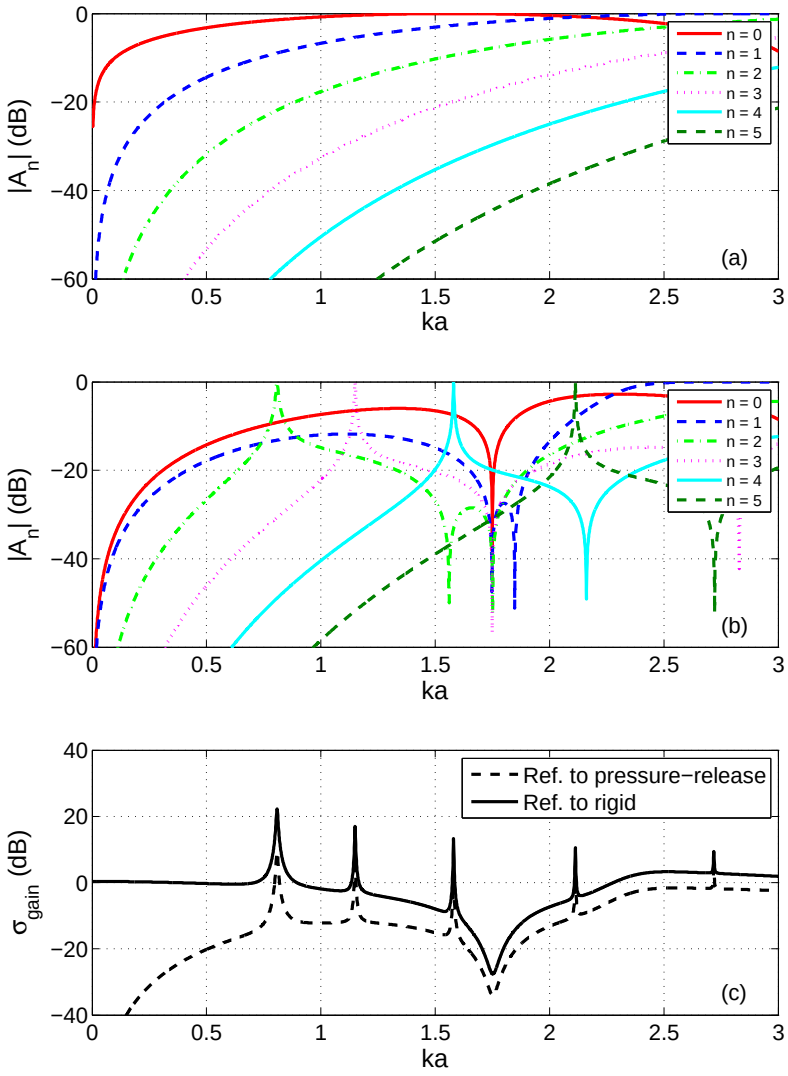

Figure 5.12: Magnitude of the scattering coefficients (in dB) for a hollow (pressure-release) sphere: (a) uncloaked, and (b) cloaked using a single elastic layer with $\nu_c = 0.3$ and $\dfrac{b}{a} = 1.30$, designed to cancel the first 4 modes at $k_{d,0}a = 1.75$, with the material properties listed in Table 5.4. The scattering gain (in dB) is given in (c), referenced to the scattering strength of a pressure-release sphere (dashed) and a rigid sphere (solid).

gain using the scattering strength of a rigid sphere as a reference is therefore also plotted in Figure 5.12(c), and is represented by a black solid line.

Comparing these two ways of expressing the scattering strength, it can be seen that the most significant difference occurs at low frequencies, for which the pressure-release referenced results suggest that there is a significant scattering reduction. This is somewhat deceiving, since almost *any* stiff coating would produce a similar result. It is therefore decided that the rigid sphere reference should be used when inspecting the utility of a layer to cloak a compliant scatterer, since this metric provides a better indication of the scattering reduction achieved. Examining the scattering gain, it is noted that the reduction is only about 25 dB (relative to a rigid sphere) at $k_{d,0}a = 1.75$, even though the first 4 scattering modes are cancelled. From Figure 5.12(b), it is seen that the scattering reduction is limited by the relative proximity of the $n = 4$ modal resonance to $k_{d,0}a = 1.75$.

Finally, it is worthwhile to inspect the usefulness of an anti-resonance cloak design for a commonly encountered example of scattering from a compliant sphere: a spherical air bubble in water. Due to the large difference in density and bulk modulus between these two fluids, the air bubble in this case appears very similar to that of a pressure-release surface. Inspecting the properties given in Table 5.4, the difference in the cloaking layer parameters between a pressure-release (vaccuum) and air is only about 0.1%.

To highlight this simiarlity, the results of Figure 5.12 are replotted for an air bubble in water in Figure 5.13. Examining each mode in the uncloaked and cloaked configuration confirms the similar nature of the case of a pressure-release sphere and an air bubble in water. The only apparent difference in the case of the air bubble is presence of very narrow resonances occurring through the entire frequency band. Upon a closer examination, these resonances originate in the uncloaked air bubble,

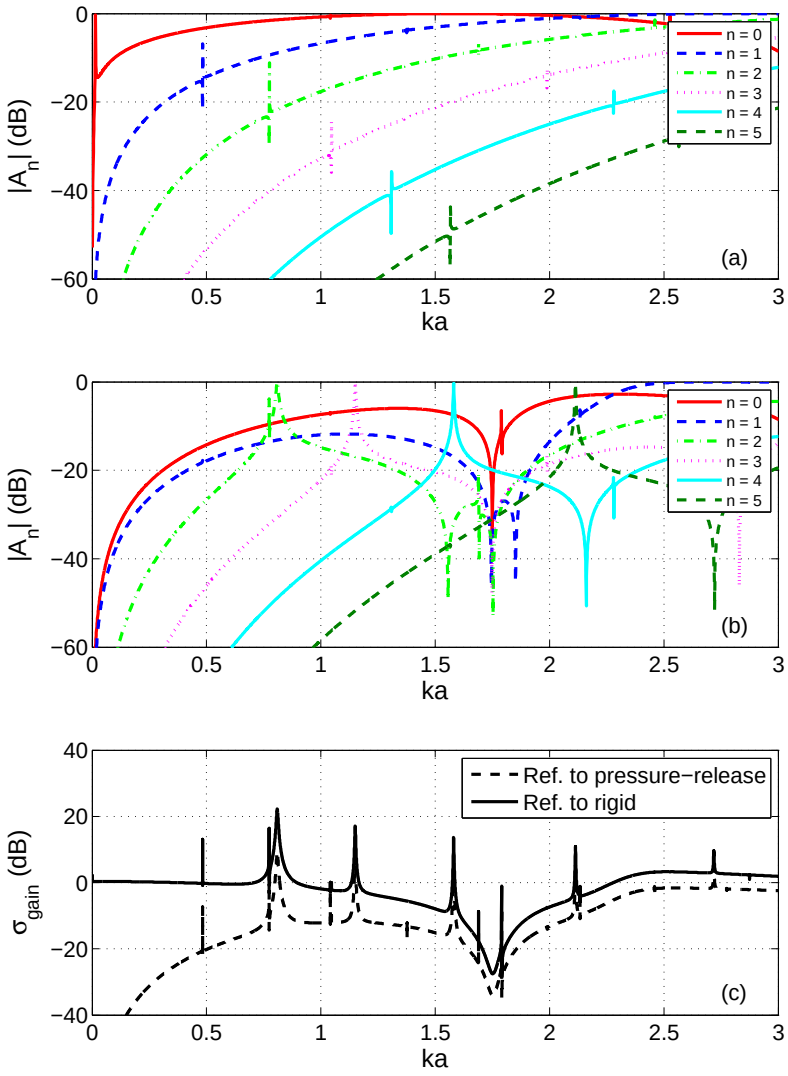

Figure 5.13: Magnitude of the scattering coefficients (in dB) for a spherical air bubble in water: (a) uncloaked, and (b) cloaked using a single elastic layer with $\nu_c = 0.3$ and $\dfrac{b}{a} = 1.30$, designed to cancel the first 4 modes at $k_{d,0}a = 1.75$, with the material properties listed in Table 5.4. The scattering gain (in dB) is given in (c), referenced to the scattering strength of a pressure-release sphere (dashed) and a rigid sphere (solid).

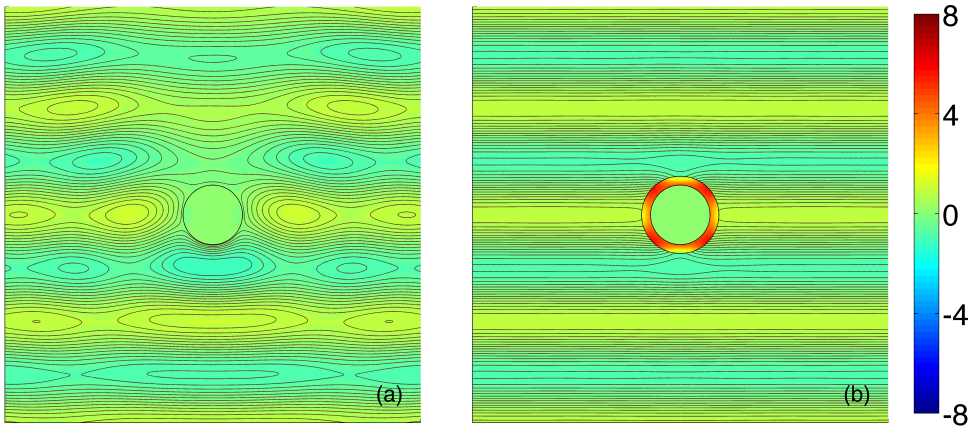

Figure 5.14: Real part of total pressure field for a spherical air bubble in water: (a) uncloaked, and (b) cloaked using a single elastic layer with $\nu_c = 0.3$ and $\frac{b}{a} = 1.30$, designed to cancel the first 4 modes at $k_{d,0}a = 1.75$, with the material properties listed in Table 5.4. The color scale for the pressure is normalized to the amplitude of the incident wave, which is a time-harmonic plane wave traveling from bottom to top with a frequency of $k_{d,0}a = 1.75$.

and correspond to the modal resonances within the air bubble itself. It is worth noting that losses in true systems will likely eliminate these internal resonances.

To demonstrate the effectiveness of this anti-resonance cloak at $k_{d,0}a = 1.75$, the real part of the total pressure field is presented in Figure 5.14(a) and (b) for an uncloaked and cloaked air bubble in water, respectively. In the uncloaked case, the incident field is significantly disrupted due to the scattering from the air bubble. With the cloaking layer, it can be seen that the incident field is restored, with only minimal disruption occurring in the nearfield of the air bubble.

Although only a single elastic layer was investigated here, the principles developed in this chapter can readily be applied to more complex configurations.

Using an elastic cloaking layer, it was shown that manipulation of shear properties enables the use of modal anti-resonances to achieve additional cancellation of scattering modes beyond the non-resonant modes utilized in plasmonic cloaks.

In this chapter, the use of anti-resonances within an elastic layer were shown to be able to increase the number modes which could be eliminated by a single layer cloak. By increasing the number of modes which were cancelled, it was shown that this increased the scattering reduction of the cloaking layer at a given design frequency, and allowed for higher design frequencies to be considered. The next step, therefore, is to examine the effects of adding additional layers, and how this can be used to further increase the number of modes which can be eliminated, which is the topic of the next chapter.

Chapter 6

Investigation of acoustic plasmonic cloaking using multiple layers

The most practical means to achieve the cancellation of multiple higher order modes is to consider a plasmonic cloak design consisting of multiple layers. To investigate the necessary layer properties, an analytic solution is developed for the special case consisting of two fluid layers, which is presented in Section 6.1. Although the usefulness of analytic techniques for multilayered cloaks is limited by the increasing complexity of the corresponding expressions, an approximate solution for two thin layers can guide the design of more complicated configurations, as developed in Section 6.2. The nature of this solution is considered first for the case of a rigid, immovable sphere in Section 6.3, followed by a consideration of elasticity in Section 6.4 in both the core and the outer cloaking layer. These results are expanded to include multiple alternating fluid and elastic layers in Section 6.5, using the solution for two thin fluid layers as a guide.

6.1 Exact analytic expressions

In this section, a multilayered acoustic plasmonic cloak consisting of two fluid shells will be considered. Although at first glance this may appear to represent only a modest increase in complexity over the single layer solutions developed in Chapter 4, there are several important novel features compared to the single layer case. First, the cloaking properties for each of the two fluid layers are significantly different from each other, and from those of a single layer. Understanding these differences is

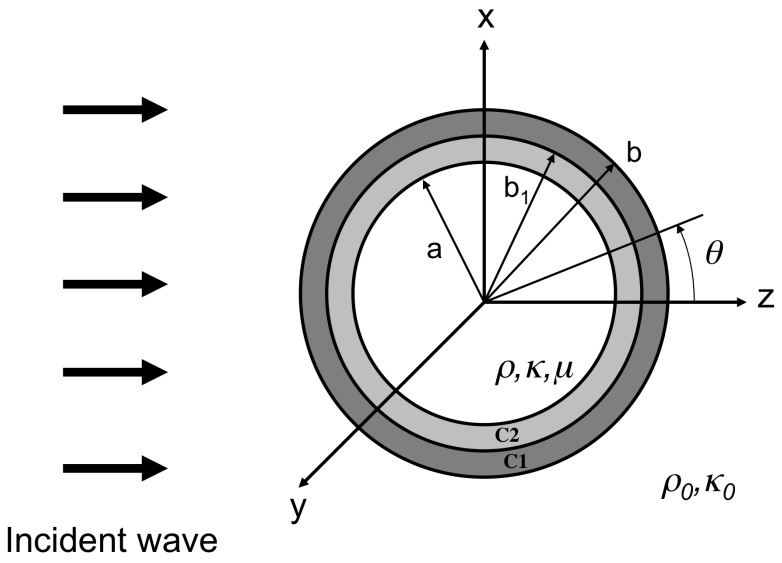

Figure 6.1: A time-harmonic incident plane wave in a fluid medium impinging on an isotropic elastic core of radius a coated in two concentric shells of uniform thickness with outer radius b. The surrounding medium has density ρ_0 and bulk modulus κ_0, and the elastic core has density ρ, bulk modulus κ and shear modulus μ.

important for the development of more complicated multilayered acoustic plasmonic cloaks. Second, due to the increased complexity of the expressions and to the presence of additional cloaking layer parameters, the analytic formulation developed for two fluid layers does not reduce down to compact, explicit expressions, as was achieved for a single layer. Instead, a system of coupled equations is developed that can be solved implicitly, generalizeable to multilayered configurations. Finally, the two layer acoustic plasmonic cloak demonstrates that the addition of more layers allows for the simultaneous cancellation of more modes, which is a key benefit of using a plasmonic cloak consisting of multiple isotropic layers.

To develop an analytic solution, the same process as described in Section 4.1 will be followed to produce an expression for the cloaking condition of the n^{th} mode

in terms of the cloaking layer properties. For the case of an isotropic elastic core coated with two fluid layers consistent with Figure C.1, Equation (4.1) becomes

$$\begin{vmatrix} u_{11}^{(n)} & u_{12}^{(n)} & u_{13}^{(n)} & 0 & 0 & 0 & 0 \\ u_{21}^{(n)} & u_{22}^{(n)} & u_{23}^{(n)} & 0 & 0 & 0 & 0 \\ 0 & u_{32}^{(n)} & u_{33}^{(n)} & u_{34}^{(n)} & u_{35}^{(n)} & 0 & 0 \\ 0 & u_{42}^{(n)} & u_{43}^{(n)} & u_{44}^{(n)} & u_{45}^{(n)} & 0 & 0 \\ 0 & 0 & 0 & u_{54}^{(n)} & u_{55}^{(n)} & u_{56}^{(n)} & u_{57}^{(n)} \\ 0 & 0 & 0 & u_{64}^{(n)} & u_{65}^{(n)} & u_{66}^{(n)} & u_{67}^{(n)} \\ 0 & 0 & 0 & 0 & 0 & u_{76}^{(n)} & u_{77}^{(n)} \end{vmatrix} = 0, \tag{6.1}$$

where the non-zero terms are given by

$$u_{11}^{(n)} = k_{d,0} b \, j_n'(k_{d,0} b), \tag{6.2}$$

$$u_{12}^{(n)} = k_{d,c1} b \, j_n'(k_{d,c1} b), \tag{6.3}$$

$$u_{13}^{(n)} = k_{d,c1} b \, n_n'(k_{d,c1} b), \tag{6.4}$$

$$u_{21}^{(n)} = j_n(k_{d,0} b), \tag{6.5}$$

$$u_{22}^{(n)} = \overline{\rho}_{c1} \, j_n(k_{d,c1} b), \tag{6.6}$$

$$u_{23}^{(n)} = \overline{\rho}_{c1} \, n_n(k_{d,c1} b), \tag{6.7}$$

$$u_{32}^{(n)} = k_{d,c1} b_1 \, j_n'(k_{d,c1} b_1), \tag{6.8}$$

$$u_{33}^{(n)} = k_{d,c1} b_1 \, n_n'(k_{d,c1} b_1), \tag{6.9}$$

$$u_{34}^{(n)} = k_{d,c2} b_1 \, j_n'(k_{d,c2} b_1), \tag{6.10}$$

$$u_{35}^{(n)} = k_{d,c2} b_1 \, n_n'(k_{d,c2} b_1), \tag{6.11}$$

$$u_{42}^{(n)} = \overline{\rho}_{c1} \, k_{d,c1} b_1 \, j_n(k_{d,c1} b_1), \tag{6.12}$$

$$u_{43}^{(n)} = \overline{\rho}_{c1} \, k_{d,c1} b_1 \, n_n(k_{d,c1} b_1), \tag{6.13}$$

$$u_{44}^{(n)} = \overline{\rho}_{c2} \, k_{d,c2} b_1 \, j_n(k_{d,c2} b_1), \tag{6.14}$$

$$u_{45}^{(n)} = \overline{\rho}_{c2} \, k_{d,c2} b_1 \, n_n(k_{d,c2} b_1), \tag{6.15}$$

$$u_{54}^{(n)} = k_{d,c2}a\, j_n'(k_{d,c2}a), \tag{6.16}$$

$$u_{55}^{(n)} = k_{d,c2}a\, n_n'(k_{d,c2}a), \tag{6.17}$$

$$u_{56}^{(n)} = -k_{\mathrm{d}}a\, j_n'(k_{\mathrm{d}}a), \tag{6.18}$$

$$u_{57}^{(n)} = -n(n+1)\, j_n(k_{\mathrm{s}}a), \tag{6.19}$$

$$u_{64}^{(n)} = \overline{\rho}_{c2}\, j_n(k_{d,c2}a), \tag{6.20}$$

$$u_{65}^{(n)} = \overline{\rho}_{c2}\, n_n(k_{d,c2}a), \tag{6.21}$$

$$u_{66}^{(n)} = 2\overline{\rho}\left\{\left[\frac{n(n+1)}{(k_{\mathrm{s}}a)^2} - \frac{1}{2}\right] j_n(k_{\mathrm{d}}a) - 2\frac{k_{\mathrm{d}}a}{(k_{\mathrm{s}}a)^2} j_n'(k_{\mathrm{d}}a)\right\}, \tag{6.22}$$

$$u_{67}^{(n)} = 2\overline{\rho}\frac{n(n+1)}{(k_{\mathrm{s}}a)^2}\left[k_{\mathrm{s}}a j_n'(k_{\mathrm{s}}a) - j_n(k_{\mathrm{s}}a)\right], \tag{6.23}$$

$$u_{76}^{(n)} = k_{\mathrm{d}}a\, j_n'(k_{\mathrm{d}}a) - j_n(k_{\mathrm{d}}a), \tag{6.24}$$

$$u_{77}^{(n)} = \left[n(n+1) - 1 - \frac{1}{2}(k_{\mathrm{s}}a)^2\right] j_n(k_{\mathrm{s}}a) - k_{\mathrm{s}}a\, j_n'(k_{\mathrm{s}}a), \tag{6.25}$$

with $\overline{\rho}_{c1} = \rho_{c1}/\rho_0$, $\overline{\rho}_{c2} = \rho_{c2}/\rho_0$ and $\overline{\rho} = \rho/\rho_0$.

Examining Equations (6.1)–(6.25), it is apparent that the elements in different columns in Equation (6.1) are functions of only one single material property. It is observed that column 1 depends on the surrounding fluid properties, columns 2 and 3 on the outer cloaking layer, columns 4 and 5 on the inner cloaking layer, and columns 6 and 7 on the elastic core material. This is similar to the results for a single fluid layer, given by Equations (4.1)–(4.17). Except for the additional fluid cloaking layer (and its interfaces), the elements within each of these columns have the same form in each case.

In particular, it is noted that the elements given by Equations (4.10)–(4.11), (4.14)–(4.17) and Equations (6.18)–(6.19), (6.22)–(6.25) for the core material are identical, except for the indices of the element, which change based on the total size of U_n. Therefore, for the case of two fluid cloaking layers, the function Υ_n from

Equation (4.25) can be written as

$$\Upsilon_n = \begin{cases} \frac{u_{56}^{(n)} u_{77}^{(n)} - u_{57}^{(n)} u_{76}^{(n)}}{u_{66}^{(n)} u_{77}^{(n)} - u_{67}^{(n)} u_{76}^{(n)}}, & \text{for an elastic core,} \\ \frac{u_{56}^{(n)}}{u_{66}^{(n)}}, & \text{for a fluid core,} \end{cases} \tag{6.26}$$

or more generally for the case when U_n is a $q \times q$ determinant as

$$\Upsilon_n = \begin{cases} \frac{u_{q-2,q-1}^{(n)} u_{q,q}^{(n)} - u_{q-2,q}^{(n)} u_{q,q-1}^{(n)}}{u_{q-1,q-1}^{(n)} u_{q,q}^{(n)} - u_{q-1,q}^{(n)} u_{q,q-1}^{(n)}}, & \text{for an elastic core,} \\ \frac{u_{q-2,q-1}^{(n)}}{u_{q-1,q-1}^{(n)}}, & \text{for a fluid core.} \end{cases} \tag{6.27}$$

To evaluate the determinant given by Equation (6.1), use of Equation (4.22) yields

$$\begin{aligned} &\left[u_{11}^{(n)}\eta_{11}^{(n)} - u_{21}^{(n)}\eta_{12}^{(n)}\right]\left[u_{44}^{(n)}\left(u_{55}^{(n)} - \Upsilon_n u_{65}^{(n)}\right) - u_{45}^{(n)}\left(u_{54}^{(n)} - \Upsilon_n u_{64}^{(n)}\right)\right] \\ -&\left[u_{11}^{(n)}\eta_{21}^{(n)} - u_{21}^{(n)}\eta_{22}^{(n)}\right]\left[u_{34}^{(n)}\left(u_{55}^{(n)} - \Upsilon_n u_{65}^{(n)}\right) - u_{35}^{(n)}\left(u_{54}^{(n)} - \Upsilon_n u_{64}^{(n)}\right)\right] = 0, \end{aligned} \tag{6.28}$$

where Υ_n is given by Equation (6.26) and the η terms are given by

$$\boldsymbol{\eta}_n = \begin{bmatrix} \eta_{11}^{(n)} & \eta_{12}^{(n)} \\ \eta_{21}^{(n)} & \eta_{22}^{(n)} \end{bmatrix} = \begin{bmatrix} \left(u_{22}^{(n)} u_{33}^{(n)} - u_{23}^{(n)} u_{32}^{(n)}\right) & \left(u_{12}^{(n)} u_{33}^{(n)} - u_{13}^{(n)} u_{32}^{(n)}\right) \\ \left(u_{22}^{(n)} u_{43}^{(n)} - u_{23}^{(n)} u_{42}^{(n)}\right) & \left(u_{12}^{(n)} u_{43}^{(n)} - u_{13}^{(n)} u_{42}^{(n)}\right) \end{bmatrix} = 0. \tag{6.29}$$

Examining Equation (6.29), it can be seen that $\boldsymbol{\eta}_n$ is only dependent on the material properties of the outer fluid cloaking layer. Likewise, the terms $u_{i4}^{(n)}$ and $u_{i5}^{(n)}$ (with $i = 3, 4, 5 \text{ or } 6$) are only dependent on the material properties of the inner fluid cloaking layer. Therefore, it can be seen that the bracketed items in Equation (6.28) contains terms which depend on either the inner cloaking layer properties (and the core material properties), or the outer cloaking layer properties (and the surrounding fluid properties).

Although Equation (6.28) represents a relatively compact expression for the cloaking condition of the n^{th} mode, its expansion by the substitution of the exact expressions given by Equations (6.2)–(6.25) would produce a complicated, intractable equation. To reduce this expression to a manageable form while still retaining its practical applicability for finding layer properties leading to plasmonic acoustic cloaking, a thin shell approximation can be made following the process outlined in Section 4.1.2, which is discussed in the next section.

6.2 Two fluid cloaking layers

To understand the basic behavior of a multilayered plasmonic acoustic cloak at moderate frequencies, the simplest configuration will be explored analytically– the case of an isotropic sphere coated with two, thin fluid layers. Following the development of Section 4.1.2, the components of the determinant U_n which describe the cloaking layers will be expanded about $k_{d,c1}b_1$, where the radius $r = b_1$ is the interface between the two layers. Thus, the Taylor series for the spherical Bessel functions are given by

$$j_n(k_{d,c1}b) \approx j_n(k_{d,c1}b_1) + k_{d,c1}b_1\delta_1\, j_n'(k_{d,c1}b_1) + (k_{d,c1}b_1)^2\delta_1^2\, j_n''(k_{d,c1}b_1), \quad (6.30)$$

$$j_n(k_{d,c2}a) \approx j_n(k_{d,c2}b_1) - k_{d,c2}b_1\delta_2\, j_n'(k_{d,c2}b_1) + (k_{d,c2}b_1)^2\delta_2^2\, j_n''(k_{d,c2}b_1), \quad (6.31)$$

where $\delta_1 = (b - b_1)/a$ and $\delta_2 = (b_1 - a)/a$ are the shell thicknesses of the outer and inner cloaking layer, respectively, normalized by the core radius a. Note that Equations (6.30)–(6.31) may be written for any spherical Bessel functions. In these equations, terms of order $(k_{d,c}b_1\delta)^2$ have been retained to ensure sufficient accuracy in the resulting expressions for the cloaking layer properties. Even though it will be assumed that the shells are geometrically small ($\delta \ll 1$), large values of the outer layer density are required in some cases, so that the assumption $k_{d,c}a\,\delta \ll 1$ is not

valid. However, by retaining the second order terms, the less restrictive condition of $(k_{d,c}a\,\delta)^2 \ll 1$ can be applied.

To evaluate the cloaking condition using two fluid layers, a thin shell approximation is obtained by substituting Equations (6.2)–(6.25) and (6.30)–(6.31) into Equations (6.28)–(6.29). After some algebraic manipulation, and neglecting terms of order δ^3, this gives

$$
\begin{aligned}
\overline{\rho}_{c1}\overline{\rho}_{c2}\Bigg\{ & \Big[\big[(1-\delta_2)-\overline{\rho}_{c2}\delta_2\Upsilon_n\big]\overline{\mathcal{F}}'_n-\Upsilon_n\big[(1+\delta_1)\overline{\mathcal{F}}_n-\overline{\rho}_{c1}\delta_1\overline{\mathcal{F}}'_n\big]\Big] \\
& \qquad \times \mathrm{W}_n^{(\mathrm{i})}(k_{d,c1}b_1)\mathrm{W}_n^{(\mathrm{i})}(k_{d,c2}b_1) \\
& -\delta_2\big[\overline{\mathcal{F}}'_n+\overline{\rho}_{c2}\delta_2\Upsilon_n k_{d,0}b_1\,j'_n(k_{d,0}b_1)\big]k_{d,c2}b_1\mathrm{W}_n^{(\mathrm{i})}(k_{d,c1}b_1)\mathrm{W}_n^{(\mathrm{ii})}(k_{d,c2}b_1) \\
& -\Upsilon_n\delta_1\big[\overline{\mathcal{F}}_n-\overline{\rho}_{c1}\delta_1 k_{d,0}b_1\,j'_n(k_{d,0}b_1)\big]k_{d,c1}b_1\mathrm{W}_n^{(\mathrm{ii})}(k_{d,c1}b_1)\mathrm{W}_n^{(\mathrm{i})}(k_{d,c2}b_1) \\
& +\delta_2^2 k_{d,0}b_1\,j'_n(k_{d,0}b_1)(k_{d,c2}b_1)^2\mathrm{W}_n^{(\mathrm{i})}(k_{d,c1}b_1)\mathrm{W}_n^{(\mathrm{iv})}(k_{d,c2}b_1) \\
& -\Upsilon_n\delta_1^2\,j_n(k_{d,0}b_1)(k_{d,c1}b_1)^2\mathrm{W}_n^{(\mathrm{iv})}(k_{d,c1}b_1)\mathrm{W}_n^{(\mathrm{i})}(k_{d,c2}b_1)\Bigg\} \\
+\overline{\rho}_{c1}\Bigg\{ & \delta_2\big[\overline{\mathcal{F}}_n+\delta_1\,j_n(k_{d,0}b_1)-\overline{\rho}_{c1}\delta_1 k_{d,0}b_1\,j'_n(k_{d,0}b_1)+\overline{\rho}_{c2}\delta_2\Upsilon_n\,j_n(k_{d,0}b_1)\big] \\
& \qquad \times (k_{d,c2}b_1)^2\mathrm{W}_n^{(\mathrm{i})}(k_{d,c1}b_1)\mathrm{W}_n^{(\mathrm{iii})}(k_{d,c2}b_1) \\
& +\delta_1\delta_2\,j_n(k_{d,0}b_1)k_{d,c1}b_1(k_{d,c2}b_1)^2\mathrm{W}_n^{(\mathrm{ii})}(k_{d,c1}b_1)\mathrm{W}_n^{(\mathrm{iii})}(k_{d,c2}b_1) \\
& -\delta_2^2\,j_n(k_{d,0}b_1)(k_{d,c2}b_1)^3\mathrm{W}_n^{(\mathrm{i})}(k_{d,c1}b_1)\mathrm{W}_n^{(\mathrm{v})}(k_{d,c2}b_1)\Bigg\} \\
+\overline{\rho}_{c2}\Bigg\{ & \delta_1\big[\overline{\mathcal{F}}_n-\delta_2\,j_n(k_{d,0}b_1)-\overline{\rho}_{c1}\delta_1 k_{d,0}b_1\,j'_n(k_{d,0}b_1)+\overline{\rho}_{c2}\delta_2\Upsilon_n\,j_n(k_{d,0}b_1)\big] \\
& \qquad \times (k_{d,c1}b_1)^2\mathrm{W}_n^{(\mathrm{iii})}(k_{d,c1}b_1)\mathrm{W}_n^{(\mathrm{i})}(k_{d,c2}b_1) \\
& -\delta_1\delta_2\,j_n(k_{d,0}b_1)(k_{d,c1}b_1)^2k_{d,c2}b_1\mathrm{W}_n^{(\mathrm{iii})}(k_{d,c1}b_1)\mathrm{W}_n^{(\mathrm{ii})}(k_{d,c2}b_1) \\
& +\delta_1^2\,j_n(k_{d,0}b_1)(k_{d,c1}b_1)^3\mathrm{W}_n^{(\mathrm{v})}(k_{d,c1}b_1)\mathrm{W}_n^{(\mathrm{i})}(k_{d,c2}b_1)\Bigg\} = 0,
\end{aligned}
\tag{6.32}
$$

where

$$
\overline{\mathcal{F}}_n = j_n(k_{d,0}b_1) + k_{d,0}b_1\,\delta_1\,j'_n(k_{d,0}b_1), \tag{6.33}
$$

$$
\overline{\mathcal{F}}'_n = k_{d,0}b_1\big[(1+\delta_1)\,j'_n(k_{d,0}b_1) + k_{d,0}a\,\delta_1\,j''_n(k_{d,0}b_1)\big], \tag{6.34}
$$

and

$$\mathrm{W}_n^{(\mathrm{i})}(z) = j_n(z)n_n'(z) - j_n'(z)n_n(z) = \frac{1}{z^2}, \tag{6.35}$$

$$\mathrm{W}_n^{(\mathrm{ii})}(z) = j_n(z)n_n''(z) - j_n''(z)n_n(z) = -\frac{2}{z^3}, \tag{6.36}$$

$$\mathrm{W}_n^{(\mathrm{iii})}(z) = j_n'(z)n_n''(z) - j_n''(z)n_n'(z) = \frac{1}{z^2}\left[1 - \frac{n(n+1)}{z^2}\right], \tag{6.37}$$

$$\mathrm{W}_n^{(\mathrm{iv})}(z) = j_n(z)n_n'''(z) - j_n'''(z)n_n(z) = -\frac{1}{z^2}\left[1 - \frac{n(n+1)+6}{z^2}\right], \tag{6.38}$$

$$\mathrm{W}_n^{(\mathrm{v})}(z) = j_n'(z)n_n'''(z) - j_n'''(z)n_n'(z) = -\frac{2}{z^3}\left[1 - \frac{2n(n+1)}{z^2}\right]. \tag{6.39}$$

From Equations (6.35)–(6.39), it can be seen that the somewhat complicated products of spherical Bessel functions (and derivatives) reduce to simple algebraic quantities. It is important to note that these are not approximations, but exact expressions. The identities given in Equations (6.35)–(6.37) were used for the case of a single fluid cloaking layer, and Equations (6.38)–(6.39) can be derived from these equations using the relationship between derivatives based on the recursion relations of spherical Bessel functions [69]. The details of this derivation are given in Appendix B.

Substitution of the algebraic expressions on the right hand side of Equations (6.35)–(6.39) into Equation (6.32), the cloaking condition for the n^{th} mode reduces to

$$\begin{aligned}
&\overline{\gamma}_n + \Upsilon_n \overline{\mathcal{F}}_n' \left[\overline{\rho}_{c1}\delta_1 + \overline{\rho}_{c2}\delta_2\right] + (k_{d,0}b_1)^2 \Bigg\{ \left[\overline{\mathcal{F}}_n - \overline{\rho}_{c1}\delta_1 \overline{\mathcal{G}}_n + \overline{\rho}_{c2}\delta_2 \Upsilon_n j_n(k_{d,0}b_1) \right] \frac{\delta_1}{\overline{\kappa}_{c1}} \\
&\qquad + \left[\overline{\mathcal{F}}_n - \overline{\rho}_{c1}\delta_1 k_{d,0}b_1 j_n'(k_{d,0}b_1) - \overline{\rho}_{c2}\delta_2 \overline{\mathcal{G}}_n \right] \frac{\delta_2}{\overline{\kappa}_{c2}} \Bigg\} \\
&- n(n+1) \Bigg\{ \overline{\mathcal{F}}_n \left[\frac{\delta_1}{\overline{\rho}_{c1}} + \frac{\delta_2}{\overline{\rho}_{c2}} \right] - \frac{\overline{\rho}_{c1}}{\overline{\rho}_{c2}} \delta_1\delta_2 k_{d,0}b_1 j_n'(k_{d,0}b_1) + \frac{\overline{\rho}_{c2}}{\overline{\rho}_{c1}} \delta_1\delta_2 \Upsilon_n j_n(k_{d,0}b_1) \Bigg\} = 0,
\end{aligned} \tag{6.40}$$

where

$$\overline{\mathcal{G}}_n = k_{d,0}b_1\, j_n'(k_{d,0}b_1) - \Upsilon_n j_n(k_{d,0}b_1), \tag{6.41}$$

$$\begin{aligned}\overline{\gamma}_n = {} & (1+\delta_2)\overline{\mathcal{F}}_n' - \Upsilon_n\overline{\mathcal{F}}_n + k_{d,0}b_1 j_n'(k_{d,0}b_1)\Big[\delta_2^2\big[2n(n+1)+6\big] + \delta_1^2 n(n+1)\Big] \\ & + \Upsilon_n j_n(k_{d,0}b_1)\Big[\delta_1 + \delta_2^2 n(n+1) + \delta_1^2\big[2n(n+1)+6\big]\Big].\end{aligned} \tag{6.42}$$

Through the use of the identities given in Equations (6.35)–(6.39), the transcendental relationship among the cloaking layer properties given by Equation (6.32) may be replaced by the much simpler algebraic expression of Equation (6.40). Although it is sufficient to use Equations (6.40)–(6.42) to numerically solve for the desired modes to be cancelled, the objective here is to develop approximate explicit expressions for the cloaking layer properties, in order to provide a way to determine an appropriate initial guess for the numerical solution.

Based on previous investigations of multilayered fluids [28] and the use of these structures for acoustic metamaterials and cloaking applications [12, 15], one would expect the benefits of increasing the number of fluid layers to be dominated by the inertial effects of each layer. To illustrate this, first consider the case in which the densities of each layer are the same, so that $\overline{\rho}_{c1} = \overline{\rho}_{c2} \equiv \overline{\rho}_{c0}$. In this case, Equation (6.40) becomes

$$\begin{aligned}\overline{\gamma}_n + \Upsilon_n\overline{\mathcal{F}}_n'\overline{\rho}_{c0}\big[\delta_1+\delta_2\big] + (k_{d,0}b_1)^2\Bigg\{ & \overline{\mathcal{F}}_n\left[\frac{\delta_1}{\overline{\kappa}_{c1}} + \frac{\delta_2}{\overline{\kappa}_{c2}}\right] \\ & - \overline{\rho}_{c0}\Big[\delta_1\overline{\mathcal{G}}_n - \delta_2\Upsilon_n j_n(k_{d,0}b_1)\Big]\frac{\delta_1}{\overline{\kappa}_{c1}} - \overline{\rho}_{c0}\Big[\delta_1 k_{d,0}b_1 j_n'(k_{d,0}b_1) + \delta_2\overline{\mathcal{G}}_n\Big]\frac{\delta_2}{\overline{\kappa}_{c2}}\Bigg\} \\ & - n(n+1)\Bigg\{\overline{\mathcal{F}}_n\frac{1}{\overline{\rho}_{c0}}\big[\delta_1+\delta_2\big] - \delta_1\delta_2 k_{d,0}b_1 j_n'(k_{d,0}b_1) + \delta_1\delta_2\Upsilon_n j_n(k_{d,0}b_1)\Bigg\} = 0.\end{aligned} \tag{6.43}$$

Examining this relationship, it is clear that the bulk moduli $\overline{\kappa}_{c1}$ and $\overline{\kappa}_{c2}$ have independently very little effect, appearing only in terms of order δ^2. Instead, the

compressibility is dominated by the effective bulk modulus of the two fluid layers given by

$$\frac{1}{\overline{\kappa}_{c0}} = \left[\frac{\delta_1}{\delta_0}\frac{1}{\overline{\kappa}_{c1}} + \frac{\delta_2}{\delta_0}\frac{1}{\overline{\kappa}_{c2}}\right], \tag{6.44}$$

where $\delta_0 = \delta_1 + \delta_2$. Furthermore, neglecting terms of order δ^2 in Equation (6.43) yields

$$\overline{\gamma}_n + \Upsilon_n \overline{\mathcal{F}}'_n \overline{\rho}_{c0}\delta_0 + (k_{d0}b_1)^2 \overline{\mathcal{F}}_n \frac{\delta_0}{\overline{\kappa}_{c0}} - n(n+1)\overline{\mathcal{F}}_n \frac{\delta_0}{\overline{\rho}_{c0}} = 0. \tag{6.45}$$

Comparing Equation (6.45) with Equation (4.61), it is apparent that this is simply the solution for a single fluid layer with effective density $\overline{\rho}_{c0}$ and effective bulk modulus $\overline{\kappa}_{c0}$. Even though the bulk moduli of each layer can be independently varied, the effective bulk modulus dominates the scattering cancellation effect for the first two scattering modes. Therefore, having two fluid layers with the same density does not allow for additional scattering modes to be cancelled compared to a single layer.

For this reason, we focus on cases in which the densities in the two layers are very different, i.e., (1) $\overline{\rho}_{c1} \gg \overline{\rho}_{c2}$, and (2) $\overline{\rho}_{c1} \ll \overline{\rho}_{c2}$. Within each one of these limits, Equation (6.40) reduces to a simpler form, allowing for explicit expressions for the cloaking conditions.

6.2.1 Region 1: $\overline{\rho}_{c1} \gg \overline{\rho}_{c2}$

Assuming that $\overline{\rho}_{c1} \gg \overline{\rho}_{c2}$, Equation (6.40) becomes

$$\begin{aligned}
&\overline{\gamma}_n + \Upsilon_n \overline{\mathcal{F}}'_n \overline{\rho}_{c1}\delta_1 + (k_{d,0}b_1)^2 \Bigg\{ \left[\overline{\mathcal{F}}_n - \overline{\rho}_{c1}\delta_1 \overline{\mathcal{G}}_n\right]\frac{\delta_1}{\overline{\kappa}_{c1}} \\
&\quad + \left[\overline{\mathcal{F}}_n - \overline{\rho}_{c1}\delta_1 k_{d,0}b_1 j'_n(k_{d,0}b_1) + \overline{\rho}_{c2}\delta_2 \Upsilon_n j_n(k_{d,0}b_1)\right]\frac{\delta_2}{\overline{\kappa}_{c2}} \Bigg\} \\
&\quad - n(n+1)\left\{\overline{\mathcal{F}}_n \frac{\delta_2}{\overline{\rho}_{c2}} - \frac{\overline{\rho}_{c1}}{\overline{\rho}_{c2}}\delta_1\delta_2 k_{d,0}b_1 j'_n(k_{d,0}b_1)\right\} = 0.
\end{aligned} \tag{6.46}$$

To determine expressions for the cloaking layer properties, a system of equations can be obtained by writing Equation (6.46) for the modes $n=0$ through $n=3$, in a similar manner to the approach taken for the single fluid layer. However, cancellation of all 4 modes would require at least one negative parameter. To examine the range where $\overline{\rho}_{c1}$, $\overline{\kappa}_{c1}$, $\overline{\rho}_{c2}$ and $\overline{\kappa}_{c2}$ are all positive, a cloak will be sought that cancels the first 3 modes: $n=0$ (monopole), $n=1$ (dipole) and $n=2$ (quadrupole).

With three equations prescribing the cancellation of each mode, only three of the cloaking layer properties will be explicitly determined, with the remaining property acting as a parameter. Thus, unlike the case of a single fluid cloaking layer which has one optimal solution, in this case one obtains a family of solutions from which a design can be selected. For the case $\overline{\rho}_{c1} \gg \overline{\rho}_{c2}$, the three independent variables solved for will be $\overline{\rho}_{c1}$, $\overline{\kappa}_{c1}$, and $\overline{\rho}_{c2}$, with $\overline{\kappa}_{c2}$ kept as a free parameter.

To obtain solutions for each of the independent variables, each modal equation will be used to solve for one of the variables in terms of the others, systematically eliminating each of the variables. Solving Equation (6.46) with $n=0$ yields

$$\overline{\kappa}_{c1} = \frac{\delta_1 (k_{d,0} b_1)^2 \left[\overline{\rho}_{c1}\delta_1 \overline{\mathcal{G}}_0 - \overline{\mathcal{F}}_0\right]}{\overline{\gamma}_0 + \overline{\rho}_{c1}\delta_1 \Upsilon_0 \overline{\mathcal{F}}'_0 + (k_{d,0}b_1)^2 \left[\overline{\mathcal{F}}_0 - \overline{\rho}_{c1}\delta_1 k_{d,0} b_1 j'_0(k_{d,0}b_1) + \overline{\rho}_{c2}\delta_2 \Upsilon_0 j_0(k_{d,0}b_1)\right] \dfrac{\delta_2}{\overline{\kappa}_{c2}}}. \tag{6.47}$$

Substitution of Equation (6.47) into Equation (6.46) yields an expression relating the two remaining independent variables, $\overline{\rho}_{c1}$ and $\overline{\rho}_{c2}$, and the parameter $\overline{\kappa}_{c2}$,

$$\left[\delta_2 \zeta_3^{(n)} (k_{d,0}b_1)^2 \frac{\delta_2}{\overline{\kappa}_{c2}}\right] \overline{\rho}_{c2}^2 + \left[\zeta_2^{(n)} + \zeta_1^{(n)} (k_{d,0}b_1)^2 \frac{\delta_2}{\overline{\kappa}_{c2}}\right] \overline{\rho}_{c2} - n(n+1)\delta_2 \zeta_0^{(n)} = 0, \tag{6.48}$$

where

$$\zeta_0^{(n)} = a_0^{(n)} (\overline{\rho}_{c1}\delta_1)^2 + b_0^{(n)} \overline{\rho}_{c1}\delta_1 + c_0^{(n)}, \tag{6.49}$$

$$\zeta_1^{(n)} = a_1^{(n)} (\overline{\rho}_{c1}\delta_1)^2 + b_1^{(n)} \overline{\rho}_{c1}\delta_1 + c_1^{(n)}, \tag{6.50}$$

$$\zeta_2^{(n)} = a_2^{(n)}(\overline{\rho}_{c1}\delta_1)^2 + b_2^{(n)}\overline{\rho}_{c1}\delta_1 + c_2^{(n)}, \tag{6.51}$$

$$\zeta_3^{(n)} = a_3^{(n)}(\overline{\rho}_{c1}\delta_1)^2 + b_3^{(n)}\overline{\rho}_{c1}\delta_1 + c_3^{(n)}, \tag{6.52}$$

with

$$a_0^{(n)} = -k_{d,0}b_1 j_n'(k_{d,0}b_1)\overline{\mathcal{G}}_0, \tag{6.53}$$

$$b_0^{(n)} = \overline{\mathcal{F}}_n\overline{\mathcal{G}}_0 + k_{d,0}b_1 j_n'(k_{d,0}b_1)\overline{\mathcal{F}}_0, \tag{6.54}$$

$$c_0^{(n)} = -\overline{\mathcal{F}}_0\overline{\mathcal{F}}_n, \tag{6.55}$$

$$a_1^{(n)} = k_{d,0}b_1\big[\Upsilon_0 j_0(k_{d,0}b_1)j_n'(k_{d,0}b_1) - \Upsilon_n j_n(k_{d,0}b_1)j_0'(k_{d,0}b_1)\big], \tag{6.56}$$

$$b_1^{(n)} = -\big[\Upsilon_0 j_0(k_{d,0}b_1)\overline{\mathcal{F}}_n - \Upsilon_n j_n(k_{d,0}b_1)\overline{\mathcal{F}}_0\big], \tag{6.57}$$

$$c_1^{(n)} = 0, \tag{6.58}$$

$$a_2^{(n)} = \Upsilon_n\overline{\mathcal{F}}_n\overline{\mathcal{G}}_0 - \Upsilon_0\overline{\mathcal{F}}_0\overline{\mathcal{G}}_n, \tag{6.59}$$

$$b_2^{(n)} = \big[\overline{\gamma}_n\overline{\mathcal{G}}_0 - \overline{\gamma}_0\overline{\mathcal{G}}_n\big] - \big[\Upsilon_n\overline{\mathcal{F}}_n\overline{\mathcal{G}}_0 - \Upsilon_0\overline{\mathcal{F}}_0\overline{\mathcal{G}}_n\big], \tag{6.60}$$

$$c_2^{(n)} = -\big[\overline{\gamma}_n\overline{\mathcal{F}}_0 - \overline{\gamma}_0\overline{\mathcal{F}}_n\big], \tag{6.61}$$

$$a_3^{(n)} = 0, \tag{6.62}$$

$$b_3^{(n)} = \Upsilon_n j_n'(k_{d,0}b_1)\overline{\mathcal{G}}_0 - \Upsilon_0 j_0'(k_{d,0}b_1)\overline{\mathcal{G}}_n, \tag{6.63}$$

$$c_3^{(n)} = -\big[\Upsilon_n j_n'(k_{d,0}b_1)\overline{\mathcal{F}}_0 - \Upsilon_0 j_0'(k_{d,0}b_1)\overline{\mathcal{F}}_n\big]. \tag{6.64}$$

Solving Equation (6.48) with $n=1$ for $\overline{\rho}_{c2}$ yields two roots, given by

$$\overline{\rho}_{c2} = R\left[-1 \pm \sqrt{1 + 2\varepsilon\delta_2^2}\right], \tag{6.65}$$

where

$$R = \frac{\zeta_2^{(1)} + \zeta_1^{(1)}(k_{d,0}b_1)^2\dfrac{\delta_2}{\overline{\kappa}_{c2}}}{2\delta_2\zeta_3^{(1)}(k_{d,0}b_1)^2\dfrac{\delta_2}{\overline{\kappa}_{c2}}}, \tag{6.66}$$

$$\varepsilon = \frac{4\zeta_0^{(1)}\zeta_3^{(1)}(k_{d,0}b_1)^2\dfrac{\delta_2}{\overline{\kappa}_{c2}}}{\left[\zeta_2^{(1)} + \zeta_1^{(1)}(k_{d,0}b_1)^2\dfrac{\delta_2}{\overline{\kappa}_{c2}}\right]^2}. \tag{6.67}$$

Assuming that $2\varepsilon\delta_2^2 \ll 1$, the two roots reduce to

$$\overline{\rho}_{c2}^{(1)} = R\varepsilon\delta_2^2 = \frac{2\delta_2\zeta_0^{(1)}}{\zeta_2^{(1)} + \zeta_1^{(1)}(k_{d,0}b_1)^2\dfrac{\delta_2}{\overline{\kappa}_{c2}}}, \tag{6.68}$$

$$\overline{\rho}_{c2}^{(2)} = -2R = -\frac{\zeta_2^{(1)} + \zeta_1^{(1)}(k_{d,0}b_1)^2\dfrac{\delta_2}{\overline{\kappa}_{c2}}}{\delta_2\zeta_3^{(1)}(k_{d,0}b_1)^2\dfrac{\delta_2}{\overline{\kappa}_{c2}}}, \tag{6.69}$$

where the superscripts $^{(1)}$ and $^{(2)}$ denote the different roots of Equation (6.48).

Examining the two possible values of $\overline{\rho}_{c2}$, it is noted that $\overline{\rho}_{c2}^{(1)}$ is proportional to δ_2, and $\overline{\rho}_{c2}^{(2)}$ is proportional to δ_2^{-1}. Since $\delta_2 \ll 1$, this indicates that the magnitude of $\overline{\rho}_{c2}^{(1)}$ will be significantly smaller than $\overline{\rho}_{c2}^{(2)}$. Furthermore, comparing these roots to Equation (6.48) it is observed that Equations (6.68) and (6.69) correspond to the solution for the limiting cases when $\overline{\rho}_{c2} \ll 1$ and $\overline{\rho}_{c2} \gg 1$, respectively. Therefore, to ensure validity of the assumption that $\overline{\rho}_{c1} \gg \overline{\rho}_{c2}$, Equation (6.68) must be used in this case. Although it is not apparent from Equation (6.48), it will be shown later in this section that this root is positive within the range considered here.

To determine $\overline{\rho}_{c1}$, Equation (6.68) can be substituted into Equation (6.48) with $n=2$. The leads to a 4^{th} order polynomial, given by

$$q_4(\overline{\rho}_{c1}\delta_1)^4 + q_3(\overline{\rho}_{c1}\delta_1)^3 + q_2(\overline{\rho}_{c1}\delta_1)^2 + q_1\overline{\rho}_{c1}\delta_1 + q_0 = 0, \tag{6.70}$$

where

$$q_0 = 2c_0^{(1)}c_2^{(2)} - 6c_0^{(2)}c_2^{(1)}, \tag{6.71}$$

$$q_1 = 2\left\{b_0^{(1)}c_2^{(2)} + c_0^{(1)}\left[b_2^{(2)} + b_1^{(2)}(k_{d,0}b_1)^2\frac{\delta_2}{\overline{\kappa}_{c2}}\right]\right\} - 6\left\{b_0^{(2)}c_2^{(1)} + c_0^{(2)}\left[b_2^{(1)} + b_1^{(1)}(k_{d,0}b_1)^2\frac{\delta_2}{\overline{\kappa}_{c2}}\right]\right\}, \tag{6.72}$$

$$q_2 = 2\left\{a_0^{(1)}c_2^{(2)} + b_0^{(1)}\left[b_2^{(2)} + b_1^{(2)}(k_{d,0}b_1)^2\frac{\delta_2}{\overline{\kappa}_{c2}}\right] + c_0^{(1)}\left[a_2^{(2)} + a_1^{(2)}(k_{d,0}b_1)^2\frac{\delta_2}{\overline{\kappa}_{c2}}\right]\right\} - 6\left\{a_0^{(2)}c_2^{(1)} + b_0^{(2)}\left[b_2^{(1)} + b_1^{(1)}(k_{d,0}b_1)^2\frac{\delta_2}{\overline{\kappa}_{c2}}\right] + c_0^{(2)}\left[a_2^{(1)} + a_1^{(1)}(k_{d,0}b_1)^2\frac{\delta_2}{\overline{\kappa}_{c2}}\right]\right\}, \tag{6.73}$$

$$q_3 = 2\left\{a_0^{(1)}\left[b_2^{(2)} + b_1^{(2)}(k_{d,0}b_1)^2\frac{\delta_2}{\overline{\kappa}_{c2}}\right] + b_0^{(1)}\left[a_2^{(2)} + a_1^{(2)}(k_{d,0}b_1)^2\frac{\delta_2}{\overline{\kappa}_{c2}}\right]\right\} - 6\left\{a_0^{(2)}\left[b_2^{(1)} + b_1^{(1)}(k_{d,0}b_1)^2\frac{\delta_2}{\overline{\kappa}_{c2}}\right] + b_0^{(2)}\left[a_2^{(1)} + a_1^{(1)}(k_{d,0}b_1)^2\frac{\delta_2}{\overline{\kappa}_{c2}}\right]\right\}, \tag{6.74}$$

$$q_4 = 2a_0^{(1)}\left[a_2^{(2)} + a_1^{(2)}(k_{d,0}b_1)^2\frac{\delta_2}{\overline{\kappa}_{c2}}\right] - 6a_0^{(2)}\left[a_2^{(1)} + a_1^{(1)}(k_{d,0}b_1)^2\frac{\delta_2}{\overline{\kappa}_{c2}}\right], \tag{6.75}$$

where the coefficients $a_m^{(n)}$, $b_m^{(n)}$ and $c_m^{(n)}$ are given by Equations (6.53)–(6.61). Although the roots can be determined numerically using a polynomial root solver, a solution is sought such that $(\overline{\rho}_{c1}\delta_1)^2 \ll 1$ to ensure that $(k_{d,c1}b_1)^2 \ll 1$. Assuming $(\overline{\rho}_{c1}\delta_1)^2 \ll 1$, Equation (6.70) becomes

$$q_2(\overline{\rho}_{c1}\delta_1)^2 + q_1\overline{\rho}_{c1}\delta_1 + q_0 \approx 0, \tag{6.76}$$

in which case

$$\overline{\rho}_{c1} = \frac{-q_1 \pm \sqrt{q_1^2 - 4q_0q_2}}{2\delta_1 q_2}. \tag{6.77}$$

Although this approximation is limited to relatively small values of $(\overline{\rho}_{c1}\delta_1)^2$, this solution can still result in a cloaking layer which is much denser than the surrounding fluid, since $\delta_1 \ll 1$. This can be observed in Equation (6.77), in which the value of $\overline{\rho}_{c1}$ is proportional to δ_1^{-1}.

Using the results developed in this section, the required cloaking layer properties can be determined. Given a design frequency $k_{d,0}a$ and shell thicknesses δ_2 and δ_1, $\overline{\rho}_{c1}$, $\overline{\rho}_{c2}$ and $\overline{\kappa}_{c1}$ can be determined using Equations (6.77), (6.68) and (6.47), respectively. The fourth cloaking layer property $\overline{\kappa}_{c2}$ is a free parameter, which leads to an entire family of possible designs.

6.2.2 Region 2: $\overline{\rho}_{c1} \ll \overline{\rho}_{c2}$

Assuming that $\overline{\rho}_{c1} \ll \overline{\rho}_{c2}$, Equation (6.40) simplifies to

$$\overline{\gamma}_n + \Upsilon_n \overline{\mathcal{F}}'_n \overline{\rho}_{c2}\delta_2 + (k_{d,0}b_1)^2 \Bigg\{ \left[\overline{\mathcal{F}}_n - \overline{\rho}_{c1}\delta_1 k_{d,0}b_1 j'_n(k_{d,0}b_1) + \overline{\rho}_{c2}\delta_2 \Upsilon_n j_n(k_{d,0}b_1) \right] \frac{\delta_1}{\overline{\kappa}_{c1}} + \left[\overline{\mathcal{F}}_n - \overline{\rho}_{c2}\delta_2 \overline{\mathcal{G}}_n \right] \frac{\delta_2}{\overline{\kappa}_{c2}} \Bigg\} - n(n+1) \Bigg\{ \overline{\mathcal{F}}_n \frac{\delta_1}{\overline{\rho}_{c1}} + \frac{\overline{\rho}_{c2}}{\overline{\rho}_{c1}} \delta_1\delta_2 \Upsilon_n j_n(k_{d,0}b_1) \Bigg\} = 0. \quad (6.78)$$

Comparing this expression to Equation (6.46), it is found that both have the same form. Specifically, Equation (6.46) can be obtained from Equation (6.78) by swapping the layer subscripts (so that $\overline{\rho}_{c1} \leftrightarrow \overline{\rho}_{c2}$, $\overline{\kappa}_{c2} \leftrightarrow \overline{\kappa}_{c1}$ and $\delta_2 \leftrightarrow \delta_1$), and switching the terms $-k_{d,0}b_1 j'_n(k_{d,0}b_1)$ and $\Upsilon_n j_n(k_{d,0}b_1)$.

Given this analogous relationship between Equation (6.46) and Equation (6.78), the cloaking layer properties for the case when $\overline{\rho}_{c1} \ll \overline{\rho}_{c2}$ can be written as

$$\overline{\kappa}_{c2} = \frac{\delta_2 (k_{d,0}b_1)^2 \left[\overline{\rho}_{c2}\delta_2 \overline{\mathcal{G}}_0 - \overline{\mathcal{F}}_0 \right]}{\overline{\gamma}_0 + \overline{\rho}_{c2}\delta_2 \Upsilon_0 \overline{\mathcal{F}}'_0 + (k_{d,0}b_1)^2 \left[\overline{\mathcal{F}}_0 - \overline{\rho}_{c1}\delta_1 k_{d,0}b_1 j'_0(k_{d,0}b_1) + \overline{\rho}_{c2}\delta_2 \Upsilon_0 j_0(k_{d,0}b_1) \right] \frac{\delta_1}{\overline{\kappa}_{c1}}}, \quad (6.79)$$

$$\overline{\rho}_{c1} = \frac{2\delta_1 \overline{\zeta}_0^{(1)}}{\overline{\zeta}_2^{(1)} + \overline{\zeta}_1^{(1)} (k_{d,0}b_1)^2 \frac{\delta_1}{\overline{\kappa}_{c1}}}, \quad (6.80)$$

$$\overline{\rho}_{c2} = \frac{-\bar{q}_1 \pm \sqrt{\bar{q}_1^2 - 4\bar{q}_0\bar{q}_2}}{2\delta_2 \bar{q}_2}, \quad (6.81)$$

where

$$\overline{\zeta}_0^{(n)} = \bar{a}_0^{(n)} (\overline{\rho}_{c2}\delta_2)^2 + \bar{b}_0^{(n)} \overline{\rho}_{c1}\delta_1 + c_0^{(n)}, \quad (6.82)$$

$$\overline{\zeta}_1^{(n)} = \bar{a}_1^{(n)}(\overline{\rho}_{c2}\delta_2)^2 + \bar{b}_1^{(n)}\overline{\rho}_{c1}\delta_1 + c_1^{(n)}, \tag{6.83}$$

$$\overline{\zeta}_2^{(n)} = a_1^{(n)}(\overline{\rho}_{c2}\delta_2)^2 + b_1^{(n)}\overline{\rho}_{c1}\delta_1 + c_1^{(n)}, \tag{6.84}$$

$$\bar{a}_0^{(n)} = \Upsilon_n j_n(k_{d,0}b_1)\overline{\mathcal{G}}_0, \tag{6.85}$$

$$\bar{b}_0^{(n)} = \overline{\mathcal{F}}_n\overline{\mathcal{G}}_0 - \Upsilon_n j_n(k_{d,0}b_1)\overline{\mathcal{F}}_0, \tag{6.86}$$

$$\bar{a}_1^{(n)} = -k_{d,0}b_1\big[\Upsilon_0 j_0(k_{d,0}b_1)j_n'(k_{d,0}b_1) - \Upsilon_n j_n(k_{d,0}b_1)j_0'(k_{d,0}b_1)\big], \tag{6.87}$$

$$\bar{b}_1^{(n)} = k_{d,0}b_1\big[j_n(k_{d,0}b_1)j_0'(k_{d,0}b_1) - j_n'(k_{d,0}b_1)j_0(k_{d,0}b_1)\big], \tag{6.88}$$

and

$$\bar{q}_0 = 2c_0^{(1)}c_2^{(2)} - 6c_0^{(2)}c_2^{(1)}, \tag{6.89}$$

$$\begin{aligned}\bar{q}_1 = {} & 2\left\{\bar{b}_0^{(1)}c_2^{(2)} + c_0^{(1)}\left[b_2^{(2)} + \bar{b}_1^{(2)}(k_{d,0}b_1)^2\frac{\delta_2}{\overline{\kappa}_{c2}}\right]\right\} \\ & -6\left\{\bar{b}_0^{(2)}c_2^{(1)} + c_0^{(2)}\left[b_2^{(1)} + \bar{b}_1^{(1)}(k_{d,0}b_1)^2\frac{\delta_2}{\overline{\kappa}_{c2}}\right]\right\},\end{aligned} \tag{6.90}$$

$$\begin{aligned}\bar{q}_2 = {} & 2\left\{\bar{a}_0^{(1)}c_2^{(2)} + \bar{b}_0^{(1)}\left[b_2^{(2)} + \bar{b}_1^{(2)}(k_{d,0}b_1)^2\frac{\delta_2}{\overline{\kappa}_{c2}}\right] + c_0^{(1)}\left[a_2^{(2)} + \bar{a}_1^{(2)}(k_{d,0}b_1)^2\frac{\delta_2}{\overline{\kappa}_{c2}}\right]\right\} \\ & -6\left\{\bar{a}_0^{(2)}c_2^{(1)} + \bar{b}_0^{(2)}\left[b_2^{(1)} + \bar{b}_1^{(1)}(k_{d,0}b_1)^2\frac{\delta_2}{\overline{\kappa}_{c2}}\right] + c_0^{(2)}\left[a_2^{(1)} + \bar{a}_1^{(1)}(k_{d,0}b_1)^2\frac{\delta_2}{\overline{\kappa}_{c2}}\right]\right\},\end{aligned} \tag{6.91}$$

with all other constants the same as defined in Section 6.2.1. For the case $\overline{\rho}_{c1} \ll \overline{\rho}_{c2}$, the three independent variables are $\overline{\kappa}_{c1}$, $\overline{\rho}_{c2}$ and $\overline{\rho}_{c1}$, with $\overline{\kappa}_{c1}$ remaining a free parameter. Given a design frequency $k_{d,0}a$, and shell thicknesses δ_2 and δ_1, the cloaking layer properties $\overline{\kappa}_{c1}$, $\overline{\rho}_{c2}$ and $\overline{\rho}_{c1}$ can be determined using Equations (6.79)–(6.81) for a given value of $\overline{\kappa}_{c1}$.

6.3 Cloaking of a rigid sphere using two fluid layers

In the previous section, the explicit solutions for the cloaking layer properties were derived under a thin-shell approximation. Although evaluation of these

expressions can provide significant insight into understanding the behavior of a two-layer acoustic plasmonic cloak, the solutions do not provide an easy interpretation, and the dependence on each input parameter is not obvious. Specifically, the value of the cloaking layer properties vary depending on the design frequency, shell thicknesses and properties of the core material in non-trivial ways. In order to provide more insights into these general solutions, an investigation of how these input parameters affect the required cloaking layer properties for the limiting case of a rigid, immovable sphere is considered in the following section.

In Section 6.2, the core material properties were lumped into a single parameter Υ_n for each of the n modes, and is given by Equation (6.26). Following the method described in Section 4.2, taking the limit of a rigid, immovable spherical core corresponds to $\Upsilon_n \to 0$. Taking this limit for the two regions analyzed in the previous section, the equations for the cloaking layer properties can be significantly simplified. Using these simplified expressions, the fundamental features of the cloaking layer properties of a two fluid layer acoustic plasmonic cloak will be explored.

6.3.1 Region 1: $\overline{\rho}_{c1} \gg \overline{\rho}_{c2}$

To analyze the design of a two layer plasmonic acoustic cloak for a rigid, immovable sphere, consider the analytic expressions developed in Section 6.2.1 for $\overline{\rho}_{c1} \gg \overline{\rho}_{c2}$. Taking $\Upsilon_n \to 0$, Equation (6.47) for $\overline{\kappa}_{c1}$ becomes

$$\overline{\kappa}_{c1} = \frac{\delta_1 (k_{d,0} b_1)^2 \left[\overline{\rho}_{c1} \delta_1 k_{d,0} b_1 j_0'(k_{d,0} b_1) - \overline{\mathcal{F}}_0\right]}{\overline{\gamma}_0 - (k_{d,0} b_1)^2 \left[\overline{\rho}_{c1} \delta_1 k_{d,0} b_1 j_0'(k_{d,0} b_1) - \overline{\mathcal{F}}_0\right] \dfrac{\delta_2}{\overline{\kappa}_{c2}}}. \tag{6.92}$$

Examination of the coefficients given by Equations (6.53)–(6.61) in the limit of $\Upsilon_n \to 0$, it is observed that

$$a_1^{(n)} = b_1^{(n)} = a_2^{(n)} = 0. \tag{6.93}$$

Therefore, Equation (6.68) reduces to

$$\overline{\rho}_{c2} = 2\delta_2 \frac{a_0^{(1)}(\overline{\rho}_{c1}\delta_1)^2 + b_0^{(1)}\overline{\rho}_{c1}\delta_1 + c_0^{(1)}}{b_2^{(1)}\overline{\rho}_{c1}\delta_1 + c_2^{(1)}}. \tag{6.94}$$

Maintaining the restriction that $(\overline{\rho}_{c1}\delta_1)^2 \ll 1$, Equation (6.70) represents the solution for $\overline{\rho}_{c1}$. The sign of the square root is then selected to ensure a positive density, which corresponds to root obtained using the "+" sign.

The expressions for q_0, q_1 and q_2 given by Equation (6.93) simplify quite considerably, no longer depending on $\overline{\kappa}_{c2}$, implying the required values of $\overline{\rho}_{c1}$ and $\overline{\rho}_{c2}$ are independent of the bulk moduli of the cloaking layers. Furthermore, the expressions for the cloaking layer densities in Equations (6.77) and (6.94), it is observed that the shell thickness δ_2 appears in the *numerator* of $\overline{\rho}_{c2}$, while the shell thickness δ_1 appears in the *denominator* of $\overline{\rho}_{c1}$. Since it has been assumed that the shell thicknesses are small, these results yield values of $\overline{\rho}_{c1}$ which are much larger than $\overline{\rho}_{c2}$, which is consistent with the initial assumption that $(\overline{\rho}_{c1}\delta_1)^2 \ll 1$.

Figures 6.2(a) and (b) illustrate the variation of $\overline{\rho}_{c1}$ with δ_1 and $\overline{\rho}_{c2}$ with δ_2, respectively. In these figures, the approximate analytic results obtained using Equations (6.70) and (6.94) are shown with a dashed line, and the exact numerical solution is represented by the solid line and black stars. The numerical solutions were obtained by the minimization of the scattered fields associated with the first three modes, and solved using the thin shell results as initial guesses for each value of $\overline{\kappa}_{c2}$, denoted as black circles. Very good agreement is observed between the approximate analytic results and the exact numerical solutions. Both highlight the dominant effects of $\overline{\rho}_{c2}$ increasing linearly with δ_2, and of $\overline{\rho}_{c1}$ varying as δ_1^{-1}. Even though the thin shell results predict the correct functional dependence with respect to δ_1, the deviation from the exact solution increases for larger δ_1. This is due to

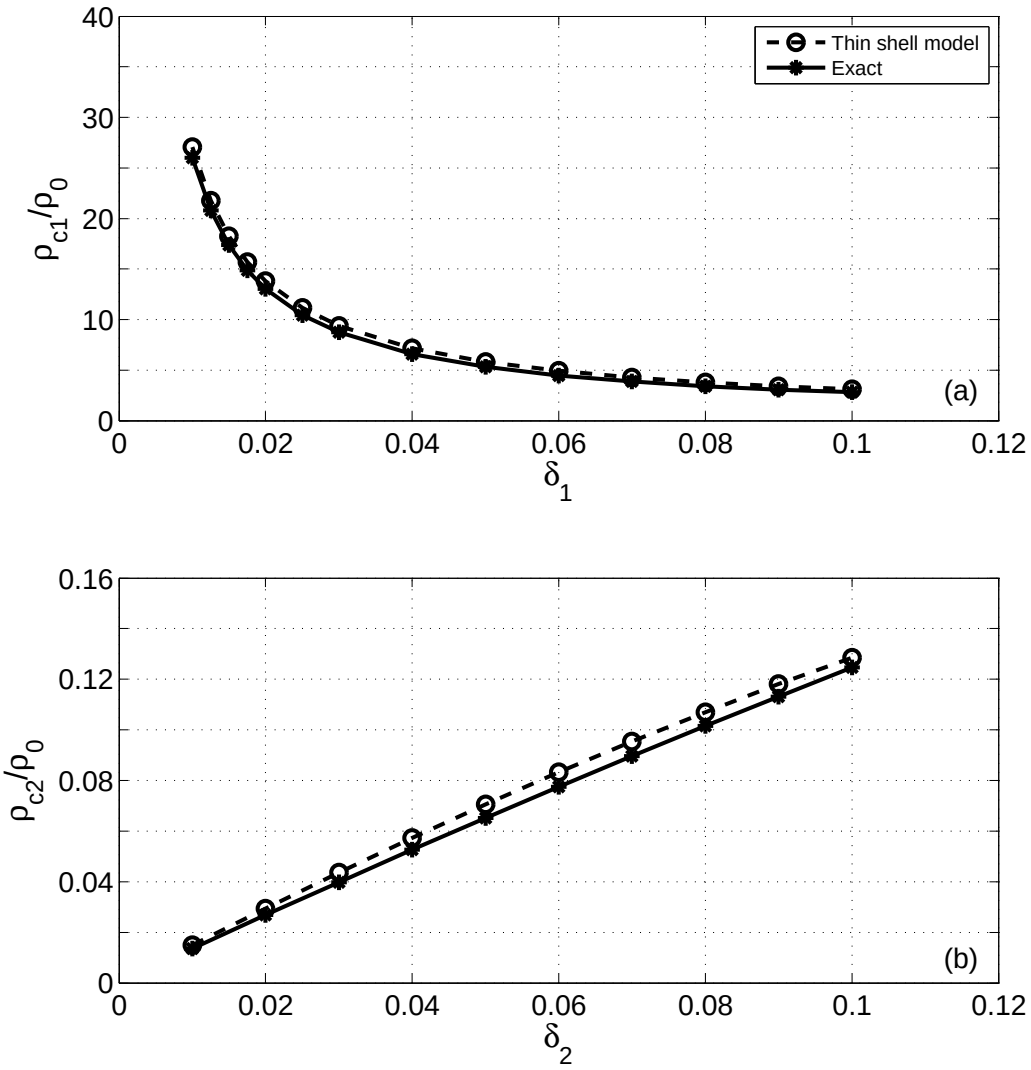

Figure 6.2: Variation in cloaking layer density as a function of the shell thickness, for the (a) outer cloaking layer and (b) inner cloaking layer. The two layer fluid cloak is enclosing a rigid, immovable sphere at $k_{d,0}a = 1.0$, with (a) $\delta_2 = 0.01$, (b) $\delta_1 = 0.01$. The cloaking layer densities are normalized by the density of the fluid in the surrounding medium, and the shell thickness is normalized by the radius of the inner sphere. Thin shell results are calculated using Equations (6.77) and (6.94).

the fact that, as the shell thickness becomes thicker, the thin shell assumption is less accurate, as expected.

Equation (6.92) allows the determination of $\overline{\kappa}_{c1}$, based on the shell thickness δ_1 and the value of $\overline{\rho}_{c1}$ and $\overline{\kappa}_{c2}$. Although $\overline{\rho}_{c1}$ varies significantly with δ_1, in Equation (6.92) it appears only as the product $\overline{\rho}_{c1}\delta_1$. As a function of the shell thickness, $\overline{\kappa}_{c2}$ is primarily dependent on the presence of δ_1 in the numerator of Equation (6.92), as illustrated in Figure 6.3(a).

Although the shell thickness influences the magnitude of $\overline{\kappa}_{c1}$ required for cloaking, the most significant variable influencing $\overline{\kappa}_{c1}$ is $\overline{\kappa}_{c2}$. Looking at the denominator in Equation (6.92), the presence of the difference between the coefficient $\overline{\gamma}_0$ and a term containing $\overline{\kappa}_{c2}$ suggests the possibility of a pole occurring in the parameter space. This trend is observed in Figure 6.3(b) in both the analytic results and exact numerical solution. For values of $\overline{\kappa}_{c2}$ below a critical point, the resulting $\overline{\kappa}_{c1}$ becomes negative. Since only positive layer properties are considered in this work, this asymptote corresponds to the minimum allowable $\overline{\kappa}_{c2}$ and sets a lower bound on the range of the parameter space. Due to the rapid rate of change as $\overline{\kappa}_{c2}$ approaches this minimum value, it can be seen that the differences in $\overline{\kappa}_{c1}$ given by the analytic model and exact solutions can become more significant. However, the analytic solution for $\overline{\kappa}_{c1}$ is still sufficient to converge to an exact solution, while capturing the underlying nature of the relationship between $\overline{\kappa}_{c1}$ and $\overline{\kappa}_{c2}$.

6.3.2 Region 2: $\overline{\rho}_{c1} \ll \overline{\rho}_{c2}$

In Section 6.2.2, analytic expressions were developed for the case when $\overline{\rho}_{c1} \ll \overline{\rho}_{c2}$. These expressions are simplified in the case of a rigid, immovable sphere, by

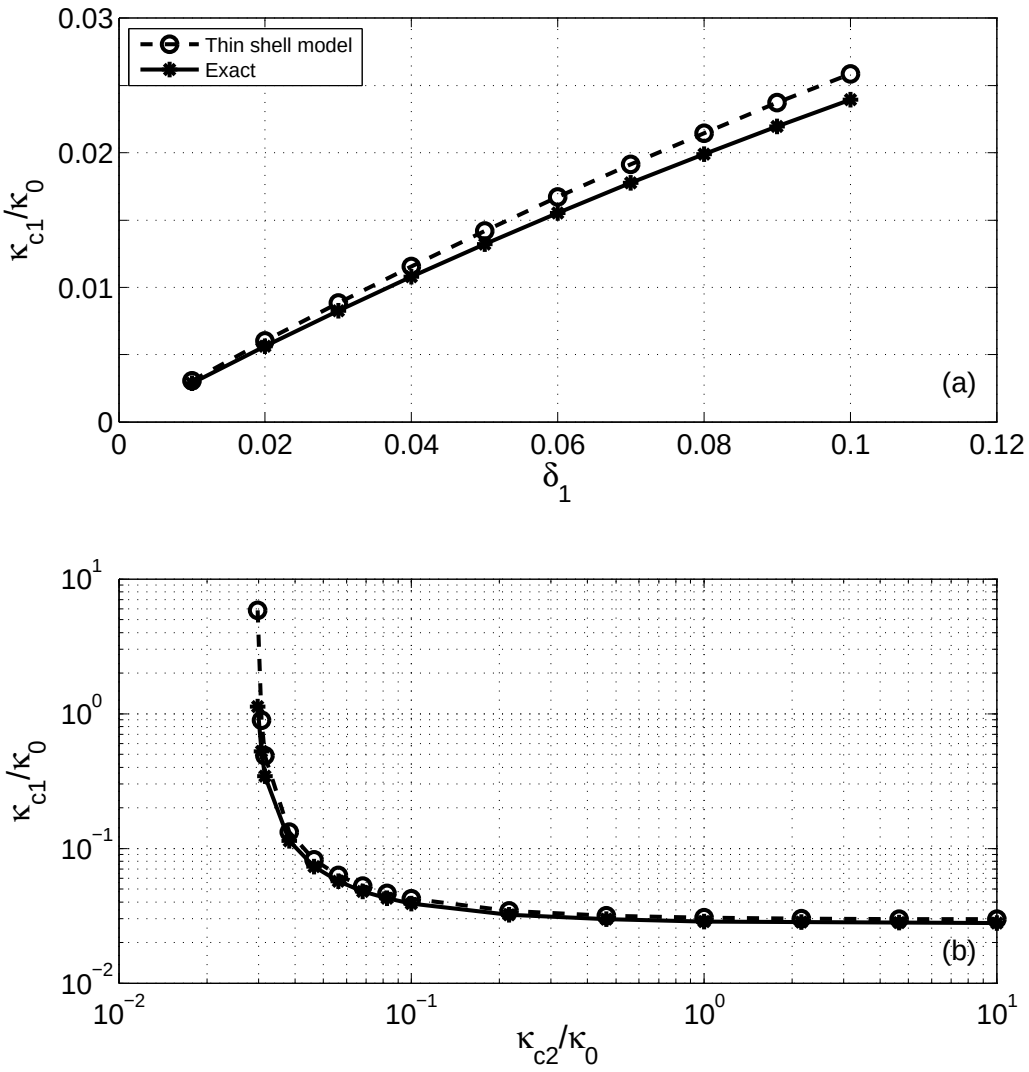

Figure 6.3: Variation in the bulk modulus of the outer cloaking layer κ_{c1} as a function of the (a) shell thickness δ_1 and (b) inner cloaking layer bulk modulus κ_{c2}, enclosing a rigid, immovable sphere at $k_{d,0}a = 1.0$. In (a) $\delta_2 = 0.01$ with $\overline{\kappa}_{c2} = 1$, and (b) $\delta_1 = \delta_2 = 0.01$. The cloaking layer bulk modulus is normalized by the bulk modulus of the fluid in the surrounding medium, and the shell thickness is normalized by the radius of the inner sphere. Thin shell results are calculated using Equation (6.92).

taking the limit of $\Upsilon_n \to 0$ in Equation (6.79):

$$\overline{\kappa}_{c2} = \frac{\delta_2 (k_{d,0} b_1)^2 \left[\overline{\rho}_{c2} \delta_2 k_{d,0} b_1 j_0'(k_{d,0} b_1) - \overline{\mathcal{F}}_0 \right]}{\overline{\gamma}_0 - (k_{d,0} b_1)^2 \left[\overline{\rho}_{c1} \delta_1 k_{d,0} b_1 j_0'(k_{d,0} b_1) - \overline{\mathcal{F}}_0 \right] \dfrac{\delta_1}{\overline{\kappa}_{c1}}}. \tag{6.95}$$

Considering the coefficients given by Equations (6.59)–(6.61) and (6.85)–(6.88), it is observed that in the limit of $\Upsilon_n \to 0$,

$$\bar{a}_0^{(n)} = \bar{a}_1^{(n)} = a_2^{(n)} = 0. \tag{6.96}$$

Therefore, Equation (6.80) reduces to

$$\overline{\rho}_{c1} = 2\delta_1 \frac{\bar{b}_0^{(1)} \overline{\rho}_{c2} \delta_2 + c_0^{(1)}}{b_2^{(1)} \overline{\rho}_{c2} \delta_2 + c_2^{(1)} + \bar{b}_1^{(1)} (k_{d,0} b_1)^2 \dfrac{\delta_1}{\overline{\kappa}_{c1}}}. \tag{6.97}$$

Although Equation (6.97) is very similar in form to Equation (6.94), an important difference is noticed in that Equation (6.97) retains a dependence on $\overline{\kappa}_{c1}$ arising from $b_1^{(n)} \neq 0$, whereas Equation (6.94) is independent of the bulk modulus. Similarly, using Equation (6.96), the expressions for $\bar{q}_0$, $\bar{q}_1$, and $\bar{q}_2$ can be simplified, but there is still is a dependence on $\overline{\kappa}_{c1}$ which remains in both $\bar{q}_1$ and $\bar{q}_2$. Therefore, using Equation (6.81), $\overline{\rho}_{c2}$ will also have a dependence on $\overline{\kappa}_{c1}$. The dependence of $\overline{\kappa}_{c2}$, $\overline{\rho}_{c2}$, and $\overline{\rho}_{c1}$ on $\overline{\kappa}_{c1}$ is shown Figure 6.4(a)–(c), respectively.

From Figure 6.4(a) and (b), both $\overline{\kappa}_{c2}$ and $\overline{\rho}_{c2}$ asymptotically become infinite as $\overline{\kappa}_{c1}$ decreases towards a critical point, beyond which both cloaking layer properties would need to be negative. This asymptotic behavior is also observed in the required value of $\overline{\rho}_{c1}$ in Figure 6.4(c), except that it approaches $-\infty$.

Another important characteristic is the presence of a lower limit for the positive values of $\overline{\rho}_{c2}$ and $\overline{\kappa}_{c2}$, which occur as $\overline{\kappa}_{c1} \to \infty$. For $\overline{\rho}_{c2}$, this leads to values which are quite large; for $\delta_1 = 0.01$ illustrated in Figure 6.4, the lower limit is $\overline{\rho}_{c2} = 1879$. Besides the practical problems of achieving such a high density, this

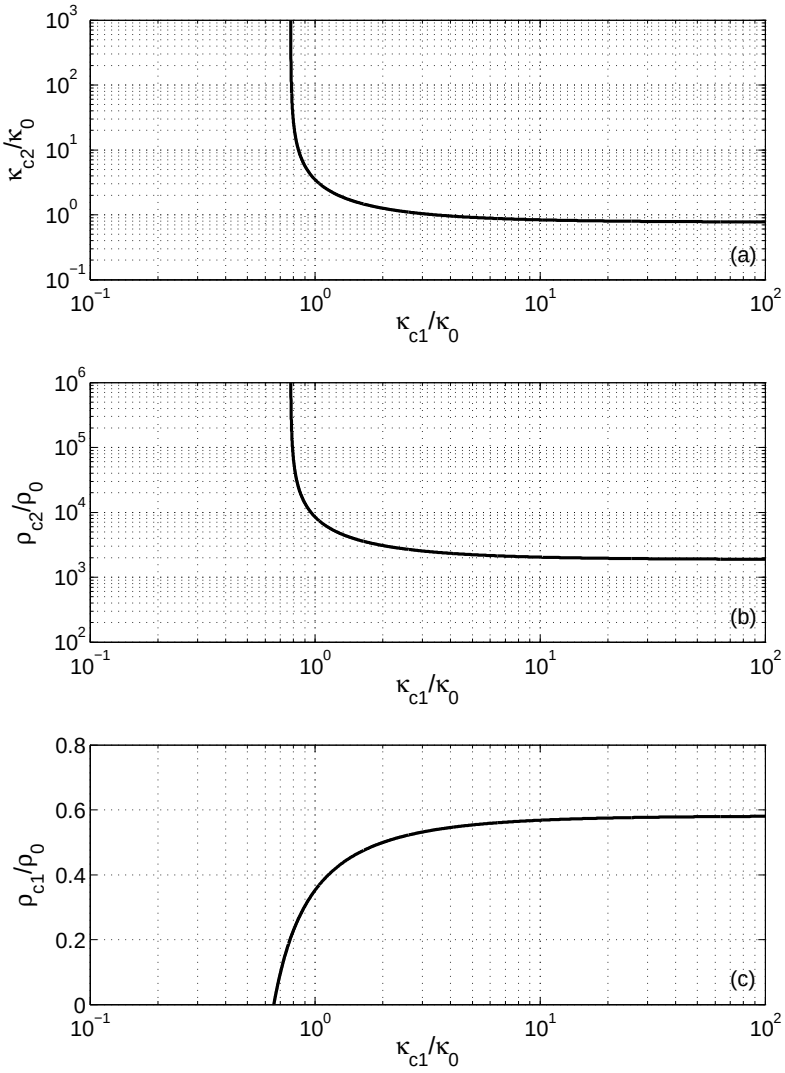

Figure 6.4: Variation as a function of outer cloaking layer bulk modulus κ_{c1} for (a) the inner cloaking layer bulk modulus κ_{c2} (b) the inner cloaking layer density ρ_{c2} and (c) the outer cloaking layer density ρ_{c1}, enclosing a rigid, immovable sphere for $\delta_1 = \delta_2 = 0.01$ at $k_{d,0}a = 2.0$. The cloaking layer properties are normalized by those of the fluid in the surrounding medium. Thin shell results are calculated using Equations (6.81), (6.95) and (6.97).

leads to $k_{d,c2}b_1\delta_2 \approx 1$, which suggests that the layer is not small enough compared to the wavelength to be considered a thin, and would require retaining higher order terms to achieve sufficient accuracy.

6.4 Elastic effects

In this section, the effects of elasticity in the core and in the cloaking layers will be considered. First, the more general case of a penetrable sphere will be considered, with the core material consisting of an isotropic elastic solid. Therefore, the analytic expressions for the cloaking layer properties will be more complex, since Υ_n will be nonzero and given by Equation (6.26), and the resulting $\overline{\rho}_{c1}$, $\overline{\rho}_{c2}$ and $\overline{\kappa}_{c1}$ will all vary as a function of $\overline{\kappa}_{c2}$.

After exploring the behavior of various common elastic solids, the details of the resulting reduction on the scattering strength will be examined for a specific case of a steel sphere in water. Using this example, the broad applicability of the equations developed in Section 6.2.1 will be illustrated for both a two fluid cloaking layer and when elastic (shear) effects are considered in the outer cloaking layer.

6.4.1 Penetrable elastic core

To examine the cloaking layer properties when the core material is an isotropic elastic solid, Figure 6.5 shows $\overline{\rho}_{c1}$, $\overline{\rho}_{c2}$ and $\overline{\kappa}_{c1}$ as a function of $\overline{\kappa}_{c2}$ for $\delta_1 = \delta_2 = 0.04$ and $k_{d,0}a = 2.0$. The results for three different isotropic elastic solids commonly used in engineering applications are presented: steel, aluminum and glass. The surrounding fluid in each case is water. For comparison, the results for a rigid, immovable sphere are also shown.

Comparing the results for the three elastic solids to that of the rigid sphere, the same general trends can be found for each cloaking layer property. In Fig-

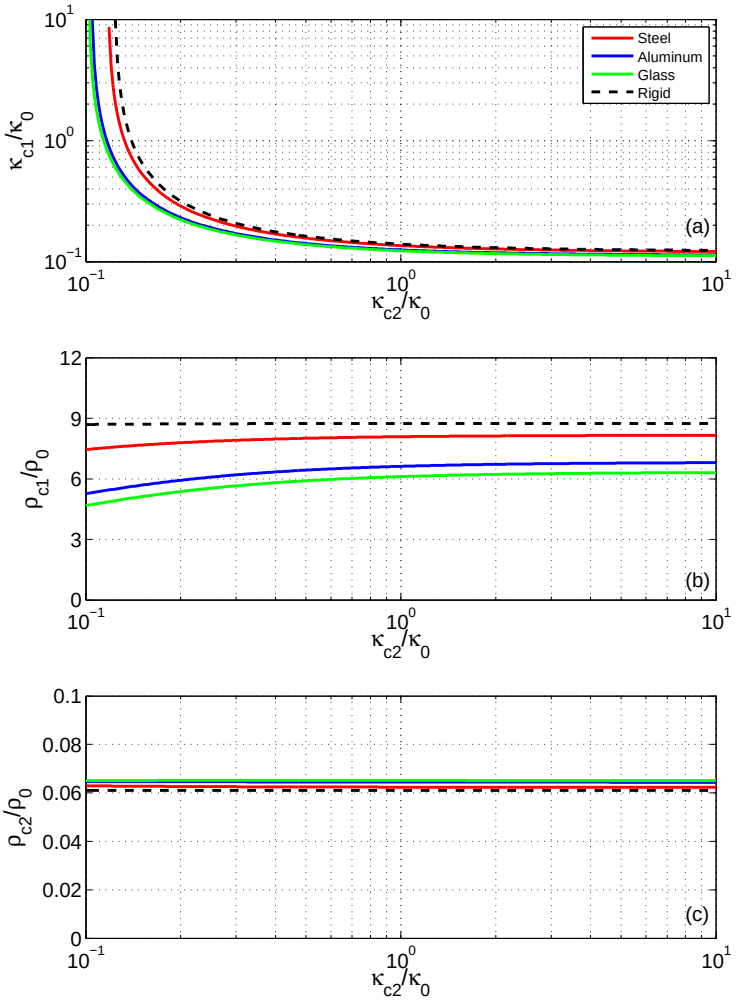

Figure 6.5: Variation as a function of inner cloaking layer bulk modulus κ_{c2} for (a) the outer cloaking layer bulk modulus κ_{c1} (b) the outer cloaking layer density ρ_{c1} and (c) the inner cloaking layer density ρ_{c2} for $\delta_1 = \delta_2 = 0.04$ at $k_{d,0}a = 2.0$. Curves are shown for 4 different core materials: steel (solid red line), aluminum (solid blue line), glass (solid green line) and a rigid, immovable sphere (dashed black line). Material properties are listed in Table 4.1. The cloaking layer properties are normalized by those of the fluid in the surrounding medium, which is water. Thin shell results are calculated using Equations (6.77), (6.92) and (6.94).

ure 6.5(a), $\overline{\kappa}_{c1}$ exhibits the same asymptotic behavior for all cases, though the point where $\overline{\kappa}_{c1} \to \infty$ occurs at a slightly lower value of $\overline{\kappa}_{c2}$ for the elastic core materials.

In Figure 6.5(b), the variation of $\overline{\rho}_{c1}$ with $\overline{\kappa}_{c2}$ is illustrated. In Section 6.3 it was observed that the cloaking layer densities for a rigid, immovable sphere were independent of $\overline{\kappa}_{c2}$. In Figure 6.5(b), it can be observed that elastic core materials exhibit a slight decrease in the value of $\overline{\rho}_{c1}$ for smaller values of $\overline{\kappa}_{c2}$, in contrast with the case of a rigid, immovable core. However, the most significant variation occurs in the overall magnitude of $\overline{\rho}_{c1}$, which decreases with the density and bulk modulus of the elastic material. Specifically, it can be observed that the value of $\overline{\rho}_{c1}$ required in this configuration for a glass or aluminum sphere is about a third of that of a rigid sphere. Even for a steel sphere, with a density and bulk modulus much larger than water, this value is about 10% less than if the sphere were perfectly rigid.

Figure 6.5(c) reports the variation of $\overline{\rho}_{c2}$, which shows that this parameter is much less sensitive to the core material properties, compared to $\overline{\rho}_{c1}$. The small change in the magnitude which arises when considering elastic core materials leads to slightly larger value of $\overline{\rho}_{c2}$. In addition, there is negligible change as $\overline{\kappa}_{c2}$ is varied over several orders of magnitude.

6.4.2 Scattering strength reduction using two fluid layers

In the analysis of the two layer cloak up to this point, the focus has been on determining the necessary cloaking layer properties and understanding their relationship to achieve an optimal design. However, it has not been verified yet how the acoustic cloak would ultimately perform. To explore the functionality of the cloak, consider a steel sphere in water, covered by two fluid cloaking layers with thicknesses $\delta_1 = \delta_2 = 0.04$, $\overline{\kappa}_{c2} = 0.175$ and a design frequency of $k_{d,0}a = 2.0$. The cloaking layer properties used in this case are given in Table 6.1.

Solution type	$\overline{\rho}_{c1}$	$\overline{\kappa}_{c1}$	$\overline{\rho}_{c2}$	$\overline{\kappa}_{c2}$
Analytic (thin-shell approx.)	7.738	0.361	0.063	0.175
Exact (fluid/fluid)	7.700	0.213	0.049	0.175
Exact (elastic/fluid)	8.081	0.262	0.056	0.175

Table 6.1: Cloaking layer properties for a steel sphere in water, coated by an acoustic plasmonic cloak consisting of two layers with shell thicknesses $\delta_1 = \delta_2 = 0.04$ and a design frequency of $k_{d,0}a = 2.0$. Solutions are given based on analytic thin-shell expressions, exact solutions for the case of two fluid layers, and exact solutions for the case of a fluid inner layer and isotropic elastic outer layer with $\nu_{c1} = 0.3$.

To examine the effectiveness of the cloak at $k_{d,0}a = 2.0$, Figure 6.6(a) and (b) show the real part of the total pressure field for an uncloaked and cloaked steel sphere in water, excited by a time harmonic incident pressure wave impinging from bottom to top. For the uncloaked sphere shown in the top panel of Figure 6.6, there is significant perturbation of the pressure field in and around the object.

Figure 6.6(b) indicates that the optimized cloaking layers dramaticly change in the pressure field in the surrounding fluid and within the elastic sphere, showing that the incident wave is almost completely undisturbed by the cloaked sphere. Since the plasmonic acoustic cloak was designed to cancel the scattered field in the surrounding fluid, it is also seen that the incident pressure field still interacts with the steel sphere, though the resulting stress field within the sphere is more uniform than when uncloaked. With the scattered field cancelled, the total pressure acting on the outer surface of the steel sphere is equal to the incident pressure, and so the pressure in the steel sphere is phases matched to the incoming wave. Based on this characteristic, an acoustic plasmonic cloak of this type therefore may enable the design of an *ideal sensor*, allowing for detection of an incident acoustic wave without almost any disruption of the pressure field [56].

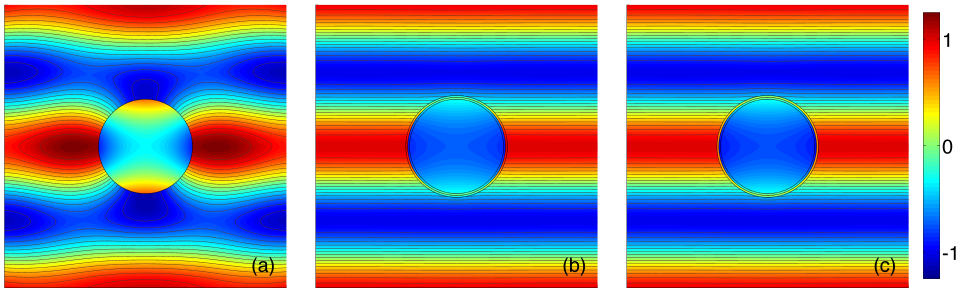

Figure 6.6: Real part of the total pressure field for a steel sphere in water at $k_{d,0}a = 2.0$: (a) uncloaked, (b) cloaked using two fluid layers, and (c) cloaked using a fluid inner layer and an elastic outer layer. For the cloaked spheres, each layer of the cloak has a shell thickness of $\delta = 0.04$. The color scale for the pressure is normalized by the amplitude for the incident wave, which is a time-harmonic plane wave impinging from bottom to top.

To analyze the frequency dependence of the plasmonic acoustic cloak functionality, the magnitude of the first 6 scattering coefficients is plotted for the uncloaked and cloaked configurations in Figure 6.7(a) and (b), respectively. Comparing Figure 6.7(a) and (b), the effect of adding the cloaking layer is clearly seen at the design frequency of $k_{d,0}a = 2.0$, where nulls in the $n = 0$, $n = 1$ and $n = 2$ scattering modes are aligned. The resulting scattered field at the design frequency can be expressed in terms of the scattering gain, given by Equation (4.80), which is plotted in Figure 6.7(c). From this plot, it can be seen that the scattering strength is reduced by 35 dB at $k_{d,0}a = 2.0$, where the first three scattering modes are cancelled. Interestingly, away from the design frequency significant scattering reduction is also obtained. In particular, the scattering strength is reduced by 20 dB over a range of $k_{d,0}a$ from 0 to almost 2.5. This reduction in scattering strength, though more modest, extends even up to $k_{d,0}a = 5$ and beyond. These observations are verified by results obtained using COMSOL, for which there is excellent agreement over the

entire band shown in Figure 6.7(c). Details on the implementation of the COMSOL simulation are given in Appendix C.

6.4.3 Practical considerations for implementation

Given the ability of the plasmonic acoustic cloak described in the previous section to significantly reduce the scattering strength of a spherical target in water, an important question to consider is what type of materials could be used to create such a structure. The cloaking layer properties presented in the previous section require two fluid layers, with the cloaking layer properties given in Table 6.1. For the specific case considered here, the bulk modulus of each layer is approximately 0.2 times that of water. The density of the outer layer needs to be large, roughly equal to that of steel, while the density of the inner layer is very low, about 5% of the density of water.

Since no naturally occurring fluids exhibit such properties, alternative methods would be required to obtain the necessary combinations of densities and bulk moduli. One possible means would be the use of acoustic metamerials, which have been proposed for other acoustic cloaking applications [12][21]-[16]. Unlike acoustic cloaks developed using coordinate transformation techniques, the layers for this design are simply isotropic fluids, but require extreme values not found in nature.

One promising method to achieve the necessary material properties consists in creating an effective fluid using a microstructure consisting of smooth beads. Such a structure would allow for the density and bulk modulus of the effective fluid to be varied based on the composition and volume fraction of the beads. Use of a lubricated bead microstructure has also been proposed as a means for creating an *acoustic metafluid*, based on the requirements for transformation-based acoustic cloaks [21].

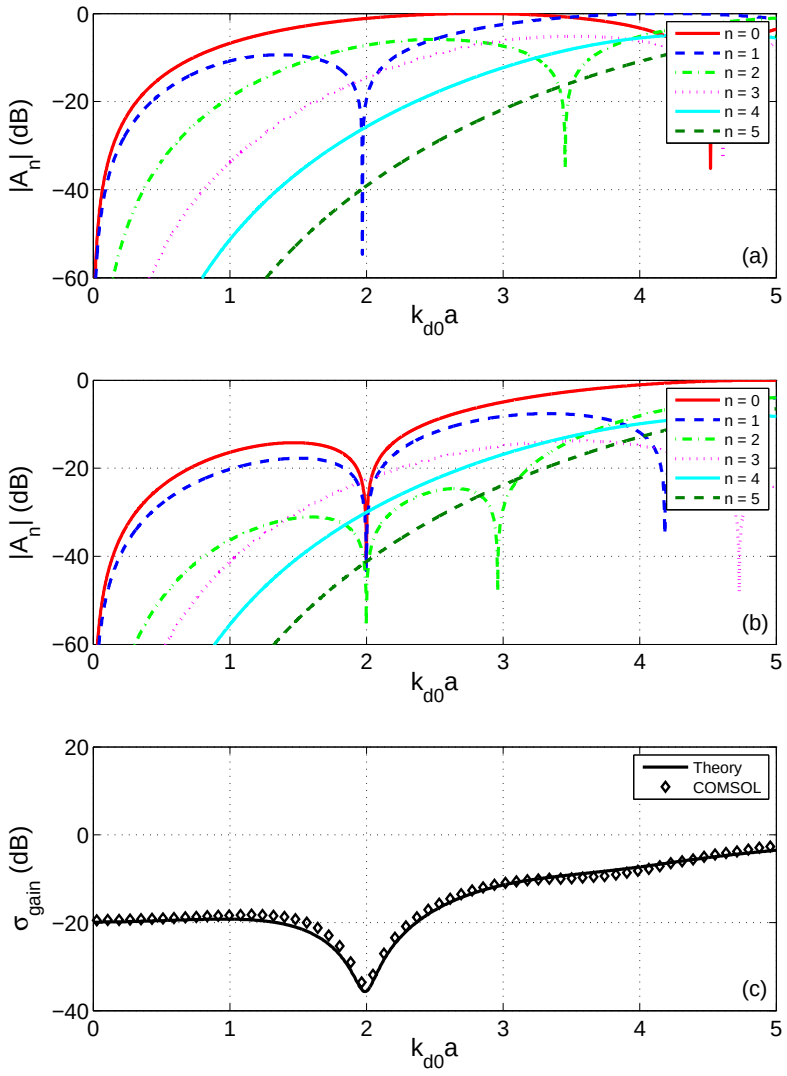

Figure 6.7: Scattering coefficients (in dB) for an (a) uncloaked and (b) cloaked steel sphere in water. The cloak consists of two fluid layers with $\delta_1 = \delta_2 = 0.04$, which cancels the first three scattering modes at $k_{d,0}a = 2.0$. The scattering gain in dB, relative to the uncloaked scatterer, is given in (c) for the exact theoretical solution and using finite elements (COMSOL).

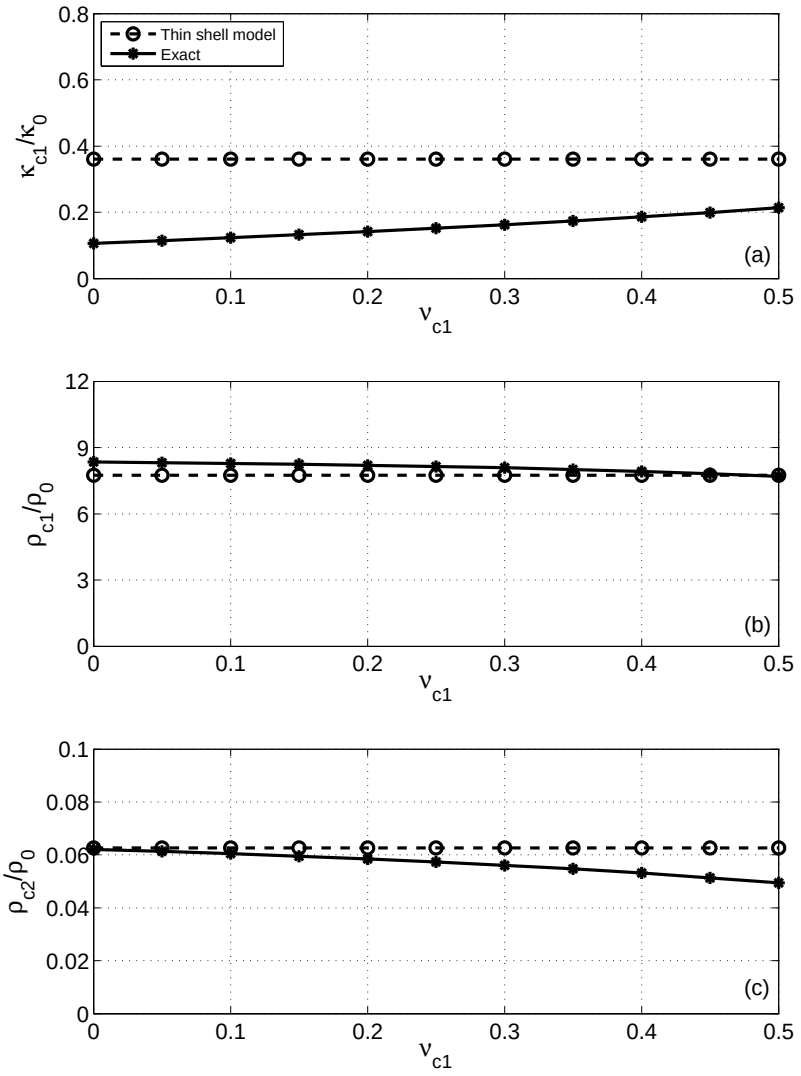

Figure 6.8: Variation as a function of outer cloaking layer Poisson's ratio ν_{c1} for (a) the outer cloaking layer bulk modulus κ_{c1} (b) the inner cloaking layer density ρ_{c1} and (c) the outer cloaking layer density ρ_{c2}, enclosing a steel sphere in water for $\delta_1 = \delta_2 = 0.04$ at $k_{d,0}a = 2.0$. The cloaking layer properties are normalized by those of the fluid in the surrounding medium. Thin shell results are calculated using Equations (6.77), (6.92) and (6.94).

Although the design procedure presented in this paper has assumed that the cloak consists of two fluid layers, in practice this would require some sort of elastic materials to maintain the structure of the cloak. To determine the effect of using an isotropic elastic solid for the outer layer, Figure 6.8 shows the variation with the cloaking layer properties of the Poisson's ratio in the outer layer, ν_{c1}. Using the thin fluid shell model results as an initial guess, the exact solution for each value of ν_{c1} is determined using the numerical techniques described in Section 3.4. Since the analytic thin-shell expressions developed in this work assume only fluid layers, these results tacitly assume Poisson's ratio is 0.5 and therefore appear constant in the plots. Although there is some deviation in the magnitude of the cloaking layer properties when the outer layer is elastic compared to the fluid layer solution, the different is relatively modest and suggests that the use of the analytic results developed in Section 6.2 can be applied to get a good initial guess also when an outer layer is elastic.

To compare the effectiveness of this configuration, the real part of the total pressure field is plotted in Figure 6.6(c). In this configuration, the inner layer is a fluid and the outer layer is an isotropic elastic solid, with $\nu_{c1} = 0.3$. Comparing Figure 6.6(c) with the two fluid layer case shown in Figure 6.6(b), it is clear that the performance of the two are identical at the design frequency of $k_{d,0}a = 2.0$.

To evaluate the scattering reduction and bandwidth with an elastic outer layer, Figure 6.9(a) and (b) shows the magnitude of the first 6 scattering coefficients for the uncloaked and cloaked configurations, respectively, using the cloaking layer properties listed in Table 6.1. The scattering gain is presented in Figure 6.9(c), with the elastic layer and the fluid-only cloaking layer solution shown together for comparison. In the vicinity of the design frequency $k_{d,0}a = 2.0$ and above, the scattering modes and scattering gain are nearly identical to the case with two fluid

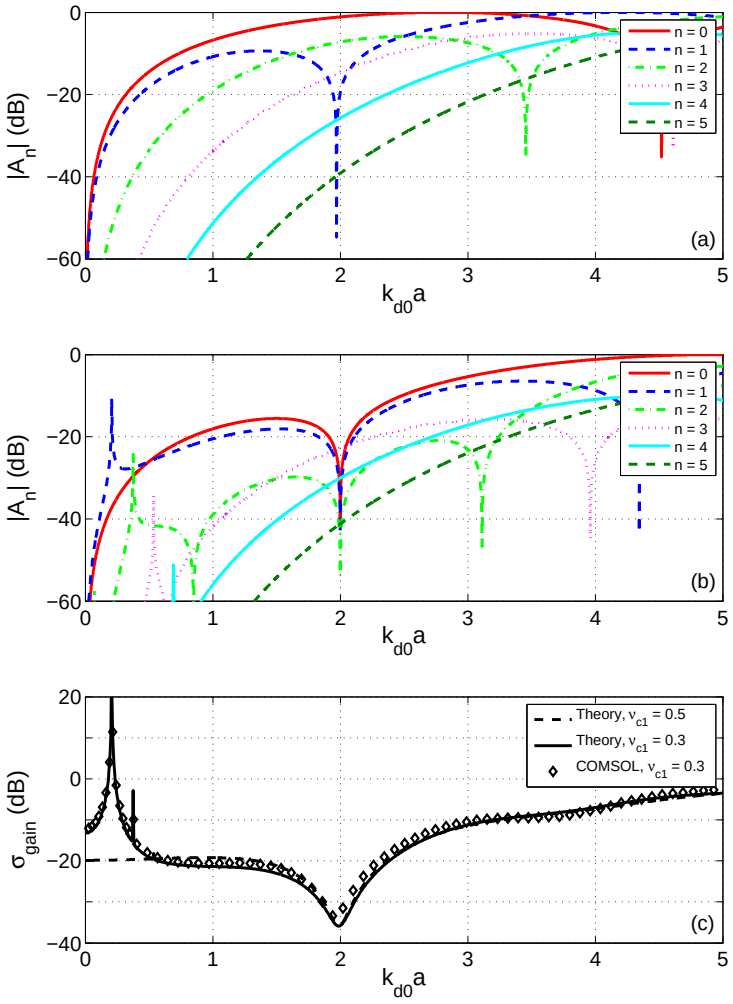

Figure 6.9: Scattering coefficients (in dB) for an (a) uncloaked and (b) cloaked steel sphere in water. The cloak consists of an inner fluid layer and outer elastic layer with $\delta_1 = \delta_2 = 0.04$, which cancels the first three scattering modes at $k_{d,0}a = 2.0$. The Poisson's ratio of the outer elastic layer is 0.3. The scattering gain in dB, relative to the uncloaked scatterer, is given in (c) for the exact theoretical solution and using finite elements (COMSOL) for the case when the outer layer is an isotropic elastic solid. The scattering gain for the case of a fluid outer layer (dashed) is given for reference.

layers. At low frequencies, however, there is a large peak in the the scattering gain. This is associated with the $n=1$ (dipole) resonance within the outer cloaking layer itself, which arises from the excitation of axisymmetric Lamb waves, and its behavior is also captured with remarkable precision using COMSOL. These resonances can also be found in the higher order modes, though the increase in the scattering gain is dominated by the response from the dipole mode.

6.5 Alternating fluid-fluid and fluid-elastic layers

Guided by the detailed analytic investigation presented in Sections 6.1 and 6.2, significant reductions in the scattering strength were demonstrated in Sections 6.3 and 6.4 using two plasmonic cloaking layers. Although such a thorough development would be desired for plasmonic cloaks consisting of any arbitrary number of layers, the increasing complexity of the system makes it impractical to obtain explicit expressions for the cloaking layer properties. Therefore, exact solutions for each configuration must be determined numerically for each specific configuration of interest.

Although any arbitrary layering scheme can be proposed, the lack of any analytic expressions to guide the design can make it difficult to determine which configurations will work. In addition, for the cases when there are three or more layers, even performing a parametric study for each independent layer property can be complicated and time consuming. Without any guide for determining an appropriate initial guess or introduction of a complex design space search algorithm, there is no way to determine beforehand whether or not such a parametric study will yield a solution for a plasmonic cloak, or simply one of the numerous anti-resonance cloaks which are examined in Chapter 5.

Alternatively, one method for developing a multilayer cloak is to use two

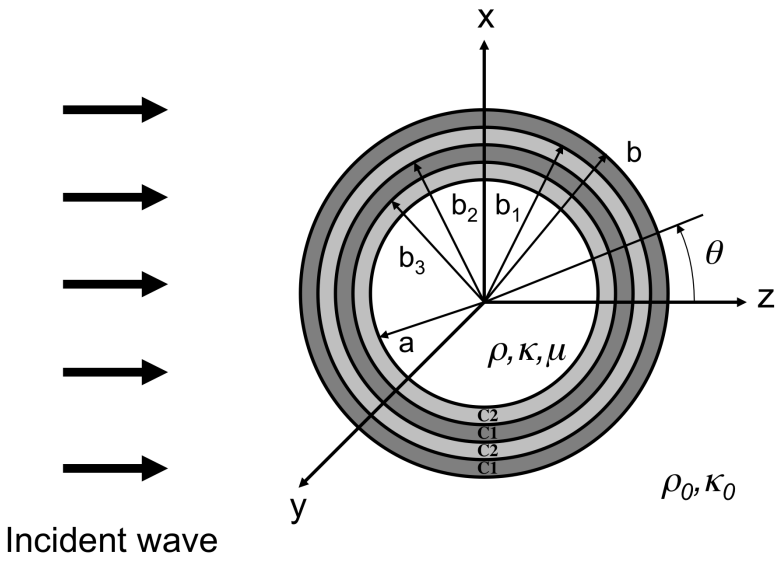

Figure 6.10: A time-harmonic incident plane wave in a fluid medium impinging on an isotropic elastic core of radius a coated in four concentric shells of uniform thickness with outer radius b. The layers consist of alternating materials *C1* and *C2*, respectively, starting with the outermost layer. The surrounding medium has density ρ_0 and bulk modulus κ_0, and the elastic core has density ρ, bulk modulus κ and shear modulus μ.

cloaking layer materials in an alternating laminate scheme, an example of which is illustrated in Figure 6.10. By varying the layer thicknesses, this enables one to cancel different modes, while limiting the parameter space by searching for only two sets of cloaking material properties. Furthermore, the two layer plasmonic cloaking results developed in previous sections of this chapter can be used to guide the selection of the cloaking layer properties. Such an approach has been used extensively in designing transformation-based acoustic cloaks, providing a relatively simple means of designing functionally-graded anisotropic cloaks with alternating fluid layers [15, 27].

To highlight how this method relates to the two layer configurations devel-

Solution type	$\overline{\rho}_{c1}$	$\overline{\kappa}_{c1}$	$\overline{\rho}_{c2}$	$\overline{\kappa}_{c2}$
Exact (fluid/fluid)	8.6465	0.2242	0.0213	0.2000
Exact (elastic/fluid)	8.3770	0.1469	0.0239	0.2204

Table 6.2: Cloaking layer properties for a four layer acoustic plasmonic cloak for a steel sphere in water at a design frequency of $k_{d,0}a = 2.0$. The shell thicknesses δ of the four layers, in order of the outermost to innermost layer, are 0.0135, 0.0642, 0.0037 and 0.0046, respectively. Exact solutions obtained numerically for the case of four fluid layers, and the case of alternating fluid and isotropic elastic layers with $\nu_{c1} = 0.3$.

oped in the previous section, consider a four layer design illustrated in in Figure 6.10 for the case of a steel sphere in water at $k_{d,0}a = 2.0$. Using the results from Table 6.1 for the two layer case, a solution for a four layer plasmonic acoustic cloak can be obtained numerically and the relevant properties are presented in Table 6.2.

Figure 6.11(a) and (b) show the magnitude of the scattering coefficients for the uncloaked and cloaked configurations, respectively, for the case when both cloaking layer materials are fluids. From Figure 6.11(b) it is clear that the first four modes are cancelled at $k_{d,0}a = 2.0$ with the cloaking layers present. The resulting scattering gain is presented in Figure 6.11(c), from which it is seen that the scattering strength is reduce by 70 dB compared with the uncloaked steel sphere at $k_{d,0}a = 2.0$. Away from the design frequency, there is still significant reduction in the scattering strength, with a 30 dB or more reduction below $k_{d,0}a = 2.0$, with a more modest reduction achieved up to about $k_{d,0}a = 5.0$, at which point the scattering strength is the same as the uncloaked steel sphere.

These results show a noticeable improvement over those obtained for the two fluid layer case. Recall that for the two fluid layer case shown in Figure 6.7, only the first three modes were cancelled. Furthermore, contributions from the remaining modes (in particular the $n = 3$ mode), limit the total scattering reduction achieved

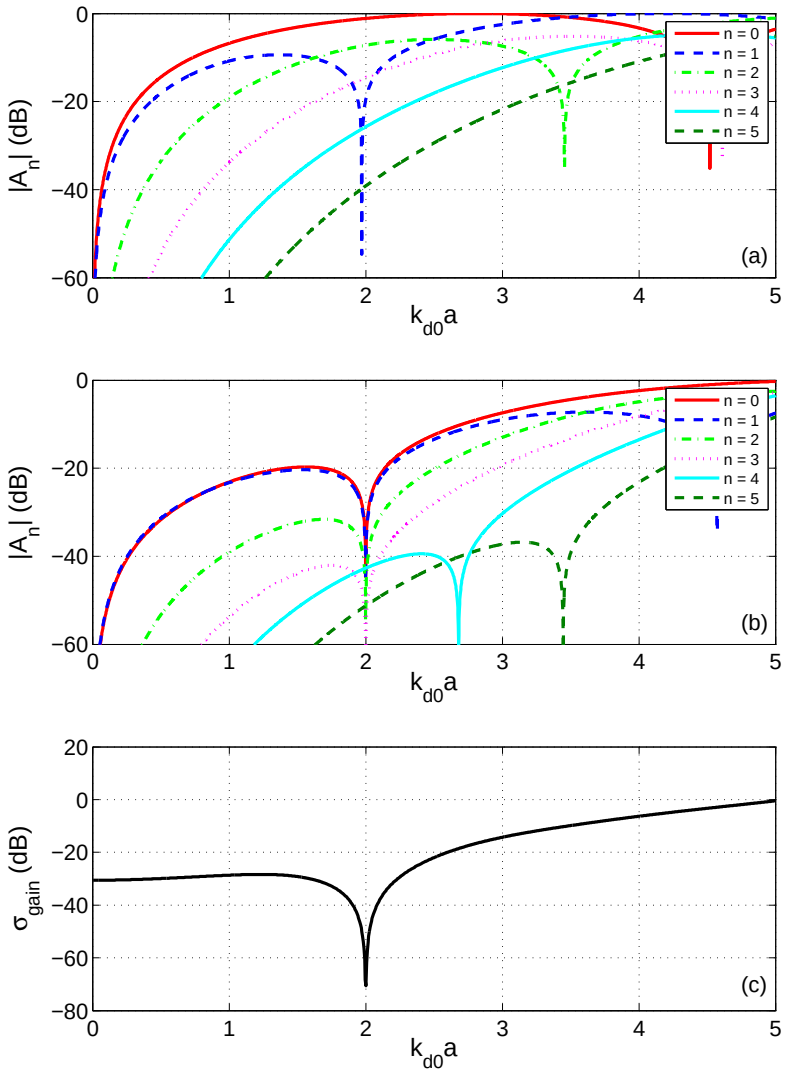

Figure 6.11: Scattering coefficients (in dB) for an (a) uncloaked and (b) cloaked steel sphere in water. The cloak consists of four fluid layers, which cancels the first four scattering modes at $k_{d,0}a = 2.0$. The cloaking layer properties are given in Table 6.2. The scattering gain in dB, relative to the uncloaked scatterer, is given in (c).

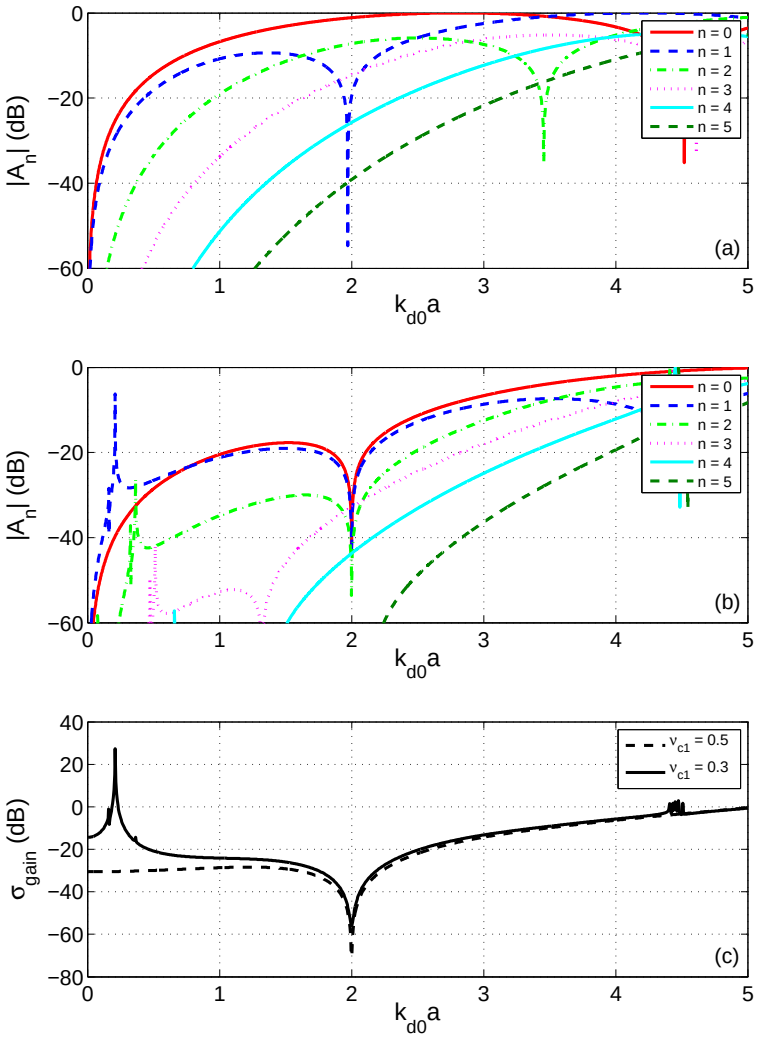

Figure 6.12: Scattering coefficients (in dB) for an (a) uncloaked and (b) cloaked steel sphere in water. The cloak consists of a four layer cloak, consisting of alternating fluid and elastic layers, which cancels the first three scattering modes at $k_{d,0}a = 2.0$. The Poisson's ratio of the elastic layer is 0.3, and the cloaking layer properties are given in Table 6.2. The scattering gain in dB, relative to the uncloaked scatterer, is given in (c) for the case when the outer alternating layer is fluid (dashed) and elastic (solid).

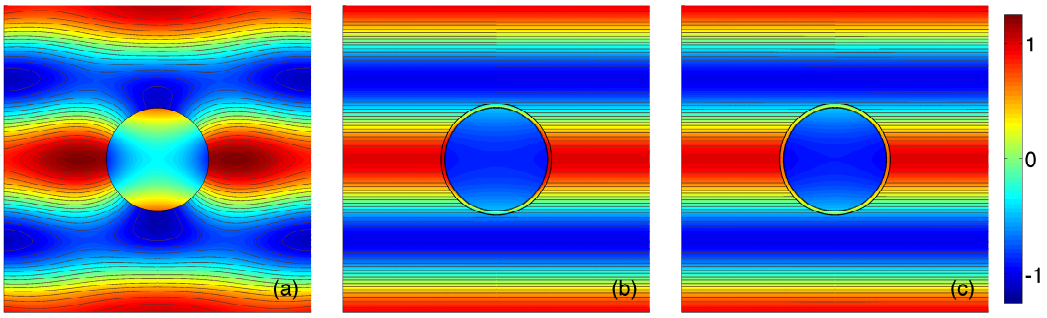

Figure 6.13: Real part of the total pressure field for a steel sphere in water at $k_{d,0}a = 2.0$: (a) uncloaked, (b) cloaked using four fluid layers, and (c) cloaked using alternating fluid and elastic layers. The cloaking layer properties are given in Table 6.2. The color scale for the pressure is normalized by the amplitude for the incident wave, which is a time-harmonic plane wave impinging from bottom to top.

at $k_{d,0}a = 2.0$ to 35 dB.

Examining the effectiveness for the four layer configuration consisting of alternating fluid and elastic materials, Figure 6.12(a) and (b) show the magnitude of the scattering coefficients when the steel sphere is uncloaked and cloaked, respectively. In this case, only the first three modes are cancelled, although all of the higher modes are significantly reduced. As a result, a 55 dB reduction in the scattering strength is observed at $k_{d,0}a = 2.0$, as shown in Figure 6.12(c). It is seen that like the two layer cloak with an elastic outer layer, there are low frequency modal resonances apparent for $n \geq 1$, the same as those observed in Figure 6.9.

To illustrate the effect of the cloak at the design frequency, Figure 6.13(a)–(c) shows the real part of the total pressure field for a steel sphere in water when uncloaked, coated in a four fluid layer cloak, and coated in a four layer cloak consisting of alternating fluid and elastic materials, respectively. With the addition of the coatings, it is seen that the disruptions in the time-harmonic incident wave are eliminated for both cloaked configurations.

Through the use of alternating cloaking layers, it has been shown that superior reduction in the scattering strength can be achieved, through the cancellation (or significant reduction) of higher scattering modes. Although only a relatively simply design consisting of four layers was presented, these results can be applied to more complicated cloak configurations. Despite the improved performance within the vicinity of the design frequency, it was observed that an alternating-layer design does not eliminate the low frequency dipole resonance which occurs when elastic cloaking layers are used.

To address this issue, a more detailed analysis must be undertaken to examine the elastodynamics of spherical elastic layers. In particular, an examination of materials with transverse isotropy allows for independent control of the radial and transverse stiffnesses of each layer to address the low frequency dipole resonance, and likely lead to an improved broadband acoustic plasmonic cloak. The following chapter therefore presents an investigation of the effects of transversely isotropic cloaking layers on the resulting scattered field.

Chapter 7

Theoretical formulation for spherically isotropic elastic layers

Although numerous materials exhibit isotropic behavior that can accurately be described by the methods of Chapter 3, there also many whose elastic properties are different along different axes. This is known as elastic anisotropy. Although some homogeneous structures may possess anisotropy (such as those occurring in crystalline materials), many anisotropic elastic materials are heterogeneous compositions.

Of particular interest in many fields of science and engineering are materials which exhibit the simplest case of anisotropy, known as *transverse isotropy*. Transverse isotropy is defined by three orthogonal planes of symmetry, one of which is isotropic [35], as illustrated in Figure 7.1(a). In addition to providing more degrees of freedom, a transversely isotropic material can provide the ability to independently control the elastic properties of a layer in both the normal and tangential direction. Utilizing these qualities can lead to a more robust acoustic cloak compared with one comprised of only isotropic elastic materials.

For spherical geometry, the use of a transversely isotropic spherically symmetric shell is described as *spherical isotropy*, which is characterized by isotropic properties for rotation about any axis through the center of the sphere [78], and is illustrated in Figure 7.1(b). In the following sections, the formulation for achieving scattering cancellation using multiple spherically isotropic layers are presented. In

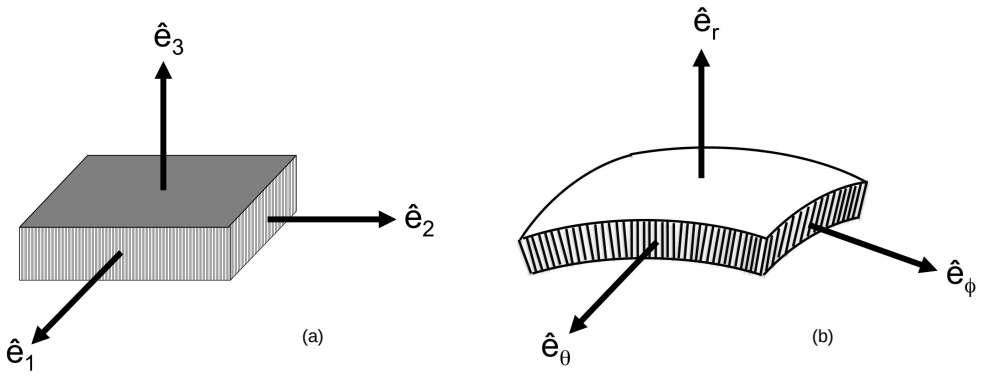

Figure 7.1: Geometry of the anisotropic media considered in this chapter, for a material with (a) transverse isotropy, and (b) spherical isotropy.

Section 7.1, the elastodynamics of a spherically isotropic material are presented. In contrast with an isotropic elastic material, it is observed that the method of potentials developed in Section 3.1 is not a practical means of obtaining a solution for spherically isotropic shells.

To obtain a solution for the scattering from multiple spherically isotropic shells, the historical development of solution techniques are examined in Section 7.2. Based on this analysis, solutions for the stress and displacement are obtained at the interfaces of each spherically isotropic layer, the details of which are given in Section 7.3. Applying boundary conditions at the interface of the outer spherically isotropic shell and the surrounding fluid medium, a linear system of equations in terms of the scattering coefficients similar to Equation (3.21) is obtained in Section 7.4. This form allows the cloaking condition $A_n^{(0)} = 0$ to be evaluated for multiple spherically isotropic shells.

7.1 Spherical isotropy

For a linear elastic transversely isotropic material, the stiffness tensor $\mathbf{C}$ contains 5 independent elastic constants, so the stress-strain relationship can be expressed as [61]

$$\begin{bmatrix} T_{11} \\ T_{22} \\ T_{33} \\ T_{23} \\ T_{13} \\ T_{12} \end{bmatrix} = \begin{bmatrix} C_{11} & C_{12} & C_{13} & 0 & 0 & 0 \\ C_{12} & C_{11} & C_{13} & 0 & 0 & 0 \\ C_{13} & C_{13} & C_{33} & 0 & 0 & 0 \\ 0 & 0 & 0 & C_{44} & 0 & 0 \\ 0 & 0 & 0 & 0 & C_{44} & 0 \\ 0 & 0 & 0 & 0 & 0 & C_{66} \end{bmatrix} \begin{bmatrix} \varepsilon_{11} \\ \varepsilon_{22} \\ \varepsilon_{33} \\ 2\varepsilon_{23} \\ 2\varepsilon_{13} \\ 2\varepsilon_{12} \end{bmatrix}, \tag{7.1}$$

where the fourth-order stiffness $\mathbf{C}$ and second-order stress $\mathbf{T}$ and strain $\boldsymbol{\varepsilon}$ from Equation (3.3) have been presented using a contracted notation, known as Voigt notation, making use of the symmetry of the tensors. Note that the constant C_{66} is not an independent parameter, and can be written as

$$C_{66} = \frac{1}{2}(C_{11} - C_{12})\,. \tag{7.2}$$

Based on Equation (7.1), a coordinate system can be defined such that

$$(\hat{e}_1, \hat{e}_2, \hat{e}_3) \rightarrow (\hat{e}_\theta, \hat{e}_\varphi, \hat{e}_r)\,, \tag{7.3}$$

leading to a stress-strain relationship for a spherically isotropic material that can be written as

$$T_{\theta\theta} = C_{11}\,\varepsilon_{\theta\theta} + C_{12}\,\varepsilon_{\varphi\varphi} + C_{13}\,\varepsilon_{rr}, \tag{7.4}$$

$$T_{\varphi\varphi} = C_{12}\,\varepsilon_{\theta\theta} + C_{11}\,\varepsilon_{\varphi\varphi} + C_{13}\,\varepsilon_{rr}, \tag{7.5}$$

$$T_{rr} = C_{13}\,\varepsilon_{\theta\theta} + C_{13}\,\varepsilon_{\varphi\varphi} + C_{33}\,\varepsilon_{rr}, \tag{7.6}$$

$$T_{r\theta} = 2\,C_{44}\,\varepsilon_{r\theta}, \tag{7.7}$$

$$T_{r\varphi} = 2\,C_{44}\,\varepsilon_{r\varphi}, \tag{7.8}$$

$$T_{\theta\varphi} = (C_{11} - C_{12})\;\varepsilon_{\theta\varphi}. \tag{7.9}$$

To determine the dynamic behavior, Equations (7.4)–(7.9) can be combined with the equations of motion and strain-displacement relations, which are given by Equations (3.1) and (3.2), respectively. In cartesian coordinates, the method of potentials described in Section 3.1 can be applied, yielding wave equations for the displacement potentials, solutions of which can be expressed as an expansion in terms of spherical Bessel functions in the form of Equations (3.15)–(3.18).

For curvilinear coordinates, the method of potentials can be applied to cylindrical geometries with a transversely isotropic shell, including the case of a plane wave incident at variable angles relative to the cylinder [79]. For the case of spherical geometry exhibiting spherical isotropy, however, the use of displacement potentials do not lead to the simplified expressions satisfying the wave equation. To highlight this, it can be observed that the reduction to the wave equation in terms of the displacement potentials arises from the orthogonality of the irrotational and solenoidal components of Equation (3.7). Therefore, for the spherically isotropic case an expression is sought in the form of

$$\bar{M}\,\nabla\,(\nabla\cdot\mathbf{u}) - \bar{\mu}\nabla\times(\nabla\times\mathbf{u}) = \rho\ddot{\mathbf{u}}, \tag{7.10}$$

where $\bar{M}$ and $\bar{\mu}$ represent effective quantities for plane wave and shear moduli, respectfully. Evaluating Equation (7.10) in spherical coordinates assuming azimuthal symmetry yields

$$\begin{aligned}\bar{M}\,&\left\{\frac{\partial^2 u_r}{\partial r^2}+\frac{2}{r}\frac{\partial u_r}{\partial r}-\frac{2}{r^2}u_r+\frac{1}{r\sin\theta}\frac{\partial}{\partial\theta}\left[\left(\frac{\partial u_\theta}{\partial r}-\frac{1}{r}u_\theta\right)\sin\theta\right]\right\}\\ &-\bar{\mu}\,\frac{1}{r}\left\{\frac{\partial}{\partial\theta}\left[\frac{\partial u_\theta}{\partial r}+\frac{1}{r}u_\theta-\frac{1}{r}\frac{\partial u_r}{\partial\theta}\right]+\left[\frac{\partial u_\theta}{\partial r}+\frac{1}{r}u_\theta-\frac{1}{r}\frac{\partial u_r}{\partial\theta}\right]\cot\theta\right\} = \rho\ddot{u}_r,\end{aligned} \tag{7.11}$$

$$\bar{M}\,\frac{1}{r}\left\{\frac{\partial}{\partial\theta}\left[\frac{\partial u_r}{\partial r}+\frac{2}{r}u_r+\frac{1}{r}\frac{\partial u_\theta}{\partial\theta}\right]+\frac{1}{r}\cot\theta\frac{\partial u_\theta}{\partial\theta}-\frac{1}{r}u_\theta\cot^2\theta-\frac{1}{r}u_\theta\right\}$$
$$+\,\bar{\mu}\left\{\frac{\partial^2 u_\theta}{\partial r^2}+\frac{2}{r}\frac{\partial u_\theta}{\partial r}-\frac{1}{r}\frac{\partial^2 u_r}{\partial r\partial\theta}\right\}=\rho\ddot{u}_\theta, \quad (7.12)$$

where u_r and u_θ are the radial and tangential components of the displacement, respectively. Combining Equations (7.4)–(7.9) with Equations (3.1) and (3.2), the analogous formulation for a spherically isotropic shell is

$$C_{33}\left\{\frac{\partial^2 u_r}{\partial r^2}+\frac{2}{r}\frac{\partial u_r}{\partial r}-\underline{\frac{\alpha}{C_{33}}\frac{2}{r^2}u_r}+\frac{1}{r\sin\theta}\frac{\partial}{\partial\theta}\left[\left(\underline{\underline{\frac{\beta}{C_{33}}\frac{\partial u_\theta}{\partial r}}}-\underline{\underline{\frac{\alpha}{C_{33}}\frac{1}{r}u_\theta}}\right)\sin\theta\right]\right\}$$
$$-\,C_{44}\frac{1}{r}\left\{\frac{\partial}{\partial\theta}\left[\frac{\partial u_\theta}{\partial r}+\frac{1}{r}u_\theta-\frac{1}{r}\frac{\partial u_r}{\partial\theta}\right]+\left[\frac{\partial u_\theta}{\partial r}+\frac{1}{r}u_\theta-\frac{1}{r}\frac{\partial u_r}{\partial\theta}\right]\cot\theta\right\}=\rho\ddot{u}_r, \quad (7.13)$$

$$C_{11}\frac{1}{r}\left\{\frac{\partial}{\partial\theta}\left[\underline{\frac{\beta}{C_{11}}\frac{\partial u_r}{\partial r}}+\underline{\left(1+\frac{\beta}{C_{11}}\right)\frac{1}{r}u_r}+\frac{1}{r}\frac{\partial u_\theta}{\partial\theta}\right]+\frac{1}{r}\cot\theta\frac{\partial u_\theta}{\partial\theta}\right.$$
$$\left.-\,\frac{1}{r}u_\theta\cot^2\theta-\underline{\underline{\frac{\gamma}{C_{11}}\frac{1}{r}u_\theta}}\right\}+C_{44}\left\{\frac{\partial^2 u_\theta}{\partial r^2}+\frac{2}{r}\frac{\partial u_\theta}{\partial r}-\frac{1}{r}\frac{\partial^2 u_r}{\partial r\partial\theta}\right\}=\rho\ddot{u}_\theta, \quad (7.14)$$

where

$$\alpha=C_{11}+C_{12}-C_{13}, \quad (7.15)$$

$$\beta=C_{13}+2C_{44}, \quad (7.16)$$

$$\gamma=C_{12}+2C_{44}. \quad (7.17)$$

Comparing Equations (7.11) and (7.12) with Equations (7.13) and (7.14), it is clear that the spherically isotropic case contains all the same terms as the general form for a potential solution, with the shear modulus corresponding to C_{44}, and the equivalent isotropic plane wave moduli corresponding to C_{33} for the radial direction and C_{11} for the tangential direction. Although each term in the general form is represented, the coefficients of several terms do not match, and are highlighted in the expressions by a single underline for functions of the radial displacement and a

double underline for those which depend on tangential displacement. The coefficients of these underlined terms are given by a ratio of a transversely isotropic stiffness, denoted by either α, β or γ, and the equivalent isotropic elastic modulus. These ratios therefore represent a measure of the anisotropy of the elastic medium, and the relative effect of this anisotropy on the orthogonality of the wave propagation in different directions.

Looking at Equations (7.13) and (7.14), the underlined terms appear only in the terms multiplied by the effective plane wave modulus, which corresponds to compressional waves in the radial and tangential direction, respectively. For these modes of propagation, the solutions of the form given by Equations (3.17) and (3.18) are not valid unless the ratios $\frac{\alpha}{C_{33}}$, $\frac{\beta}{C_{11}}$, $\frac{\beta}{C_{33}}$ and $\frac{\gamma}{C_{11}}$ are unity. Consider the limiting case of an isotropic elastic medium, for which

$$C_{11} = C_{33} = \lambda + 2\mu, \tag{7.18}$$

$$C_{12} = C_{13} = \lambda, \tag{7.19}$$

$$C_{44} = \mu. \tag{7.20}$$

Combining these expressions with Equations (7.15)–(7.17) yields

$$\frac{\alpha}{C_{33}} = \frac{\beta}{C_{33}} = \frac{\beta}{C_{11}} = \frac{\gamma}{C_{11}} = 1, \tag{7.21}$$

in which case Equations (7.13) and (7.14) reduce to Equation (3.7), as expected. By definition, however, this will not be true for a transversely isotropic layer. To obtain an elastic medium which obeys Equation (7.21) requires $C_{11} = C_{33}$ and $\alpha = \beta = \gamma$, from which it is clear that only isotropic mediums, which have the properties given by Equations (7.18)–(7.20), can achieve this condition. It is therefore necessary to employ a different solution technique than the method of potentials to solve the scattering problem for the case of spherically isotropic shells.

7.2 Historical development of solution techniques

To solve for the stresses and displacements of a spherically isotropic medium, one cannot expect *a priori* to have a solution consisting of a series expansion with spherical Bessel functions that describe the r dependence of each mode, as was assumed in Equations (3.15)–(3.18). A separable series solution can be written more generally, however, and in spherical coordinates for the case of azimuthal symmetry takes the form

$$F(r,\theta) = \sum_{n=0}^{\infty} f_n(r) P_n(\cos\theta), \tag{7.22}$$

where $F(r,\theta)$ is the variable of interest with $e^{-i\omega t}$ time-harmonic dependence suppressed, $f_n(r)$ is an arbitrary function which depends only on r, and P_n is the Legrendre polynomial. Rewriting the equations of motion in terms of $F(r,\theta)$ and applying the boundary conditions, a system of equations can be developed, and solved for the unknown functions f_n for each mode.

The approach of using a decomposition of field variables for the problem of spherically isotropic shells was first derived by Hu [80], in which a series expansion in the form of Equation (7.22) for the displacement potentials were used to obtain the displacements and stresses for the case of free vibrations and later for various static loading conditions [81]. Unfortunately, using this form precludes the reduction to a pair of Helmholtz equations in terms of the potentials used given in Equations (3.13) and (3.14) and utilized in Sec 3.1 to simplify the analysis, while retaining the disadvantage of the higher order derivatives which arise in defining the potential fields.

Alternatively, the decomposition of the field variables can be achieved by separating the displacement into *auxiliary functions*, which were defined in terms of the components of the displacement using linear combinations of the auxiliary

functions and their derivatives with respect to the azimuthal or polar angles only. This was first applied to the case of spherical isotropy to determine the free vibrations of an unloaded hollow spherical shell [82, 83], based on similar work done by Prasad for isotropic spherical shells [84]. To address problems in which the shell has spatially varying properties in the radial direction, Shul'ga *et al.* investigated the free response of a hollow sphere with multiple discrete spherically isotropic layers, using a modified approach which defined auxiliary functions for both displacement and stress given by [85]

$$u_\theta = \frac{1}{\sin\theta}\frac{\partial u_1}{\partial \varphi} - \frac{\partial u_2}{\partial \theta}, \tag{7.23}$$

$$u_\varphi = \frac{\partial u_1}{\partial \theta} + \frac{1}{\sin\theta}\frac{\partial u_2}{\partial \varphi}, \tag{7.24}$$

$$T_{r\theta} = \frac{1}{\sin\theta}\frac{\partial T_1}{\partial \varphi} - \frac{\partial T_2}{\partial \theta}, \tag{7.25}$$

$$T_{r\varphi} = \frac{\partial T_1}{\partial \theta} + \frac{1}{\sin\theta}\frac{\partial T_2}{\partial \varphi}, \tag{7.26}$$

where u_1, u_2, T_1, and T_2 are the pairs of auxiliary functions for displacement and stress, respectively. These were then used in conjunction with the radial displacement u_r and radial stress T_{rr}. Following application of the boundary conditions at each outer surface leads to a system of equations which could then numerically solved for the auxiliary functions.

Apparently unaware of this previous work, Chen and Ding later developed a similar approach using the auxiliary functions given by Equations (7.23)–(7.26) independently for the same problem [86, 87]. However, the formulation obtained by Chen and Ding is more compact, consisting of systems of first-order ordinary differential equations (ODEs) which are more numerically efficient to implement. The resulting system of equations closely resembles those used for state-space analysis, and is therefore often simply referred to as the "state-space method" [87, 88]. This method is examined in more detail in Section 7.3.

Although the state-space method and the similar formulation first presented by Shul'ga *et al.* allow for an effective means to analyze a sphere coated with multiple spherically isotropic layers, these works were originally limited to free vibrations of coated hollow spheres. Although later expanded to include the effects of a surrounding inviscid fluid medium [86] and a coated fluid-filled sphere [89], the scattering problem was surprisingly not addressed in the literature until recent years. In 2002, Scandrett [88] used this method to formulate the scattered field from a spherically isotropic piezoelectric layer, coated with an isotropic elastic outer layer. Later work by Hasheminejad and Maleki [78] used the state-space method to model the scattering from multiple concentric spherically isotropic layers with a fluid-filled core, and investigated the effect bonding between layers has on the scattered field.

7.3 State-space formulation

In this work, the development of a solution for the scattering from an isotropic sphere coated with multiple spherically isotropic shells will be based on the state-space method closely following the works of Scandrett [88] and Hasheminejad and Maleki [78]. It will be assumed that the incident wave is a time-harmonic plane wave, impinging upon an isotropic sphere coated with spherically isotropic shells, using the same geometry given by Figure 3.1.

The first step is to define a stress function, Σ, which is given by

$$\Sigma_{ij} = rT_{ij}, \tag{7.27}$$

where i and j represent the coordinate directions (r, θ, φ). Employing the stress function defined by Equation (7.27) for the case of azimuthal symmetry, the equations of motion given by Equation (3.1) are expressed in spherical coordinates as

$$r\frac{\partial \Sigma_{rr}}{\partial r} + \frac{\partial \Sigma_{r\theta}}{\partial \theta} + \Sigma_{rr} - (\Sigma_{\theta\theta} + \Sigma_{\varphi\varphi}) + \Sigma_{r\theta}\cot\theta = -\rho\omega^2 r^2 u_r, \tag{7.28}$$

$$r\frac{\partial \Sigma_{r\theta}}{\partial r} + \frac{\partial \Sigma_{\theta\theta}}{\partial \theta} + 2\Sigma_{r\theta} + (\Sigma_{\theta\theta} - \Sigma_{\varphi\varphi})\cot\theta = -\rho\omega^2 r^2 u_\theta. \tag{7.29}$$

Similarly, the stress-displacement relations can be found by combining Equations (7.4)–(7.9) and Equation (3.2) with Equation (7.27) which yields

$$\Sigma_{rr} = C_{33}\, r\frac{\partial u_r}{\partial r} + C_{13}\left(2u_r + u_\theta \cot\theta + \frac{\partial u_\theta}{\partial \theta}\right), \tag{7.30}$$

$$\Sigma_{\theta\theta} = C_{13}\, r\frac{\partial u_r}{\partial r} + C_{11}\left(u_r + \frac{\partial u_\theta}{\partial \theta}\right) + C_{12}\left(u_r + u_\theta \cot\theta\right), \tag{7.31}$$

$$\Sigma_{\varphi\varphi} = C_{13}\, r\frac{\partial u_r}{\partial r} + C_{12}\left(u_r + \frac{\partial u_\theta}{\partial \theta}\right) + C_{11}\left(u_r + u_\theta \cot\theta\right), \tag{7.32}$$

$$\Sigma_{r\theta} = C_{44}\left(r\frac{\partial u_\theta}{\partial r} + \frac{\partial u_r}{\partial \theta} - u_\theta\right), \tag{7.33}$$

$$\Sigma_{r\varphi} = \Sigma_{\theta\varphi} = 0, \tag{7.34}$$

Rewriting the displacement and stress in the tangential directions in terms of auxiliary functions yields [88]

$$u_\theta = \frac{1}{\sin\theta}\frac{\partial \psi}{\partial \varphi} - \frac{\partial G}{\partial \theta}, \tag{7.35}$$

$$u_\varphi = \frac{\partial \psi}{\partial \theta} + \frac{1}{\sin\theta}\frac{\partial G}{\partial \varphi}, \tag{7.36}$$

$$\Sigma_{r\theta} = \frac{1}{\sin\theta}\frac{\partial \Sigma_1}{\partial \varphi} - \frac{\partial \Sigma_2}{\partial \theta}, \tag{7.37}$$

$$\Sigma_{r\varphi} = \frac{\partial \Sigma_1}{\partial \theta} + \frac{1}{\sin\theta}\frac{\partial \Sigma_2}{\partial \varphi}, \tag{7.38}$$

where G, ψ, Σ_1 and Σ_2 are the displacement and stress auxiliary functions, respectively. Comparing these equations with Equations (7.23)–(7.26) used by Shul'ga *et al.*, it is clear that although both use the same form to define the auxiliary functions, the state-space method makes use of the stress function Σ, rather than the actual physical stress T. Assuming azimuthal symmetry, for which $u_\varphi = T_{r\varphi} = T_{\theta\varphi} = 0$ and derivatives with respect to φ are zero, Equations (7.36) and (7.38) reduce to

$$\frac{\partial \psi}{\partial \theta} = \frac{\partial \Sigma_1}{\partial \theta} = 0. \tag{7.39}$$

It is clear from Equation (7.39) that the functions ψ and Σ_1 are proportional to θ, multiplied by an arbitrary constant. Based on the periodicity of the θ dependence for a spherical domain, however, this means that the constants for ψ and Σ_1 must be equal to zero, yielding $\psi = \Sigma_1 = 0$.

From Equations (7.35) and (7.37), the expressions for the remaining functions G and Σ_2 with azimuthal symmetry reduce to

$$u_\theta = -\frac{\partial G}{\partial \theta}, \tag{7.40}$$

$$\Sigma_{r\theta} = -\frac{\partial \Sigma_2}{\partial \theta}. \tag{7.41}$$

Substitution of Equations (7.40) and (7.41) into Equations (7.28)–(7.32) and the rearrangement of terms leads to the system of equations [78]

$$r\frac{\partial}{\partial r}\begin{bmatrix} \Sigma_{rr} \\ \Sigma_2 \\ G \\ u_r \end{bmatrix} = \begin{bmatrix} 2\beta - 1 & \nabla_\theta^2 & \gamma_1 \nabla_\theta^2 & -2\gamma_1 - \rho(\omega r)^2 \\ \beta & -2 & \gamma_2 \nabla_\theta^2 - 2C_{66} - \rho(\omega r)^2 & -\gamma_1 \\ 0 & \frac{1}{C_{44}} & 1 & 1 \\ \frac{1}{C_{33}} & 0 & \beta \nabla_\theta^2 & -2\beta \end{bmatrix} \begin{bmatrix} \Sigma_{rr} \\ \Sigma_2 \\ G \\ u_r \end{bmatrix}, \tag{7.42}$$

where

$$\beta = \frac{C_{13}}{C_{33}}, \tag{7.43}$$

$$\gamma_1 = 2C_{13}\beta - (C_{11} + C_{12}), \tag{7.44}$$

$$\gamma_2 = C_{13}\beta - C_{11} = \frac{1}{2}\gamma_1 - C_{66}, \tag{7.45}$$

and the operator ∇_θ^2 is given by

$$\nabla_\theta^2 = \frac{\partial^2}{\partial \theta^2} + \cot\theta \frac{\partial}{\partial \theta}. \tag{7.46}$$

From the general separable series form given by Equation (7.22), the independent variables Σ_{rr}, Σ_2, G_n, and u_r (called *state variables* in a state-space

formulation) can be expanded in terms of spherical harmonics,

$$\Sigma_{rr}(r,\theta) = \sum_{n=0}^{\infty} \Sigma_{rr,n}(r) P_n(\cos\theta), \tag{7.47}$$

$$\Sigma_2(r,\theta) = \sum_{n=0}^{\infty} \Sigma_{2,n}(r) P_n(\cos\theta), \tag{7.48}$$

$$G(r,\theta) = \sum_{n=0}^{\infty} G_n(r) P_n(\cos\theta), \tag{7.49}$$

$$u_r(r,\theta) = \sum_{n=0}^{\infty} u_{r,n}(r) P_n(\cos\theta). \tag{7.50}$$

Based on the recurrence formulas for the Legendre polynomials [34]

$$\left(1-z^2\right) P_n''(z) - 2zP_n' = -l_n P_n(z), \tag{7.51}$$

where $l_n = n(n+1)$, and therefore the ∇_θ^2 operating on a separable function $F(r,\theta)$ given by Equation (7.22) can be written in terms of $P_n(\cos\theta)$ as

$$\nabla_\theta^2 F(r,\theta) = -\sum_{n=0}^{\infty} l_n \, f_n(r) \, P_n(\cos\theta). \tag{7.52}$$

This equation, along with Equations (7.47)–(7.50), can be substituted into Equation (7.42) to yield a system of equations for the n^{th} mode of the series expansion as a function of r only,

$$r\frac{d}{dr}\begin{bmatrix} \Sigma_{rr,n} \\ \Sigma_{2,n} \\ G_n \\ u_{r,n} \end{bmatrix} = \begin{bmatrix} 2\beta-1 & -l_n & -l_n\gamma_1 & -2\gamma_1-\rho(\omega r)^2 \\ \beta & -2 & -l_n\gamma_2-2C_{66}-\rho(\omega r)^2 & -\gamma_1 \\ 0 & \frac{1}{C_{44}} & 1 & 1 \\ \frac{1}{C_{33}} & 0 & -l_n\beta & -2\beta \end{bmatrix} \begin{bmatrix} \Sigma_{rr,n} \\ \Sigma_{2,n} \\ G_n \\ u_{r,n} \end{bmatrix}. \tag{7.53}$$

As illustrated in Figure 3.1, a total of N discrete shells make up the coating, where each shell is assumed to have a uniform density ρ_s and thickness $h_s = b_{s-1} - b_s$ (for $s = 1, 2, \ldots, N$), where $b_{s-1} > b_s$ and here $b_N = a$ is the radius of the inner sphere.

To rewrite the derivative on the left hand side of Equation (7.53) from $r\frac{d}{dr} \rightarrow \frac{d}{d\xi}$, a change of variable for the s^{th} layer can be used [78]

$$r = b_s e^{\xi} \qquad (0 \leq \xi \leq \xi_s), \tag{7.54}$$

which expressed with ξ as the dependent parameter leads to $\xi(r) = \ln\left(\frac{r}{b_s}\right)$ and $\xi_s = \ln\left(\frac{b_{s-1}}{b_s}\right)$. To ensure numerical stability, the state variables can be normalized to the properties of the inner layer (layer N in Figure 3.1), such that [78]

$$\overline{\Sigma}_{rr,n} = \frac{\Sigma_{rr,n}}{a\,\kappa_0}, \qquad\qquad \overline{\Sigma}_{2,n} = \frac{\Sigma_{2,n}}{a\,\kappa_0}, \tag{7.55}$$

$$\overline{G}_n = \frac{G_n}{a}, \qquad\qquad \overline{u}_{r,n} = \frac{u_{r,n}}{a}. \tag{7.56}$$

Substitution of Equations (7.54)–(7.56) into Equation (7.53) yields

$$\frac{d}{d\xi}\begin{bmatrix} \overline{\Sigma}_{rr,n} \\ \overline{\Sigma}_{2,n} \\ \overline{G}_n \\ \overline{u}_{r,n} \end{bmatrix} = \begin{bmatrix} 2\beta_s - 1 & -l_n & -l_n\overline{\gamma}_1 & -2\overline{\gamma}_1 - \frac{\rho_s}{\rho_0}\left(\Omega\frac{b_s}{a}\right)^2 e^{2\xi} \\ \beta_s & -2 & -l_n\overline{\gamma}_2 - 2\frac{C_{66}^{(s)}}{\kappa_0} - \frac{\rho_s}{\rho_0}\left(\Omega\frac{b_s}{a}\right)^2 e^{2\xi} & -\overline{\gamma}_1 \\ 0 & \frac{\kappa_0}{C_{44}^{(s)}} & 1 & 1 \\ \frac{\kappa_0}{C_{33}^{(s)}} & 0 & -l_n\beta_s & -2\beta_s \end{bmatrix} \begin{bmatrix} \overline{\Sigma}_{rr,n} \\ \overline{\Sigma}_{2,n} \\ \overline{G}_n \\ \overline{u}_{r,n} \end{bmatrix}, \tag{7.57}$$

where

$$\beta_s = \frac{C_{13}^{(s)}}{C_{33}^{(s)}}, \tag{7.58}$$

$$\overline{\gamma}_1^{(s)} = \frac{\gamma_1^{(s)}}{\kappa_0} = 2\frac{C_{13}^{(s)}}{\kappa_0}\beta^{(s)} - \left(\frac{C_{11}^{(s)} + C_{12}^{(s)}}{\kappa_0}\right), \tag{7.59}$$

$$\overline{\gamma}_2^{(s)} = \frac{\gamma_2^{(s)}}{\kappa_0} = \frac{1}{2}\overline{\gamma}_1^{(s)} - \frac{C_{66}^{(s)}}{\kappa_0} = \frac{C_{13}^{(s)}}{\kappa_0}\beta^{(s)} - \frac{C_{11}^{(s)}}{\kappa_0}, \tag{7.60}$$

$$\Omega^2 = (\omega a)^2\,\frac{\rho_0}{\kappa_0} = (k_{d,0}a)^2. \tag{7.61}$$

Written in this manner, Equation (7.57) takes the form of a first-order ODE in terms of ξ, given by

$$\frac{d}{d\xi}\mathbf{x}_{n,s}(\xi) = \mathbf{M}_{n,s}(\xi)\,\mathbf{x}_{n,s}(\xi)\ , \tag{7.62}$$

where the state vector for the n^{th} mode and s^{th} layer is

$$\mathbf{x}_{n,s} = \begin{bmatrix}\overline{\Sigma}_{rr,n} & \overline{\Sigma}_{2,n} & \overline{G}_n & \overline{u}_{r,n}\end{bmatrix}^{\mathrm{T}}. \tag{7.63}$$

From this system of equations, a local transfer function is sought relating the state variables at the inner edge of the s^{th} layer, denoted by $\xi = 0$ according to Equation (7.54), and the state variables at a distance ξ within the layer. This can be achieved by expressing the state vector $\mathbf{x}$ in terms of its Maclaurin series

$$\mathbf{x}_{n,s}(\xi) = \mathbf{x}_{n,s}(0) + \frac{\mathbf{x}^{(1)}_{n,s}(0)}{1!}\xi + \frac{\mathbf{x}^{(2)}_{n,s}(0)}{2!}\xi^2 + \cdots + \frac{\mathbf{x}^{(q)}_{n,s}(0)}{q!}\xi^q + \cdots\ , \tag{7.64}$$

where the notation $\mathbf{x}^{(q)}$ denotes the q^{th} derivative of $\mathbf{x}$ with respect to ξ. Using the product rule with Equation (7.62), one obtains the derivatives on the right hand side of Equation (7.64) can be evaluated as

$$\begin{aligned}
\mathbf{x}^{(1)}_{n,s}(0) &= \mathbf{M}_{n,s}(0)\,\mathbf{x}_{n,s}(0) \\
&\equiv \overline{\mathbf{M}}^{(1)}_{n,s}(0)\,\mathbf{x}_{n,s}(0), \qquad (7.65)\\
\mathbf{x}^{(2)}_{n,s}(0) &= \mathbf{M}^{(1)}_{n,s}(0)\,\mathbf{x}_{n,s}(0) + \mathbf{M}_{n,s}(0)\,\mathbf{x}^{(1)}_{n,s}(0) \\
&= \left[\mathbf{M}^{(1)}_{n,s}(0) + \mathbf{M}_{n,s}(0)\,\overline{\mathbf{M}}^{(1)}_{n,s}(0)\right]\mathbf{x}_{n,s}(0) \\
&\equiv \overline{\mathbf{M}}^{(2)}_{n,s}(0)\,\mathbf{x}_{n,s}(0), \qquad (7.66)
\end{aligned}$$

$$
\begin{aligned}
\mathbf{x}_{n,s}^{(3)}(0) &= \mathbf{M}_{n,s}^{(2)}(0)\,\mathbf{x}_{n,s}(0) + \mathbf{M}_{n,s}^{(1)}(0)\,\mathbf{x}_{n,s}^{(1)}(0) + \mathbf{M}_{n,s}(0)\,\mathbf{x}_{n,s}^{(2)}(0) \\
&= \left[\mathbf{M}_{n,s}^{(2)}(0) + \mathbf{M}_{n,s}^{(1)}(0)\,\overline{\mathbf{M}}_{n,s}^{(1)}(0) + \mathbf{M}_{n,s}(0)\,\overline{\mathbf{M}}_{n,s}^{(2)}(0)\right]\mathbf{x}_{n,s}(0) \\
&\equiv \overline{\mathbf{M}}_{n,s}^{(3)}(0)\,\mathbf{x}_{n,s}(0), \qquad (7.67) \\
&\vdots \\
\mathbf{x}_{n,s}^{(q)}(0) &= \Big[c_1^q\mathbf{M}_{n,s}^{(q-1)}(0) + c_2^q\mathbf{M}_{n,s}^{(q-2)}(0)\,\overline{\mathbf{M}}_{n,s}^{(1)}(0) \\
&\qquad\qquad + \cdots + c_q^q\mathbf{M}_{n,s}(0)\,\overline{\mathbf{M}}_{n,s}^{(q-1)}(0)\Big]\mathbf{x}_{n,s}(0) \\
&\equiv \overline{\mathbf{M}}_{n,s}^{(q)}(0)\,\mathbf{x}_{n,s}(0), \qquad (7.68)
\end{aligned}
$$

where the coefficients $c_k^q = c_{k-1}^{q-1} + c_k^{q-1}$ with $c_1^q = c_q^q = 1$ and $k = 2, \ldots, q-1$. Combining Equations (7.64)–(7.68) yields a relationship between the state vector $\mathbf{x}$ at the outer boundary of the layer at $\xi = \xi_s$ and the inner boundary $\xi = 0$,

$$
\mathbf{x}_{n,s}(\xi_s) = \mathbf{A}_{n,s}(\xi_s)\mathbf{x}_{n,s}(0), \qquad (7.69)
$$

where $\mathbf{A}_{n,s}$ represents the local transfer function for the s^{th} layer given by

$$
\mathbf{A}_{n,s}(\xi_s) = \mathbf{I} + \frac{\overline{\mathbf{M}}_{n,s}^{(1)}(0)}{1!}\xi_s + \frac{\overline{\mathbf{M}}_{n,s}^{(2)}(0)}{2!}\xi_s^2 + \cdots + \frac{\overline{\mathbf{M}}_{n,s}^{(q)}(0)}{q!}\xi_s^q + \cdots, \qquad (7.70)
$$

with $\mathbf{I}$ denoting the identity matrix.

The local transfer function allows the state variables of an individual layer at one boundary to be related to those on the other boundary. By applying the appropriate boundary conditions at each interface where the inner edge of one layer meets the outer edge of another, a relationship for an arbitrary number of layers can be developed. The conditions on the normal and transverse components of displacement and stress (and similarly to the auxiliary functions used as the state variables) can be applied at each interface, which can be expressed in the form [78]

$$
\mathbf{x}_{n,s-1}^{+}(\xi_{s-1}) = \mathbf{J}_{n,s}\mathbf{x}_{n,s}^{-}(\xi_s), \quad (s = 2, \ldots, N) \qquad (7.71)
$$

where $\mathbf{J}_{n,s}$ is the interfacial transfer matrix and the superscripts "+" and "-" referred to the outer and inner edge of the interface, respectively.

In general, the interface transfer matrix can account for discontinuous boundaries, such as those arising from partial or complete debonding between the layers [78]. In the present work, perfectly bonded interfaces will be assumed, in which case the components of displacement and stress are continuous across the interface, and therefore $\mathbf{J}_{n,s}$ simply reduces to the identity matrix. In this case, applying the boundary conditions between all the layers yields

$$\mathbf{x}_{n,1}(\xi_1) = \left(\prod_{s=1}^{N} \mathbf{A}_{n,s}(\xi_s) \right) \mathbf{x}_{n,N}(0) \equiv \mathbf{S}_n \mathbf{x}_{n,N}(0), \tag{7.72}$$

where $\mathbf{S}_n$ represents the global transfer function relating the state variables on the inner and outer boundaries of a multilayered shell.

7.4 Relation to the scattered field in an isotropic medium

Although the results from the previous section describe the state-space method for the formulation of the elastodynamics of multiple spherically isotropic layers, these expressions need to be connected to the incident and scattered field in the surrounding fluid medium. This will follow the same process as outlined in Section 3.2 for isotropic coatings– applying the boundary conditions at the interfaces with the target and the surrounding fluid medium, setting up a linear system of equations in terms of the scattering coefficients and then seeking a solution where $A_n^{(0)} = 0$.

To apply the boundary conditions in terms of the normalized state variables given by Equations (7.55)–(7.56), the solutions derived using the method of potentials for isotropic media in Equations (3.15)–(3.18) can be rewritten as

$$\mathbf{x}_{n,0}^{(\mathrm{inc})}(r) = \frac{1}{a\, r} \left[\boldsymbol{\alpha}_n^{(0)} j_n(k_{d,0} r) + \boldsymbol{\alpha}_n'^{(0)} k_{d,0} r j_n'(k_{d,0} r) \right], \tag{7.73}$$

$$\mathbf{x}_{n,0}^{(\mathrm{sc})}(r) = \frac{1}{a\,r} A_n^{(0)} \left[\boldsymbol{\alpha}_n^{(0)} h_n(k_{d,0} r) + \boldsymbol{\alpha}_n'^{(0)} k_{d,0} r h_n'(k_{d,0} r) \right], \tag{7.74}$$

$$\begin{aligned} \mathbf{x}_n^{(\mathrm{core})}(r) = \frac{1}{a\,r} \Bigg\{ & A_n^{(\mathrm{core})} \left[\boldsymbol{\alpha}_n^{(\mathrm{core})} j_n(k_{d,\mathrm{core}} r) + \boldsymbol{\alpha}_n'^{(\mathrm{core})} k_{d,\mathrm{core}} r j_n'(k_{d,\mathrm{core}} r) \right] \\ & + C_n^{(\mathrm{core})} \left[\boldsymbol{\beta}_n^{(\mathrm{core})} j_n(k_{s,\mathrm{core}} r) + \boldsymbol{\beta}_n'^{(\mathrm{core})} k_{s,\mathrm{core}} r j_n'(k_{s,\mathrm{core}} r) \right] \Bigg\}, \end{aligned} \tag{7.75}$$

where $\mathbf{x}_n$ is the radially dependent normalized state vector given by Equation (7.63), expressed in terms of the scattering coefficients $A_n^{(m)}$ and $C_n^{(m)}$ and the coefficient vectors $\boldsymbol{\alpha}_n^{(m)}$, $\boldsymbol{\alpha}_n'^{(m)}$, $\boldsymbol{\beta}_n^{(m)}$, and $\boldsymbol{\beta}_n'^{(m)}$ for the n^{th} mode and m^{th} material. Expressions for the coefficient vectors are developed in Appendix A, which for an isotropic elastic solid can be written as

$$\boldsymbol{\alpha}_n^{(m)}(r) = \begin{bmatrix} 2\overline{\mu}_m l_n - (\overline{\lambda}_m + 2\overline{\mu}_m)(k_{d,m} r)^2 \\ -2\overline{\mu}_m \\ 1 \\ 0 \end{bmatrix}, \qquad \boldsymbol{\alpha}_n'^{(m)} = \begin{bmatrix} -4\overline{\mu}_m \\ 2\overline{\mu}_m \\ 0 \\ 1 \end{bmatrix}, \tag{7.76}$$

$$\boldsymbol{\beta}_n^{(m)}(r) = \begin{bmatrix} -2\overline{\mu}_m l_n \\ 2\overline{\mu}_m \left[l_n - 1 - \frac{1}{2}(k_{s,m} r)^2 \right] \\ 1 \\ l_n \end{bmatrix}, \qquad \boldsymbol{\beta}_n'^{(m)} = \begin{bmatrix} 2\overline{\mu}_m l_n \\ -2\overline{\mu}_m \\ 1 \\ 0 \end{bmatrix}, \tag{7.77}$$

where

$$\overline{\lambda}_m = \frac{\lambda_m}{\kappa_0}, \qquad \overline{\mu}_m = \frac{\mu_m}{\kappa_0}, \tag{7.78}$$

$l_n = n(n+1)$, λ_m is Lamé's first parameter and μ_m is the shear modulus for the m^{th} material. To obtain the coefficient vectors for an inviscid fluid, the shear modulus in Equations (7.76)–(7.77) can be set to zero, in which case λ_m reduces to the adiabatic bulk modulus and $\boldsymbol{\alpha}_n'^{(m)} = \boldsymbol{\beta}_n'^{(m)} = 0$.

To properly apply the boundary conditions, continuity of the stress and displacement at the interfaces must be rewritten in terms of the state variables.

Consider the case illustrated in Figure 3.1 of a fluid surrounding medium and an isotropic elastic core of radius a coated with multiple spherically isotropic shells with outer radius b. For the boundary between an inviscid fluid and an elastic solid (either isotropic or spherically isotropic), continuity of the normal component of stress and displacement, in addition to zero tangential stress at the interface $r=b$ yields

$$\overline{\Sigma}^{(1)}_{rr,n}\big|_{r=b} - \overline{\Sigma}^{(sc)}_{rr,n}\big|_{r=b} = \overline{\Sigma}^{(inc)}_{rr,n}\big|_{r=b}\,, \tag{7.79}$$

$$\overline{\Sigma}^{(1)}_{2,n}\big|_{r=b} = 0\,, \tag{7.80}$$

$$\overline{u}^{(1)}_{r,n}\big|_{r=b} - \overline{u}^{(sc)}_{r,n}\big|_{r=b} = \overline{u}^{(inc)}_{r,n}\big|_{r=b}\,. \tag{7.81}$$

Using the global transfer function defined by Equation (7.72), the state variables in the outermost layer (*medium 1*) can be expressed in terms of the states variables in the innermost layer (*medium N*), in which case the boundary conditions at $r=b$ become

$$\left[S_{n,11}\overline{\Sigma}^{(N)}_{rr,n} + S_{n,12}\overline{\Sigma}^{(N)}_{2,n} + S_{n,13}\overline{G}^{(N)}_{n} + S_{n,14}\overline{u}^{(N)}_{r,n}\right]\Big|_{r=a} - \overline{\Sigma}^{(sc)}_{rr,n}\big|_{r=b} = \overline{\Sigma}^{(inc)}_{rr,n}\big|_{r=b}\,, \tag{7.82}$$

$$\left[S_{n,21}\overline{\Sigma}^{(N)}_{rr,n} + S_{n,22}\overline{\Sigma}^{(N)}_{2,n} + S_{n,23}\overline{G}^{(N)}_{n} + S_{n,24}\overline{u}^{(N)}_{r,n}\right]\Big|_{r=a} = 0\,, \tag{7.83}$$

$$\left[S_{n,41}\overline{\Sigma}^{(N)}_{rr,n} + S_{n,42}\overline{\Sigma}^{(N)}_{2,n} + S_{n,43}\overline{G}^{(N)}_{n} + S_{n,44}\overline{u}^{(N)}_{r,n}\right]\Big|_{r=a} - \overline{u}^{(sc)}_{r,n}\big|_{r=b} = \overline{u}^{(inc)}_{r,n}\big|_{r=b}\,, \tag{7.84}$$

where $S_{n,ij}$ denote the element in the i^{th} row and j^{th} column of the global transfer function of the n^{th} mode, S_n.

For the interface between a spherically isotropic layer and an isotropic elastic medium core, the boundary conditions for a perfectly bonded interface are the continuity of the normal and tangential components of the traction and displacement. Applying these conditions at the interface $r=a$ in terms of the state variables,

$$\overline{\Sigma}^{(N)}_{rr,n}\big|_{r=a} = \overline{\Sigma}^{(\text{core})}_{rr,n}\big|_{r=a}\,, \tag{7.85}$$

$$\overline{\Sigma}_{2,n}^{(N)}\big|_{r=a} = \overline{\Sigma}_{2,n}^{(\text{core})}\big|_{r=a}\,, \tag{7.86}$$

$$\overline{G}_{n}^{(N)}\big|_{r=a} = \overline{G}_{n}^{(\text{core})}\big|_{r=a}\,, \tag{7.87}$$

$$\overline{u}_{r,n}^{(N)}\big|_{r=a} = \overline{u}_{r,n}^{(\text{core})}\big|_{r=a}\,. \tag{7.88}$$

Substitution of these expressions into Equations (7.82)–(7.84) yields

$$\Big[S_{n,11}\overline{\Sigma}_{rr,n}^{(\text{core})} + S_{n,12}\overline{\Sigma}_{2,n}^{(\text{core})} + S_{n,13}\overline{G}_{n}^{(\text{core})} + S_{n,14}\overline{u}_{r,n}^{(\text{core})}\Big]\Big|_{r=a} - \overline{\Sigma}_{rr,n}^{(sc)}\big|_{r=b} = \overline{\Sigma}_{rr,n}^{(inc)}\big|_{r=b}\,, \tag{7.89}$$

$$\Big[S_{n,21}\overline{\Sigma}_{rr,n}^{(\text{core})} + S_{n,22}\overline{\Sigma}_{2,n}^{(\text{core})} + S_{n,23}\overline{G}_{n}^{(\text{core})} + S_{n,24}\overline{u}_{r,n}^{(\text{core})}\Big]\Big|_{r=a} = 0\,, \tag{7.90}$$

$$\Big[S_{n,41}\overline{\Sigma}_{rr,n}^{(\text{core})} + S_{n,42}\overline{\Sigma}_{2,n}^{(\text{core})} + S_{n,43}\overline{G}_{n}^{(\text{core})} + S_{n,44}\overline{u}_{r,n}^{(\text{core})}\Big]\Big|_{r=a} - \overline{u}_{r,n}^{(sc)}\big|_{r=b} = \overline{u}_{r,n}^{(inc)}\big|_{r=b}\,, \tag{7.91}$$

which relate the state variables in the surrounding medium to that of the isotropic elastic core. To write these expressions in terms of the scattering coefficients in each isotropic medium, use of Equations (7.73)–(7.78) produces a system of equations given by

$$\begin{bmatrix} d_{11}^{(n)} & d_{12}^{(n)} & d_{13}^{(n)} \\ d_{21}^{(n)} & d_{22}^{(n)} & d_{23}^{(n)} \\ d_{31}^{(n)} & d_{32}^{(n)} & d_{33}^{(n)} \end{bmatrix} \begin{bmatrix} A_n^{(0)} \\ A_n^{(\text{core})} \\ C_n^{(\text{core})} \end{bmatrix} = \begin{bmatrix} r_1^{(n)} \\ r_2^{(n)} \\ r_3^{(n)} \end{bmatrix}, \tag{7.92}$$

where

$$\begin{aligned}
d_{11}^{(n)} &= k_{d,0}b\, h_n'(k_{d,0}b), \\
d_{12}^{(n)} &= -\frac{b}{a}(k_{d,0}a)^2\Big[\eta_4^{(n)} j_n(k_{d,\text{core}}a) + \eta_4'^{(n)} k_{d,\text{core}}a\, j_n'(k_{d,\text{core}}a)\Big], \\
d_{13}^{(n)} &= -\frac{b}{a}(k_{d,0}a)^2\Big[\zeta_4^{(n)} j_n(k_{s,\text{core}}a) + \zeta_4'^{(n)} k_{s,\text{core}}a\, j_n'(k_{s,\text{core}}a)\Big], \\
d_{21}^{(n)} &= -\frac{1}{2}h_n(k_{d,0}b), \\
d_{22}^{(n)} &= -\frac{a}{b}\frac{\rho}{\rho_0}\Big[\eta_1^{(n)} j_n(k_{d,\text{core}}a) + \eta_1'^{(n)} k_{d,\text{core}}a\, j_n'(k_{d,\text{core}}a)\Big],
\end{aligned}$$

$$
\begin{aligned}
d_{23}^{(n)} &= -\frac{a}{b}\frac{\rho}{\rho_0}\left[\zeta_1^{(n)} j_n(k_{s,\text{core}}a) + \zeta_1'^{(n)} k_{s,\text{core}}a\, j_n'(k_{s,\text{core}}a)\right],\\
d_{31}^{(n)} &= 0,\\
d_{32}^{(n)} &= \frac{a}{b}\frac{\rho}{\rho_0}\left[\eta_2^{(n)} j_n(k_{d,\text{core}}a) + \eta_2'^{(n)} k_{d,\text{core}}a\, j_n'(k_{d,\text{core}}a)\right],\\
d_{33}^{(n)} &= \frac{a}{b}\frac{\rho}{\rho_0}\left[\zeta_2^{(n)} j_n(k_{s,\text{core}}a) + \zeta_2'^{(n)} k_{s,\text{core}}a\, j_n'(k_{s,\text{core}}a)\right], \qquad (7.93)\\
r_1^{(n)} &= -k_{d,0}b j_n'(k_{d,0}b),\\
r_2^{(n)} &= \frac{1}{2} j_n(k_{d,0}b),\\
r_3^{(n)} &= 0, \qquad (7.94)
\end{aligned}
$$

with

$$
\begin{aligned}
\eta_i^{(n)} &= \big[\frac{2n(n+1)}{(k_{s,\text{core}}a)^2} - 1\big] S_{n,i1} - \frac{2}{(k_{s,\text{core}}a)^2} S_{n,i2} + \frac{1}{(k_{d,0}a)^2} S_{n,i3},\\
\eta_i'^{(n)} &= -\frac{4}{(k_{s,\text{core}}a)^2} S_{n,i1} + \frac{2}{(k_{s,\text{core}}a)^2} S_{n,i2} + \frac{1}{(k_{d,0}a)^2} S_{n,i4}, \qquad (7.95)\\
\zeta_i^{(n)} &= -\frac{2n(n+1)}{(k_{s,\text{core}}a)^2} S_{n,i1} + \big[\frac{2n(n+1)-2}{(k_{s,\text{core}}a)^2} - 1\big] S_{n,i2}\\
&\quad + \frac{1}{(k_{d,0}a)^2} S_{n,i3} + \frac{n(n+1)}{(k_{d,0}a)^2} S_{n,i4},\\
\zeta_i'^{(n)} &= \frac{2n(n+1)}{(k_{s,\text{core}}a)^2} S_{n,i1} - \frac{2}{(k_{s,\text{core}}a)^2} S_{n,i2} + \frac{1}{(k_{d,0}a)^2} S_{n,i3}. \qquad (7.96)
\end{aligned}
$$

The set of equations given (7.92)–(7.96) represent a generalized model for the scattered acoustic field from an isotropic elastic sphere coated with an arbitrary number of spherically isotropic elastic layers, based on a state-space formulation. Prescribing the cloaking condition of $A_n^{(0)} = 0$, this can provide a robust model for examining cloaking using the scattering cancellation approach. Although each of the coating layers has been assumed to be spherically isotropic, using Equation (7.18)–(7.20) it can be seen that this formulation is equally valid for isotropic elastic layers as well. For even just a single isotropic elastic layer, it is necessary to solve a 7x7

matrix using the method potentials (see Appendix A), as opposed to the 3x3 linear system given by Equation (7.92). For each additional isotropic elastic layer using the method of potentials, each dimension of the matrix increases by 4, so that 2 isotropic elastic layers would yield an 11x11 matrix, 3 isotropic elastic layers would yield a 15x15 matrix, and so forth.

Although efficient numerical schemes exist, solving such large matrices quickly becomes computationally expensive. More importantly, analytic solutions of such large matrices obtained by evaluating the determinants (such as those prescribed by Equations (3.26)–(3.28)), even in the limits of low frequency or thin shells, becomes impractical even for the case of a single elastic layer using the formulation developed with the method of potentials. For the state-space formulation, the solution for the scattering coefficient in the surrounding fluid medium in Equation (7.92) can be solved for explicitly using Cramer's rule, such that

$$A_n^{(0)} = \frac{\begin{vmatrix} r_1^{(n)} & d_{12}^{(n)} & d_{13}^{(n)} \\ r_2^{(n)} & d_{22}^{(n)} & d_{23}^{(n)} \\ r_3^{(n)} & d_{32}^{(n)} & d_{33}^{(n)} \end{vmatrix}}{\begin{vmatrix} d_{11}^{(n)} & d_{12}^{(n)} & d_{13}^{(n)} \\ d_{21}^{(n)} & d_{22}^{(n)} & d_{23}^{(n)} \\ d_{31}^{(n)} & d_{32}^{(n)} & d_{33}^{(n)} \end{vmatrix}} \equiv -\frac{U^{(n)}}{U^{(n)} + i\, V^{(n)}}, \tag{7.97}$$

where

$$U^{(n)} = \begin{vmatrix} \mathfrak{Re}\left[d_{11}^{(n)}\right] & d_{12}^{(n)} & d_{13}^{(n)} \\ \mathfrak{Re}\left[d_{21}^{(n)}\right] & d_{22}^{(n)} & d_{23}^{(n)} \\ \mathfrak{Re}\left[d_{31}^{(n)}\right] & d_{32}^{(n)} & d_{33}^{(n)} \end{vmatrix} = - \begin{vmatrix} r_1^{(n)} & d_{12}^{(n)} & d_{13}^{(n)} \\ r_2^{(n)} & d_{22}^{(n)} & d_{23}^{(n)} \\ r_3^{(n)} & d_{32}^{(n)} & d_{33}^{(n)} \end{vmatrix}, \tag{7.98}$$

and

$$V^{(n)} = \begin{vmatrix} \mathfrak{Im}\left[d_{11}^{(n)}\right] & d_{12}^{(n)} & d_{13}^{(n)} \\ \mathfrak{Im}\left[d_{21}^{(n)}\right] & d_{22}^{(n)} & d_{23}^{(n)} \\ \mathfrak{Im}\left[d_{31}^{(n)}\right] & d_{32}^{(n)} & d_{33}^{(n)} \end{vmatrix}. \tag{7.99}$$

The significant advantage of the compact form achieved using the state-space formulation can be seen in Equations (7.97)–(7.99), in which the determinants of 3x3 matrices are prescribed, regardless of the number of elastic layers in the cloak. Additional complexity due to multiple layers, however, manifests itself in the η, η', ζ, and ζ' terms. Specifically, these terms contain the elements of the global transfer function which, as defined by Equation (7.72), is a product of the local transfer function for each layer. The limitations of this state-space formulation lie in these local transfer functions, which are written as a Maclaurin series expansions about the edge of the layer. For thicker layers, more terms in the series expansion must be retained to obtain an accurate solution, while much fewer are need for acoustically thin shells.

To demonstrate the effectiveness of using spherically isotropic layers, consider the example of a steel sphere in water coated with a bilayer plasmonic cloak, explored in Sections 6.4.2 and 6.4.3. In this previous examination, it was observed that when the outer fluid layer is replaced by an isotropic elastic layer, a large low-frequency resonance appears, which potentially can limit the bandwidth and inhibits the overall goal of reducing the scattering strength. The source of this was attributed to the resonances arising from circumferential waves traveling within the elastic layer, analogous to antisymmetric Lamb waves present in flat plates.

To mitigate these effects, one possible approach is to change the tangential properties of the elastic layer. This process is illustrated in Figure 7.2, and consists

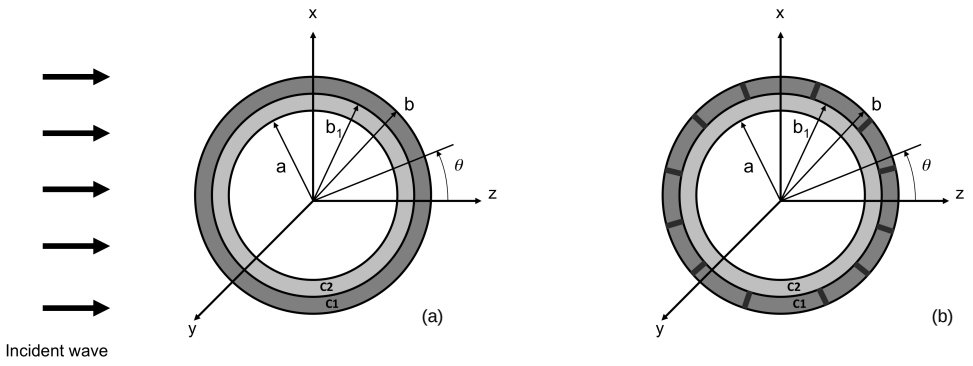

Figure 7.2: Comparison of a two layer cloak with an inner fluid layer and (a) an isotropic elastic outer layer, previously described in Chapter 6, and (b) an anisotropic (spherically isotropic) elastic layer. One possible way for creating the necessary anisotropy is illustrated in (b) using a compliant *kerf filler*, shown in black.

of inserting thin sections of a different material. In engineering applications, a small cut or groove is sometimes referred to as a *kerf*, and the resulting material inserted is called *kerf filler*. Note that the material properties of the kerf filler will have a significant affect on the tangential wave motion within the elastic layer, though its impact on the radial motion will be minimal.

An example of the effect of the tangential elastic layer properties on the effectiveness of the cloak is shown in Figure 7.3. Examining the magnitude of the scattering coefficients, it is seen that the first three modes are successfully cancelled, whereas the low-frequency resonance is significantly reduced in frequency. Otherwise, the modal characteristics of the cloaked steel sphere using a spherically isotropic elastic layer remain nearly unchanged compared with the isotropic elastic layer case, shown in Figure 6.9. This effect is highlighted in Figure 7.3(c), which shows a comparison of the scattering gain between the cases with the isotropic and anisotropic outer layer.

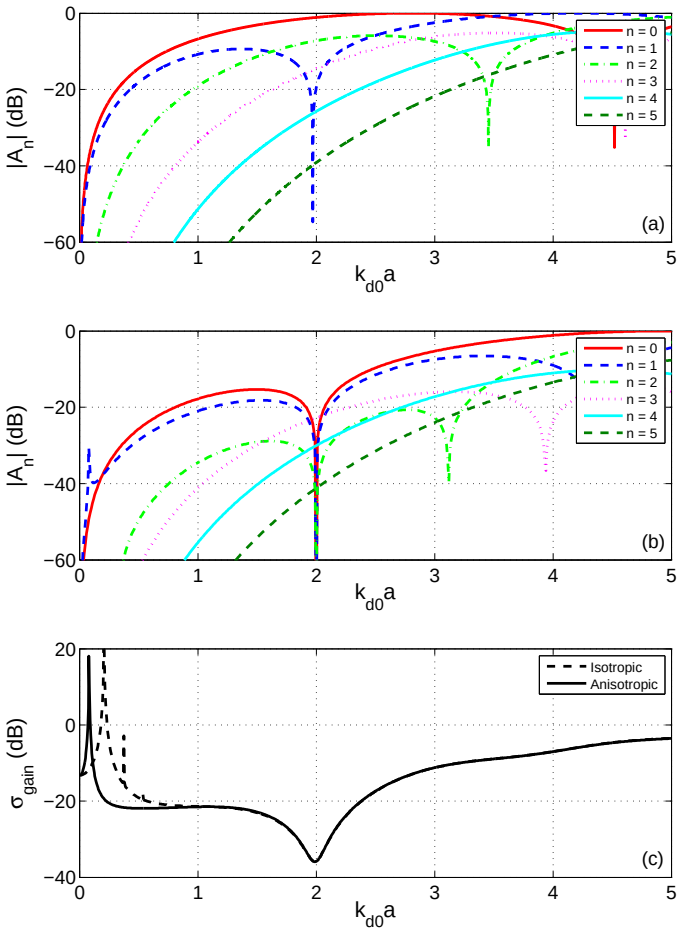

Figure 7.3: Scattering coefficients (in dB) for an (a) uncloaked and (b) cloaked steel sphere in water. The cloak consists of an inner fluid layer and outer elastic layer with $\delta_1 = \delta_2 = 0.04$, which cancels the first three scattering modes at $k_{d,0}a = 2.0$. The outer layer shown is spherically isotropic, with the same properties as the isotropic elastic case given in Table 6.1, except that the coefficient C_{11} in Equation 7.1 is scaled by a factor of 0.1. The scattering gain in dB, relative to the uncloaked scatterer, is given in (c) for the exact theoretical solution when the outer layer is a spherically isotropic elastic solid. The scattering gain for the case of a isotropic elastic outer layer (dashed) is given for reference.

Adjusting only a single property of the anisotropic layer, the analysis presented here highlights the usefulness and importance of anisotropy on a plasmonic cloaking layer. Although this is a relatively simple example, it highlights how consideration of even relatively modest anisotropy, though analytically complex, is a potentially powerful tool in designing and developing practical and effective acoustic plasmonic cloaks.

Chapter 8

Conclusions

8.1 General conclusions and contributions

The objective of this work was to investigate the physical parameters necessary for, and the feasibility of, designing an acoustic cloak using a scattering cancellation approach for an elastic sphere surrounded by fluid and elastic layers. Recall that the tasks associated with this objective were expressed by two questions:

1. How can the acoustic field scattered from a spherical object be significantly reduced or cancelled?

2. How can a realizable cloak be achieved?

The next two sections are dedicated to describing the results of examining each of these questions, and the contributions that have been made in the process.

8.1.1 How the acoustic field scattered from a spherical object can be significantly reduced or cancelled

The first of these questions was addressed in Chapters 2 and 3. Although significant reduction in the scattering strength is limited to finite bandwidths, in Chapter 2 the scattering cancellation approach was shown to have a key advantage in that it can be implemented using a single homogeneous layer. This makes it far more feasible to realize than either transformation-based cloaks or anomalous resonance cloaks, which currently are limited by fabrication of the metamaterials, due to unusual properties which must be achieved and the complexity of the arrangements.

Despite successfully being implemented for EM waves, plasmonic cloaks had not been investigated for acoustic waves prior to the current work being undertaken. For spherically symmetric geometries, it was pointed out that there is not an exact analogy between EM and acoustic waves. As a result, in Chapter 3 the acoustic scattering cancellation formulation was developed from fundamental acoustic and elastodynamic principles. Using the insight gained from the previous work for EM waves, one obtains solutions for the cloaking layers which were established by setting each mode of the scattering coefficient equal to zero. It was also observed that the number of modes making a substantial contribution to the scattered field increased as the size of the object increased relative to the wavelength, requiring more layers to significantly reduce the scattering strength. The formulation developed here allows for any large (but finite) number of fluid or isotropic layers, leading to a correspondingly large number of modes to be cancelled.

8.1.2 How a realizable cloak is achieved

The second question presented in relation to the thesis objective was investigated throughout the remainder of the thesis, being addressed in Chapters 4–7. For the single layer plasmonic cloak discussed in Chapter 4, it was observed that only the first two modes of the scattering coefficient could be cancelled. This is in agreement with the solutions obtained for the case of EM waves. In the quasi-static limit, these results matched previous acoustic analyses, which showed that the monopole term depends only on the compressibility of the coated object, and the dipole term depends only on the density.

As in the scattering cancellation of EM waves using a single layer, a target with properties *greater* than the surrounding medium requires a cloak with properties which are *less* than those of the surrounding medium. In water, this means that

acoustic scattering cancellation can be achieved using ordinary, homogenous materials which can be constructed from materials which are found in nature. Thus, no metamaterials or microscale resonant structures, like those of plasmonic materials utilized for EM waves, are required to implement this type of cloak for underwater applications.

Despite only two scattering modes being cancelled simultaneously using a single layer, significant scattering reductions were observed for practical examples. At ka near unity, metal spheres in water coated with a thin single cloaking layer reduced the scattering strength by 40 dB compared to the uncloaked sphere. Although these results are impressive considering the relative simplicity of the cloak, several limitations were observed. First, the operability is limited to relatively low frequencies, since there are more significant contributions from higher order modes as the frequency increases. Also, plasmonic cloaking using a single layer cannot be applied to all possible targets. In particular, it was seen that a single fluid layer of outer radius b was restricted to targets of radius a with bulk moduli greater than $(a/b)^3$, and limited to targets with densities less than $(b/a)^3$ for elastic targets.

Expanding upon the single layer plasmonic cloak, it is shown in Chapter 5 that an anti-resonance cloak can be created, utilizing the shear wave anti-resonance within an elastic layer to cancel additional modes. Although anti-resonances have been shown to create narrowband regions of reduced scattering strength for EM waves, these lack of an equivalent mechanism to the elastodynamic shear effects, highlighting that this is a novel feature of acoustic scattering cancellation and a noteworthy contribution. Furthermore, anti-resonance acoustic cloaks can be implemented for cases in which a single plasmonic cloak and target combination were not otherwise possible. The main limitation that arises using these type of cloaks, however, is a narrowing of the overall bandwidth, due to the shear wave resonances

within the cloaking layer.

In Chapter 6, the effects of additional plasmonic layers were presented, and it was found that additional isotropic elastic or fluid layers can be used to cancel more modes. This allows higher design frequencies to be considered, and for a given design frequency can lead to a significant reduction in scattering strength compared to a single layer cloak. A detailed analysis is presented for a configuration consisting of two fluid layers. Although this represents a relatively simple design for a multilayer cloak, it is demonstrated that these solutions can readily be used to create more complex arrangements using alternating layer schemes.

Examining the cloaking layer properties which are required for a two layer configuration, it is observed that the design is driven by the inertial effects within each layer. Specifically, it is seen that the inner layer has a density much *smaller* than that of the surrounding medium, much like the case of a single layer cloak, while the outer layer requires a density which is much *larger* than the surrounding medium. Conversely, the dominant feature determining the compressibility is the effective compressibility of the two layer coating, rather than each of the layers individually. This allows for the bulk modulus of one of the layers to be treated as a design parameter, yielding an entire family of possible designs, rather than a single optimal solution as seen for a single layer plasmonic cloak.

Using an isotropic elastic layer instead of a fluid for the outer layer, similar results to the two fluid layer case are reported. However, use of an elastic layer adds a low frequency resonance, corresponding to the axisymmetric Lamb wave in the elastic layer. Even though the necessary cloak properties for either the fluid or elastic outer layer are nearly identical, the existence of the non-zero shear in the elastic layer acts as a restoring force leading to this phenomenon. The predicted reduction in the scattering strength was verified using COMSOL, which showed

excellent agreement across the entire frequency band of interest. Typical reductions in the scattering strength for a steel sphere in water were 35 dB using two layers and up to 70 dB using four layers, achieved at $ka = 2.0$. Using only fluid layers, the reduction below the design frequency is 20 dB or more, with modest reductions observed up to $ka = 5.0$. For an elastic outer layer, the reduction below the design frequency iss not achieved due to the low frequency resonance, but a similar modest reduction is seen above the design frequency up to $ka = 5.0$.

To address the low frequency resonance observed with elastic layers, a formulation for scattering cancellation using spherically isotropic layers was developed in Chapter 7. To accomplish this, the scattering cancellation formulation is re-derived to allow for multiple layers with spherical isotropy. This allows for the tangential stiffness to to be varied independent of the radial stiffness, thereby allowing for the mitigation of the low frequency resonance within the frequency band of interest, improving the broadband response of the cloak.

The results developed in this thesis create a theoretical framework to understand and design an effective acoustic cloak using a scattering cancellation approach, which has never previously been examined for acoustic waves. Although guided by prior work for EM applications, the detailed examination of the elastodynamics represents a significant departure from that done with EM waves, which are analogous to the acosutic case in which only fluids are considered. Furthermore, due to the non-existent issues limiting the bandwidth and realization of EM plasmonic cloaks, namely causality and the necessity for resonant structures to construct a cloak, this leads to significant broadband scattering reductions for acoustic waves.

8.2 Suggestions for future work

Given the successful demonstration of the theoretical implementation of acoustic scattering cancellation, the next obvious step would be experimental fabrication and testing. This step is particularly important, since the biggest challenge to the implementation of acoustic cloaks has been creating the materials necessary to match those prescribed by the theory. Although this task is difficult, the results demonstrated in this thesis have two advantageous features with regards to the feasibility of constructing an acoustic cloak: (i) the possibility of using ordinary materials with homogeneous properties instead of needing to design and develop acoustic metamaterials or metafluids, and (ii) significant reductions in the scattering strength can be achieved using simple configurations of only one or two layers.

Although ordinary materials with homogeneous properties can be utilized to create a cloak in water, expansion of this analysis for air applications would require the use of acoustic metamaterials, creating materials with either extremely low (but positive) or negative densities. The use of these materials for plasmonic cloaking is potentially promising, given that much of the difficulties faced in previous acoustic metamaterials research has been driven by the extreme properties and strong gradients required by transformation-based cloaks. Future research could also build upon developments in EM plasmonic cloaking, which have demonstrated the feasibility of overcoming this particular challenge.

One of the novel features of the plasmonic cloak is that the pressure field on the interior is non-zero. In particular, the elimination of the scattered pressure field acting on the surface of cloaked object means the total pressure is equal in magnitude and phase to the incident pressure. This enables one to explore the fascinating concept of an *ideal acoustic sensor*, which is able to measure an incident pressure wave without disruption of the wave itself. Applications of such a device

could be used for a wide range of acoustic measurements, particularly those involving closely packed arrays or near-field testing. This could be accomplished using a piezoelectric inner shell, which is a traditional method for making hydrophones enabling the acoustic pressure to be converted to an electric voltage. Due to the coupling between the electric and mechanical properties, a piezoelectric shell exhibits spherical isotropy [88, 90]. Building upon the analysis presented in Chapter 7 for a multilayered spherically isotropic cloak, a spherically isotropic piezoelectric layer could be added, allowing for the investigation and design of a cloaked acoustic sensor.

Although the focus of this thesis was on the investigation of the cloaking effects associated with a scattering cancellation approach, the method represents a more general process of describing the scattered field as a sum of the modes and then adding a coating to control the strength of each relevant mode. Thus, it is also possible to utilize these techniques to change the acoustic scattering from an object, rather than to simply hide or 'cloak' it. Possible applications for this include imaging, underwater navigation, and acoustic metamaterial design. The design of some acoustic metamaterials, such as sonic crystals, use the frequency dependent scattering from a lattice of elastic inclusions to create the desired exotic macroscopic properties. By coating the inclusions and using the methods developed in this thesis, a wide range of scattering patterns can be designed, even at the relatively long wavelengths (compared to the size of the inclusion) typically used in such a structure.

For the case of underwater navigation, the techniques described in this thesis could be used in the design of sonar reflectors, such as a *sonar bell*. For example, it would be possible to design a coating which cancelled the monopole and quadrupole modes to produce a non-resonant, broadband directional scatterer dominated by the dipole mode. Using a similar concept for the design of biomedical contrast agents

could lead to improved ultrasonic imaging. This could even be used in conjunction with the cloaking concepts presented in this thesis, to create a contrast agent which is cloaked for some frequencies, and a strong scatterers at others. Although these are just a few specific applications, the theoretical methods to control the scattered field of an acoustic object demonstrated here enables both improved and expanded designs of acoustic systems and a deeper appreciation of a fundamental acoustic phenomenon.

Appendices

Appendix A

Linear system of equations derivation for scattering from isotropic sphere coated with isotropic shells

A.1 Basic formulation

To determine the coefficients in $\boldsymbol{\mathcal{D}}^{(n)}$ and $\bar{\mathsf{r}}^{(n)}$ for the linear system given by Equation (3.20) which can be solved for the n^{th} mode of the unknown scattering coefficients, continuity of the stress and displacement at each interface must be evaluated. To do so, expressions for the stress (pressure) and displacement in each elastic (or fluid) layer or in the core material will need to be determined. Using the *method of potentials* described in Section 3.1, the stress and displacement are expressed in terms of two scalar displacement potentials, ϕ and χ, which are given by Equations (3.15)–(3.18). From Equations (3.2), (3.4), and (3.8), the components of displacement u and stress T in spherical coordinates assuming azimuthal symmetry become [91]

$$u_r = \frac{\partial}{\partial r}\left(\phi + \frac{\partial}{\partial r}(r\chi)\right) + rk_s^2\chi, \tag{A.1}$$

$$u_\theta = \frac{1}{r}\frac{\partial}{\partial \theta}\left(\phi + \frac{\partial}{\partial r}(r\chi)\right), \tag{A.2}$$

$$T_{rr} = -\lambda k_d^2\phi + 2\mu\frac{\partial}{\partial r}\left[\frac{\partial}{\partial r}\left(\phi + \frac{\partial}{\partial r}(r\chi)\right) + rk_s^2\chi\right], \tag{A.3}$$

$$T_{r\theta} = \mu\frac{\partial}{\partial \theta}\left[2\frac{\partial}{\partial r}\left[\frac{1}{r}\left(\phi + \frac{\partial}{\partial r}(r\chi)\right)\right] + k_s^2\chi\right]. \tag{A.4}$$

Using Equations (A.1)–(A.4), expressions for the displacement and stress in the radial and tangential directions can be evaluated at the interface of each medium.

In the resulting expressions, the partial derivatives of ϕ and χ with respect to r yield higher order derivatives of the spherical Bessel functions, namely, terms containing $j_n''(kr)$ and $j_n'''(kr)$. As shown in Appendix B, these higher order derivatives can be written as

$$j_n''(z) = \frac{1}{z^2}\left[\left(n(n+1) - z^2\right)j_n(z) - 2z\, j_n'(z)\right], \tag{A.5}$$

$$j_n'''(z) = \frac{1}{z^3}\left[-4\left(n(n+1) - \frac{1}{2}z^2\right)j_n(z) + (n^2+n+6-z^2)z\, j_n'(z)\right]. \tag{A.6}$$

The exact expressions for the coefficients of $\boldsymbol{\mathcal{D}}^{(n)}$ and $\bar{\mathsf{r}}^{(n)}$ depend on the the specific configuration of the submerged coated sphere. In particular, the number and exact formulation of the coefficients depends on the type of materials (whether they are isotropic elastic solids or fluids), and how many layers the coating is comprised of. The case of a single elastic layer coating an elastic sphere is presented in Section A.2, and a more general formulation for multilayered coatings is described Section A.4.

A.2 Solution for a single layer coated sphere

Consider an elastic sphere coated with a single elastic layer surrounded by a fluid, which is illustrated in Figure 5.1. In this case, Equation (3.20) reduces to

$$\begin{bmatrix} d_{11}^{(n)} & d_{12}^{(n)} & d_{13}^{(n)} & d_{14}^{(n)} & d_{15}^{(n)} & 0 & 0 \\ d_{21}^{(n)} & d_{22}^{(n)} & d_{23}^{(n)} & d_{24}^{(n)} & d_{25}^{(n)} & 0 & 0 \\ 0 & d_{32}^{(n)} & d_{33}^{(n)} & d_{34}^{(n)} & d_{35}^{(n)} & 0 & 0 \\ 0 & d_{42}^{(n)} & d_{43}^{(n)} & d_{44}^{(n)} & d_{45}^{(n)} & d_{46}^{(n)} & d_{47}^{(n)} \\ 0 & d_{52}^{(n)} & d_{53}^{(n)} & d_{54}^{(n)} & d_{55}^{(n)} & d_{56}^{(n)} & d_{57}^{(n)} \\ 0 & d_{62}^{(n)} & d_{63}^{(n)} & d_{64}^{(n)} & d_{65}^{(n)} & d_{66}^{(n)} & d_{67}^{(n)} \\ 0 & d_{72}^{(n)} & d_{73}^{(n)} & d_{74}^{(n)} & d_{75}^{(n)} & d_{76}^{(n)} & d_{77}^{(n)} \end{bmatrix} \begin{bmatrix} A_n^{(0)} \\ A_n^{(\mathrm{c})} \\ B_n^{(\mathrm{c})} \\ C_n^{(\mathrm{c})} \\ D_n^{(\mathrm{c})} \\ A_n^{(\mathrm{core})} \\ C_n^{(\mathrm{core})} \end{bmatrix} = \begin{bmatrix} r_1^{(n)} \\ r_2^{(n)} \\ 0 \\ 0 \\ 0 \\ 0 \\ 0 \end{bmatrix}. \tag{A.7}$$

The components of the linear system are given by

$$d_{11}{}^{(n)} = -k_{d,0}b\, h_n^{(1)\prime}(k_{d,0}b), \tag{A.8}$$

$$d_{12}{}^{(n)} = k_{d,c}b\, j_n'(k_{d,c}b), \tag{A.9}$$

$$d_{13}{}^{(n)} = k_{d,c}b\, n_n'(k_{d,c}b), \tag{A.10}$$

$$d_{14}{}^{(n)} = n(n+1)\, j_n(k_{s,c}b), \tag{A.11}$$

$$d_{15}{}^{(n)} = n(n+1)\, n_n(k_{s,c}b), \tag{A.12}$$

$$d_{21}{}^{(n)} = \frac{1}{2}h_n^{(1)}(k_{d,0}b), \tag{A.13}$$

$$d_{22}{}^{(n)} = \overline{\rho}_c \frac{1}{(k_{s,c}b)^2}\left\{\left[n(n+1) - \frac{1}{2}(k_{s,c}b)^2\right] j_n(k_{d,c}b) - 2k_{d,c}b\, j_n'(k_{d,c}b)\right\}, \tag{A.14}$$

$$d_{23}{}^{(n)} = \overline{\rho}_c \frac{1}{(k_{s,c}b)^2}\left\{\left[n(n+1) - \frac{1}{2}(k_{s,c}b)^2\right] n_n(k_{d,c}b) - 2k_{d,c}b\, n_n'(k_{d,c}b)\right\}, \tag{A.15}$$

$$d_{24}{}^{(n)} = \overline{\rho}_c \frac{1}{(k_{s,c}b)^2} n(n+1)\left[k_{s,c}b\, j_n'(k_{s,c}b) - j_n(k_{s,c}b)\right], \tag{A.16}$$

$$d_{25}{}^{(n)} = \overline{\rho}_c \frac{1}{(k_{s,c}b)^2} n(n+1)\left[k_{s,c}b\, n_n'(k_{s,c}b) - n_n(k_{s,c}b)\right], \tag{A.17}$$

$$d_{32}{}^{(n)} = k_{d,c}b\, j_n'(k_{d,c}b) - j_n(k_{d,c}b), \tag{A.18}$$

$$d_{33}{}^{(n)} = k_{d,c}b\, n_n'(k_{d,c}b) - n_n(k_{d,c}b), \tag{A.19}$$

$$d_{34}{}^{(n)} = \left[n(n+1) - 1 - \frac{1}{2}(k_{s,c}b)^2\right] j_n(k_{s,c}b) - k_{s,c}b\, j_n'(k_{s,c}b), \tag{A.20}$$

$$d_{35}{}^{(n)} = \left[n(n+1) - 1 - \frac{1}{2}(k_{s,c}b)^2\right] n_n(k_{s,c}b) - k_{s,c}b\, n_n'(k_{s,c}b), \tag{A.21}$$

$$d_{42}{}^{(n)} = k_{d,c}a\, j_n'(k_{d,c}a), \tag{A.22}$$

$$d_{43}{}^{(n)} = k_{d,c}a\, n_n'(k_{d,c}a), \tag{A.23}$$

$$d_{44}{}^{(n)} = n(n+1)\, j_n(k_{s,c}a), \tag{A.24}$$

$$d_{45}{}^{(n)} = n(n+1)\, n_n(k_{s,c}a), \tag{A.25}$$

$$d_{46}{}^{(n)} = -k_{\rm d} a\, j_n'(k_{\rm d} a), \tag{A.26}$$

$$d_{47}{}^{(n)} = -n(n+1)\, j_n(k_{\rm s} a), \tag{A.27}$$

$$d_{52}{}^{(n)} = j_n(k_{d,c} a), \tag{A.28}$$

$$d_{53}{}^{(n)} = n_n(k_{d,c} a), \tag{A.29}$$

$$d_{54}{}^{(n)} = k_{s,c} a\, j_n'(k_{s,c} a) + j_n(k_{s,c} a), \tag{A.30}$$

$$d_{55}{}^{(n)} = k_{s,c} a\, n_n'(k_{s,c} a) + n_n(k_{s,c} a), \tag{A.31}$$

$$d_{56}{}^{(n)} = -j_n(k_{\rm d} a), \tag{A.32}$$

$$d_{57}{}^{(n)} = -\left[k_{\rm s} a j_n'(k_{\rm s} a) + j_n(k_{\rm s} a)\right], \tag{A.33}$$

$$d_{62}{}^{(n)} = \overline{\rho}_c \frac{1}{(k_{s,c} a)^2} \left\{ \left[n(n+1) - \frac{1}{2}(k_{s,c} a)^2 \right] j_n(k_{d,c} a) - 2 k_{d,c} a\, j_n'(k_{d,c} a) \right\}, \tag{A.34}$$

$$d_{63}{}^{(n)} = \overline{\rho}_c \frac{1}{(k_{s,c} a)^2} \left\{ \left[n(n+1) - \frac{1}{2}(k_{s,c} a)^2 \right] n_n(k_{d,c} a) - 2 k_{d,c} a\, n_n'(k_{d,c} a) \right\}, \tag{A.35}$$

$$d_{64}{}^{(n)} = \overline{\rho}_c \frac{1}{(k_{s,c} a)^2} n(n+1) \left[k_{s,c} a\, j_n'(k_{s,c} a) - j_n(k_{s,c} a) \right], \tag{A.36}$$

$$d_{65}{}^{(n)} = \overline{\rho}_c \frac{1}{(k_{s,c} a)^2} n(n+1) \left[k_{s,c} a\, n_n'(k_{s,c} a) - n_n(k_{s,c} a) \right], \tag{A.37}$$

$$d_{66}{}^{(n)} = -\overline{\rho} \frac{1}{(k_{\rm s} a)^2} \left\{ \left[n(n+1) - \frac{1}{2}(k_{\rm s} a)^2 \right] j_n(k_{\rm d} a) - 2 k_{\rm d} a\, j_n'(k_{\rm d} a) \right\}, \tag{A.38}$$

$$d_{67}{}^{(n)} = -\overline{\rho} \frac{1}{(k_{\rm s} a)^2} n(n+1) \left[k_{\rm s} a\, j_n'(k_{\rm s} a) - j_n(k_{\rm s} a) \right], \tag{A.39}$$

$$d_{72}{}^{(n)} = \overline{\rho}_c \frac{1}{(k_{s,c} a)^2} \left[k_{d,c} a\, j_n'(k_{d,c} a) - j_n(k_{d,c} a) \right], \tag{A.40}$$

$$d_{73}{}^{(n)} = \overline{\rho}_c \frac{1}{(k_{s,c} a)^2} \left[k_{d,c} a\, n_n'(k_{d,c} a) - n_n(k_{d,c} a) \right], \tag{A.41}$$

$$d_{74}{}^{(n)} = \overline{\rho}_c \frac{1}{(k_{s,c} a)^2} \left\{ \left[n(n+1) - 1 - \frac{1}{2}(k_{s,c} a)^2 \right] j_n(k_{s,c} a) - k_{s,c} a\, j_n'(k_{s,c} a) \right\}, \tag{A.42}$$

$$d_{75}{}^{(n)} = \overline{\rho}_c \frac{1}{(k_{s,c} a)^2} \left\{ \left[n(n+1) - 1 - \frac{1}{2}(k_{s,c} a)^2 \right] n_n(k_{s,c} a) - k_{s,c} a\, n_n'(k_{s,c} a) \right\}, \tag{A.43}$$

$$d_{76}^{(n)} = -\overline{\rho}\frac{1}{(k_{\mathrm{s}}a)^2}\left[k_{\mathrm{d}}a\, j_n'(k_{\mathrm{d}}a) - j_n(k_{\mathrm{d}}a)\right], \tag{A.44}$$

$$d_{77}^{(n)} = -\overline{\rho}\frac{1}{(k_{\mathrm{s}}a)^2}\left\{\left[n(n+1)-1-\frac{1}{2}(k_{\mathrm{s}}a)^2\right]j_n(k_{\mathrm{s}}a) - k_{\mathrm{s}}a\, j_n'(k_{\mathrm{s}}a)\right\}, \tag{A.45}$$

$$r_1^{(n)} = k_{d,0}b\, j_n'(k_{d,0}b), \tag{A.46}$$

$$r_2^{(n)} = -\frac{1}{2}j_n(k_{d,0}b), \tag{A.47}$$

where $\overline{\rho}_c = \rho_c/\rho_0$ and $\overline{\rho} = \rho/\rho_0$.

Although it is possible to obtain these expressions as limiting cases of previous work [67, 92], they have not been presented in the form used here and thus are included for completeness. When the core material sphere is a fluid, application of the boundary conditions yields a 6×6 linear system. The elements of this linear system are simply a reduced form of $d_{ij}^{(n)}$ and $r_i^{(n)}$, obtained by removing the rows and columns where $i=5$ and $j=7$ and taking $\mu\to0$, or equivalently, $1/k_{\mathrm{s}}\to0$. The resulting linear system matches those derived in previous work [64].

In the work presented in this thesis, the scattering coefficients represent the complex amplitudes of the displacement potentials. To relate these results to the acoustic pressure p in medium m, note that

$$p = \rho_m\omega^2\phi. \tag{A.48}$$

Since the the pressure is often the primary variable of interest in acoustic scattering problems, some previous work has used *pressure* scattering coefficients instead of those of the scalar potentials [93]. The relationship between the pressure scattering coefficients and the displacement potential scattering coefficients of each medium can be determined using Equation (A.48).

A.3 Solution for an elastic sphere coated with two fluid layers

Consider an elastic sphere coated with two fluid layers and surrounded by a fluid, as illustrated in Figure C.1. In this case, Equation (3.20) reduces to

$$\begin{bmatrix} d_{11}^{(n)} & d_{12}^{(n)} & d_{13}^{(n)} & 0 & 0 & 0 & 0 \\ d_{21}^{(n)} & d_{22}^{(n)} & d_{23}^{(n)} & 0 & 0 & 0 & 0 \\ 0 & d_{32}^{(n)} & d_{33}^{(n)} & d_{34}^{(n)} & d_{35}^{(n)} & 0 & 0 \\ 0 & d_{42}^{(n)} & d_{43}^{(n)} & d_{44}^{(n)} & d_{45}^{(n)} & 0 & 0 \\ 0 & 0 & 0 & d_{54}^{(n)} & d_{55}^{(n)} & d_{56}^{(n)} & d_{57}^{(n)} \\ 0 & 0 & 0 & d_{64}^{(n)} & d_{65}^{(n)} & d_{66}^{(n)} & d_{67}^{(n)} \\ 0 & 0 & 0 & 0 & 0 & d_{76}^{(n)} & d_{77}^{(n)} \end{bmatrix} \begin{bmatrix} A_n^{(0)} \\ A_n^{(\mathrm{c1})} \\ B_n^{(\mathrm{c1})} \\ A_n^{(\mathrm{c2})} \\ B_n^{(\mathrm{c2})} \\ A_n^{(\mathrm{core})} \\ C_n^{(\mathrm{core})} \end{bmatrix} = \begin{bmatrix} r_1^{(n)} \\ r_2^{(n)} \\ 0 \\ 0 \\ 0 \\ 0 \\ 0 \end{bmatrix}. \tag{A.49}$$

The components of the linear system are given by

$$d_{11}{}^{(n)} = -\, k_{d,0} b\, h_n^{(1)\prime}(k_{d,0} b), \tag{A.50}$$

$$d_{12}{}^{(n)} = k_{d,c1} b\, j_n'(k_{d,c1} b), \tag{A.51}$$

$$d_{13}{}^{(n)} = k_{d,c1} b\, n_n'(k_{d,c1} b), \tag{A.52}$$

$$d_{21}{}^{(n)} = \frac{1}{2} h_n^{(1)}(k_{d,0} b), \tag{A.53}$$

$$d_{22}{}^{(n)} = \overline{\rho}_{c1}\, j_n(k_{d,c1} b), \tag{A.54}$$

$$d_{23}{}^{(n)} = \overline{\rho}_{c1}\, n_n(k_{d,c1} b), \tag{A.55}$$

$$d_{32}{}^{(n)} = k_{d,c1} b_1\, j_n'(k_{d,c1} b_1), \tag{A.56}$$

$$d_{33}{}^{(n)} = k_{d,c1} b_1\, n_n'(k_{d,c1} b_1), \tag{A.57}$$

$$d_{34}{}^{(n)} = k_{d,c2} b_1\, j_n'(k_{d,c2} b_1), \tag{A.58}$$

$$d_{35}{}^{(n)} = k_{d,c2} b_1\, n_n'(k_{d,c2} b_1), \tag{A.59}$$

$$d_{42}{}^{(n)} = \overline{\rho}_{c1}\, k_{d,c1} b_1\, j_n(k_{d,c1} b_1), \tag{A.60}$$

$$d_{43}{}^{(n)} = \overline{\rho}_{c1}\, k_{d,c1} b_1\, n_n(k_{d,c1} b_1), \tag{A.61}$$

$$d_{44}{}^{(n)} = \overline{\rho}_{c2}\, k_{d,c2} b_1\, j_n(k_{d,c2} b_1), \tag{A.62}$$

$$d_{45}{}^{(n)} = \overline{\rho}_{c2}\, k_{d,c2} b_1\, n_n(k_{d,c2} b_1), \tag{A.63}$$

$$d_{54}{}^{(n)} = k_{d,c2} a\, j_n'(k_{d,c2} a), \tag{A.64}$$

$$d_{55}{}^{(n)} = k_{d,c2} a\, n_n'(k_{d,c2} a), \tag{A.65}$$

$$d_{56}{}^{(n)} = -k_{\mathrm{d}} a\, j_n'(k_{\mathrm{d}} a), \tag{A.66}$$

$$d_{57}{}^{(n)} = -n(n+1)\, j_n(k_{\mathrm{s}} a), \tag{A.67}$$

$$d_{64}{}^{(n)} = \overline{\rho}_{c2}\, j_n(k_{d,c2} a), \tag{A.68}$$

$$d_{65}{}^{(n)} = \overline{\rho}_{c2}\, n_n(k_{d,c2} a), \tag{A.69}$$

$$d_{66}{}^{(n)} = 2\overline{\rho}\left\{ \left[\frac{n(n+1)}{(k_{\mathrm{s}} a)^2} - \frac{1}{2} \right] j_n(k_{\mathrm{d}} a) - 2 \frac{k_{\mathrm{d}} a}{(k_{\mathrm{s}} a)^2} j_n'(k_{\mathrm{d}} a) \right\}, \tag{A.70}$$

$$d_{67}{}^{(n)} = 2\overline{\rho} \frac{n(n+1)}{(k_{\mathrm{s}} a)^2} \left[k_{\mathrm{s}} a j_n'(k_{\mathrm{s}} a) - j_n(k_{\mathrm{s}} a) \right], \tag{A.71}$$

$$d_{76}{}^{(n)} = k_{\mathrm{d}} a\, j_n'(k_{\mathrm{d}} a) - j_n(k_{\mathrm{d}} a), \tag{A.72}$$

$$d_{77}{}^{(n)} = \left[n(n+1) - 1 - \frac{1}{2}(k_{\mathrm{s}} a)^2 \right] j_n(k_{\mathrm{s}} a) - k_{\mathrm{s}} a\, j_n'(k_{\mathrm{s}} a), \tag{A.73}$$

$$r_1{}^{(n)} = k_{d,0} b\, j_n'(k_{d,0} b), \tag{A.74}$$

$$r_2{}^{(n)} = -\frac{1}{2} j_n(k_{d,0} b), \tag{A.75}$$

where $\overline{\rho}_{c1} = \rho_{c1}/\rho_0$, $\overline{\rho}_{c2} = \rho_{c2}/\rho_0$ and $\overline{\rho} = \rho/\rho_0$. The resulting linear system matches those derived in previous work [94].

A.4 Solution for a submerged sphere covered with a multilayer coating

Consider the case of a spherical isotropic elastic core coated by N isotropic layers (either elastic or fluid), as illustrated in Figure 3.1. The linear system of equations which describe this configuration are given by Equation (3.20). The values of $\boldsymbol{\mathcal{D}}^{(n)}$ and $\vec{\mathsf{r}}^{(n)}$ are presented for the applicable regions of this configuration, with the results for the surrounding fluid medium, multilayer coating and core material given in Sections A.4.1, A.4.2 and A.4.3, respectively.

A.4.1 Surrounding fluid medium

The coefficients contained within $\mathbf{D}_{1,0}^{(n)}$ and $\vec{r}_0^{(n)}$ depend on the properties of the surrounding fluid medium and the outer radius b, and are given by

$$\mathbf{D}_{1,0}^{(n)}(1,1) = -k_{d,0} b \, h_n^{(1)\prime}(k_{d,0} b), \tag{A.76}$$

$$\mathbf{D}_{1,0}^{(n)}(1,2) = \frac{1}{2} h_n^{(1)}(k_{d,0} b), \tag{A.77}$$

$$\mathbf{D}_{1,0}^{(n)}(1,3) = 0, \tag{A.78}$$

$$\vec{r}_0^{(n)}(1,1) = k_{d,0} b \, j_n'(k_{d,0} b), \tag{A.79}$$

$$\vec{r}_0^{(n)}(1,2) = -\frac{1}{2} j_n(k_{d,0} b), \tag{A.80}$$

$$\vec{r}_0^{(n)}(1,3) = 0, \tag{A.81}$$

A.4.2 Multilayer coating

For the m^{th} layer of a coating comprised of N isotropic layers, there are two coefficient matrices $\mathbf{D}_{m,m}^{(n)}$ and $\mathbf{D}_{m+1,m}^{(n)}$, corresponding to the outer and inner interfaces, respectively. These matrices, which depend on the properties of the m^{th} layer of the coating and the radius of the interface b_m. When the m^{th} layer is an

isotropic elastic solid at the interface with another elastic material,

$$\mathbf{D}^{(n)}_{q,m}(1,1) = k_{d,m}b_q\, j'_n(k_{d,m}b_q), \tag{A.82}$$

$$\mathbf{D}^{(n)}_{q,m}(1,2) = k_{d,m}b_q\, n'_n(k_{d,m}b_q), \tag{A.83}$$

$$\mathbf{D}^{(n)}_{q,m}(1,3) = n(n+1)j_n(k_{s,m}b_q), \tag{A.84}$$

$$\mathbf{D}^{(n)}_{q,m}(1,4) = n(n+1)n_n(k_{s,m}b_q), \tag{A.85}$$

$$\mathbf{D}^{(n)}_{q,m}(2,1) = j_n(k_{d,m}b_q), \tag{A.86}$$

$$\mathbf{D}^{(n)}_{q,m}(2,2) = n_n(k_{d,m}b_q), \tag{A.87}$$

$$\mathbf{D}^{(n)}_{q,m}(2,3) = k_{s,m}b_q\, j'_n(k_{s,m}b_q) + j_n(k_{s,m}b_q), \tag{A.88}$$

$$\mathbf{D}^{(n)}_{q,m}(2,4) = k_{s,m}b_q\, n'_n(k_{s,m}b_q) + n_n(k_{s,m}b_q), \tag{A.89}$$

$$\mathbf{D}^{(n)}_{q,m}(3,1) = \overline{\rho}_{c,m}\left\{\left[\frac{n(n+1)}{(k_{s,m}b_q)^2} - \frac{1}{2}\right] j_n(k_{d,m}b_q) - 2\frac{k_{d,m}b_q}{(k_{s,m}b_q)^2} j'_n(k_{d,m}b_q)\right\}, \tag{A.90}$$

$$\mathbf{D}^{(n)}_{q,m}(3,2) = \overline{\rho}_{c,m}\left\{\left[\frac{n(n+1)}{(k_{s,m}b_q)^2} - \frac{1}{2}\right] n_n(k_{d,m}b_q) - 2\frac{k_{d,m}b_q}{(k_{s,m}b_q)^2} n'_n(k_{d,m}b_q)\right\}, \tag{A.91}$$

$$\mathbf{D}^{(n)}_{q,m}(3,3) = \overline{\rho}_{c,m}n(n+1)\left\{\frac{1}{k_{s,m}b_q} j'_n(k_{s,m}b_q) - \frac{1}{(k_{s,m}b_q)^2} j_n(k_{s,m}b_q)\right\}, \tag{A.92}$$

$$\mathbf{D}^{(n)}_{q,m}(3,4) = \overline{\rho}_{c,m}n(n+1)\left\{\frac{1}{k_{s,m}b_q} n'_n(k_{s,m}b_q) - \frac{1}{(k_{s,m}b_q)^2} n_n(k_{s,m}b_q)\right\}, \tag{A.93}$$

$$\mathbf{D}^{(n)}_{q,m}(4,1) = \overline{\rho}_{c,m}\frac{1}{(k_{s,m}b_q)^2}\left[k_{d,m}b_q\, j'_n(k_{d,m}b_q) - j_n(k_{d,m}b_q)\right], \tag{A.94}$$

$$\mathbf{D}^{(n)}_{q,m}(4,2) = \overline{\rho}_{c,m}\frac{1}{(k_{s,m}b_q)^2}\left[k_{d,m}b_q\, n'_n(k_{d,m}b_q) - n_n(k_{d,m}b_q)\right], \tag{A.95}$$

$$\mathbf{D}^{(n)}_{q,m}(4,3) = \overline{\rho}_{c,m}\left\{\left[\frac{n(n+1)-1}{(k_{s,m}b_q)^2} - \frac{1}{2}\right] j_n(k_{s,m}b_q) - \frac{1}{k_{s,m}b_q} j'_n(k_{s,m}b_q)\right\}, \tag{A.96}$$

$$\mathbf{D}^{(n)}_{q,m}(4,4) = \overline{\rho}_{c,m}\left\{\left[\frac{n(n+1)-1}{(k_{s,m}b_q)^2} - \frac{1}{2}\right] n_n(k_{s,m}b_q) - \frac{1}{k_{s,m}b_q} n'_n(k_{s,m}b_q)\right\}, \tag{A.97}$$

where $q{=}m, m{+}1$. At the interface with a fluid, $\mathbf{D}^{(n)}_{q,m}$ becomes

$$\mathbf{D}^{(n)}_{q,m}(1,1) = k_{d,m}b_q\, j'_n(k_{d,m}b_q), \tag{A.98}$$

$$\mathbf{D}^{(n)}_{q,m}(1,2) = k_{d,m}b_q\, n'_n(k_{d,m}b_q), \tag{A.99}$$

$$\mathbf{D}^{(n)}_{q,m}(1,3) = n(n+1)j_n(k_{s,m}b_q), \tag{A.100}$$

$$\mathbf{D}^{(n)}_{q,m}(1,4) = n(n+1)n_n(k_{s,m}b_q), \tag{A.101}$$

$$\mathbf{D}^{(n)}_{q,m}(2,1) = \overline{\rho}_{c,m}\left\{\left[\frac{n(n+1)}{(k_{s,m}b_q)^2} - \frac{1}{2}\right] j_n(k_{d,m}b_q) - 2\frac{k_{d,m}b_q}{(k_{s,m}b_q)^2} j'_n(k_{d,m}b_q)\right\}, \tag{A.102}$$

$$\mathbf{D}^{(n)}_{q,m}(2,2) = \overline{\rho}_{c,m}\left\{\left[\frac{n(n+1)}{(k_{s,m}b_q)^2} - \frac{1}{2}\right] n_n(k_{d,m}b_q) - 2\frac{k_{d,m}b_q}{(k_{s,m}b_q)^2} n'_n(k_{d,m}b_q)\right\}, \tag{A.103}$$

$$\mathbf{D}^{(n)}_{q,m}(2,3) = \overline{\rho}_{c,m}n(n+1)\left\{\frac{1}{k_{s,m}b_q} j'_n(k_{s,m}b_q) - \frac{1}{(k_{s,m}b_q)^2} j_n(k_{s,m}b_q)\right\}, \tag{A.104}$$

$$\mathbf{D}^{(n)}_{q,m}(2,4) = \overline{\rho}_{c,m}n(n+1)\left\{\frac{1}{k_{s,m}b_q} n'_n(k_{s,m}b_q) - \frac{1}{(k_{s,m}b_q)^2} n_n(k_{s,m}b_q)\right\}, \tag{A.105}$$

$$\mathbf{D}^{(n)}_{q,m}(3,1) = \overline{\rho}_{c,m}\frac{1}{(k_{s,m}b_q)^2}\left[k_{d,m}b_q\, j'_n(k_{d,m}b_q) - j_n(k_{d,m}b_q)\right], \tag{A.106}$$

$$\mathbf{D}^{(n)}_{q,m}(3,2) = \overline{\rho}_{c,m}\frac{1}{(k_{s,m}b_q)^2}\left[k_{d,m}b_q\, n'_n(k_{d,m}b_q) - n_n(k_{d,m}b_q)\right], \tag{A.107}$$

$$\mathbf{D}^{(n)}_{q,m}(3,3) = \overline{\rho}_{c,m}\left\{\left[\frac{n(n+1)-1}{(k_{s,m}b_q)^2} - \frac{1}{2}\right] j_n(k_{s,m}b_q) - \frac{1}{k_{s,m}b_q} j'_n(k_{s,m}b_q)\right\}, \tag{A.108}$$

$$\mathbf{D}^{(n)}_{q,m}(3,4) = \overline{\rho}_{c,m}\left\{\left[\frac{n(n+1)-1}{(k_{s,m}b_q)^2} - \frac{1}{2}\right] n_n(k_{s,m}b_q) - \frac{1}{k_{s,m}b_q} n'_n(k_{s,m}b_q)\right\}. \tag{A.109}$$

When both layers at the interface are fluids, $\mathbf{D}^{(n)}_{q,m}$ reduces to

$$\mathbf{D}^{(n)}_{q,m}(1,1) = k_{d,m}b_q\, j'_n(k_{d,m}b_q), \tag{A.110}$$

$$\mathbf{D}^{(n)}_{q,m}(1,2) = k_{d,m}b_q\, n'_n(k_{d,m}b_q), \tag{A.111}$$

$$\mathbf{D}^{(n)}_{q,m}(2,1) = -\frac{1}{2}\,\overline{\rho}_{c,m}\, j_n(k_{d,m}b_q), \tag{A.112}$$

$$\mathbf{D}^{(n)}_{q,m}(2,2) = -\frac{1}{2}\,\overline{\rho}_{c,m}\, n_n(k_{d,m}b_q). \tag{A.113}$$

A.4.3 Core material

Consider a spherical core of radius a, comprised of an isotropic elastic solid. When the inner layer of the coating is elastic, $\mathbf{D}^{(n)}_{N+1,\mathrm{core}}$ is given by,

$$\mathbf{D}^{(n)}_{N+1,\mathrm{core}}(1,1) = -k_{\mathrm{d}}a\, j'_n(k_{\mathrm{d}}a), \tag{A.114}$$

$$\mathbf{D}^{(n)}_{N+1,\mathrm{core}}(1,2) = -n(n+1)j_n(k_{\mathrm{s}}a), \tag{A.115}$$

$$\mathbf{D}^{(n)}_{N+1,\mathrm{core}}(2,1) = -j_n(k_{\mathrm{d}}a), \tag{A.116}$$

$$\mathbf{D}^{(n)}_{N+1,\mathrm{core}}(2,2) = -\left[k_{\mathrm{s}}a\, j_n'(k_{\mathrm{s}}a) + j_n(k_{\mathrm{s}}a)\right], \tag{A.117}$$

$$\mathbf{D}^{(n)}_{N+1,\mathrm{core}}(3,1) = -\overline{\rho}\left\{\left[\frac{n(n+1)}{(k_{\mathrm{s}}a)^2} - \frac{1}{2}\right] j_n(k_{\mathrm{d}}a) - 2\frac{k_{\mathrm{d}}a}{(k_{\mathrm{s}}a)^2} j_n'(k_{\mathrm{d}}a)\right\}, \tag{A.118}$$

$$\mathbf{D}^{(n)}_{N+1,\mathrm{core}}(3,2) = -\overline{\rho}\frac{n(n+1)}{(k_{\mathrm{s}}a)^2}\left[k_{\mathrm{s}}a j_n'(k_{\mathrm{s}}a) - j_n(k_{\mathrm{s}}a)\right], \tag{A.119}$$

$$\mathbf{D}^{(n)}_{N+1,\mathrm{core}}(4,1) = -\overline{\rho}\frac{1}{(k_{\mathrm{s}}a)^2}\left[k_{\mathrm{d}}a\, j_n'(k_{\mathrm{d}}a) - j_n(k_{\mathrm{d}}a)\right], \tag{A.120}$$

$$\mathbf{D}^{(n)}_{N+1,\mathrm{core}}(4,2) = -\overline{\rho}\left\{\left[\frac{n(n+1)-1}{(k_{\mathrm{s}}a)^2} - \frac{1}{2}\right] j_n(k_{\mathrm{s}}a) - \frac{1}{k_{\mathrm{s}}a} j_n'(k_{\mathrm{s}}a)\right\}. \tag{A.121}$$

When the inner layer of the coating is a fluid, $\mathbf{D}^{(n)}_{N+1,\mathrm{core}}$ becomes

$$\mathbf{D}^{(n)}_{N+1,\mathrm{core}}(1,1) = -k_{\mathrm{d}}a\, j_n'(k_{\mathrm{d}}a), \tag{A.122}$$

$$\mathbf{D}^{(n)}_{N+1,\mathrm{core}}(1,2) = -n(n+1)j_n(k_{\mathrm{s}}a), \tag{A.123}$$

$$\mathbf{D}^{(n)}_{N+1,\mathrm{core}}(2,1) = -\overline{\rho}\left\{\left[\frac{n(n+1)}{(k_{\mathrm{s}}a)^2} - \frac{1}{2}\right] j_n(k_{\mathrm{d}}a) - 2\frac{k_{\mathrm{d}}a}{(k_{\mathrm{s}}a)^2} j_n'(k_{\mathrm{d}}a)\right\}, \tag{A.124}$$

$$\mathbf{D}^{(n)}_{N+1,\mathrm{core}}(2,2) = -\overline{\rho}\frac{n(n+1)}{(k_{\mathrm{s}}a)^2}\left[k_{\mathrm{s}}a j_n'(k_{\mathrm{s}}a) - j_n(k_{\mathrm{s}}a)\right], \tag{A.125}$$

$$\mathbf{D}^{(n)}_{N+1,\mathrm{core}}(3,1) = -\overline{\rho}\frac{1}{(k_{\mathrm{s}}a)^2}\left[k_{\mathrm{d}}a\, j_n'(k_{\mathrm{d}}a) - j_n(k_{\mathrm{d}}a)\right], \tag{A.126}$$

$$\mathbf{D}^{(n)}_{N+1,\mathrm{core}}(3,2) = -\overline{\rho}\left\{\left[\frac{n(n+1)-1}{(k_{\mathrm{s}}a)^2} - \frac{1}{2}\right] j_n(k_{\mathrm{s}}a) - \frac{1}{k_{\mathrm{s}}a} j_n'(k_{\mathrm{s}}a)\right\}, \tag{A.127}$$

When both the core and the inner layer of the coating are fluids, $\mathbf{D}^{(n)}_{N+1,\mathrm{core}}$ reduces to

$$\mathbf{D}^{(n)}_{N+1,\mathrm{core}}(1,1) = -k_{\mathrm{d}}a\, j_n'(k_{\mathrm{d}}a), \tag{A.128}$$

$$\mathbf{D}^{(n)}_{N+1,\mathrm{core}}(2,1) = \frac{1}{2}\overline{\rho}\, j_n(k_{\mathrm{d}}a), \tag{A.129}$$

Appendix B

Derivation of expressions containing products of spherical Bessel functions of the first and second kind

In this section, the following identities relating the product of spherical Bessel function are developed,

$$j_n(z)n_n'(z) - j_n'(z)n_n(z) = \frac{1}{z^2}, \tag{B.1}$$

$$j_n(z)n_n''(z) - j_n''(z)n_n(z) = -\frac{2}{z^3}, \tag{B.2}$$

$$j_n'(z)n_n''(z) - j_n''(z)n_n'(z) = \frac{1}{z^2}\left[1 - \frac{n(n+1)}{z^2}\right], \tag{B.3}$$

$$j_n(z)n_n'''(z) - j_n'''(z)n_n(z) = -\frac{1}{z^2}\left[1 - \frac{n(n+1)+6}{z^2}\right], \tag{B.4}$$

$$j_n'(z)n_n'''(z) - j_n'''(z)n_n'(z) = -\frac{2}{z^3}\left[1 - \frac{2n(n+1)}{z^2}\right], \tag{B.5}$$

where j_n and n_n are the spherical Bessel functions of the first and second kind, respectively, and the prime denotes the derivative with respect to the argument. These relationships, which arise from evaluating the cloaking criterion for thin shells in Sections 4.1.2 and 6.2, serve an important function in simplifying the analytic formulation for the cloak properties, which are contained within the arguments of the spherical Bessel functions. Specifically, these identities allow the relationship between the cloak properties to be converted from a transcendental relationship to a far simpler algebraic expression.

The derivation of these identities can be formulated by defining the terms

on the left-hand side of Equations (B.1)–(B.5) as

$$y_1(z) = j_n(z)n_n'(z) - j_n'(z)n_n(z), \tag{B.6}$$

$$y_2(z) = j_n(z)n_n''(z) - j_n''(z)n_n(z), \tag{B.7}$$

$$y_3(z) = j_n'(z)n_n''(z) - j_n''(z)n_n'(z), \tag{B.8}$$

$$y_4(z) = j_n(z)n_n'''(z) - j_n'''(z)n_n(z), \tag{B.9}$$

$$y_5(z) = j_n'(z)n_n'''(z) - j_n'''(z)n_n'(z). \tag{B.10}$$

Differentiation of Equation (B.6) yields

$$y_1'(z) = j_n(z)n_n''(z) - j_n''(z)n_n(z) = y_2(z). \tag{B.11}$$

Recall that j_n and n_n satisfy Bessel's equation in spherical coordinates, which can be expressed as

$$z^2 f''(z) + 2zf'(z) + \left[z^2 - n(n+1)\right] f(z) = 0, \tag{B.12}$$

where $f(z)$ is any function that is a solution to this expression, namely, a spherical Bessel function. This leads to

$$f''(z) = \frac{1}{z^2}\left\{ \left[n(n+1) - z^2\right] f(z) - 2zf'(z)\right\}, \tag{B.13}$$

which shows that the second derivative of a spherical Bessel function can be expressed in terms of the function and first derivative.

Substitution of Equation (B.13) into Equation (B.11) yields

$$y_1'(z) = -\frac{2}{z}\left[j_n(z)n_n'(z) - j_n'(z)n_n(z)\right] = -\frac{2}{z}y_1(z). \tag{B.14}$$

Equation (B.6) therefore represents a first-order ordinary differential equation, which yields the general solution

$$y_1(z) = \frac{C}{z^2}, \tag{B.15}$$

where C is a constant of integration. To determine this constant, consider the limit of $y_1(z)$ as $z \to 0$. The limiting behavior of j_n and n_n for small arguments given by Equations (4.30)–(4.37) yields $C=1$, and thus

$$y_1(z) = j_n(z)n'_n(z) - j'_n(z)n_n(z) = \frac{1}{z^2}. \tag{B.16}$$

The solution for $y_2(z)$ can be obtained directly from this result. Since $y_2(z)=y'_1(z)$, substitution of Equation (B.16) into Equation (B.14) yields

$$y_2(z) = j_n(z)n''_n(z) - j''_n(z)n_n(z) = -\frac{2}{z^3}. \tag{B.17}$$

To evaluate $y_3(z)$, Equation (B.13) can be substituted into Equation (B.8), so that

$$y_3(z) = \left[1 - \frac{n(n+1)}{z^2}\right]\left[j_n(z)n'_n(z) - j'_n(z)n_n(z)\right], \tag{B.18}$$

which through the use of Equation (B.16) reduces to

$$y_3(z) = j'_n(z)n''_n(z) - j''_n(z)n'_n(z) = \frac{1}{z^2}\left[1 - \frac{n(n+1)}{z^2}\right]. \tag{B.19}$$

Before evaluating Equation (B.4) and (B.5), the relationship between the third derivative of the spherical Bessel function with respect to the argument must be considered. Differentiation of Equation (B.13) will yield an expression for $f'''(z)$, in terms of $f''(z)$, $f'(z)$ and $f(z)$. Using Equation (B.13) to rewrite $f'''(z)$ in terms of $f'(z)$ and $f(z)$ only, one obtains

$$f'''_n(z) = \frac{1}{z^3}\left\{ -4\left[n(n+1) - \frac{1}{2}z^2\right] f_n(z) + (n^2+n+6-z^2)z\, f'_n(z)\right\}. \tag{B.20}$$

Using Equation (B.20) combined with the results from Equation (B.16), Equations (B.9) and (B.10) reduce to the desired form,

$$y_4(z) = j_n(z)n'''_n(z) - j'''_n(z)n_n(z) = -\frac{1}{z^2}\left[1 - \frac{n(n+1)+6}{z^2}\right], \tag{B.21}$$

$$y_5(z) = j'_n(z)n'''_n(z) - j'''_n(z)n'_n(z) = -\frac{2}{z^3}\left[1 - \frac{2n(n+1)}{z^2}\right]. \tag{B.22}$$

Appendix C

Verification of results using COMSOL multiphysics

To verify the methods and results developed throughout this thesis, the COMSOL multiphysics software package was used. Unlike the spherical harmonic expansions used here, COMSOL uses finite element analysis to solve problems of arbitrary 2D and 3D geometries. Using the acoustics module in COMSOL version 4.1, a 2D axisymmetric domain was created. Although only a 2D model, this is identical to the assumption of azimuthal symmetry used to develop the analytic expressions in Chapter 3.

Figure C.1 shows a comparison between the analytic geometry used in this thesis, illustrated in (a), and the COMSOL model shown in (b). In both cases, a time-harmonic incident wave propagating from left to right impinges on the spherical object. For the analytic examples investigated throughout this work, the object is surrounded by an unbounded space containing water. Finite domains are required for finite element analysis, and so the COMSOL model uses a hemispherical boundary with a radiation condition to mimic an unbounded fluid medium, as observed in Figure C.1(b).

To simulate a time-harmonic plane wave impinging upon the spherical object, the spatial distribution of the complex incident pressure field was prescribed as

$$p_{\text{inc}} = e^{-ik_{\text{w}}x}, \tag{C.1}$$

where k_{w} is the wavenumber in water. In COMSOL, this is accomplished by defin-

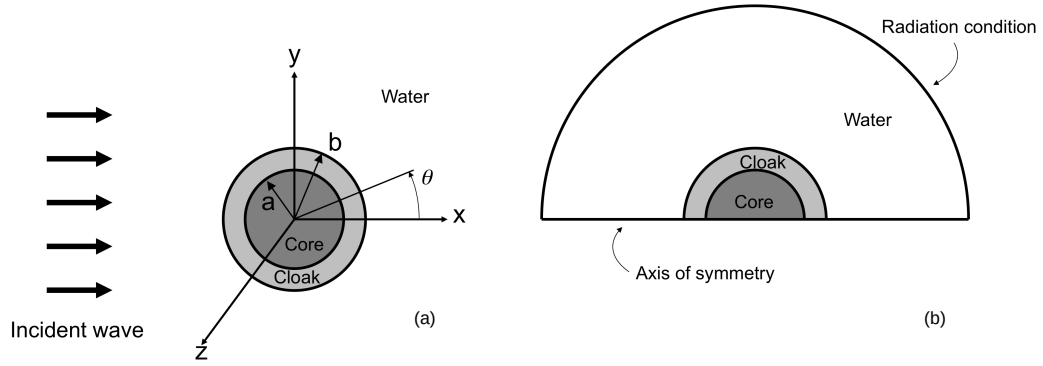

Figure C.1: (a) A time-harmonic incident plane wave in a fluid medium impinging on a spherical core of radius a coated in a cloak of radius b, and (b) the equivalent configuration in COMSOL.

ing a *background field* in the surrounding water. To provide a comparison with the analytic models, the scattered farfield pressure is sought as a function of the angle θ. In COMSOL, these values are obtained by selecting a surface (in the 2D axisymmetric model these surfaces appear as lines), and calculating the farfield pressure by numerically evaluating the product rp_{sc}, where r is the radial distance form the center of the spherical object and p_{sc} is the scattered acoustic pressure, in the limit of $r \to \infty$.

In this particular case, the outer perimeter was chosen to evaluate the farfield scattered pressure in the COMSOL model. At each point on the perimeter evaluated, the position of this point corresponds to a particular angle θ. For each frequency analyzed, the values of the farfield scattered pressure at each angle were exported to compare with the analytic results. One metric which is utilized to compare the analytic results throughout this thesis is the scattering gain, which is a measure of the total scattering cross-section of the cloaked object relative to the uncloaked

object. In the farfield, this expression reduces to

$$\sigma_{\text{gain}} = \frac{\int_0^{\pi} \left|p_{\text{sc}}^{\text{cloak}}\right|^2 d\theta}{\int_0^{\pi} \left|p_{\text{sc}}^{\text{ref}}\right|^2 d\theta}, \tag{C.2}$$

where $p_{\text{sc}}^{\text{cloak}}$ and $p_{\text{sc}}^{\text{cloak}}$ are the farfield scattered acoustic pressures in the cloaked and reference (uncloaked) configurations, respectively.

Although there was excellent agreement with the analytic results illustrated in Figures 5.9, 6.7 and 6.9, correctly implementing the model in COMSOL required some non-intuitive steps due to the design of the software. First, by defining a *background field* in the surrounding medium, this served as the incident wave. However, for the case when other fluids are present in the model, the background field in these layers must be defined using the wavenumber for the surrounding water and *not* the wavenumber for the fluid itself. In this configuration, the background field represents the wave field which would exist if the fluid layer were not there. In addition, once the correct scattered acoustic pressure field is achieved, it was observed that the farfield calculation that COMSOL performs only gives the real part of the pressure. Therefore, to obtain the necessary complex pressure field to solve for the scattering gain in Equation (C.2), solutions for the 'imaginary' part of the pressure field were obtained by introducing a $\pi/2$ phase shift to the background pressure prescribed in Equation (C.1).

Index

Bibliography

[1] G. C. Gaunaurd, "Elastic and acoustic resonance wave scattering", Applied Mechanics Reviews **42**, 143–192 (1989).

[2] J. B. Pendry, D. Schurig, and D. R. Smith, "Controlling electromagnetic fields", Science **312**, 1780–1782 (2006).

[3] D. Schurig, J. J. Mock, B. J. Justice, S. A. Cummer, J. B. Pendry, A. F. Starr, and D. R. Smith, "Metamaterial electromagnetic cloak at microwave frequencies", Science **314**, 977–980 (2006).

[4] U. Leonhardt, "Optical conformal mapping", Science **312**, 1777–1780 (2006).

[5] W. Cai, U. K. Chettiar, A. V. Kildishev, and V. M. Shalaev, "Optical cloaking with metamaterials", Nature Photonics **1**, 224–227 (2007).

[6] G. W. Milton and N.-A. P. Nicorovici, "On the cloaking effects asociated with anomalous localized resonance", Proc. R. Soc. A **462**, 3027–3059 (2006).

[7] A. Greenleaf, Y. Kurylev, M. Lassas, and G. Uhlmann, "Full-wave inviscibility of active devices at all frequencies", Comm. in Math. Phys. **275**, 748–789 (2007).

[8] D. A. B. Miller, "On perfect cloaking", Optics Express **14**, 12457–12446 (2006).

[9] A. Yaghjian and S. Maci, "Alternative derivation of electromagnietic cloaks and concentrators", New. J. Phys. **10** (2008).

[10] P. Alitalo, O. Luukkonen, L. Jylhä, J. Venermo, and S. A. Tretyakov, "Transmission-line networks cloaking objects from electromagnetic fields", IEEE Trans. Antennas Propagation **56**, 416–424 (2008).

[11] S. Tretyakov, P. Alitalo, O. Luukkonen, and C. Simovski, "Broadband electromagnetic cloaking of long cylindrical objects", Phys. Rev. Lett. **103** (2009).

[12] S. A. Cummer and D. Schurig, "One path to acoustic cloaking", New J. Phys. **9** (2007).

[13] L.-W. Cai and J. Sánchez-Dehesa, "Analysis of cummer-schurig acoustic cloaking", New. J. Phys. **9** (2007).

[14] S. A. Cummer, B.-I. Popa, D. Schurig, D. R. Smith, J. B. Pendry, M. Rahm, and A. Starr, "Scattering theory derivation of a 3d acoustic cloaking shell", Phys. Rev. Lett. **74** (2008).

[15] D. Torrent and J. Sánchez-Dehesa, "Acoustic cloaking in two dimensions: a feasible approach", New. J. Phys. **10** (2008).

[16] D. Torrent and J. Sánchez-Dehesa, "Anisotropic mass density by two-dimensional acoustic metamaterials", New. J. Phys. **10** (2008).

[17] C. L. Scandrett, J. E. Boisvert, and T. R. Howarth, "Acoustic cloaking using layered pentamode materials", J. Acoust. Soc. Am. **127**, 2856–2864 (2010).

[18] C. Ren, Z. Xiang, and Z. Cen, "Layered and isotropic acoustic cloak design based on conformal transformation acoustics", SCIENCE CHINA Physics, Mechanics & Astronomy **54**, 593–597 (2011).

[19] C. N. Layman, T. P. Martin, K. M. Moore, D. C. Calvo, and G. J. Orris, "Designing acoustic transformation devices using fluid homogenization of an elastic substructure", Applied Physics Letters **99**, 163503 (2011).

[20] Z. Chang, J. Hu, G. Hu, R. Tao, and Y. Wang, "Controlling elastic waves with isotropic materials", Applied Physics Letters **98**, 121904 (2011).

[21] A. N. Norris, "Acoustic cloaking theory", Proc. R. Soc. A **464**, 2411–2434 (2008).

[22] G. W. Milton, M. Briane, and J. R. Willis, "On cloaking for elasticity and physical equations with a transformation invariant form", New. J. Phys. **8** (2006).

[23] M. Farhat, S. Enoch, S. Guenneau, and A. B. Movchan, "Broadband cylindrical acoustic cloak for linear surface waves in a fluid", Phys. Rev. Lett. **101**, 134501 (2008).

[24] M. Farhat, S. Guenneau, S. Enoch, and A. B. Movchan, "Cloaking bending waves propagating in thin elastic plates", Phys. Rev. B **79**, 033102 (2009).

[25] M. Farhat, S. Guenneau, and S. Enoch, "Ultrabroadband elastic cloaking in thin plates", Phys. Rev. Lett. **103**, 024301 (2009).

[26] A. N. Norris, "Acoustic cloaking in 2d and 3d using finite mass", arXiv:0802.0701v1 [physics.flu-dyn] (2008).

[27] Y. Cheng, F. Yang, J. Y. Xu, and X. J. Liu, "A multilayer structured acoustic cloak with homogeneous isotropic materials", Appl. Phys. Lett. **92** (2008).

[28] M. Schoenberg and P. N. Sen, "Properties of a periodically stratified acoustic half-space and its relation to a biot fluid", J. Acoust. Soc. Am. **73**, 61–67 (1983).

[29] A. N. Norris and A. J. Nagy, "Acoustic metafluids made from three acoustic fluids", J. Acoust. Soc. Am. **128**, 1606 (2010).

[30] S. Zhang, C. Xia, and N. Fang, "Broadband acoustic cloak for ultrasound waves", Phys. Rev. Lett. **106**, 024301 (2011).

[31] B.-I. Popa, L. Zigoneanu, and S. A. Cummer, "Experimental acoustic ground cloak in air", Phys. Rev. Lett. **106**, 253901 (2011).

[32] D. Torrent, A. Håkansson, F. Cervera, and J. Sánchez-Dehesa, "Homogenization of two-dimensional clusters of rigid rods in air", Phys. Rev. Lett. **96**, 204302 (2006).

[33] D. Torrent and J. Sánchez-Dehesa, "Broadband acoustic cloaks based on the homogenization of layered materials", Wave Motion **48**, 497 – 504 (2011).

[34] D. T. Blackstock, *Fundamentals of Physical Acoustics*, 1st edition (John Wiley & Sons, New York) (2000).

[35] R. Christensen, *Mechanics of Composite Materials* (Dover Publications) (2005).

[36] G. W. Milton and A. V. Cherkaev, "Which elasticity tensors are realizeable", J. Eng. Mater. Tech. **117**, 483–493 (1995).

[37] A. N. Norris, "Periodic metal structures for acoustic wave control", J. Acoust. Soc. Am. **130**, 2359 (2011).

[38] A. N. Norris, "Acoustic metafluids", J. Acoust. Soc. Am. **125**, 839–849 (2009).

[39] N. A. Nicorovici, G. W. Milton, R. C. McPhedran, and L. C. Botten, "Quasistatic cloaking of two-dimensional polarizable discrete systems by anomalous resonance", Opt. Express **15**, 6314–6323 (2007).

[40] N. A. Nicorovici, R. C. McPhedran, and G. W. Milton, "Optical and dielectric properties of partially resonant composites", Phys. Rev. B **49**, 8479–8482 (1994).

[41] N. Fang, D. Xi, J. Xu, M. Ambati, W. Srituravanich, C. Sun, and X. Zhang, "Ultrasonic metamaterials with negative modulus", Nature Mater. **5**, 452–456 (2006).

[42] X. Zhou and G. Hu, "Analytic model of elastic metamaterials with local resonances", Phys. Rev. B **79**, 195109 (2009).

[43] A. Alù and N. Engheta, "Plasmonic and metamaterial cloaking: physical mechanisms and potentials", J. Opt. A **10** (2008).

[44] M. D. Guild, M. R. Haberman, and A. Alù, "Plasmonic cloaking and scattering cancelation for electromagnetic and acoustic waves", Wave Motion **48**, 468 – 482 (2011).

[45] A. Alù and N. Engheta, "Achieving transparency with plasmonic and metamaterial coatings", Phys. Rev. E **72** (2005).

[46] C. H. Papas, *Theory of Electromagnetic Wave Propagation* (Dover, New York) (1988).

[47] A. Alù and N. Engheta, "Polarizibilities and effective parameters for collections of spherical nano-particles formed by pairs of concentric double-negative (dng), single negative (sng) and/or double-positive (dps) metamaterial layers", J. Appl. Phys. **97** (2005).

[48] J. D. Jackson, *Classical Electrodynamics* (Wiley, New York) (1998).

[49] W. Murray and W. Barnes, "Plasmonic materials", Advanced Materials **19**, 3771–3782 (2007).

[50] A. Alù and N. Engheta, "Cloaking and transparency for collections of particles with metamaterial and plasmonic covers", Opt. Expr. **15**, 7578–7590 (2007).

[51] A. Alù and N. Engheta, "Multifrequency optical invisibility cloak with layered plasmonic shells", Phys. Rev. Lett. **100** (2008).

[52] A. Alù and N. Engheta, "Plasmonic materials in transparency and cloaking problems: mechanism, robustness and physical insights", Opt. Expr. **15**, 3318–3332 (2007).

[53] A. Alù and N. Engheta, "Robustness in design and background variations in metamaterial/plasmonic cloaking", Radio Science **43** (2008).

[54] D. Rainwater, A. Kerkhoff, K. Melin, J. C. Soric, G. Moreno, and A. Alù, "Experimental verification of three-dimensional plasmonic cloaking in free-space", New Journal of Physics **14**, 013054 (2012).

[55] A. Alù and N. Engheta, "Cloaking a sensor", Phys. Rev. Lett. **102**, 233901 (2009).

[56] A. Alù and N. Engheta, "Cloaking a receiving antenna or a sensor with plasmonic metamaterials", Metamaterials **4**, 153–159 (2010).

[57] A. Alù and N. Engheta, "Cloaked near-field scanning optical microscope tip for non-invasive near-field imaging", Phys. Rev. Lett. **105**, 263906 (2010).

[58] G. Milton, *The Theory of Composites* (Cambridge University Press, Cambridge, UK) (2002).

[59] X. Zhou, G. Hu, and T. Lu, "Elastic wave transparency of a sollid sphere coated with metamaterials", Phys. Rev. B **77** (2008).

[60] K. Graff, *Wave Motion in Elastic Solids* (Dover Publications) (1975).

[61] J. L. Rose, *Ultrasonic Waves in Solid Media*, 1st edition (Cambridge University Press, Cambridge, UK) (2004).

[62] C. G. Gray and B. G. Nickel, "Debye potential representation of vector fields", Am. J. Phys. **46**, 735–736 (1978).

[63] J. J. Faran, "Sound scattering by solid cylinders and spheres", J. Acoust. Soc. Am. **23**, 405–418 (1951).

[64] R. R. Goodman and R. Stern, "Reflection and transmission of sound by elastic spherical shells", J. Acoust. Soc. Am. **34**, 338–344 (1962).

[65] R. Hickling, "Analysis of echos from a solid elastic sphere in water", J. Acoust. Soc. Am. **34** (1962).

[66] R. Hickling, "Analysis of echos from a hollow metallic sphere in water", J. Acoust. Soc. Am. **34**, 1124–1137 (1964).

[67] L. W. Anson and R. C. Chivers, "Ultrasonic scattering from spherical shells including viscous and thermal effects", J. Acoust. Soc. Am. **93**, 1687–1699 (1993).

[68] A. D. Pierce, *Acoustics: An Introduction To Its Physical Principles and Applications* (Acoustical Soc. of America) (1989).

[69] M. Abramowitz and I. A. Stegun, *Handbook of Mathematical Functions: With Formulas, Graphs and Mathematical Tables* (Dover, New York) (1972).

[70] The Mathworks, Inc., *Optimization Toolbox* (2009).

[71] J. R. Silvester, "Determinants of block matrices", The Mathematical Gazette **84**, 460–467 (2000).

[72] R. S. Lakes and W. J. Drugan, "Dramatically stiffer elastic composite materials due to a negative stiffness phase?", J. Mech. Phys. Solids **50**, 979–1009 (2002).

[73] J. G. Berryman, "Long-wavelength propagation in composite elastic media i. spherical inclusions", J. Acoust. Soc. Am. **68**, 1809–1819 (1980).

[74] Z. Hashin and S. Shtrikman, "A variational approach to the theory of the elastic behavior of multi-phase materials", J. Mech. Phys. Solids **11**, 127–140 (1963).

[75] L. Landau, E. Lifshitz, A. Kosevich, and L. Pitaevskiĭ, *Theory of Elasticity*, Theoretical Physics (Butterworth-Heinemann) (1986).

[76] M. C. Junger and D. Feit, *Sound, Structures, and Their Interaction* (The Acosutical Society of America) (1993).

[77] L. E. Kinsler, A. R. Frey, A. B. Coppens, and J. V. Sanders, *Fundamentals of Acoustics*, 4th edition (John Wiley & Sons, New York) (2000).

[78] S. Hasheminejad and M. Maleki, "Acoustic wave interaction with a laminated transversely isotropic spherical shell with imperfect bonding", Archive of Applied Mechanics **79**, 97–112 (2009).

[79] F. Honarvar and A. Sinclair, "Acoustic wave scattering from transversely isotropic cylinders", J. Acoust. Soc. Am. **100**, 57–63 (1996).

[80] H.-C. Hu, "On the general theory of elasticity for a spherically isotropic medium", Acta Sci. Sin. **3**, 247–260 (1954).

[81] W. T. Chen, "On some problems in spherically isotropic elastic materials", ASME J. Appl. Mech. **33**, 539–546 (1966).

[82] C. V. Ramakrishnan and A. H. Shah, "Vibration of an aelotropic spherical shell", J. Acoust. Soc. Am. **47**, 1366–1374 (1970).

[83] H. Cohen and A. H. Shah, "Free vibrations of a spherically isotropic hollow sphere", Acustica **26**, 329–333 (1972).

[84] C. Prasad, "On vibrations of spherical shells", J. Acoust. Soc. Am. **36**, 489–494 (1964).

[85] N. A. Shul'ga, A. Y. Grigorenko, and T. L. Efimova, "Free non-axisymmetric oscillations of a thick-walled, nonhomogeneous, transversally [sic] isotropic, hollow sphere", Soviet Appl. Mech. **24**, 439–444 (1988).

[86] H. J. Ding and W. Q. Chen, "Natural frequencies of an elastic spherically isotropic hollow sphere submerged in a compressible medium", J. Sound Vib. **192**, 173–198 (1996).

[87] W. Q. Chen and H. J. Ding, "A state-space-based stress analysis of a multilayered spherical shell with spherical isotropy", Journal of Applied Mechanics **68**, 109–114 (2001).

[88] C. Scandrett, "Scattering and active acoustic control from a submerged spherical shell", J. Acoust. Soc. Am. **111**, 893–907 (2002).

[89] W. Q. Chen and H. J. Ding, "Natural frequencies of a fluid-filled anistropic spherical shell", J. Acoust. Soc. Am. **105**, 174–182 (1999).

[90] O. Wilson, *Introduction to Theory and Design of Sonar Transducers* (Peninsula, Los Altos, CA) (1988).

[91] G. C. Gaunaurd and H. Uberall, "Rst analysis of monostatic and bistatic acoustic echoes from an elastic sphere", J. Acoust. Soc. Am. **73**, 1–12 (1983).

[92] A. M. Baird, F. H. Kerr, and D. J. Townend, "Wave propagation in a viscoelastic medium having fluid-filled microspheres", J. Acoust. Soc. Am. **105**, 1527–1538 (1999).

[93] G. C. Gaunaurd and M. F. Werby, "Sound scattering by resonantly excited, fluid-loaded, elastic spherical shells", J. Acoust. Soc. Am. **90**, 2536–2550 (1991).

[94] Y. Hu, S. Qin, and Q. Jiang, "Characteristics of acoustic scattering from a double-layered micro shell for encapsulated drug delivery.", IEEE Trans Ultrason Ferroelectr Freq Control **51**, 809–821 (2004).